5-2018

Liposomal discovery of diacylglycerol (DAG)-binding proteins and the use of signaling lipids to improve nanodrug delivery

Samuel Isaac Mattern-Schain
University of Tennessee

To the Graduate Council:

I am submitting herewith a dissertation written by Samuel Isaac Mattern-Schain entitled "Liposomal discovery of diacylglycerol (DAG)-binding proteins and the use of signaling lipids to improve nanodrug delivery." I have examined the final electronic copy of this dissertation for form and content and recommend that it be accepted in partial fulfillment of the requirements for the degree of Doctor of Philosophy, with a major in Chemistry.

Michael D. Best, Major Professor

We have read this dissertation and recommend its acceptance:

David C. Baker, Francisco N. Barrera Olivares, Tessa R. Calhoun

Accepted for the Council:
Dixie L. Thompson

Vice Provost and Dean of the Graduate School

(Original signatures are on file with official student records.)

Liposomal discovery of diacylglycerol (DAG)-binding proteins and the use of signaling lipids to improve nanodrug delivery

A Dissertation Presented for the

Doctor of Philosophy

Degree

The University of Tennessee, Knoxville

Samuel Isaac Mattern-Schain

May 2018

Acknowledgments

Over my graduate career, I have been trained, supported and advised by several incredible individuals who motivate me with their knowledge, work ethic and skill. Dr. Best, you are responsible for my love of the natural sciences and our shared passion for the supramolecular has made working in your lab a joy. Your talent as an educator is inspiring, and I've learned too much from you to measure. Beyond that, you have been my first line of defense in times of crisis, a mentor, and a friend. I will be forever grateful for your wisdom and patience, and of course the opportunity to enter the world of liposomal technology. Dr. Andrew Bayer, as a senior member in the Best group you could not have been a better teacher to me, you are a true synthetic wizard. Dr. Kathrin Tschersch, as a postdoc in the Best lab you taught me what it meant to be an interdisciplinary scientist and your lessons have been fundamental to honing my skills as a collaborator. Other past Best group members, especially Dr. Tanei Ricks, Dr. Shahrina Alam and Dr. Stuart Whitehead, you will forever be remembered for the trials we conquered together and all the laughter we shared. Adam and Alexa, we have worked so closely with one another and I cannot thank you enough for your assistance and more importantly for making it fun. Alex, Lucia aka 'Drizzle', Jinchao, Zhengsu and all the other Best lab members past and present, it has been a pleasure to share this journey with you and become friends along the way.

I am also very grateful for the guidance and support I've received from my doctoral committee: Dr. Tessa Calhoun, Dr. David Baker and Dr. Francisco Barrera. Dr. Baker, it has a been a pleasure teaching together year after year. The opportunity to learn from you has been an honor. Dr. Barrera, thank you for all you have taught me about biology and, more importantly, what you taught me about being a scientist in general, especially early on in my graduate career. Dr. Calhoun, thank you for joining my committee. You are an inspiring chemist and you were very patient with me when I kept borrowing your key to use the DLS! In all seriousness, I've learned many lessons from all of you that I will not soon forget.

Dr. Deidra Mountain and Trey Fisher, I am eternally grateful for the opportunities your lab has presented me with. It has always been a pleasure working with you two, Conner, Stacy and everyone else in your research group. Your expertise and innovative collaboration has been invaluable to my progression as a scientist.

Kenneth Lum and everyone else that accommodated me at the Cravatt lab. Your direction and hands-on support was instrumental to my work. Ken, I learned so much from you in such a brief period, it was amazing.

Dr. Daiane Santana Alves, thank you so much for your tireless work to provide us with materials crucial to our projects. Haden Scott and Justin Westerfield, also of the Barrera lab, thank you for your generous supply of expertise, and supplies. Sujata Argawal, thank you for your accommodation, support and wonderful company whenever I was working in the UTIA Genomics Hub. Dr. John Dunlap, thank you for your consultation and instrument access. Dr. Carlos Steren, I'm grateful for your time and support, you are an invaluable asset to the UTK chemistry department. Dr. Natalie Sadlar and Dr. Aaron Wright of Pacific Northwest National Lab, thank you for training me early in my graduate career. Dr. Shawn Campagna, Allen, and Abigail, thank you for your generous donation of time and equipment.

Dr. Brian Long, Dr. Chris Baker, Dr. Jon Camden, and Dr. Steven Neal, thank you all for the advice and support during my graduate career. To everyone else at the chemistry department that has made working there a joy, thank you.

Lastly, thank you to my family and friends. You know who you are so I won't name names, but your constant yet often-unrequited loving attention while I've been away pursuing my scientific interests has been crucial to keeping me going.

This work is dedicated to two individuals. Dad, you taught me that learning is a lifelong endeavor and to finish what I start. Vanessa, we all miss you but don't worry, Ryan and Claire are in good hands.

Abstract

The protein signaling activities of the glycerolipid diacylglycerol (DAG) form the impetus for the projects described herein. DAG's governance of cellular functions involves activation of peripheral membrane proteins (PMPs) at bilayer surfaces, which includes the activation of protein kinase C (PKC) to regulate oncogenesis. In addition to enzymatic signal transduction, DAG influences membrane mechanics and is a central lipid metabolite. Relatively little is known about DAG when compared to more common signaling lipids such as phosphatidylinositol polyphosphates (PIP_ns). This is due in part to the surreptitious nature of PMP operation and the complexity of natural bilayers. We developed a liposomal platform to identify PMP binding as a function of specific lipids. Synthetic, photocrosslinking lipids with clickable tags are incorporated into liposomes to capture and enrich proteins. Affinity-based protein profiling (AfBPP) experiments initially demonstrated proteome-wide increases in affinity when using DAG or phosphatidic acid (PA) as chase lipids. With the aid of collaborators at The Scripps Research Institute (TSRI), we optimized our AfBPP protocol to label select proteins as a function of liposomal DAG content when a generic lipid probe was also present in the membrane. The generic probe strategy varies natural lipid content with consistent probe concentration between liposomal treatments, this is called the *lipomimetic* approach. Lipid specific probes have also been applied to liposomal AfBPP, which is termed the *lipospecific* approach.

In a separate project, we tested to see if DAG could potentiate the cell-association of a liposomal delivery system (LDS). LDSs are a rapidly expanding field; most existing nanodrugs are liposomal. Strategies for increasing LDS efficacies often undermine clinical translatability. Incorporating natural signaling lipids into nanodrugs architectures is a clinically viable targeting strategy. A polyethylene glycol (PEG) decorated (PEGylated) liposome bearing a cell penetrating peptide (CPP) was doped with DAG and/or PS and significant, dose-dependent increases in association to target cells were observed. We also advanced LDSs with new technologies for controlling vesicle release and fusion. Liposomes have limitless utility as theranostic tools and platforms for biochemical investigations. Herein, we bring liposomal technologies closer to their scientific and clinical potentials.

Table of Contents

Preamble – 1

Chapter 1: Introduction – 2

1.1: Glycerophospholipids – 2

Form and function of glycerolipids – 2

Membrane proteins – 8

Peripheral membrane proteins – 8

1.2: Cellular functions of DAG and related lipids – 10

DAG and PKC – 12

DAG function – 14

Dag and immune response – 15

DAG and Alzheimer's Disease – 16

PA – 17

PS – 19

SM – 19

DAG and Cancer – 20

Nanodomains: to raft or not to raft – 24

Nanodomain analyses – 26

Implications of rafting – 27

1.3: Relevant advances in chemical biology – 28

The liposome – 28

Liposomal theranostics – 31

Click chemistry – 35

Activity-based protein profiling (ABPP) – 37

Photoaffinity tags – 38

Bifunctional lipid probes – 39

Liposomal chemical biology – 41

Chapter 2: Liposomal affinity-based protein profiling (AfBPP) – 45

2.1: Introduction – 45

Lipomimetic and lipospecific AfBPP – 45

Probe design – 48

Labeling studies – 51

Controls – 53

2.2: Results – 54

Validation using known protein targets – 54

DAG-based labeling in lipomimetic studies using generic probe **7** – 56

Lipomimetic labeling with other chase lipids – 57

Lipospecific studies with diazirine DAG probe **3** – 59

Lipospecific studies with PA probes – 62

Conclusion – 65

2.3: Materials, methods and optimization – 65

Synthesis of key intermediate 15 – 65

Synthesis of single azide-tail benzophenone probe 8 – 69

General procedures for liposomal AfBPP – 71

Liposome formation – 71

Preparing cell lysates – 73

General incubation procedure – 74

Photocrosslinking – 74

Click enrichment – 75

Gel loading/running – 76

Fluorescent imaging and staining – 76

Optimizing labeling studies – 77

SDS treatment – 77

Other incubation ingredients – 78

Click enrichment – 79

Precipitation/wash – 80

Gel loading procedure for Protocol B – 83

2.3.b: Additional experimental data – 83

Lipospecific DAG probe results – 84

Lipomimetic DAG and PA studies using benzophenone probe **5** – 84

Lipomimetic studies comparing the lipid affinities of HIV capsid protein (CA) – 86

2.4: Future work – 86

Size exclusion-based liposomal protein extraction (SELPE) – 94

Discussion – 96

Chapter 3: Targeting nanodrugs using natural signaling lipids – 98

3.1: Introduction – 98

Actively targeting nanocarriers to specific cell types – 100

Cell Penetrating peptides – 103

An R8-LDS for treating vascular disease through gene silencing – 104

Experimental design – 107

Controls – 107

LDS formulations – 108

3.2: Results – 110

DAG-potentiated cell association to VSMCs – 110

PS-potentiated cell association to VSMCs – 113

DAG-potentiated cell association to VECs – 114

PS-potentiated cell association to VECs – 115

Encapsulation efficiency of optimal DAG/PS liposomes – 117

DLS size and zeta potential studies of optimal DAG/PS formulations – 118

Combinatorial cell association studies in VSMCs using DAG and PS – 118

Future work: Cargo delivery profiles by qPCR & cytotoxicity assays – 119

Discussion – 120

3.3: Methods – 121

Liposome formation and characterization – 121

Cell culture – 123

Measuring cell association – 123

Measuring encapsulation efficiency – 124

Acknowledgments – 124

Chapter 4: Active targeting using natural signaling lipids – 125

4.1: Introduction – 125

Existing strategies for controlling liposomal release – 126

A photocleavable PC-analog for controlled release of liposomal cargo – 127

Inducing membrane fusion using clickable lipids – 130

4.2: Verifying mixing of aqueous cargo between fused liposomes – 132

The terbium-trichloride ($TbCl_3$)-dipicholinic acid (DPA) content mixing assay – 133

Results – 133

Methods – 135

4.3: The future of triggered release – 137

Epilogue – 139

References – 141

Appendix – 164

Vita – 190

List of Figures

Figure 1.1: Seven common lipids and their chemical structures – 1

Figure 1.2: Phospholipid cone angles and self-assembled structures – 2

Figure 1.3: Self-assembled structures of phospholipids in aqueous media – 5

Figure 1.4: Four common fatty acids with their trivial names – 7

Figure 1.5: A cartoon schematic of a liquid ordered (Lo) nanodomain accommodating a membrane protein at the hydrophilic face of a bilayer membrane – 9

Figure 1.6: An illustration of the plasma membrane – 11

Figure 1.7: Conventional and novel PKC regulatory domains – 13

Figure 1.8: A DAG-centric map of relevant cell signaling pathways – 21

Figure 1.9: A cartoon of membrane rafting – 25

Figure 1.10: TEM image of liposomes – 30

Figure 1.11: The enhanced permeability and retention (EPR) of nanocarriers at target sites – 33

Figure 1.12: Click chemistry used to create functional liposomal nanocarriers – 36

Figure 1.13: Two common photoaffinity tags – 39

Figure 1.14: Examples of recently-developed functional lipid probes – 40

Figure 1.15: A lipomimetic affinity-based protein profiling strategy – 44

Figure 2.1: Lipospecific experimental design – 46

Figure 2.2: Two different lipid-specific probe architectures – 47

Figure 2.3: Generic probes for lipomimetic studies – 48

Figure 2.4: Synthesis of the para-methoxy benzyl (PMB) protected azido DAG analog **15** – 49

Figure 2.5: Facile synthesis of single azide-tail generic probe **8** – 50

Figure 2.6: Outline of Protocol A for liposomal protein profiling – 52

Figure 2.7: Protocol B volumes and reagents for liposomal protein profiling – 53

Figure 2.8: A PS-Annexin lipomimetic proof of concept experiment – 54

Figure 2.9: A PS-Annexin lipomimetic proof of concept experiment – 55

Figure 2.10: Volumes of incubation ingredients and click reagents for lipomimetic studies in isolated proteins – 56

Figure 2.11: A lipomimetic PA study screening the HIV-1 capsid protein CA **–** 56

Figure 2.12: A lipomimetic DAG study in Hek cell extracts with DAG-specific protein labeling – 57
Figure 2.13: A lipomimetic and competitive lipospecific DAG study in Hek cell extracts with DAG-specific protein labeling – 58
Figure 2.14: A lipomimetic PA study in t24 cancer cell extracts – 59
Figure 2.15: A lipomimetic PIP3 study in t24 extracts – 60
Figure 2.16: A lipospecific DAG experiment in t24 cancer cell extracts using size exclusion column enrichment (SEC) pre-click – 61
Figure 2.17: A competitive lipospecific DAG/PA experiment – 62
Figure 2.18: A lipospecific PA study in t24 extracts – 63
Figure 2.19: A lipospecific PA study in yeast cell extracts – 64
Figure 2.20: A spreadsheet to output stock solution volumes for lipid film formation – 72
Figure 2.21: Optimal click reagent concentrations and corresponding volumetric ratios – 75
Figure 2.22: Structures of click ligands – 79
Figure 2.23: A lipomimetic study performed using single tail benzophenone probe **8** with the solvent wash/precipitation step with an extra water wash and top phase removal – 82
Figure 2.24: A gel experiment comparing lipospecific use of an amide-linked bifunctional DAG probe with a lipomimetic DAG study – 85
Figure 2.25: Fluorescent image of a lipospecific study using amide linked DAG probe **1a** – 86
Figure 2.26: Fluorescent image of a lipomimetic study using GP **5** – 87
Figure 2.27: Lipomimetic PS study of CA protein – 88
Figure 2.28: Lipomimetic PA study of CA protein – 89
Figure 2.29: Lipomimetic PS study of CA protein – 90
Figure 2.30: Lipomimetic DAG study of CA protein – 91
Figure 2.31: Fluorescently labeled aliquots from MS studies at TSRI – 93
Figure 2.32: Synthesis of crosslinking-only benzophenone lipid **20** – 95
Figure 2.33: SELPE data – 97
Figure 3.1: A schematic representation of how the addition of DAG and/or PS potentiates the cellular association of an octa-arginine (R8) cell penetrating peptide (CPP)-functionalized liposome – 99

Figure 3.2: A cartoon depiction of active targeting – 102
Figure 3.3: A stearyl octa-arginine (R8) CPP – 104
Figure 3.4: Experimental design to test the ability of DAG and/or PS to increase delivery efficacy of an CPP liposomal nanocarrier (R8-PLP) – 108
Figure 3.5: Structures of lipid constituents used for in LDS formulations – 109
Figure 3.6: Lipid compositions of LDS formulations for initial cell association assays – 111
Figure 3.7: Fluorescent microscopy images showing increased cell association of liposomes as signaling lipid content goes up – 112
Figure 3.8: Quantified cell association data from DAG-VSMC experiments – 113
Figure 3.9: Quantified cell association data from PS-VSMC experiments – 114
Figure 3.10: Quantified cell association data from DAG-VEC experiments – 115
Figure 3.11: Quantified cell association data from PS-VEC experiments – 116
Figure 3.12: Encapsulation efficiency results – 117
Figure 3.13: Combinatorial LDS treatment groups – 118
Figure 3.14: Average diameter of DAG/PS LDS formulations – 118
Figure 3.15: Average PDI of DAG/PS LDS formulations – 120
Figure 3.16: Cell association data using combinatorial formulations of DAG/PS – 121
Figure 3.17: Representative fluorescent images from combinatorial DAG/PS cell association assays in VSMC – 122
Figure 4.1: A cartoon of triggered release from SSNs – 125
Figure 4.2: Synthesis of a photocleavable release trigger – 128
Figure 4.3: Structures of Nile red dye and the cancer drug camptothecin are compared – 130
Figure 4.4: STEM images of azido liposomes before and after incubation with cyclooctyne liposomes – 131
Figure 4.5: Structure of DPA and TbCl3 – 133
Figure 4.6: Results of the DPA and TbCl3 content mixing assay – 134
Figure 4.7: Synthetic clickable lipids – 135

List of Abbreviations

(S)TEM – (scanning) transmission microscopy
2OHOA – 2-hydroxyoleic acid
ABI1 – Abelson interactor 1
ABPP – activity based protein profiling
AD – Alzheimer's and Dementia
AfBPP – affinity-based protein profiling
AfBPP – affinity-based protein profiling
AFM – atomic force microscopy
Ag2O – silver oxide
ALS – amyotrophic lateral sclerosis
aPKC – atypical PKC
ATP – Adenosine triphosphate
BBB – blood brain barrier
Ca – Calcium
CA – HIV capsid protein
CDCl3 – deuterated chloroform
CDP – cytidine diphosphate
CHCl3 – chloroform
CL – cationic liposome
CMC – critical micelle concentration
cPKC – conventional PKC
CPP – cell penetrating peptide
CPT – camptothecin
CRC – colorectal cancer
cRGD – cyclic arginine-glycine-aspartic acid peptide
CTR1 – constitutive triple response 1 kinase
CuAAC – catalyzed azide-alkyne
CuSO4 – copper sulfate
DAG – diacylglycerol
DCM – dichloromethane
DDQ – 2,3-dichloro-5,6-dicyano-1,4-benzoquinone (DDQ
DGK – diacylglycerol kinase
DLS – dynamic light scattering
DMEM – Dulbecco's modified eagle medium
DMF – dimethyl formamide
DMSO – dimethyl sulfoxide
DOTAP – dioleoyloxypropyltrimethylammonium
Dox – doxorubicin
EDTA – ethylenediaminetetraacetic acid
EE – encapsulation efficiency
EPR – enhanced permeability and retention
ERK – extracellular signal-related kinase

EtOAc – ethyl acetate
FA – folic acid
FCS – fetal calf serum
FDA – food and drug administration
FLIM – fluorescent lifetime imaging microscopy
FRET - Förster resonance energy transfer
GAP – GTPase activity accelerating protein
GAPDH – glyceraldehyde 3-phosphate dehydrogenase
GDP – guanosine diphosphate
GFP – green fluorescent protein
GMV – giant multilamellar vesicles
GP – generic probe
GPCR – G protein-coupled receptors
GPI – glycophosphatidylinositol
GRP1 – glucose regulated protein 1
GTP – guanosine triphosphate
GTP – Guanosine triphosphate
HASMC – human aortic smooth muscle cell
Hex – hexanes
HFS – Hand-foot syndrome
HIV – human immunodeficiency virus
HRMS – high resolution mass spectrometry
HSV – herpes simplex virus
Human embryonic kidney – Hek
IAM – immobilized artificial membranes
IEDDA – inverse electron demand Diels-Alder
iFCS – inverse fluorescent correlation spectroscopy
IH – intimal hyperplasia
ILC – immobilized liposomal chromatography
IS – immunological synapse
kDa – kilodalton
KI – potassium iodide
Ld – liquid disordered
LDS – liposomal delivery system
LEP – liposome extruder purification
LiAlH4 – lithium aluminum hydride
LNC – lipid nanocapsules
Lo – liquid ordered
LPA – lysophosphatidic acid
LTSL – lysolipid thermosensitive liposomes
LUV – large unilamellar vesicles
MALDI – matrix-assisted desorption ionization
MAPK – mitogen-activated protein kinase
MAPK – P21-mitogen activated kinase

MCI – mild cognitive impairment
MeOH – methanol
MgSO4 – magnesium sulfate
MMP – matric metalloproteases
Mn – Manganese
MS – mass spectrometry
MsCl – mesyl chloride
MTOC – microtubule organizing center
mTOR – mammalian target of rapamycin
Munc-13 – mammalian uncoordinated protein 13
N – amino
NaH – Sodium hydride
NaN3 – sodium azide NaN3
NB-PC – nitrobenzyl phosphatidylcholine
NF-kappaB – nuclear factor kappa B
NFLD – non-alcoholic fatty liver disease
NLS – nuclear localization signal
NMR - nuclear magnetic resonance
NMR – nuclear magnetic resonance
nPKC – novel PKC
NPL – Non-PEGylated liposomes
PA – phosphatidic acid
PAGE – polyacrylamide gel electrophoresis
PAP – phosphatidic acid phosphatase
PBS – phosphate buffered saline
PC – phosphatidyl choline
PDI – polydispersity index
PE – phosphatidylethanolamine
PEG – polyethylene glycol
PG – phosphatidylglycerol
PDT – photodynamic therapy
pHLIP – pH low-insertion peptide
PIP – phosphatidylinositol polyphosphate
PKB/Akt – protein kinase B
PKC – protein kinase C
PKD – protein kinase D
PLC – phospholipase C
PLD – phospholipase D
PLP – PEGylated lipoparticle
PMBCl – para-methoxybenzyl chloride
PMP – peripheral membrane protein
PMT – photomultiplication tube
PNNL – pacific northwest national lab
PON1 – paraoxinase 1

PP1 – phosphatase 1
PP2A – phosphatase-2A
PP2C – phosphatase 2C
PPI – protein-protein interactions
PS – phosphatidylserine
p-TsOH – para-toluenesulfonic acid
PVD – peripheral vascular disease
qPCR – qualitative polymerase chain reaction
R8 – octa-arginine
RAF – Fibrosarcoma
Ras – Rat Sarcoma
REV – reverse phase evaporation
RNA – ribonucleic acid
RNAi – ribonucleic acid interference
rt – room temperature
RTK – receptor tyrosine kinase
SDS – sodium dodecylsulfate
SEC – size exclusion chromatography
SEC – size exclusion column
SELPE – size exclusion-based liposomal protein extraction
SHP-1 – src homology region 2 domain-containing phosphatase-1
si – short interfacing
SL-EPR – spin-labeled electro paramagnetic resonance
SM – sphingomyelin
SMS – sphingomyelin synthase
SNALP – stable nucleic acid lipid particle
SPHK – sphingosine kinase
SPR – surface plasmon resonance
SSN – stimuli sensitive nanoparticle
STED – stimulated emission depletion
SUV – small unilamellar vesicles
TAG – triacylglycerol
TAT – trans-activating transcriptional activator
$TbCl_3$ – terbium trichloride
TBAI – tetrabutylammonium iodide (TBAI)
TBTA – tris(benzyltriazolylmethyl)amine
tBuOH – tertbutyl alcohol
TCEP – tris (2-carboxyethyl) phosphine
TES – N-[tris(hydroxymethyl)methyl]-2-aminoethanesulfonic acid
THF – tetrahydrofuran
THPTA - tris(3-hydroxypropyl-triazolylmethyl) amine
TsCl – tosyl chloride
TSRI – The Scripps Research Institute
VCAM-1 – vascular cell adhesion molecule 1

VECs – vascular endothelial cells
VRL – vascular research lab
VSMCs – vascular smooth muscle cells
Zn – Zinc

PREAMBLE

Utility often precedes elucidation. Antibiotics, gunpowder, willow bark and countless more natural phenomena were harnessed by humanity before we unraveled the mechanisms of their actions. Upon discovering biochemical relationships, we may seek to explicate or exploit. Explication is crucial and often leads to further discovery. Exploitation of biological phenomena can happen at any point and should not wait for explanations to be defined. Prescient minds see opportunity in the inexplicable; Cézanne, Whitman and Escoffier emboldened their work by intuiting yet-to-be-discovered laws of vision, cognition and sense.[1] These three seminal examples are mirrored by modern-day scientists that exploit molecular proclivities to enable new technologies before said proclivities are defined fully.

Regarding lipid second messengers, much is known but little is fully understood. They are critical, ubiquitous cellular operators with unassailable abilities to modulate supramolecular membrane activities. Lipid mechanics and signal transduction can be difficult to characterize in their natural setting and are under-utilized in applied sciences such as medicine. Here, liposomes were employed as a biomimetic medium to study protein-membrane binding interactions and identify novel DAG binding proteins. Prior to achieving our goal, we applied experimental observations to harness DAG's import and increase the efficacy of a new liposomal nanodrug. Eventually, we created a selective and repeatable liposomal platform for labeling proteins in the presence of DAG. We are now working to discover new potential drug targets for a litany of diseases including cancer. Although our understanding of DAG is far from complete, it may be harnessed for immediate increases in the efficacy of liposomal delivery systems (LDSs).

Increasing LDS efficacies and studying protein-recruitment by lipid secondary messengers are the two focal points of this dissertation. We will begin with the latter, introducing relevant background in Chapter 1 and describing our novel liposomal chemical biology platforms in Chapter 2. The discussion shifts towards liposomal localization in Chapter 3 with a simple, natural solution to the targeting of liposomal delivery systems using DAG and PS. Chapter 4 presents more complex strategies to achieve the controlled release of liposomal cargo. The work described in the later chapters was aided by the literature review and experimental observations that precede them.

CHAPTER 1: INTRODUCTION

1.1 Glycerolipids

Lipids are comprised of a diverse group of biological molecules with an array of cellular functions. There are thousands of different lipids[2-3] including mono-/di-/triglycerides, sterols, hydrophobic vitamins and other fat-soluble biological molecules. Lipid functions may be as fundamental as energy storage or as complex as governing cell signal transduction and function. Glycerophospholipids, or 'phospholipids,' are the most abundant phosphatides in organisms and the most recognizable group of lipids. Herein, the focus will be on the amphiphilic glycerolipid diacylglycerol (DAG) which is the non-phosphorylated version of any of the six groups of phospholipids: phosphatidylglycerol (PG), phosphatidylserine (PS), phosphatidic acid (PA), phosphatidylethanolamine (PE), phosphatidylcholine (PC) and sphingomyelin (SM).[4]

Form and function of glycero(phospho)lipids

Lipids, namely glycerolipids and phospholipids but also cholesterol and other amphiphilic signaling molecules such as glycolipids and hormones, gain much of their utility from their shape. Within each of the groups of glycerophospholipids in Figure 1.1, different species are determined by the length and saturation of hydrocarbon tails which impacts the geometry of that lipid. Unless otherwise noted, "lipids" will henceforth be referring to one of these groups in Figure 1.1. In the case of phospholipids, their geometry is categorized by the cone angle dictated by the relative sizes

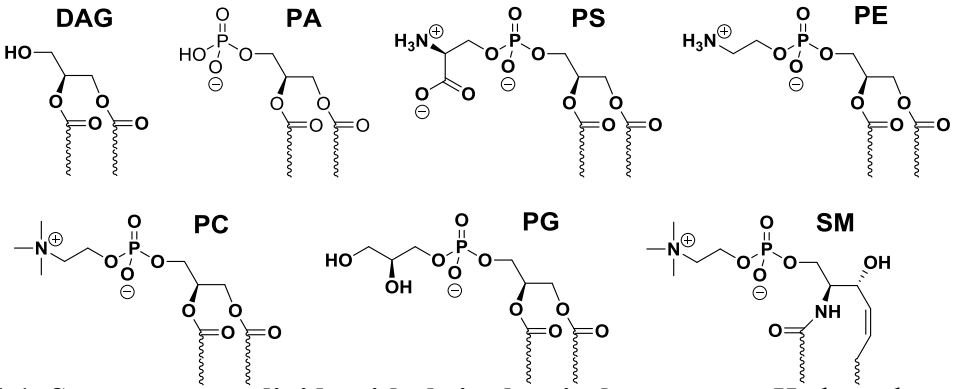

Figure 1.1: **Seven common lipids with their chemical structures.** Hydrocarbon tails vary in nature in terms of length and saturation and are represented here by truncated squiggly lines.

of headgroups to lipid tails. Cone angle dictates the type of self-assembly the lipid undergoes.[5]

Figure 1.2 on the following page presents some common lipids in this geometric context alongside different supramolecular assemblies that are formed depending on the structure of the lipid. In this way, form determines function as illustrated by preferred shapes of self-assembly. PC, for example, assembles into stable bilayers and is the most abundant mammalian lipid; eukaryotic cell membranes contain greater than 50% PC.[6]

Self-assembly results from the shared hydrophobicity of the tails gathering in a manner that leaves only the hydrophilic headgroup exposed to the aqueous media. Hydrogen bonding between polar headgroups and aqueous media outside and within the vesicles adds stability. Shared hydrophobicity brings the lipid tails together and van der Walls forces add rigidity to the lipid architecture.

Phospholipids and DAG have a glycerol backbone with acyl tails on the *sn-1* and *sn-2* carbons (see Figure 1.2)[7] that may vary in saturation and length depending on the fatty acids that are incorporated during lipid biosynthesis. If one of these acyl tails is missing, the lipid is in its 'lyso' form. The headgroup is found on the *sn-3* carbon. Three-dimensional illustration of liposomes, micelles and cellular bilayers are shown in Figure 1.3[8].

Based on supramolecular assembly properties, lipids are commonly classified as either bilayer or nonbilayer lipids. Bilayer lipids such as PC possess the appropriate geometry for residing within the curvature of bilayer membranes such as those found in cellular membranes and liposomes. Nonbilayer lipids comprise two groups: type 1 nonbilayer lipids include lyso lipids that induce positive (outward) stress on the membrane curvature, while type 2 nonbilayer lipids include DAG and PE, which have larger cone angles due to smaller headgroups, induce negative (inward) stress to phospholipid bilayers.

PE has a shape more like PC and can occupy up to 70% of membranes while DAG is missing the phosphate modality entirely and the relatively tiny hydroxyl head group gives it very strong nonbilayer properties. Thus, DAG occupies only 1-2% of healthy membranes but can be found at concentrations as high as 10% in diseased cells such as cancer.[9] This is likely related to the rapid division of cancerous cells as well as the aberrant expression of DAG-binding proteins involved in oncogenesis.

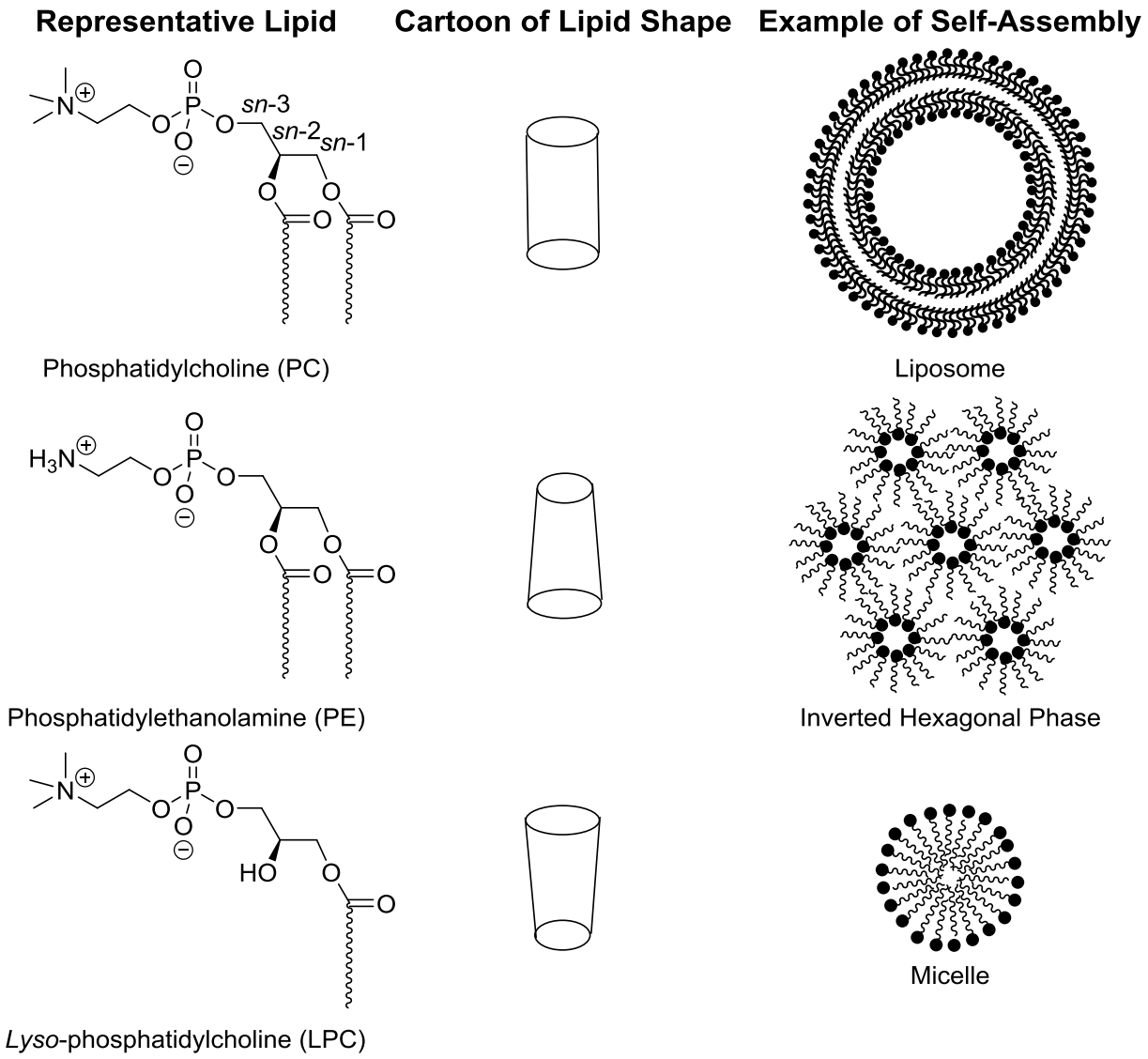

Figure 1.2: Phospholipid cone angles and self-assembled structures. PC is shown with glycerol carbons labeled for reference. PE is an example of a type 2 nonbilayer lipid, like DAG, due to a smaller headgroup. LPC is a type 1 nonbilayer lipid.[7]

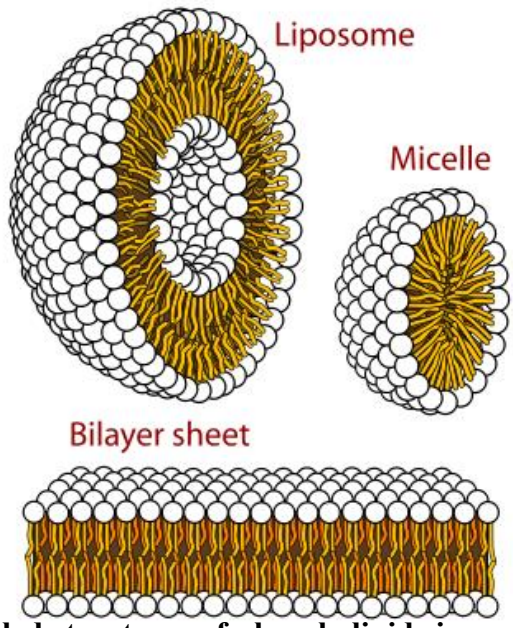

Figure 1.3: Self-assembled structures of phospholipids in aqueous media. Image is public domain, credit: Mariana Ruiz[8]

DAG, a focal point of this dissertation, will continue to serve as our exemplar lipid. Much of DAG's renown is for being the precursor for other phospholipids.[10] Lipid synthesis, or topogenesis, has been studied extensively and DAG is key for phospholipid production via the Kennedy pathway.[11] In regard to signal transduction, there is rapidly accumulating evidence for lipid governance of pathological cellular states.[6, 12-15] Still, DAG and many other lipids warrant more investigation than they currently receive. Studying lipid second messengers such as DAG may eventually help answer important questions regarding tissue-specific lipid dysregulation, something that is studied indirectly by the work presented in Chapter 3 that explores the potential of signaling lipids to modulate liposomal delivery systems (LDSs).

In addition to variable lipidomes, cells are also distinguished by the proteins they express to achieve their unique functions. It would be an oversimplification to assert that varying abundances of associated signaling lipids are always the product of protein expression. However, it is also presumptuous to assume that lipids are the driving force behind protein presentation. For example, certain proteins exist to biologically engineer DAG (synthases), others exist to metabolize it (kinases), while others yet are activated by it to regulate cellular function. Many of these proteins

operate in coordination, with abundances that may be directly or indirectly correlated to one another and their lipid activators. Lipid signaling operations are therefore too diverse and dynamic to qualify broadly and must be identified individually. As this chapter progresses, it will become clear that more research is needed to understand DAG's role in the onset and progression of cancer,[16] Alzheimer's and dementia (AD),[17] hypertension[18] and other diseases.

As stated, the dysregulation of DAG is a combinatorial consequence of it being an intermediary in the synthesis of other upregulated lipids, a signaling lipid in oncosuppressive or oncogenic cascades, and its strong nonbilayer properties due to a cone angle that may help promote fission in rapidly dividing cells and extravesicular cellular communications.[19-22] It is impossible to separate the metabolic and cell-signaling significance of lipids from their geometries as the two are closely intertwined, thus illustrating the complexities inherent to experimentation geared at studying species such as DAG.

DAG can be incorporated into stable liposomes at least as high as 25% when the other 75% is composed of a 4:1 ratios of PC:PS.[23] At high percentages such as this, however, DAG can induce liquid-disordered (Ld) nonbilayer membrane perturbations in the presence of calcium (Ca^{2+}) cations. Interestingly, increasing DAG and Ca^{2+} concentrations also potentiates the activity of certain PKC enzymes (in the presence of PS), but only up to 2.5 mM Ca^{2+}, after which the cation has a deleterious effect on enzyme activity. In the case of PKC, Ca^{2+} sensitivity hinges upon a specific C_2 binding domain and this is discussed in the upcoming section on the PKC C_1 binding domain.

The fatty acid composition of the acyl tails at the *sn-2* or *sn-3* positions of lipid species has an impact on membrane partitioning and cone angle, can vary in any of the glycerolipids, and is of importance when determining a lipid's bilayer properties. Commonly observed tails include oleic acid and palmitoleic acid, which are 18 and 16 carbons long respectively and are unsaturated meaning they each have at least one double bond. This is denoted using C:D nomenclature where C is number of carbons and D is the number of double bounds. To reference the position of the double bond one would use 'n-x' notation where x is the number of carbons from the chain's terminal methyl group at which the first double bond is found. The 'n' is often exchanged for 'omega' in nutritional literature when discussing fatty acids.

When there is more than one double bond, the location of each double bond is given as Δ^x where

x is the first carbon of each alkene using traditional numbering, which counts from the carbonyl carbon. Arachidonic acid in Figure 1.4 would be notated as follows, (20:4 (n-6) *cis, cis, cis, cis*, Δ^5, Δ^8, Δ^{11}, Δ^{13}). All the fatty acids mentioned thus far are *cis*, which is the predominant natural orientation for fatty acid double bonds. The *trans* versions have different trivial names, for example oleic acid becomes elaidic acid when the configuration of the double bond is instead *trans*.

Not surprisingly, fatty acids are incorporated into lipid structures at varying concentrations in correlation with cellular dysfunction. An analysis of total phospholipid content of the arterial tissues of heart attack victims showed significant increases in palmitic acid (16:0) and linoleic acid (18:2 (n-6)) with significant decreases of arachidonic acid (20:4 (n-6)) and all other major polyunsaturated fatty acids of n-3 and n-6.[24] DAG is no exception and among the 50+ types of diglycerides[25] found in biology there is evidence that the fatty acids composing their acyl tails are crucial to determining signaling activity,[26] including PKC activation.[27]

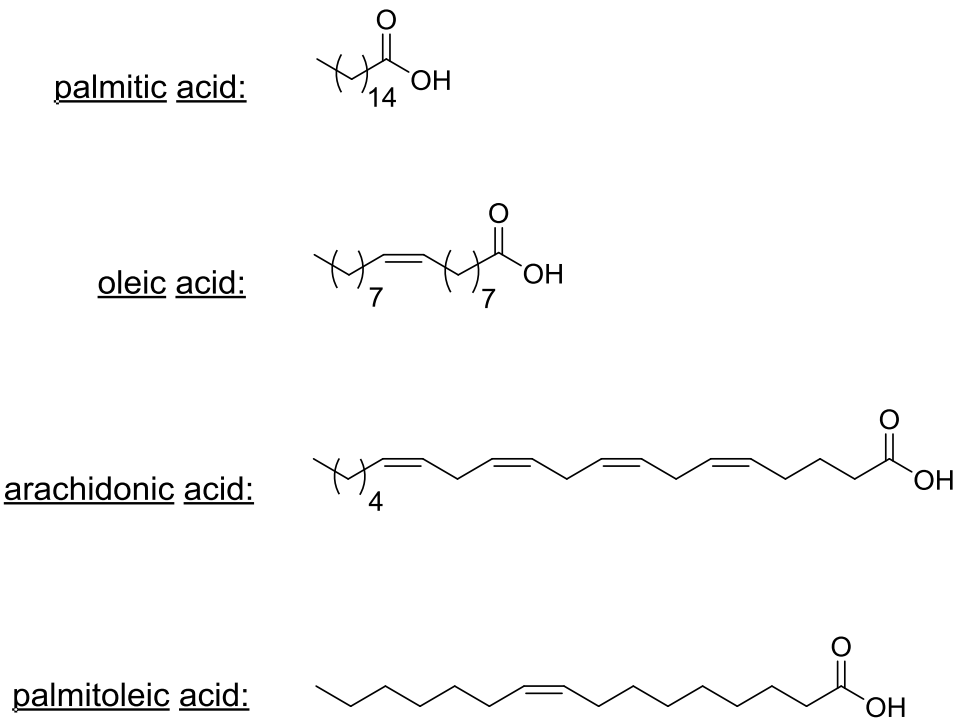

Figure 1.4: Four common fatty acids with their trivial names: palmitic acid, oleic acid, arachidonic acid and palmitoleic acid.

The causes and/or consequences of aberrant lipid expression of course vary with the type of cell, more precisely with the state of the cell, and even more precisely with each specific protein effector. Proteins justifiably remain the focal points of studies regarding cellular pathologies as well as biomedical endeavors to selectively target diseased tissues. Our entry point into exploring cellular function is lipid-centric, but discovering novel DAG-binding proteins is still the goal of the experimentation introduced in Chapter 2. As background for said experimentation, we will introduce membrane proteins and then overview of glycerophospholipid-PMP cell signaling relationships with a focus on DAG and the closely related lipids PA, PS and SM.

Membrane proteins

Each living membrane contains a proteome unique cellular function, tissue type, and state. The most abundant class of proteins are the membrane proteins, which have diverse sizes, shapes and functions.[28] Integral, or 'intrinsic', membrane proteins are deeply embedded into or through the membrane bilayer. Integral proteins that do not span from the outer to inner leaflet of the bilayer are less common and usually have lipophilic side chains to anchor them in the phospholipid bilayer, while their hydrophilic peptides remain exposed. Some integral proteins have fatty acid appendages to serve as their anchors. Most integral proteins span from the outer to inner leaflet of the bilayer and are referred to as transmembrane proteins. The integrated portions of transmembrane proteins are composed of α-helices or ß-strands. Peripheral membrane proteins (PMP)—or extrinsic proteins—do not interact directly with the hydrophobic region of the bilayer, and exhibit disparate means of membrane association.

Peripheral membrane proteins

PMPs operate transiently and reversibly. Their movement and docking can rely on any combination of electrostatics,[29] specific interactions with hydrophilic lipid headgroups,[12] indirect/nonspecific lipophilic interactions,[30] and protein-protein interactions (PPIs).[31] PPIs are typically between extrinsic and intrinsic proteins. PMP binding to a specific array of signaling lipids is represented in the schematic cartoon in Figure 1.5. When PMPs bind the bilayers in this manner it is accompanied by a change in their conformation and modulates protein function. Such reversible protein activations can be described as amphitropic regulation.[32]

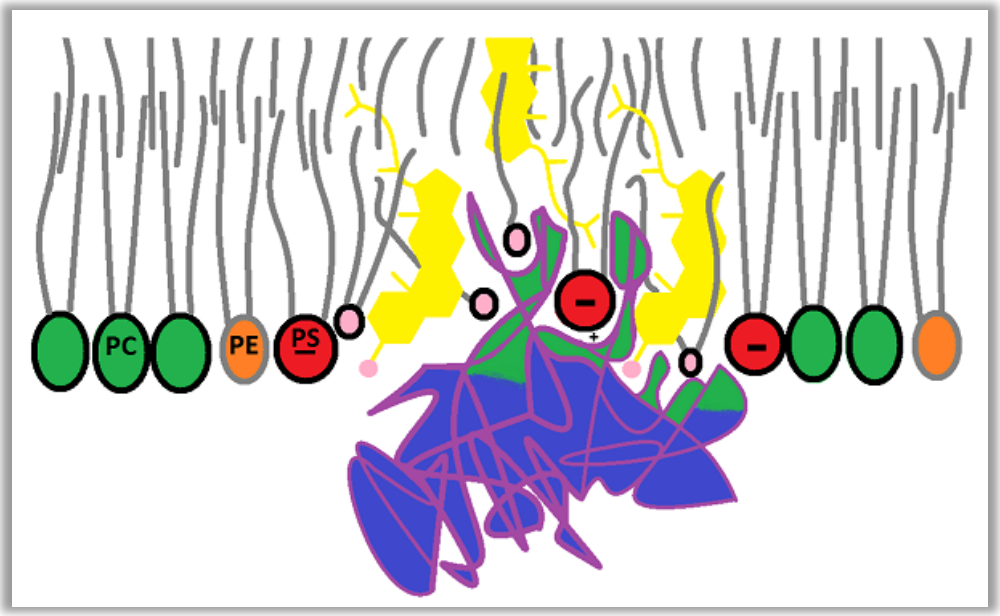

Figure 1.5: A cartoon schematic of a liquid ordered (Lo) nanodomain accommodating a PMP at the hydrophilic face of a bilayer membrane. Signaling lipids encourage membrane perturbation and recruit peripheral proteins. The pink lipids represent DAG or lyso-DAG and the yellow structures are cholesterol molecules. The blue/green shape represents a water-soluble protein with affinity for DAG and PS, such as a phorbol ester binding protein like PKC.

Amphitropic enzymes include protein kinase C (PKC) and other proteins reviewed later for their relevance to DAG. Some PMPs, such as extracellular matrix proteins, are located on the exoplasmic outer leaflet. DAG works with extracellular PMPs to shuttle signaling molecules and vesicles to enable in neuronal and immune cascades.[20, 33-34] DAG is also involved in endosomal activity within the cytosol, and it is crucial to transport at the Golgi apparatus.[22] Other PMPs, such as PKC and other signal transduction enzymes, operate internally and are thus localized at the cytosolic leaflet. PMPs have function beyond cell signaling; cytoskeletal PMPs, for example, are important structural components of erythrocyte cells.

PMP association is lipid specific.[12] The complexity of interactions and functions among PMPs make them dynamic macromolecules that are challenging to study in a natural context. The translocation of PMPs varies from Brownian to actively controlled motion.[35] Cellular and biophysical investigation of PMPs such as PKC and phospholipases have helped develop our understanding of protein-membrane interactions although there is still much more to be learned.

Phospholipases are an important subset of amphitropic PMPs. These enzymes are ubiquitous biological molecules that act by cleaving the phosphate or ester bonds of phospholipid headgroups.[36] Phospholipase activity has been experimentally tied to plant defense,[37] bacterial virulence,[38] cancer[15, 39] and much more. Several phospholipases related to DAG—and other PMPs—are presented later in this chapter.

The packing of bilayer lipids, in natural membranes or artificial vesicles, is perturbed by the presence of nonbilayer lipids. Geometric changes in lipid arrangement are mechanical yet have evolved complex biological purposes including membrane recruitment of PMPs and vesicular communication. PMPs are stimulated extrinsically to translocate about the membrane for further activation by lipid second messengers. Areas of protein translocation are liquid ordered (Lo) domains enriched with specific membrane constituents such as cholesterol and signaling lipids.[40] These domains are colloquially termed 'rafts' and are discussed in the *Nanodomains* section later in this chapter. Signal transduction depends on these unique membrane perturbations; protein-specific arrays of bulk lipids and lipid second messengers create ideal conditions for glycerophospholipid headgroup interactions with activated proteins. A lipid-specific nanodomain is represented by the cartoon schematic in Figure 1.5. This simplified depiction of 'rafting' is expanded in Figure 1.8 to include an integral membrane protein and a more transient PMP. Figure 1.6 includes several of the other membrane components omitted from Figures 1.5 and 1.9, such as glycolipids and glycoproteins.

1.2: Cellular functions of DAG and related lipids

Nearly a century ago, it was posited that there is a fatty lipoid coating two molecules thick surrounding our cells.[41] Half a century later, the phospholipid bilayer hypothesis was confirmed[42] and the fluid mosaic model for cellular membranes was proposed.[43] Once it was confirmed that phospholipid self-assembly into cellular membranes forms the building blocks of life, lipids came under more scrutiny as cellular operators. The variety of lipids per cell and their differing supramolecular behaviors is evidence enough to suggest that cellular importance of lipids extends beyond providing structure. Before long, researchers were uncovering lipid propensities to interact with metal cations and proteins to achieve isothermal regulation of cellular activities.[5] This led to

the discovery of enzymatic and electrostatic protein interactions of nonbilayer lipids, in addition to their mechanical roles, underscoring the importance of lipid secondary messengers and their fatty acid intermediaries.[6, 12, 44-48]

It is widely agreed upon now that in addition to forming cells, signaling lipids also act as metabolites and secondary messengers through protein translocation and activation. Presently, our understanding of the plasma membrane is more nuanced than it was decades ago, but still very much incomplete. What can be said for certain is that proteins and lipids work in synchronization to protect our cells and organelles, dictate cellular function, and regulate ionic gradients between the cytosol and extracellular matrix. Roughly one quarter of our proteome is comprised of membrane proteins and their tight interactions with lipids within cell bilayers is crucial for maintaining structure and the electrochemical potential that allows for adenosine triphosphate (ATP) synthesis.[49] The cell membrane is a natural phenomenon fundamental to life itself and PC—with its ideal cone angle—deserves credit for driving the self-assembly of our cells.

It is the nonbilayer glycerolipids found within the plasma membrane that are the focus of this dissertation due to innumerable biological functions they control. Such glycerolipid second messengers are generated passively upon stimulation of receptor tyrosine kinases (RTK) or seven-transmembrane receptors. The latter are now more commonly known as G protein-coupled receptors (GPCRs) and comprise the most commonly targeted group of proteins for therapeutic applications.[50]

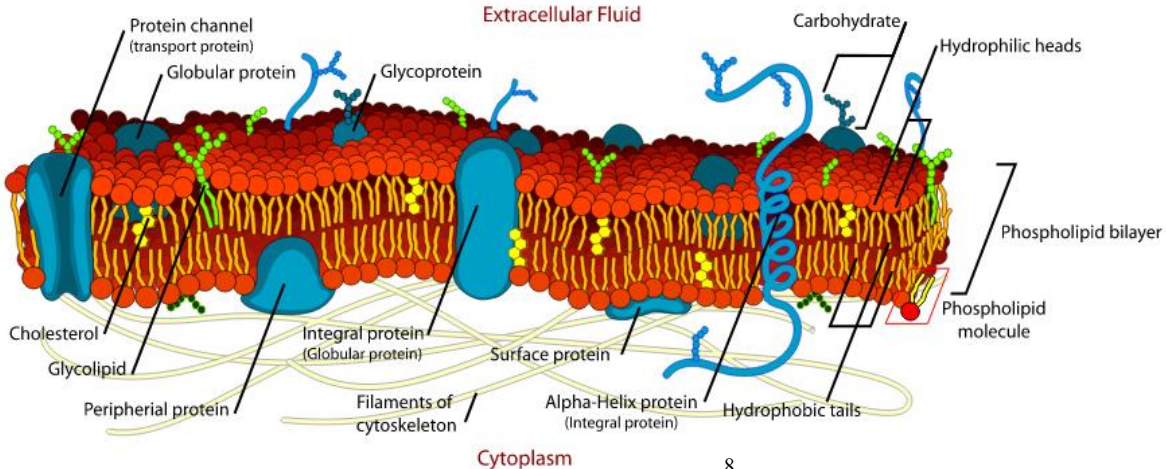

Figure 1.6: **An illustration of the plasma membrane.**[8]

The case for low abundance glycerolipids as mediators in several cellular pathologies is clearly very strong. It is no surprise that signaling lipids such as DAG are already under investigation for the roles in cancer and other diseases.

DAG and PKC

Much of what is known of DAG's cellular importance regards activation of protein kinases known as phorbol ester receptors that share a conserved binding domain colloquially known as the C_1 domain. Protein kinase C (PKC) enzymes are a type of phorbol ester binding protein and were the first to be discovered and investigated for DAG-mediated subcellular signaling activity. Phorbol esters are naturally occurring plant-derived compounds that have a protein recognition profile similar to DAG.[51] PKCs have garnered the most notoriety among DAG's protein targets thanks to a host of crucial physiological roles. We will discuss these roles in depth after briefly reviewing PKC structure.

The C_1 domain

PKCs contain two C_1 binding domains (A and B) that operate in tandem and often have DAG affinities that vary among different PKC isozymes.[52] As determined by nuclear magnetic resonance (NMR), the C_1 domains consist of two β sheets and an abbreviated C-terminal α-helix, and chelate with two Zinc (Zn^{2+}) ions through a pair of similar motifs each composed of three cysteines and a histidine.[53] The C_1 domains of non-PKC phorbol ester proteins are analogous to the C_1 domain of the PKC isozymes, however certain phorbol ester binding proteins have a disparate dormant structure that demands more drastic conformational change for activation. This suggests that significantly higher amounts of DAG are required for activation of these proteins (such as mammalian uncoordinated protein-13 or 'Munc13,' discussed later) than with PKC.[52]

There are no fewer than six other species of phorbol ester receptors for DAG capable of instigating cell signaling cascades on DAG's behalf.[54] Phorbol esters are typically poisonous plant-derived carcinogens that maintain affinity for the C_1 binding domain and lock PKC in active forms.[55] Although, some naturally derived phorbol esters have demonstrated promising therapeutic capacities.[56] The C_1 domain of DAG-binding proteins is buried until proteins are promoted to their active form by signaling molecules such as growth factors or hormones. PS is crucial at this point,

as it frees the C_1-A domain to bind DAG by first untethering it from a C_2 domain conserved among many PKC isozymes.[57] The C_2 domain binds anionic phospholipids in a calcium-dependent manner, making calcium a key cofactor for the membrane-binding of certain PKC isozymes.

***PKC** - structure*

C_1 and C_2 domains are located at the amino (N) termini of PKC enzymes where the structures of the regulatory domains determine the family of PKC.[58] Conventional PKC (cPKC) isozymes have both C_1 and C_2 domains including C_1 A and B. Novel PKC (nPKC) isozymes differ at the C_2 domain where an acidic residue is missing, thus removing the calcium requirement for anionic phospholipid binding. nPKC and cPKC isozymes also vary their respective order of presentation of residue domains, as shown in Figure 1.7 based on information found in Susan Steinberg's review of PKC structure.[58] Atypical PKCs (aPKCs) lack the C_2 domain entirely and have a disparate C_1 domain with a less-complex, cysteine-rich binding pocket. aPKC C_1 domains do not bind DAG, instead they are attracted to PIP_3 or ceramide and participate in protein-protein binding interactions. DAG activates at least eight different cPKC and nPKC isozymes. cPKC is divided into cPKCα, β1, β2 and γ. nPKC subdivides into nPKCϵ, η, and θ.[54]

In addition to the C_1 domain, many other lipid-specific protein domains have been discovered across the peripheral membrane proteome.[12] Although the structural impetuses for PMP binding pocket recognition of membrane operators such as DAG and the PIP_ns are well-understood,[59] precise mechanisms are not known for protein translocation to membrane areas rich in signaling lipids. Here, it is important to note that lipid positioning in the membrane is not static and the

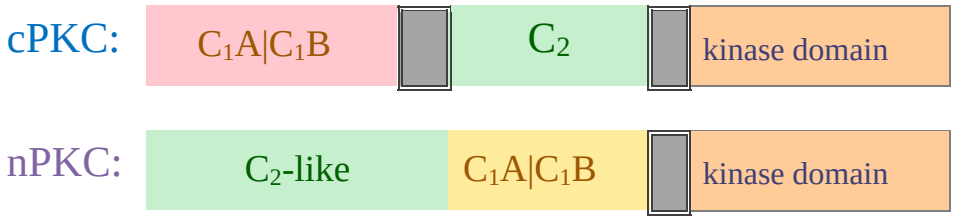

Figure 1.7: **Conventional and novel PKC regulatory domains.** Gray boxes represent hinge regions between regulatory domains and from regulatory domains to the conserved kinase domain. Kinase domain variation determines specific species within each family.[58]

collocation of signaling lipids into concentrated membrane nanodomains has been uncovered as a crucial method of lipid-instigated protein translocation. This phenomenon has been dubbed 'rafting' and will be discussed in its own section after we complete our review of DAG and related lipid second messengers.

***PKC**-activity (non-cancer-related)*

PKCs and their ilk are most often investigated with respect to oncological transformations[14, 16] but it is crucial for normal cell physiology and other diseases. For instance, PKC is also under-expressed in erythrocyte membranes of hypertensive patients[18] suggesting that PKC and DAG are important for maintaining healthy cardiac function. Just as PKC has many roles beyond regulating carcinogenesis, so too does DAG.

In addition to fighting oncogenesis and cardiac hypertrophy, DAG's activation of PKC impacts mammalian physiology in numerous other ways. PKC is crucial for cell growth, learning, memory[60] and immune response.[61] PKC isozymes also instigate profoundly important cellular events such as transcription[62] or receptor desensitization,[63] as well as participating in protein-protein crosstalk to influence a litany of other cellular functions.[54, 64] PKCs also control contraction of smooth muscle cells to allow healthy tissue function at various points in mammalian digestive tracks.[65-66]

DAG function

If we cultivate a better understanding of DAG and other signaling lipids we may advance medicinal chemistry on many fronts. Proteins are widely studied as means to therapeutic ends, yet lipids do not receive nearly as much attention despite a similar level of diversities.[67] These macromolecules work together to govern cellular behavior and it is the general aim of this dissertation to investigate such behavior from a lipidic perspective. Lipid activity is tightly controlled in biological systems and this specificity could open new avenues for research applications and targeted therapeutics.

DAG's oncological significance will be discussed at length in its own subsequent section. First, some of DAG's other functions are introduced before briefly describing the activities of closely related lipids. Lipid second messengers like DAG regulate virtually everything that goes on in the cell. DAG facilitates membrane trafficking at the Golgi complex[22] and is a pivotal part of cell

signaling cascades and lipid metabolisms related to cell proliferation,[19] hypertension,[18] immune response[34] and neuronal signaling.[21] There are many proteins that are activated by DAG or produce DAG via a related lipid effector. For ease-of-reference, these proteins will continue to be highlighted in blue to the right of the page as they appear in the text. The ultimate goal of the work described in Chapter 2 is to identify new proteins or classes of proteins that participate in DAG signaling activities.

***DGK** – non-cancer-related activity*

The most common metabolic fate of DAG is phosphorylation into PA by diacylglycerol kinases (DGKs). DAG can also be metabolized through an acyl tail removal by DAG lipase or addition of choline/ethanolamine headgroups into PC/PE, however DGK's generation of PA is the most common metabolic pathway for DAG in signaling cascades.[21] DGK isoforms have myriad functions. For example, DGK-α activates the movement and multiplication of endothelial cells stimulated by vascular endothelial growth factor, leading to angiogenesis.[68] Each of the ten DGK isozymes discovered so far have distinct localization throughout the body but have the conserved trait of protein-protein crosstalk to activate other DAG and PA binding proteins, such as PKC. Not surprisingly, DGKs contain C_1 and C_2 domains homologous to those found in PKC.

Like PKCs, DGKs are most widely investigated regarding cancer and will be touched upon again in the *DAG & Cancer* section. The physiological roles outside of cancer of the PKCs have received significantly more attention than those of the DGKs and are well-characterized in comparison. However, the physiological roles of DGK are still being uncovered. In addition to oncogenesis, DGKs have been tied to neural cascades and immune response.

DAG and Immune response

Lymphocytes, or 'T cells' communicate synaptically to effect immune response and DAG seems to be crucial for signal transduction via synaptic vesicles. Thus, the immunological synapse (IS) is another arena where DAG localization and the coordinated responses of DAG binding proteins are key for cellular communication.[34] Precise mechanisms of DAG-mediated IS signaling are still being unraveled. Evidence suggests that both the construction and metabolism of DAG are tightly controlled to achieve immunological signal transduction.[69] Recent evidence suggests that DAG maintains polarity of the microtubule organizing centers (MTOCs) of lymphocytes such

that they may exact antigen-determined responses appropriately.[34]

DAG and Alzheimer's Disease

Elevated signaling lipid content, including DAG, has been discovered in select regions of brains afflicted with Alzheimer's disease (AD). Studies have shown no discernable lipidomic alteration in the cerebellum of AD brains while other regions had site-specific elevations of certain signaling lipids.[70] DAG levels were found to be significantly higher in the prefrontal cortexes of AD brains than in the same regions of healthy brains.

Additionally, elevated DAG content was recently detected in the frontal cortex and plasma of MCI (mild cognitive impairment) subjects. A substantial number of AD patients experience MCI as a prodromal phase prior to disease onset.[17] Although DAG is not elevated in the cerebellum of AD brains, it is still a crucial lipid effector in this region through its modulation of Munc13-3, which is virtually absent in the body apart from the cerebellum.[33]

munc13

DAG activation of mammalian uncoordinated protein-13 (munc13) occurs in parallel to PKC activities. Munc13 has been investigated for its DAG-responsive regulation of synaptic transmissions, learning and motor function, and insulin release.[71] The munc-13 kinases are a family of C_1-containing phorbol ester receptors involved in neurotransmitter release from synaptic vesicles. There are three members in this family, munc13-1/2/3. Munc13-3 is cerebellum-specific and seems to play a role in learning and memory in mice.[33] Munc13-1 on the other hand, is an ever-present pre-synaptic protein in the neurons of rodent central nervous systems. Munc13-1 is also required for sustained release of insulin in mice.[71] It has also been demonstrated in mice that genetic alterations in munc13-2 expression have an array of implications for brain pathologies.[72] All three of members of the munc13 family are promising targets for developing new neurotherapeutics. Munc13s also contain the C_2 phorbol ester binding domain conserved among some but not all phorbol ester binding proteins.

DAG, along with its related species and transferases, has also been implicated in the progression of nonalcoholic fatty liver diseases (NFLD), including cirrhosis.[73] DAG has even been shown to increase the pigmentation of guinea pig skin in vivo and the melanin content of human melanocytes in vitro.[74] DAG is not only ubiquitous but also omnipotent in its regulation of

biological processes. It could be argued that virtually every phospholipid is related to DAG. To manage the scope of this introduction, the discussion that follows will be limited to DAG's siblings PA and SM and its PKC binding cofactor PS.

PA

PAP

DAG's activation of protein kinase C (PKC) involves the exchange of a phosphate group to form PA, a crucial signaling lipid that also warrants further investigation.[9] PA is similarly formed when DAG activates DGKα. DAG molecules are reformed from PA by phosphatidic acid phosphatase (PAP) and are then used in *de novo* lipid syntheses of triacylglycerol (TAG) as well as PE and PC through the Kennedy pathway via cytidine diphosphate(CDP)-DAG.[75] PAP enzymes also provide DAG for PKC activation and seem to be key regulators of mammalian lipidomics and thus cell physiology in general.

PLD and SPHK

PA is also generated by phospholipase D (PLD), a common enzyme whose main substrate is PC. PLD pumps out PA for cell signaling purposes in a variety of species including viruses, fungi, plants, and animals. PLD isozymes have been widely explored as targets for cancer therapeutics.[15] In plants, PLD is critical in cellular responses to environmental stress.[37] PA is well-studied in plants where it occupies less than 1% of total phospholipid content but seems to be a key first responder for flora by regulating sphingosine kinases (SPHKs), PLD and other enzymes in response to biotic or abiotic stress.[76] SPHKs are also present in human biology and are a subset of DGKs.[77] SPHKs (1 & 2) have complementary and/or opposing roles in simpler organisms including modulation of cell proliferation and the mediations of cellular responses to a variety of stimuli.[78] SPHKs are considered cytosolic proteins but as their location is dictated by membrane constituents such as PA they may be thought of as PMPs. SPHKs were at first thought to be redundant in mammalian tissues but subtle differences have been uncovered that suggest that SPHK1 and 2 may make promising drug targets for the selective inhibition or promotion of cellular processes.

RAF-1

PA activates the rapidly accelerated fibrosarcoma kinase-1 (RAF-1) in mammalian cells through binding at a specific amino acid sequence in the enzyme's kinase domain.[79] RAF-1 also

contains a unique binding domain for PS.[80] RAF-1 participates in the mitogen-activated protein kinase (MAPK) cascade. *BRAF* and *KRAS* are genes that encode for RAF proteins and are mutated in 40% and 10% of colorectal cancers (CRCs), respectively,[81] and combined they are mutated in 30% of all tumors and 40% of melanomas.[82] RAF inhibitors are promising anticancer agents and they act through specific inhibition of the MAPK cascade to stymie tumor growth. RAF-1 is homologous to the plant constitutive triple response 1 (CTR1) kinase which is a copper-regulator modulated by PA in response to biotic or abiotic stress.[83]

SHP-1

Protein effectors such as DAG and PA often set off signaling cascades leading to oncogenesis, mitosis, cell differentiation and proliferation. Another example of this is PA's targeted activation of Src homology region 2 domain-containing phosphatase-1 (SHP-1) of the protein tyrosine phosphatase (PTP) family. In cancerous tissues, SHP-1 is overexpressed in epithelial cells and underexpressed in hemopoietic cells.[84] PA also regulates PIP_n receptor enzymes and PTPs including SHP-1, which are crucial for many cellular functions including oncogenesis.

GAPs/mTOR/PP2A/PP1

PA is also an effector for guanosine triphosphate (GTP)ase-activity accelerating proteins (GAPs) which are crucial in regulating cellular pathways including carcinogenesis.[85] PA activates the mammalian target of rapamycin[86] (mTOR) which controls cell cycle progression/growth and switches cellular metabolisms from catabolic to anabolic.[87] PA is also known to regulate phosphatase-2A (PP2A) and phosphatase-1 (PP1) to control apoptosis, cell growth and glucose metabolisms with correlated influences on disease prevention or onset with regards to AD, human immunodeficiency virus (HIV) and herpes simplex virus (HSV).[88-91]

ABI1/PP2C

PA has also been implicated in the nuclear translocation of proteins that lack the canonical nuclear localization signal (NLS) motif.[92] An example of this is PA's governance of abscisic acid insensitive protein 1 aka Abelson interactor 1 (ABI1). ABI1's specific activation by PA also completes a signaling cycle involving PLD and phosphatase-2C (PP2C) that is crucial for regulating many cellular functions.[93]

Lysophosphatidic acid (LPA) is a critical signaling lipid as well. LPA has demonstrated increased control over cellular activity during tumor metastasis in pancreatic cancer.[13] LPA may

also help rapidly dividing cells evade apoptosis and have a protective role in neurogenesis.[94]

PS

DAG is also thought to work in conjunction with PS, a vital lipid that is typically found on the inner leaflet of cellular bilayers but flips to the outer leaflet in pathological cells.[47] The concomitant binding of multiple lipids of the same or different species adds significant complexity to the task of characterizing PMPs, which translocate to different areas of the membrane based on the affinities of their binding pockets and associated lipid constituents. PS, along with the PIP_n lipids, have been studied to a greater extent[95-100] than DAG or PA, and a thorough review of either lipid would be ancillary to this dissertation.

Annexin

PS's electrostatic untethering of C_1 domains that allows DAG to recruit and activate cPKCs is most relevant to the phenomena we seek to study.[57] Also relevant is PS's anionic character, which contributes to its biological functions. The most common example of this is the recruitment of annexins by PS-containing membranes. Annexins are a family of proteins with strong membrane affinities and a variety of roles from membrane transport to apoptosis.[101] Not surprisingly, calcium bridges facilitate PS-annexin associations just as they do when C_2 domains bind to PS. The known interaction of PS and annexin protein A5 was utilized in proof-of-concept experiments in the development of the liposomal protein screening assays described in Chapter 2. Annexins have many protein-protein and protein-phospholipid interactions and, interestingly, these include several annexin-PKC interactions, including annexin A5's negative regulation of PKC.[102] Annexins also regulate the EGRF/Ras signaling pathway.

SM

SMS/Akt

DAG is also formed by the enzymatic exchange of a choline headgroup from PC to ceramide by sphingomyelin synthase (SMS) to form SM and DAG. SM and DAG levels are correlated in cancerous tissues with low concentrations of SM implicating a poor prognosis.[103] SM is associated with inhibition of cancer pathways such as rat sarcoma (RAS) protooncogene protein P21-mitogen activated protein kinases (MAPK, also known as extracellular signal-regulated kinase (ERK)) pathway. In addition to inhibiting the RAS-MAPK/ERK oncogenic pathway, SM stymies PIP_3

activation of protein kinase B (PKB or 'Akt') as well. Akt controls crucial cellular functions including cell proliferation and migration. The promising new glioma drug minerval (2-hydroxyoleic acid, 2OHOA) has been shown to increase both SM and DAG concentrations with a concurrent reduction in PE as part of its mechanism of antitumor activity.

An exhaustive review of SM is beyond the scope of this dissertation because it is never investigated by any of the experimentation described herein. However, SM is a key cog in DAG metabolisms and in membrane nanodomains. For these reasons, SM deserves mentioning and should be considered one of the most important costars in the cellular cinema that is DAG activity. SM also serves as a facile transition to our discussion of DAG and cancer, particularly because the RAS-MAPK/ERK pathway that DAG and SM cooperatively govern has been investigated for decades as a cellular switchboard for carcinogenesis.

DAG & cancer

DAG activity is amplified in cancerous cells[16] and it is thought this is because DAG is an effector of cancer-associated proteins such as the PKCs. Only recently, however, was it discovered that cPKCs act as tumor-suppressors,[14] thus inverting the assumption that DAG's activation of PKC was involved in promoting cancer. Figure 1.8—which contains information published in a review of DGK involvement in T-cell activity,[104] as well as other lipid-protein relationships reviewed in this chapter—illustrates how convoluted DAG is in terms of cell signaling and metabolic pathways. Clearly, more investigation of DAG's second messenger activity is necessary and will unveil new angles for cancer therapeutics. What follows is a brief discussion of DAG signaling activity in relation to cancer, at least what is known. We begin where we left off in the previous section with DAG's instigation of the RAS-MAPK pathway.

RAS-MAPK/ERK

RAS refers to a super family of small guanosine triphosphatase (GTPase) proteins, one member of which was mentioned earlier with regards to SM's signaling activity. RAS are established MAPK/ERK triggers and have been widely explored as targets of cancer therapies.[105] RAS and other GTPase proteins are instrumental in the signal transduction of secondary messenger pathways that catalyze the removal of a phosphate into guanosine diphosphate (GDP). GTP is also a major source of cellular energy for the construction of macromolecules.

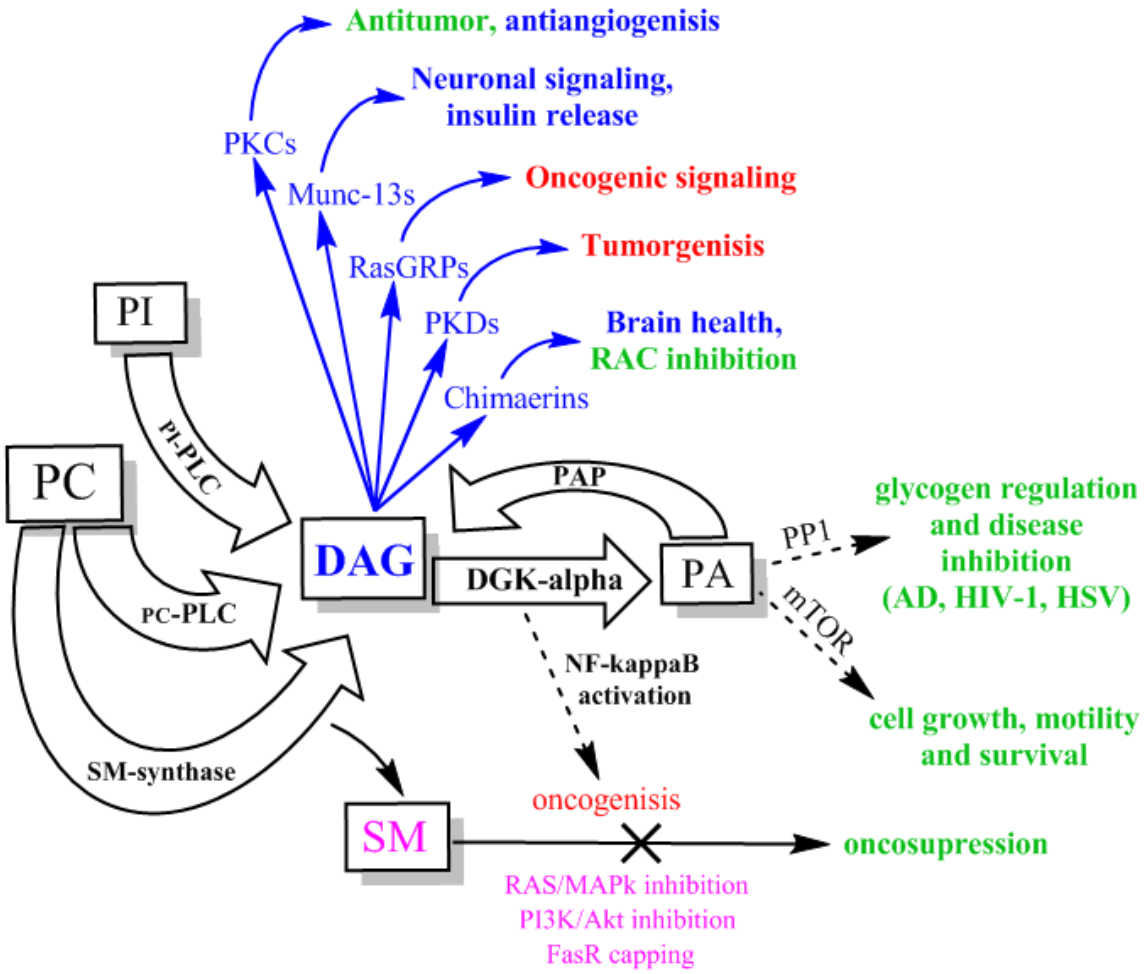

Figure 1.8: **A DAG-centric map of relevant cell signaling pathways.** The complex nature of DAG's cellular functions is illustrated. Other PA protein targets include RAF1, PIP5K, SHP1, ABI1, CTR1, SPHK1 and SPHK2.

There are many families of small GTPase proteins and they have roles in adhesion, motility, survival, cytoskeletal stability and cellular growth.[106] Flawed RAS GTPase activity leads healthy cells to become malignant cancers.

Early investigations found permanently active RAS in a variety of tumor types including 90% of pancreatic, 50% of colon and 30% of lung adenocarcinomas, 50% of thyroid tumors and 30% of acute myeloid leukemia.[107] RAS-GRP1 (glucose regulated protein 1) relies upon its activation by DAG for specific activation of MAPK/ERK kinases related to gene expression.[108] To envision how crucial this particular cell signaling cascade is, imagine the inactive RAS-GDP to be a switch in the off position. If it remains off, the cell will die. RAS-GTP however represents the on switch and when it is left on cells become invasive cancerous species.

PLC

Phospholipase C (PLC) converts PIP_3 into DAG and increases intracellular calcium cation (Ca^{2+}) concentrations. PLC is first in line to respond to RTKs and GPCRs that have been stimulated to promote lipid metabolisms, making them chief DAG producers for intracellular signaling purposes. Increased Ca^{2+} is also a hallmark of PKC activation, addressed earlier, and is a crucial factor in the signaling cascades set off by DAG and other signaling lipids. PLC is a vital operator in healthy cells and plays a significant role in cancer onset and proliferation.[39] There are 13 isozymes in the PLC family that are further divided into 6 subsets. PLCϵ is perhaps the most hotly investigated for its carcinogenic behavior and has been implicated in intestine, skin, prostate, gallbladder, bladder, lung, head and neck, colorectal, esophageal and gastric cancers.

PKD

Protein kinase D (PKD) is another highly studied DAG-binding protein and is a partner protein to PKC in cell signaling cascades crucial to a litany of functions. PKD has irons in biological fires ranging from gene expression and lymphocyte biology to cardiac hypertrophy and tumor metastasis.[64, 109] DAG is an effector of PKD isozymes 1,2 and 3 with PKD1 inhibiting invasive cellular behaviors while PKD2 and PKD3 seem to drive them. The ubiquity of PKD upregulation in malignant tumors makes it an intriguing target for new cancer therapies.

Chimaerins

Chimaerins are another family of proteins that bind DAG via a C_1 domain.[110] Chimaerins are important in brain health and development, much like the munc13 family of proteins. Chimaerins

have also been associated with breast cancer and duodenal adenocarcinomas.[111] β2-chimaerin's observed activity in cancer progression could be oncosuppressive as it contains a GAP domain at its C terminus capable of RAC inhibition. RAC proteins are a subset of the RHO family of GTPase proteins to which RAS also belongs. RAC are involved in glucose transport and best known for being highly engaged in carcinogenic cell progression.[112-113]

DGK

Diacylglycerol kinases (DGK) were introduced earlier as they are the most common route for phosphorylating DAG into PA. DGK's have been implicated in modulating cellular activity including but not limited to carcinogenesis, immune response, and neuronal signaling cascades.[21] DAG's governance of diacylglycerol kinases (DGK) such as DGK-α activates the movement and multiplication of endothelial cells stimulated by vascular endothelial growth factor, leading to angiogenesis.[68] Like PKC, DGKs are most widely investigated for their cancer-related activity.

There are at least ten different isozymes of DGK, and diacylglycerol kinase alpha (DGK-α) is perhaps the most strongly linked to cancer and is implicated in the onset and proliferation of brain gliomas, melanoma, lung cancer and other carcinomas.[114] DGK-α activity is governed by DAG and PA but therapeutic investigation has focused principally on the kinase itself, not the lipids. DGK-α is indeed a very promising drug target as it is expressed in carcinogenic melanocytes but not healthy melanocytes, and the inhibition of DGK-α induces apoptosis in tumorigenic cells by blocking its ability to instigate nuclear factor kappa B (NF-kappaB).[115] DGK-α's lipid effectors, however, deserve attention for their potential to modulate carcinogenesis.

DAG and PA are certainly not the only lipids involved in oncology. Metastasizing cancer cells require increased nonbilayer lipid content (mainly PE) for proliferation. Tumorous tissues and other diseased cells exhibit higher fatty acid concentration as a result of the requisite lipid synthase activity for proliferation.[19] The initial impetus for the investigation of nonbilayer lipids such as DAG involved their mechanical influence on fusion and fission. However, the alteration of fatty acid content in the tissue surrounding carcinomas has been shown to occur prior to metastasis in breast cancer patients, suggesting that lipid regulation may be causal as well as reactionary in terms of oncogenesis and/or oncosuppression.[116] This is further evidenced by DAG's importance as a lipid metabolite as it is an ideal intermediary in the enzymatic construction of other phospholipids, as can be observed in Figure 1.1. Several lipid synthases produce and convert DAG from/into other

lipids. In this way, the metabolic processes involving DAG blur with DAG's activity as a lipid secondary messenger.

The DAG-PA/PKC phosphorylation activation pathway already mentioned is the canonical example of this. However, DAG's peripheral membrane protein (PMP) targets range far beyond PKC. DAG's multiplicity of action and crosstalk between its pathways have made it difficult to pin down its cellular roles and capitalize on its activities therapeutically, as can be observed from the decades-long endeavors to harness PKC inhibition and/or activation (depending on the isozyme and cancer type) to inhibit tumor metastasis.[117-118]

***PKC** – cancer-related activity*

Overtime, PKC inhibition proved to be an intractable target for cancer treatment. Individual PKC isozymes have now been identified as definite tumor-suppressors.[119] Newton, Brognard and coworkers recently investigated several PKC mutations in cancer cells and concluded that PKC isozymes are, overall, not oncogenic.[14] Inhibition of PKC affords cancer the opportunity to proliferate and thus over-expression may be a non-oncogenic cellular response to carcinogenesis. Thus, cancer treatment strategies involving PKC should activate the enzyme to restore the antitumor capacities of healthy cells. Moreover, it raises questions as to what the under-expression of PKC in hypertensive patients[18] means for PKC's role in maintaining cardiac health.

Clearly, our understanding of DAG's carcinogenic activity is nascent. With each passing year, however, more experimental data supports lipid dysregulation as a global feature of cancers.[48] Furthermore, cancerous cells depend on their unique lipidome to survive the harsh tumor environments that they perpetuate, and understanding the roles of lipids in cancer may open new avenues for treatment.[120] DAG, then, stands as a key player in oncology. When considering DAG, it is important to bear in mind the complexity of the membrane context in which it operates. To this end, we will next discuss the concept of membrane nanodomains.

Nanodomains: to raft or not to raft

The original concept of biological bilayers as homogenized assemblies of amphiphiles has turned out to be far from the reality of membrane composition. In truth, our cell membranes are dynamic and actively allocate cholesterol, sphingolipids and other signaling molecules into small membrane regions in order to compartmentalize cellular functions.[121] The accepted theory to

describe the plasma membrane is as a liquid disordered (Ld) heterogenous mixture of lipids, proteins and other molecules that may or may not sequester certain membrane components into many nanoscopic liquid ordered (Lo) domains based on intermolecular affinities. These Lo domains are hypothesized to be crucial in lipid-mediated protein recruitment and single transduction, but their very presence – in living cells – is still debated. Colocalization of signaling molecules via Lo phase separation into membrane nanodomains has been dubbed 'rafting' and these rafts have elevated concentrations of the low-abundance lipids discussed herein.[122]

In lab settings, rafts order themselves based on acyl tail saturation, move as a single structural unit through the membrane, and may conglomerate with other rafts.[123] All of these observations are demonstrable in artificial membranes, with raft sizes reaching up to one micron in diameter.[124] In live cells, however, nanodomains have yet to be observed at over 5 nm,[125] which implies significantly more heterogeneity than the original natural theory of rafting allows for.

The simple answer for why raft-like events are observed in artificial systems but not their biologically active counterparts is the presence of integral membrane proteins.[126] A computer model showed that at 5-10% of total membrane area integral membrane proteins and protein

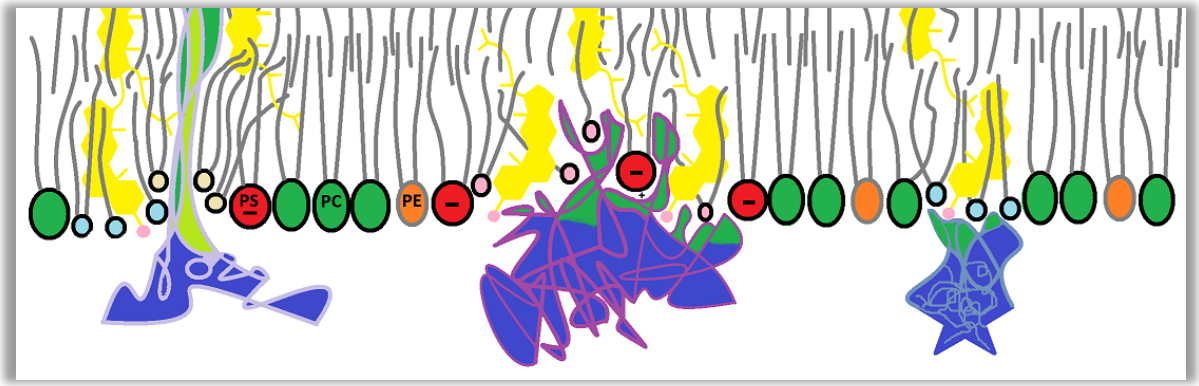

Figure 1.9: A cartoon of membrane rafting. Intrinsic (left) and extrinsic (middle, right) proteins localize to membrane domains rich in signaling lipids and cholesterol (yellow). Ld phase represented by **PC** and occasionally **PS** or **PE**. A **transmembrane integral protein**, left, is present within a Lo nanodomain with cholesterol and specific signaling lipids (mono/diacyl). Center, a Lo nanodomain is similarly formed with an activated **peripheral membrane protein (PMP)** and its preferred array of signaling lipids including PS. Right, A more transient surface **PMP** is shown with a smaller Lo nanodomain. Only the outer leaflet of the bilayer is represented, several other molecules are omitted for clarity, proteins and lipids are not to scale.

channels dramatically reduced the abilities of lipids to phase separate. Natural bilayers also contain protein channels, globular proteins, peripheral membrane proteins and surface proteins.

The complex answer for why rafts are not observed in living systems is that they happen too quickly, discretely and transiently for our current methods of detection to illustrate. However, recent technological advances are allowing researchers to qualify the membranes of living systems. Moving from laboratory recreations of membranes to actual organisms is a key step to unraveling nanodomain behavior.

Nanodomain analyses

The fragility of cells and the vitality of rafting make nanodomains elusive targets of experimental characterization. Cells are fragile and current optical microscope technology cannot image them in vivo. Ex vivo work and exogenous labels are poor recreations of the nanodomain behavior thought to occur in living organisms. Isotopic labeling techniques that label the cell and its membrane with specific amounts of hydrogen and deuterium are most promising for in vivo studies of nanodomains. Just this year, neutron scattering experiments in this vein were applied to nanodomains of lamellar bacterial phospholipid membranes and confirmed the presence of ~40 nm raft-like lateral phases.[127]

Some of the early evidence for lipid rafts made use of spin-labeled electron paramagnetic resonance (SL-EPR) to distinguish annular conglomerations of immobile lipid species stuck to the intramembranous binding domains of proteins.[128] These lipid species may include steroids or phospholipids and are determined by the binding stoichiometries inherent to different proteins and their preferred ligands.[49] Up to 100 lipid molecules[129] may be non-covalently adhered to a single protein and perturbations in lipid ordering are observed at least 1-2 nm from the protein insertion point.[130] In lab settings raft radii are significantly larger.

The fluorescent dye Laurdan is sensitive to fluctuations in membrane packing and thus has been used to investigate lipid raft existence and results suggest there are Lo domains moving coherently among the Ld matrix of the plasma membranes of rabbit erythrocytes and hamster ovary cells.[131] Phasor analysis was used to garner evidence from an adapted fluorescent lifetime imaging microscopy (FLIM) technique that suggested the membranes of intact, live cells are composed of 24% Ld domains and 76% sub-resolution Lo domains.[132] Many of these studies converge upon the

idea that there are no 'free' lipids and each and every membrane constituent is non-randomly partitioned based on affinities for proteins and other bilayer molecules.

The crux of the raft debate as it stands today lies in the size of the purported "microdomain". "Nanodomain" is used instead of "microdomain" in this dissertation to reflect the updated understanding of the concept. The initial estimation of raft sizes of 5-200 nm is now thought by detractors to be an exaggeration. Indeed, far-field fluorescence nanoscopy by stimulated emission depletion (STED) identified fleeting protein immobility of 10-20 ms in cholesterol rich membrane subcomplexes of no more than 20 nm in diameter.[133]

Recently, a glycosylphosphatidylinositol (GPI) anchored green fluorescent protein (GFP) was shown to have a Lo domain of only 1.6-2.5 nm.[130] The results of this study suggest, abstractly, that phase separation does not play a major role in protein recruitment and activation. The results also provide more evidence that the abundance of integral membrane proteins in living membranes precludes the separation of Lo and Ld phases that is so easily observed in synthetic membranes. This study was limited in its ability to track Lo phases not related to GPI-GFP so it does not, as it claims, disprove the concept of Lo rafting entirely. Rather, it underscores the true nature of rafts as ubiquitous, nanoscale, transient membrane features.

Advanced techniques such as augmented inverse fluorescence correlation spectroscopy (iFCS)[134] and course-grained molecular dynamic simulations[135] continue to be applied to rafting in artificial membranes, but more work is needed in living membranes to adequately address the nuances of natural nanodomains. Current techniques, including isotopic labeling neutron scattering experiments and recently developed super-resolution optical microscopy[40] have already confirmed several nanodomain theories and will continue to expound upon what is known of this concept.

Implications of rafting

Nanoscale Lo raft domains remain the predominant hypothesis for how membrane constituents recruit activated proteins to transmit cellular signals and how membrane proteins exert their will on lipidic environments.[40] Rafting is also suggested to be a mechanism of lipid governance towards mercurial cellular behaviors such as drug resistant cancers.[136] The concept of lipid rafts accounts for multivalent/concomitant protein-lipid binding as well. Nanodomains are well-documented if not well-understood and they should be investigated further as they contain information that may

be exploited to bring more selectivity and efficacy to the treatment of diseases such as cancer and HIV.[137] Rafting, particularly increases of cholesterol in nanodomains, has been shown to play roles in other diseased states including viral infections, hypertension and Alzheimer's.[138]

In addition to lipid composition, the curvature of a membrane's protein binding site is crucial for recruitment of proteins for signal transduction.[9] Perturbations in membrane curvature at membrane nanodomains is yet another example of how rafts facilitate protein recruitment. A raft region rich in DAG, for instance, would have significant negative stress, which likely plays a role in providing ideal docking points for DAG-binding proteins. The presence of many signaling lipids at membrane nanodomains reconciles with the multivalent binding that many proteins undergo when docking to membranes. When the complexity of membrane operations is considered fully, it becomes clear that recreating raft-like bilayer conditions is ideal for understanding lipid behavior. One ideal medium emerges by which lipid-protein phenomena may be studied and applied clinically: the liposome.

1.3: Relevant advances in chemical biology

The liposome

The same supramolecular properties that self-assemble phospholipids into cells allow for the formation of liposomes. Hydrophobic hydrocarbon tails conglomerate to expose the polar hydrophilic headgroups to aqueous media externally and within the liposomal core, as can be seen in in the liposome cross section in Figure 1.3.

These highly tunable spherical bilayer vesicles have been applied everywhere from agriculture to homeopathy and gone on to become the most common and effective nanoparticles used in drug delivery and diagnostic imaging.[7] The term 'liposome' was first used to describe lipoid droplets observed as resultant biological microbodies in a variety of animals.[139] A few years later in 1963, Bangham and coworkers identified self-assembled phospholipid bilayers by electron microscopy.[140] Bangham was joined by Weissmann and coworkers who went on to posit in 1968 that phospholipid bilayers partitioned intra- and extracellular space.[141] Two decades after liposomes were discovered, the convergence of nanotechnology and biomedical sciences amplified their clinical potential and the Food and Drug Administration (FDA) approved the liposomal

nanodrug Doxil™ in 1995, which has been administered successfully for delivery of doxorubicin (dox).[142] Cantharidin, 5-fluorouacil, cis-platin, combrestatin, docetaxel, irinotecan, mitoxantrone and paclitaxel, among others, are commonly administered liposomally.[143]

Various approaches for the formation, manipulation and application of liposomes are introduced and discussed in detail throughout this dissertation, we shall begin with a basic outline of liposome formation. The first step almost always involves mixing lipid constituents from organic stock solutions and then removing solvent to create homogenized lipid films. The most common technique for liposome formation is called thin-film hydration and proceeds by hydrating the lipid films in aqueous media with heating and mixing to promote self-assembly into giant multilamellar bilayer vesicles. Next, freeze-thaw and/or sonication can be employed to disrupt multilamellarity and size the liposomes down to large or small unilamellar vesicles (LUVs or SUVs). This may be followed by extrusion to create vesicles of uniform diameter with a low polydispersity index (PDI), size exclusion columns (SEC) or dialysis to remove un-encapsulated liposomal cargo (if present), or centrifugation to separate LUV's from SUV's.

Ethanol injection and reverse phase evaporation (REV) are also common methods for liposome formation and are presented in later chapters corresponding to their utility for the projects herein. Ethanol injection proved most effective at encapsulating short interfacing ribonucleic acid (siRNA)[144] for liposomal nanodelivery of gene silencing agents and was used for liposomal preparation in the DAG-potentiated cell association experiments described in Chapter 3. REV liposomes gained notoriety for their enhanced encapsulation of aqueous cargo and this preparation was explored for the click-promoted content mixing fusion assays described in Chapter 4.[145]

Liposomes may be characterized by many means. By far the most common and accessible method for confirming uniform size of liposomes is dynamic light scattering (DLS). DLS instruments can give average nanometer of vesicles with relative abundances at each diameter. DLS experiments can also determine charge in the form of zeta potential. It is possible to snap pictures of liposomes as well to confirm morphology. To this end, transmission electron microscopy (TEM) as well as atomic force microscopy (AFM) can be used. We have used TEM and scanning TEM (STEM) to image our liposomes in order to confirm morphology as well as fusion events (Chapter 4). An example of a TEM liposome image is shown in Figure 1.0.

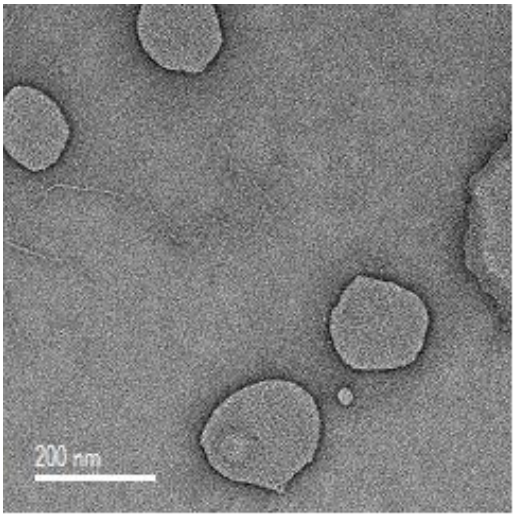

Figure 1.10: **TEM image of liposomes:** a 1.5 mM [lipid] solution of liposomes composed of 75% PC, 24% PS and 2% of a bifunctional lipid probe. The liposomes are in 1x phosphate buffered saline (PBS).

Lipophilic guests may be shuttled about within the membrane bilayer of liposomes. To achieve this, the guest is included during the formation of the lipid film. Upon hydration, the lipophilic guest will form into the bilayer up to a tolerated percentage. Lipophilic cargo or membrane modifications may be added to liposomes after formation by a process called post-insertion. Briefly, post-insertion requires forming the insertants into PE micelles, which are then incubated with the pre-formed liposomes. The less-stable micelles, through electrostatics and natural lipidic conglomeration, favor deforming and reforming into the larger, more stable liposomes.

Hydrophilic cargo is often introduced during hydration, in which case SEC or dialysis is necessary after hydration to remove unencapsulated cargo. Encapsulation of aqueous drugs can also be achieved after formation by creating concentration gradients of pH, manganese or ammonium salt (citrate, phosphate, sulfate or acetate) between extra- and intraliposomal space: drug molecules diffuse into the inner core of liposomes when they enter solution where a minor change such as protonation or chelation prevents escape.[146]

Extrusion is important when uniform size is at the crux of the experimental platform or liposomal application. Interestingly, extrusion can also be useful for ‘clean up’ of certain unencapsulated organic molecules when these molecules are lipophilic bilayer components.

Bilayers will house lipophilic guests, such as the membrane-bound dye Nile Red, but if the guests maintain some aqueous solubility they will exist extraliposomally. In the case of extraliposomal Nile Red, it will stick to the plastic filter supports used during extrusion and visible changes in sample color are observed post-extrusion in these cases. Encapsulated Nile Red is carried through extrusion within the bilayer. Therefore, extrusion is advisable for many liposomal applications, even when uniform size is not a concern. Extrusion techniques are discussed in more detail in Chapter 2.

Extrusion to remove aqueous cargo[147] not entrapped within liposomal core is also possible and requires a clever approach where liposomes are first sized above a certain diameter, 100nm for examples. Next, a smaller filter of 50nm can be used to push the liposomal solution up against a wall that is impassible for intact vesicles. The passed-through solution contains un-entrapped aqueous cargo and may be discarded. Clean buffer is passed back through the filter in the reverse direction, pushing the vesicles off the filter and back into solution. This liposome extruder purification (LEP) protocol may be repeated as many times as desired and the developers reported >93% liposome recovery and contaminant removal in a single step.[147]

Liposomes have been used extensively to study fusion and other membrane recognition events.[148] The biocompatibility and biodegradability of liposomes make them attractive in food science applications for the delivery of enzymes, nutrients and antimicrobials.[149] Various liposomal technologies have emerged over the last few decades and several relevant innovative applications are described in the upcoming *Liposomal Chemical Biology* section. Liposomes are also the obvious choice for testing and optimizing new technologies related to delivery of bioactive compounds,[150] which leads us into the vast field of liposomal delivery systems for the treatment and diagnoses of several diseases, i.e. liposomal theranostics.

Liposomal Theranostics

Self-assembled liposomal drugs and diagnostic agents have emerged over the last two decades as the preferred method for medicinal nanodelivery (‘nano’ used per the typical vesicle diameters of ~50 to ~200 nanometers). Liposomal delivery systems (LDSs) are also known as liposomal nanocarriers and they exemplify the rapidly expanding field of nanodelivery. For simplicity, ‘LDS’ will be used instead and LNC will only be used to refer to lipid nanocapsules. LNCs, incidentally,

are one of several liposome subtypes developed for specific nanodrug applications—in this case, LNCs have a long 18-month shelf life and favorable encapsulation efficiencies of aqueous drugs.[151] Small nucleic acid lipid particles SNALPs) comprise another subset of recently-developed LDS subtype. These nanodrugs are typically cationic and fusogenic. An LDS can be made fusogenic through a few different strategies, as will be described later in Figure 1.11 and later chapters. SNALPS are ideal for the transport of nucleic acid cargo, called nanovectors, for gene silencing applications.

The use of nanocarriers has allowed for significant advances in the passive targeting of tumors and other inflammatory diseases owing to the enhanced permeability and retention (EPR) effect.[152] Small drug molecules are indiscriminate, causing a wide array of side effects and creating dose-limiting toxicity. The sites of tumors, bacterial infections and other types of neoplasms or vascular injuries exhibit enlarged gaps in the surrounding endothelium. Liposomes can home drugs to target sites by keeping them in circulation until they accumulate preferentially through these widened endothelial gaps, as illustrated in Figure 1.11. This phenomenon is colloquially termed 'passive targeting' to refer to the natural advantage of putting a small drug in a larger delivery vessel.

There are several non-liposomal nanodrug platforms including lipidic micelles or lipid-coated inorganic nanoparticles, some nanoparticle delivery platforms are lipid-free such as purely polymeric micelles or carbon nanotubes. All nanoparticular delivery strategies make use of passive targeting (Figure 1.11) and will experience increases in efficacy as nebulous 'active targeting' strategies continue to be formed into nanoparticle architectures as a means for creating cell-specificity among nanoparticles. Active targeting refers to the homing of nanocarriers to target sites using peptides or other molecules with affinity for cell surface receptors characteristic of target tissues. EPR is not purely mechanical; to assert that it operates on the principle that 'big things cannot fit into small holes' would be an oversimplification of how liposomes home to neoplasms and inflammation. Enlarged endothelial gaps are a programed response to maladies ranging from bacterial infections to cancers. There is a pre-existing biological infrastructure to usher larger particles to these sites. Size, therefore, is not the only thing that leads to EPR. Circulation time, charge and biocompatibility can be utilized to potentiate EPR.[152] Furthermore, there are nuanced molecular and chemical differences between inflamed and healthy tissues that aid in this process. It is possible to go beyond EPR to target tissue microdomains where

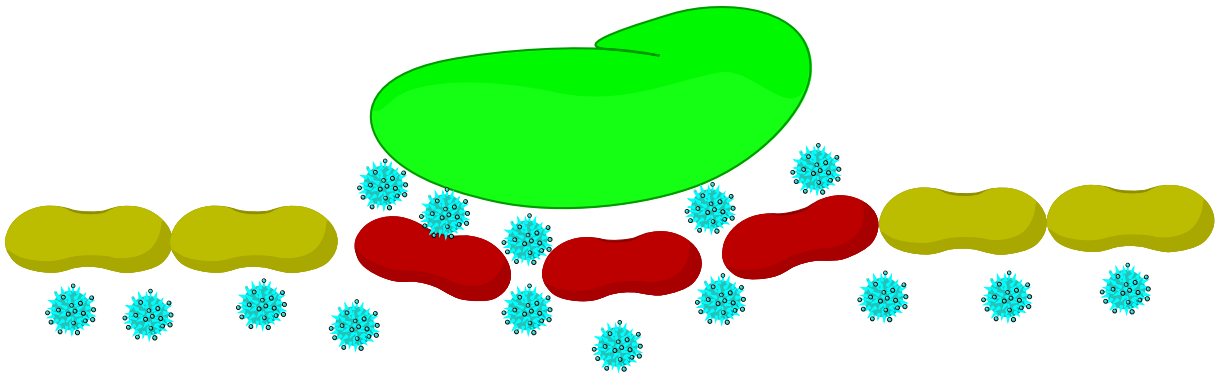

Figure 1.11: **The enhanced permeability and retention (EPR) of nanocarriers at target sites.** Liposomes are shown accumulating at a tumor (green shape) through the leaky vasculature (red) surrounding the diseased/inflamed tissue.

diseased/infected cells create unique environments. This is the forefront where passive targeting becomes active targeting.

Active targeting is touched on at the end of this section and reviewed more thoroughly at the onset of Chapter 3. The type of biological information we seek to uncover through the experimentation described herein is applicable to the active targeting of LDSs. The controlled release of cargo through 'lipid switches' or 'lipid triggers' is also a principle pursuit of Dr. Best and our research group and a review of this emergent technology begins Chapter 4, where work is presented that relates to the controlled release of LDS cargo.

Many promising drugs are cleared by our immune system before they can act. The prolonged circulation time achieved with liposomal administration is yet another advantage of using a nanodelivery system. Liposomes often make use of lipid-anchored polyethylene glycol (PEG) coatings to avoid aggregation and evade being marked by opsonins for immune system clearance.[153] PEG, however, imparts dose-limiting toxicity to PEGylated LDSs as over-exposure to PEGs leads to hand-foot syndrome (HFS). Non-PEGylated liposomes (NPL) make use of propriety compositions and manufacturing techniques to prolong circulation time and have emerged as more effective alternatives to existing PEGylated FDA-approved LDSs.[154] Liposomes have advanced therapy for cancer and several other diseases,[155-158] but there are significant strides yet to be made in terms of active targeting and the controlled release of cargo at target sites. To date, there is but one FDA-approved nanodrug, Mepact®, that is actively targeted to its cellular

destination.[159-160] Laboratory-based experimentation that bears in mind the tenants of clinical viability could start a wave of increased nanodrug efficacy with profound clinical implications.

The simple fact that liposomal architectures are comprised of naturally occurring biological molecules is one of the most attractive features of liposomal theranostics. Latent lipid mechanisms allow lipidic nanoparticles to cross the blood-brain barrier (BBB).[161] Solubility issues with drugs like Paclitaxel were formally solved with harmful adjuvants but can now be overcome with harmless liposomes.[162] Liposomes are also being used to solve multi-drug resistance in cancers,[163] as novel immunotherapies[164] and as potent inhibitors capable of acute actions that avoid unwanted systemic side effects.[165] Additionally, liposomes are now approved for use as viral vaccines, analgesics, antifungals and a photodynamic therapy to treat macular degeneration.[159]

At least 15 liposomal nanodrug formulations have been FDA approved, with many more in clinical trials.[159] Commercially available LDSs are able to deliver their cargo through temporal degradation after collecting at target sites.[7] Cholesterol is a ubiquitous component of LDS formulations, investigations into the roles of the lipid constituents of LDS architectures have focused on tuning stability and circulation time to enhance passive targeting. Such work has honed in on PG,[166] SM,[167] or PE[168] and other natural fats such as tricaprylin[169] and lecithin,[170] which have all found roles as structural components in FDA approved nanodrugs. In this way, tailoring liposomal components has led commercially available liposomal drugs such as extended-release morphine.[171] Most of the liposomal nanodrugs mentioned thus far were created decade(s) ago. There is a disconnect between lab-based nanotechnologies and clinical applicability that has kept the vast majority of actively targeted and/or triggered-release nanodrugs from making it to market, despite great promise.[172] As previously mentioned, we will return to detailed discussions of active targeting (chapter 3) and triggered release (chapter 4).

To improve localization of liposome nanocarriers we conjugated targeting groups to liposomal surfaces.[144] We have also shown that by simply incorporating DAG and/or PS into liposomal architectures we can potentiate and fine-tune the targeted cell-association of PEGylated liposomes to different tissue types (Chapter 3). To improve delivery, we have shown that release of cargo can be triggered with light[150] and that vesicle fusion can be promoted through click chemistry (Chapter 4).[148] Click chemistry is often utilized for many aspects of our projects, beyond the promotion of vesicle fusion discussed in Chapter 4. Click is used in the synthesis of lipid probes, the

modification of liposomal membranes and the enrichment of labeled proteins. Click chemistry is central to the experimentation described herein and will be reviewed next.

Click chemistry

Click chemistry describes a set of bioorthogonal reactions commonly applied in synthetic and bio-organic chemistry. The term 'click' was adopted by Barry Sharpless and others to describe a set of facile cyclization reactions that progress efficiently at ambient temperatures. Click reactions have marked utility for derivatization or conjugation of biomolecules. The essence of click chemistry is its bioorthoganality, i.e. the tolerance of all other biological functional groups that allows for selective reactivity of only azides or alkynes (or tetrazines and cyclooctenes) in complex mixtures.[173-177] Click reactions include copper-catalyzed azide-alkyne cycloaddition (CuAAC), copper-free strain-promoted azide-alkyne cycloaddition (SPAAC) and tetrazine/trans-cyclooctene inverse electron demand Diels-Alder (IEDDA) cycloaddition. In the Best lab, we have used click reactions extensively, particularly CuAAC and SPAAC.

The Best lab often also uses click synthetically as single steps in the engineering of functional lipids.[97, 148, 178-179] More examples of click chemistry used to engineer functional synthetic lipids will be seen in Chapter 2. Recently, we have begun applying click for the chemical modification of liposomal surfaces to increase efficacy in liposomal theranostics. Such modifications include the clicking of an azido cell-penetrating peptide (CPP), such as octa-arginine **2** in Figure 1.12, to a lipid anchor such as the commercially available Alkynyl-PE **1**. This work was done in development of a CPP-targeted liposomal gene-silencing drug for treating vascular injury.[144] Ultimately, post-conjugation yielded better encapsulation efficiency than the pre-modification/self-assembly strategy in Figure 1.12. Liposomal theranostics are introduced later in this chapter and the concept of targeting LDSs will be reviewed in Chapter 3.

Click chemistry has also been applied for faster delivery of toxic cargo in LDSs. Click kinetics are much greater than those of typical non-covalent targeting strategies.[180] Click-based delivery systems can localize isotopic labels to target cites (pre-modified with click partners) more quickly and thus avoid temporal degradation and content-leakage leading to poor imaging resolution and/or side-effects.[181] An exemplary strategy for pre-modifying target sites is the pH low insertion peptide (pHLIP).[182] pHLIPs may be functionalized with tetrazine before being sent to insert at the

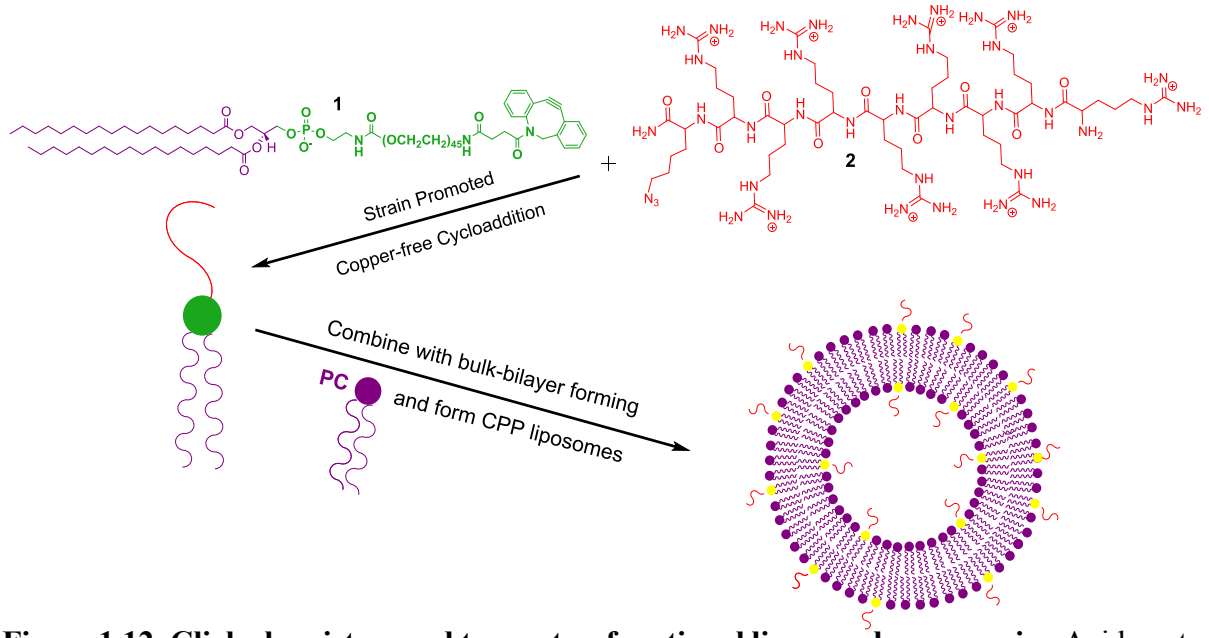

Figure 1.12: **Click chemistry used to create a functional liposomal nanocarrier.** Azido octa-arginine **2** is clicked to dibenzyl cyclooctyne lipid **1** thus enabling the formation of CPP-decorated liposomes. This work was done to aid Trey Fisher and the lab of Dr. Deidre Mountain as they developed a targeted nanodrug with greater cell association and delivery properties.

target cites with lower pH (such as tumors), followed by administration of a liposomal imaging agent targeted by the *trans*-cyclooctene IEDDA click partner.[183-185]

Preforming liposomes decorated with clickable headgroups to enable immobilization or functionalization of intact vesicles has been widely explored.[7] Use of liposomal CuAAC,[186-191] SPAAC,[192-193] and Staudinger ligations[194] have resulted in reviews devoted to methodology that allows for click-functionalized liposomes that maintain membrane integrity.[195-196] Liposomal theranostics have benefited extensively from these efforts. Liposomal doxorubicin has been modified with a HSV-1 peptide (gH625) through conjugation of a clickable gH625 analog[190] and branched neurotensin peptides, for active targeting purposes.[197] To create anticoagulant LDSs, CuAAC and the Staudinger ligation have been employed to decorate liposomes with thombomodulin.[198] Click is a powerful tool for customizing LDSs as it affords elegant options for creating lipid anchored molecules, such as CPPs that can then be formed into liposomes—this strategy is outlined in Figure 1.12. Conversely, liposomes can be pre-formed with less bulky clickable groups such that intact liposomes may have their extraliposomal surface modified after

formation. This strategy is called post-conjugation. The use of CPPs (which imbue liposomes with fusogenic properties) and other active targeting strategies are reviewed at the beginning of Chapter 3.

Click chemistry has also been applied for the fluorescence based investigation of lipid rafts and was used recently to expose protein-protein interactions that play a previously unappreciated role in the mesoscale compartmentalization of our cellular membranes.[199] A staggering amount of progress has been made on several scientific fronts thanks to click chemistry. Click reactions are among the most powerful tools at the disposal of chemical biologists. Another set of tools fundamental to the types of experimentation reviewed next and described in Chapter 2 are a set of photoreactive compounds commonly called photoaffinity tags. Click and photoaffinity tags converge to enable a robust form of chemical biology known as activity-based protein profiling (ABPP), which will be introduced next along with a discussion of photoaffinity tags.

Activity-based protein profiling (ABPP)

Activity-based proteomics uses molecular probes to identify related classes of enzymes based on conserved catalytic sites with affinities for probe architectures.[200] In this way, probe molecules tag, enrich and isolate proteins based on enzymatic activity qualified by affinity for specific probe architypes. The ABPP revolution was made possible by bifunctional probes that can A) covalently capture associated proteins and B) chemically bridge labeled probe-protein complexes to reporter molecules such as dyes or biotin.[174] Covalent capture makes use of photoactivatable crosslinking moieties and enrichment uses bioorthogonal click handles that react exclusively with reporter molecules. ABPP probes are typically soluble in the aqueous media of cellular environments. Using ABPP, chemical biologists may uncover new pathways that lead to cancer,[201] identify and characterize new members of protein families, and catalog virtually any proteome based on conserved recognition sites and protein function.

"Affinity" is used instead of "activity" to describe the adaptation of traditional ABPP to label proteins based on docking interactions during translocation. It is the preference of proteins for certain membrane composition that enable our work, rather than enzymatic activities. Thus, AfBPP is a more appropriate title for experimentation aimed at cataloging PMPs based on membrane

affinities. Our liposomal AfBPP platforms will be presented in Chapter 2.

Photoaffinity tags

Soluble bifunctional probes are often applied to the identification and characterization of biological targets based on their affinities and functions. Bifunctional, in this case, refers to their ability to capture protein targets with a photoaffinity tag and be subsequently enriched (usually via click chemistry) for visualization and/or identification. A clickable probe is useful insofar as the probe can first covalently capture target compounds prior to click enrichment. The major advancement in this realm is the photoaffinity tag. Photoaffinity tags burst onto the chemical biology scene as a means for ligands to capture and thereby facilitate the identification of protein receptors.[202] Such technologies are extremely valuable for drug discovery[203] and the study of various protein receptors. Clickable, photoactive probes provide platforms for biological mapping ranging from phospholipase activities,[204] PIP_n binding proteins,[96] and global profiling of cellular dysfunctions such as cancer.[205] Such techniques epitomize ABPP.

Two common photocrosslinking tags are the diazirine and benzophenone groups shown in Figure 1.13 with their mechanisms. A diazirine consists of nitrogen-nitrogen double bonds constrained within a three-membered ring with an additional sp^3 hybridized carbon atom tethered to the probe backbone. UV excitation promotes the escape of a far more stable diatomic N_2 molecule, leaving a nucleophilic carbene in its wake. The carbene will react to covalently insert into any nearby C-H, N-H or O-H bond—including water—thus the carbene is short-lived and will be quenched if there are no peptides nearby. Benzophenone, on the other hand, goes through a radical reaction, as seen in Figure 1.13. The diphenylketyl radical intermediate in this case can relax back into the ketone if upon initial excitation there are no hydrogen bonds nearby for it to propagate its radical insertion mechanism with.

Naturally, background labeling is a major concern when employing photocrosslinking groups. There is a demand for global identification of background labeling due to the latent natural affinities of diazirines and especially benzophenones. Benzophenones have been applied widely across science, medicine and industry for nearly 50 years, often in sunscreens, and have been studied for their pharmacokinetics, allergic and photoalergic interactions.[206-207] Happily, efforts are already underway to create inventories of background protein hits for benzophenones,

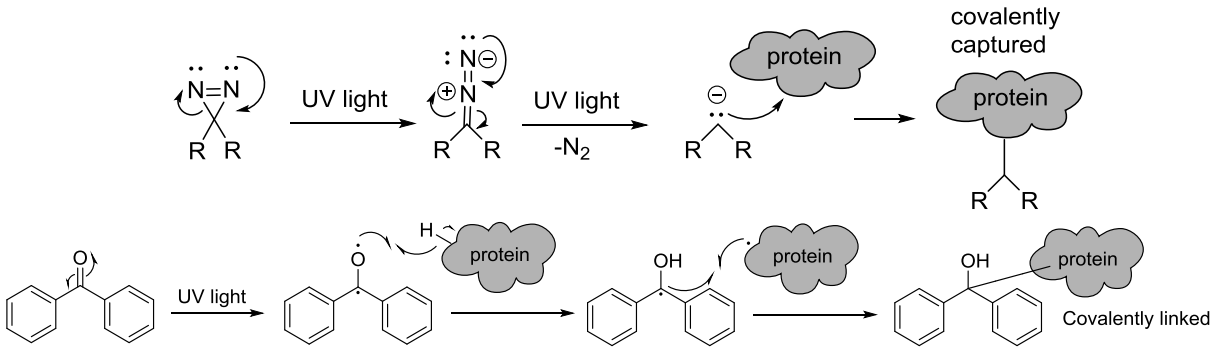

Figure 1.13: **Two common photoaffinity groups with their crosslinking mechanisms.** A diazirine photoaffinity tag is shown above and a benzophenone photoaffinity tag is shown below.

diazirines and other crosslinking groups such as aryl azides.[208]

Bifunctional lipid probes

Lipid scaffolds have been synthesized into clickable photoaffinity probes that operate in similar fashions to the hydrophilic bifunctional molecular probes first used in traditional ABPP. DAG is an intuitive architecture for synthetic intermediaries to access several bifunctional probes corresponding to natural lipids. Previous members of our research group have engineered and made use of an azido DAG species to access several bifunctional lipid probes and the bifunctional DAG version of said probe maintained affinity for PKC, thus demonstrating the efficacy of such strategies.[178] Indeed, the Best lab has advanced the field of bifunctional lipid probes on many fronts. The inositol phosphates have been studied in this manner[209] as well as phosphatidic acid[179] and phospholipids in general.[195] Ultimately, the use of crosslinking, clickable lipid probes has become an established means to label lipophilic proteins.[210]

Single-tail lipids have been studied in virtually the same way and fatty acid protein affinities have been investigated extensively using bifunctional probes.[211-212] A bifunctional probe corresponding to sphingosine, which could be thought of as lyso-sphingomyelin, was recently developed to probe sphingolipid cellular regulation.[213] Even more recently, a photocrosslinking clickable lipid probe was used to identify the active site residues in paraoxinase 1 (PON1), a protein with antioxidant and anti-atherosclerosis properties.[214] Lipid probes such as these provide universal platforms for

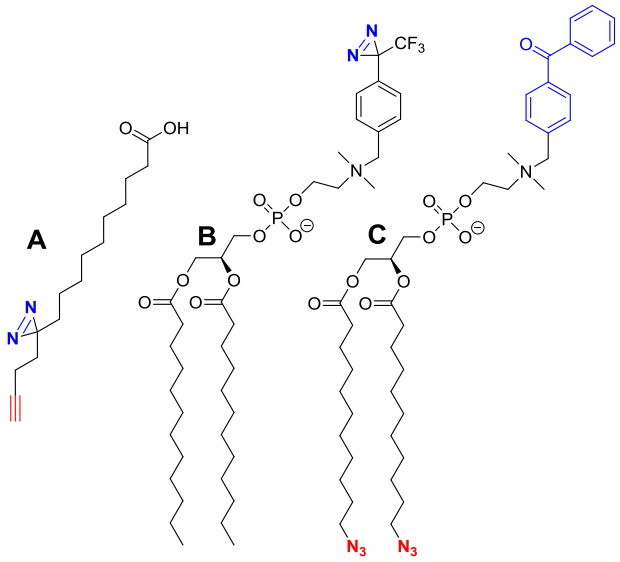

Figure 1.14: **Examples of recently-used synthetic lipid probes.** A bifunctional fatty acid probe (**A**) used by Haberkant and coworkers[200] for labeling proteins is shown, as well as monofunctional (**B**) and bifunctional (**C**) PC-based probes employed by Gubbens and coworkers.[199] Click tags are red, photocrosslinking groups are blue.

chemical proteomics in terms of protein ligandability, which has in turn revealed a marked correspondence between the lipid affinities of proteins and the active sites of drugs and/or inhibitors.[215] Lipid probes have already shed light on the mechanisms of many potent drugs and are concurrently uncovering new avenues for advanced therapies for many diseases.

To date, glycerolipid A(f)BPP has chiefly employed probes based on PC[216-217] or sometimes PE[218] as the parent architectures and liposomal iterations have been limited to the labeling of integral membrane proteins with latent bilayer affinities. Isolating proteins from complex mixtures based on affinities for different lipid headgroups—presented in a membrane context—is an attractive method for uncovering important new protein and/or lipid cellular functions. Probes that seek to identify affinity for PC are unremarkable in their specificity and/or ability to uncover new biological interactions. In assays sought to confirm affinity for a recent PC probe, results with a known PC binding partner were negative, suggesting that the probe labeled membrane proteins indiscriminately.[217]

Synthetic organic chemistry is not the only means by which bifunctional lipid probes may be engineered. For example, probes have been generated by feeding an unnatural alkyne-containing

choline to cells along with a synthetic fatty acid bearing a diazirine group so that the cells themselves generate a clickable, photo-crosslinking phospholipid probe to be used in proteomic mapping.[217] Despite this progress, the use of lipidic probes maintains many challenges that inhibit their applicability. Many lipids, particularly two-tail species, struggle to go into solution in aqueous media. Solvation effects and unwanted self-assembly phenomena such as critical micelle concentration (CMC) hinder the operation of lipid probes. Furthermore, lipid probes will maintain universal non-specific affinities for any greasy protein binding pockets and thus produce unwanted interactions when studying headgroup affinities of lipid species. A key avenue for advancing the utility of bifunctional lipid probes is the employment of liposomes as platforms for such technology.

Liposomal chemical biology

The concept of recreating the membrane context to more accurately characterize the lipidomic and proteomic behaviors therein is at least two decades old, but as it stands today liposomal chemical biology is still an expanding field. Studying membrane enzymes using proteoliposomes (bilayer vesicles created from the lipid-enriched fractions of cellular extracts) is known to be an advantageous biomimetic strategy and narrowing the liposomal contents to just phospholipids seems to have the same effect as proteoliposomes in *Escherichia coli*.[219] Liposomes present solutions for shuttling lipid probes into cellular environments or presenting lipid probes to complex mixtures of proteins in cell extracts. Anchoring lipid probes into liposomal membranes may also diminish non-specific hydrophobic interactions by burying the fatty acid tails of lipid probes into the membrane, although lipophilic proteins will of course insert themselves in the same context, and amphiphilic molecules may partition themselves into hydrophilic areas if they do not pack well into bilayers. Such are the nuances of concepts such as lipid rafting and part of the reason complex liposomal presentation of bifunctional ABPP probes is rare.

Liposomes can also create a more biomimetic environment in which to screen protein affinities, particularly when experimentation involves introducing lipidic probes to cell extracts. Incorporating liposomes into complex experimental protocols creates challenges regarding the increased lipid content that can interfere with ex vivo cellular delivery of probes and the gel electrophoresis and mass spectrometry (MS) that culminates both ex vivo and in vitro protein

profiling assays. Liposomal administration of probes to cell extracts however, is particularly intriguing as it recreates some of the biological context lost upon cell lysis, and could advance extract-based chemical biology. Considerable optimization is required to harness liposomes as platforms for the chemical investigation of protein-lipid binding interactions and such nuances are discussed in Chapter 2.

Surface plasmon resonance (SPR) has been used to characterized liposomes[220] and similar technologies have previously made use of immobilized liposomes using various attachment strategies although avidin-biotin is most common.[221] Plasmon resonant liposomes have themselves been created by coating liposomes in gold such that they are responsive to near-infrared to stimulate release of biological molecules.[222] Liposomes have also been deposited on polydopamine surfaces by forming amine-catechol conjugates to create nanofiltration technologies with potential application to water purification.[223] Studies such as these move away from traditional chemical biology and begin to blur the lines between biomedical and chemical engineering, surface science and other disciplines. The wide applicability of liposomes illustrates their versatility and positions them at the interfaces of several scientific fields, including analytical chemistry. For example, MS-based investigations of tissue samples, such as time of flight secondary ion mass spec, can be aided by liposomes to identify the presence and characterize the interplay of biological molecules characteristic of AD or other diseases.[224]

Non-vesicle lipid microarrays are common are common alternatives to ABPP using lipid probes to investigate lipid-protein interactions.[225-227] Lipid arrays are accurate ways to measure some lipid-protein interactions, although they lack the curvature and dynamics to be truly biomimetic. Liposomal microwell or microarray protein profiling overcomes this obstacle and has been performed by immobilizing liposomes on avidin plates using biotinylated vesicles.[228-229] Microarray liposomal applications have been developed further to become quantitative and are extremely convenient in their ability to provide high-throughput analyses of complex lipid interactions.[230] Advanced microarray technologies that make use of fluorescent liposomes to characterize protein-membrane binding interactions dependent on signaling lipid content, often PIP_n species, are now extremely robust and versatile.[231] Microwells with sizes correspondent to diameters of avidin-secured biotinylated liposomes have also been used to immobilize vesicles and enable membrane-based assays.[232]

Many techniques have emerged in which liposomes are the stationary phase in column chromatography and such techniques have been applied to drug discovery and molecular detection.[233-234] These techniques are often referred to as immobilized liposome chromatography (ILC) or immobilized artificial membranes (IAM). Immobilization can make use of various covalent attachment strategies to silica and other column media, or they are often immobilized through biotin-avidin interactions. Fluorescent molecules may be incorporated into liposomes that are immobilized on columns in order to gauge membrane perturbation of drugs, peptides or other molecules.[235] Yet another emerging nanotechnology involving liposomes is the creation of stabilized polymeric vesicles that make use of photo-induced cyclization reactions of tricosidinoyl lipid tails and such technologies have already been applied to the study of PIP_n species.[236] Future applications of IAM or ILC may involve polymeric liposomes or could potentially use size exclusion chromatography for the liposomal enrichment of membrane-captured proteins, as described in more detail in the 'Future work' section at the end of Chapter 2.

Liposomes have been applied in a somewhat similar fashion to the liposomal AfBPP detailed in the next chapter. Multifunctional probes have been incorporated into liposomes to label integral membrane proteins to confirm their ability to crosslink and be derivitized.[216] Much of this experimentation has been done by incorporating probes into the mitochondrial membranes of yeast extracts.

We have adopted some strategies and protocols from these works and are grateful for the headway made by other research groups. Our studies differ in probe design and application; they also have a different end goal, which is the specific detection of PMPs with specific and selective signaling lipid affinities. Figure 1.15 illustrates some of the liposomal chemical biology that will be discussed in the Chapter 2, where a generic lipid probe allows us to capture and identify proteins dependent on their natural signaling lipid affinities. The background protein hits of photocrosslinking groups is an obvious concern, as evidenced by aforementioned recent experimentation that catalogs such protein-phototag affinities.[208] This liposomal protein profiling approach outlined in Figure 1.15 controls for this by employing liposomes with only the probe (and PC) to identify non-specific (or PC-only) interactions.

Here, we present a novel platform whereby lipid probes are formed into liposomes with crosslinking groups displayed at the membrane interface. Specific lipid probes may be employed.

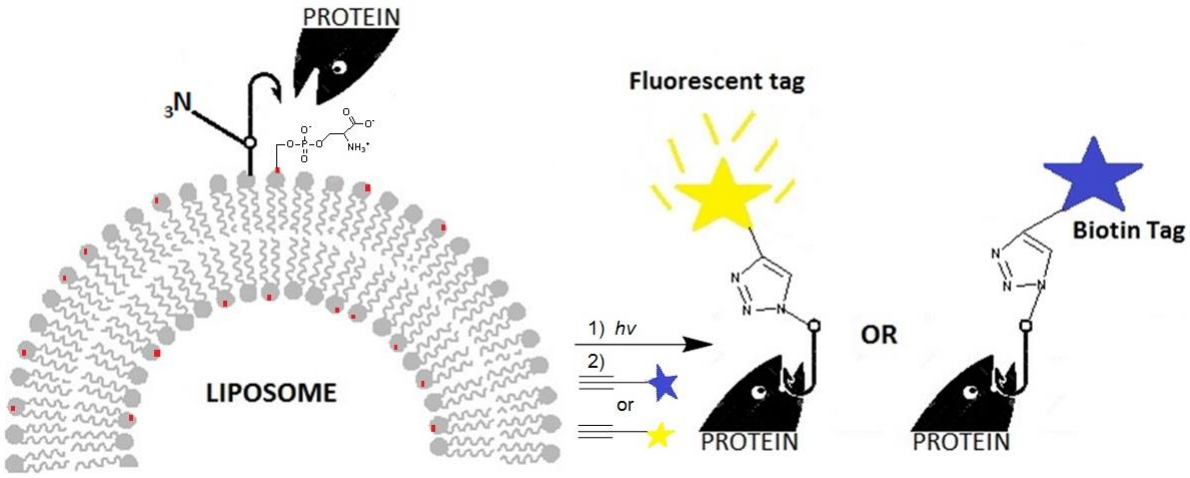

Figure 1.15: **A lipomimetic affinity-based protein profiling strategy.** A photoactive (hook) and clickable (N_3) lipid probe is applied liposomally to label proteins with a fluorescent tag for imaging or to a biotin tag for purification. This strategy identifies proteins attracted to natural chase lipids (red dots, PS in this cartoon) by incorporating a 'generic' lipid probe into liposomal treatments at a constant percentage while varying the chase lipid.

Or, a nonspecific lipid probes (or 'generic' probes) may be incorporated at a fixed percentage into liposomes with varying signaling lipid contents. Efficacy was confirmed early on using known protein-lipid binding interactions and the protocol was also applied to characterize the membrane affinities of the HIV capsid protein CA.

Probe liposomes were also mixed with complex mixtures of proteins and achieved selective labeling of low molecular weight proteins from the membrane fraction of lysed cell extracts. The location of our photoaffinity tag and the membrane composition-dependent labeling suggest that some of our hits may be PMPs. To our knowledge, similar liposomal strategies that afford tight control of membrane composition while investigating complex protein mixtures has not been previously reported, until now.

CHAPTER 2: LIPOSOMAL AFFINITY-BASED PROTEIN PROFILING (A_FBPP)

2.1: Introduction

Lipomimetic and lipospecific AfBPP

This chapter describes the development of protocols to incorporate lipid probes into liposomes to identify proteins that are recruited to the membrane surface preferentially based on membrane composition or probe architecture. Probe liposomes may be incubated with cell extracts for the discovery of protein-lipid binding interactions in a complex mixture of proteins. Probe liposomes may also be incubated with enriched lysates or isolated proteins to characterize the membrane binding behavior of specific proteins. Probes may be generic, allowing natural lipids to be screened at incremental percentages by treatment liposomes with a fixed percentage of a non-specific probe. This lipomimetic approach requires less synthesis and more accurately recreates the natural ligand-binding of proteins to membranes. Lipid-specific probes may also be used and, although this lipospecific approach is more demanding synthetically, this allows us to compare changes to probe architectures among PA and DAG-specific probes, as well the results of lipomimetic studies with generic probes (GPs). Specifically, the lipospecific approach hones in on the role of lipid headgroups in the role of recruiting PMPs.

Once we have captured and labeled proteins with a fluorophore, analysis involves separation by sodium dodecylsulfate-polyacrylamide gel electrophoresis (SDS-PAGE) and fluorescence imaging where proteins preferentially recruited to our liposomal surfaces will fluoresce more intensely due to increased probe labeling (based on variations in lipospecific probes, or natural lipid content in the lipomimetic approach). In this way, we have pursued two distinct strategies for the labeling of lipid binding proteins.

The *lipospecific* approach utilizes a probe analog of the natural lipid containing functional tags introduced within the structure. A lipospecific experiment is outlined in Figure 2.1 on the next page, where the hydroxyl group on the probe molecule indicates a probe engineered to be analogous to DAG. The *lipomimetic* approach relies on natural lipids to recruit proteins to the membrane where they are then labeled by generic probes with no analogous natural headgroup. A lipomimetic experiment with PS as the chase lipid is depicted in Figure 1.15 at the end of the

previous chapter.

The lipospecific strategy is theoretically more precise when envisioning the immediacy of the photocrosslinking event. Nonetheless, any tailoring of a natural lipid scaffold will exert changes on headgroup presentation. This becomes clear when considering how close the headgroups of DAG and many phospholipids are held to their glycerol backbone, as well as the location of some binding domains within folded protein structures. These considerations lead to the evolution of probes generated by the Best Lab from benzophenone-based to diazirine-based functional lipids.

The lipomimetic strategy makes use of nonspecific GPs that are not meant to bear any similarity to lipids of interest. In this approach, proteins are recruited by natural lipids and captured by nearby generic probes embedded in the same membranes. This approach has considerable logistical advantages and is more biomimetic because it uses natural chase lipids. It is theoretically less precise and the use of control liposomes that lack the chase lipid is crucial. Additionally, the lipospecific approach has the potential to discover binding domains while the lipomimetic does not.

In the lipospecific case, probes are used where the natural headgroup is retained at the *sn-3* position in addition to the bifunctional headgroup attached to the *sn-1* position (Figure 2.2, structures **1** and **2**). Alternatively, lipid probes may have only the photocrosslinking group attached

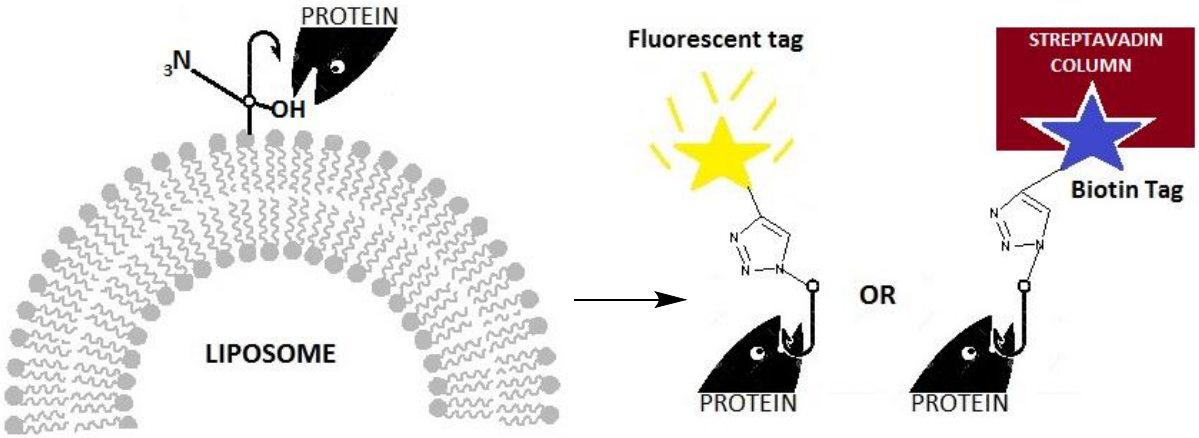

Figure 2.1: **Lipospecific experimental design.** In this cartoon the lipid-specific probe corresponds to DAG, the fishhook represents the photoaffinity tag and the azide is the click handle used to enrich (triazole ring is linkage product of enrichment with an alkyne-reporter).

to the headgroup with clickable tails inserted at the end of the lipid tails (structures **3** and **4**, Figure 2.2). In the lipomimetic case, non-specific probes (Figure 2.3, compounds **5**, **6**, **7, 8**) are used to study the labeling trends of natural lipids without the need to synthesize lipid-specific probes for each lipid of interest, also known as the 'chase lipid'.

Applying this liposomal AfBPP platform to cell extracts is attractive as a translatable technology that is more cost and time-effective and can be more easily recreated lab to lab than ex vivo work. For similar reasons, we are especially excited about the lipomimetic approach. However, it is important to note that turning the entire liposome into a probe will impart a degree of background labeling. This is accounted for by control samples using liposomes that lack the chase lipid. As we add in chase lipids such as DAG, PA, PS, or any combination thereof, we observe changes in labeling. Changes in labeling can be considered putative data and may be compared to results of lipospecific assays and, potentially, mass spectrometry data using this same experimental platform. Of course, these studies may also be applied in live cells and work has already begun to optimize such experimentation.

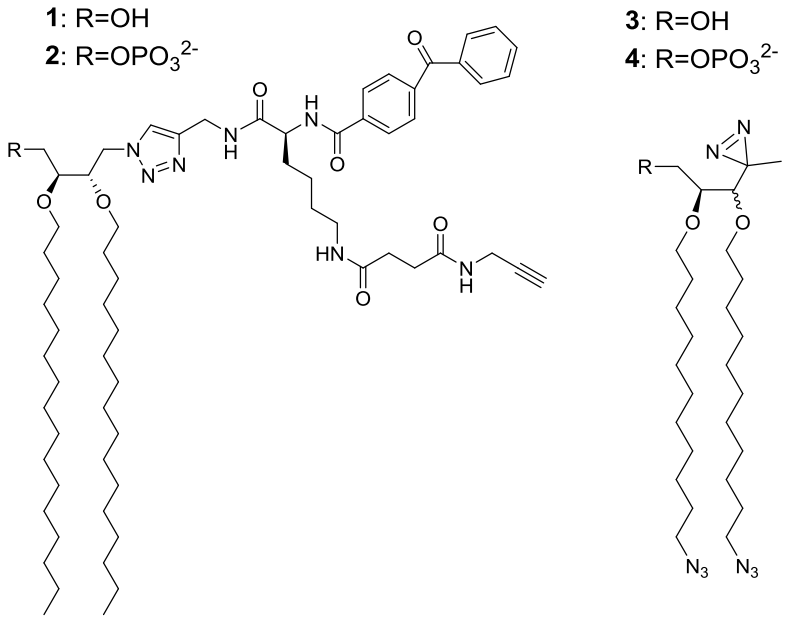

Figure 2.2: **Two different lipid-specific probe architectures.** Lipospecific probes with a bifunctional alkyne/benzophenone headgroup (**1**, **2**) or with clickable azide-tails and a diazirine headgroup (**3**, **4**) corresponding to DAG (**1**, **3**) or PA (**2**, **4**).

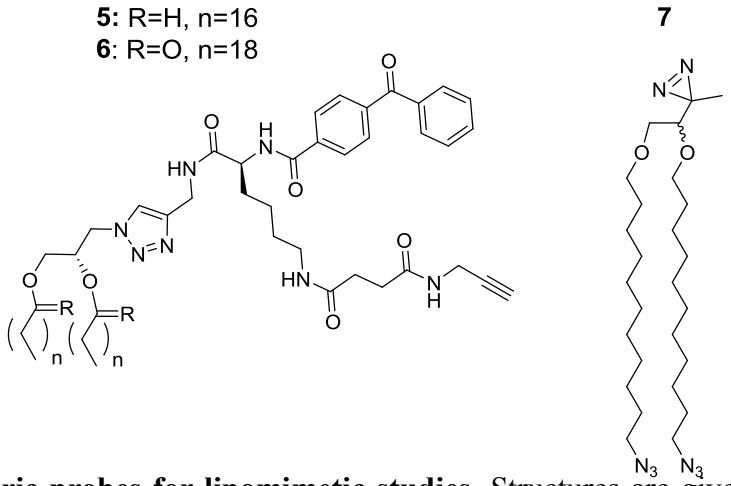

Figure 2.3: **Generic probes for lipomimetic studies.** Structures are given for probes with bifunctional alkyne/benzophenone headgroups (**5**, **6**) or clickable azide-tails with a diazirine headgroup (**7**). Syntheses by Adam Carr.

I was responsible for optimizing conditions for liposome formation, incubation, photocrosslinking, click derivatization, gel electrophoresis and fluorescence imaging of separated proteins—as detailed later in this chapter. I also synthesized a key intermediate (Figure 2.4) for lipid-specific probes **1** and **2** in Figure 2.2, as well as a simple single azide-tail benzophenone probe used in optimization studies (Figure 2.5).

Probe design

To achieve our goal of capturing and enriching PMPs, we designed bifunctional lipids that maintained amphiphilic phospholipid tendencies to form spherical bilayer membranes i.e. liposomes. The probes' synthetic alterations allow them to be activated by UV light to covalently bind nearby proteins, and be enriched by click chemistry to label or identify captured proteins. The first photoaffinity tag we tried was benzophenone, which is represented by the fishhook seen in Figures 1.14 and 2.1. We have more recently added probes bearing a diazirine photoaffinity groups as the 'fishhook.' Various combinations of azide and alkyne click handles and reporters have been experimented with; currently, we employ azide-tail probes such as **3**, **4**, and **7**.

Once we have captured and labeled proteins with a fluorophore, analysis involves separation by SDS-PAGE and fluorescence imaging where proteins preferentially recruited to our liposomal

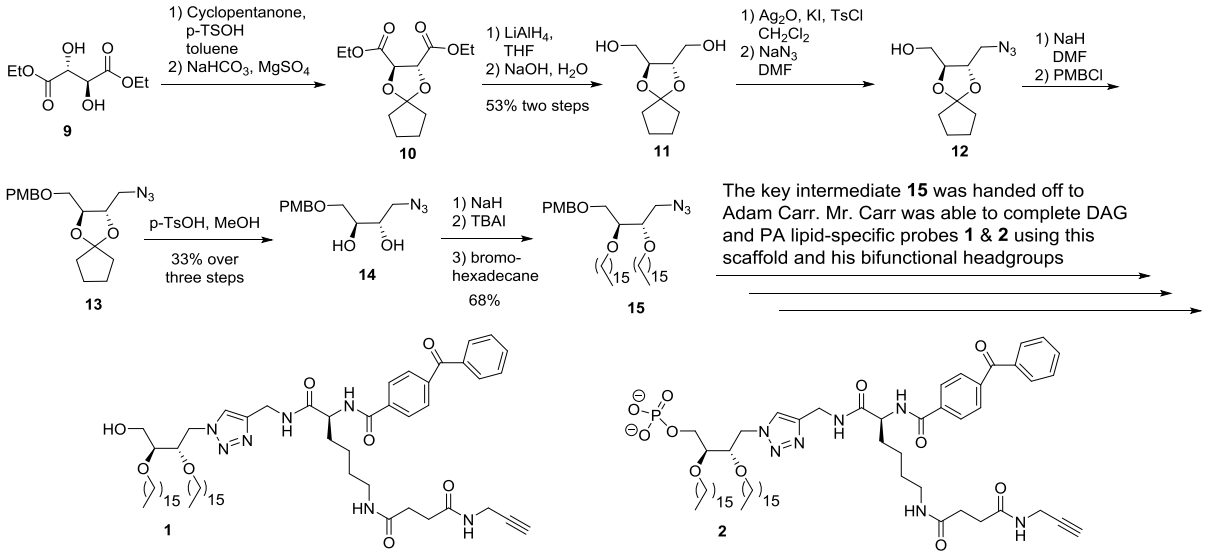

Figure 2.4: **Synthesis of *para*-methoxy benzyl (PMB) protected azido DAG analog 15**. **15** was used by Adam Carr to finish convergent syntheses of four lipid-specific probes (two with amide-linked bifunctional headgroups (not shown) and two with triazole linkages (**1** & **2**)) corresponding to DAG and PA. Synthetic details are in section 2.3, spectra are in Appendix 1.

surfaces will fluoresce more intensely due to increased probe labeling based on variations in lipospecific probes (or natural lipid content in the lipomimetic approach).

Best group member Adam Carr was chiefly responsible for synthesis of the probes. My contributions to the synthetic end of this endeavor can be found in Figures 2.4 and 2.5. The synthetic strategy is outlined here, procedural details and synthetic data can be found in Section **2.3**: *Materials and methods* with corresponding spectra contained in Appendix 1. Following the scheme in Figure 2.4: synthesis of key intermediate **15** began with acetal protection of the vicinal diol on diethyl-L-tartrate **9** using cyclopentenone to form acetal **10**. Ester reduction using lithium aluminum hydride ($LiAlH_4$) formed diol **11**. A mono-tosylation technique using silver oxide (Ag_2O), finely crushed potassium iodide (KI) and tosyl chloride (TsCl) created the primary leaving group requisite of a nucleophilic azide introduction to form the azido alcohol **12** using sodium azide (NaN_3).

Sodium hydride (NaH) was used to deprotonate the primary alcohol of **12** so that it may be protected through reaction with *para*-methoxybenzyl chloride (PMBCl). The acetal protecting

group was removed using *para*-toluenesulfonic acid (*p*-TsOH). NaH and a catalytic amount of tetrabutylammonium iodide (TBAI) were used to install lipid tails, introduced as bromohexadecane. From here, Best Lab member Adam Carr completed the synthesis by reducing the azide to an amine and conjugating to a bifunctional headgroup. These probes performed poorly in labeling experiments and are not shown. Mr. Carr also clicked the azido group to an alkynal bifunctional headgroup to form the triazole linkages shown in the final probe structures **1** and **2**. Mr. Carr's removal of the PMB protecting group using 2,3-dichloro-5,6-dicyano-1,4-benzoquinone (DDQ), not shown, completed the synthesis.

Mr. Carr's twin-azide tail synthetic probes require significant time and cost to produce. As such, a simple probe molecule that was cheaper and less demanding to construct was devised and used in test experiments to optimizing the protocol for azide-tail probes. Synthesis of single azide-tail probe **8**, shown in Figure 2.5, commenced with the conversion of bromoundecanol **16** into azido alcohol **17**.

A Finklestein-esque reaction began next by mesylating the alcohol of **18** using mesyl chloride (MsCl) in the presence of pyridine. An iodo nucleophile was than introduced to the mesylated

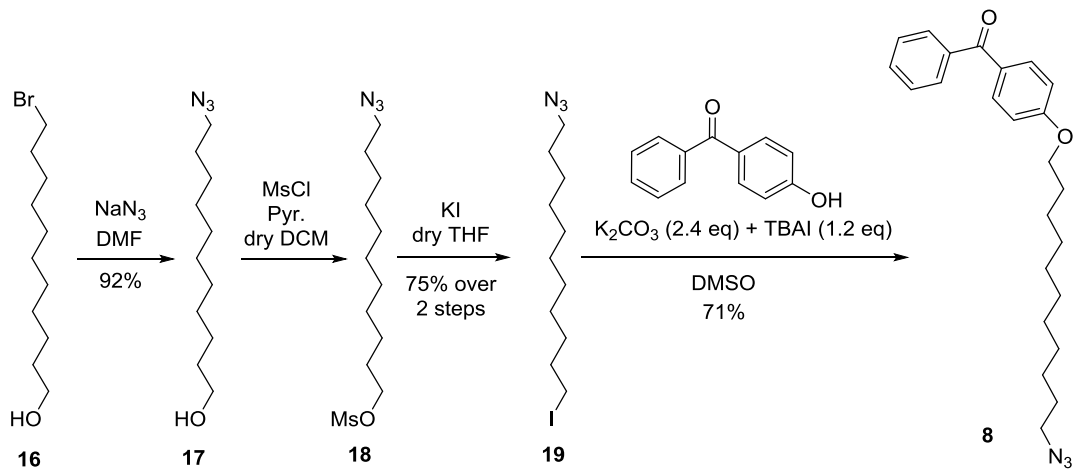

Figure 2.5: **Facile synthesis of single azide-tail generic probe 8**. Probe **8** was used in the optimization of lipomimetic conditions for azide-tail probe experiments to conserve twin-azide tail diazirine probes. The synthesis is detailed in section 2.3 and corresponding spectra are in Appendix 1.

carbon, creating iodo-azide **19**. The iodo leaving group proved to be significantly more susceptible to attack from the benzophenoxide nucleophile, which was prepared from benzophenol and potassium bicarbonate (K_2CO_3) and introduced with TBAI to create the lipophilic clickable photoaffinity probe **8**. MS characterization of azido (N_3) compounds typically gives a mass ion peak less the weight of two nitrogen atoms due to ionization of N_2. Thus, an orbitrap MS with non-fragmentation mode was used to confirm our azide withstood this reaction scheme to be introduced as click tails to probe architectures. Instrument details and characterization data are presented in *Methods* and *Appendix 1*.

Labeling studies

Thorough procedural details are presented later, followed by a discussion of experimentation to determine optimum liposomal labeling conditions in Section 2.3: *Materials, methods and optimization*. The current optimized protocol can be found in Figure 2.6. Several gel results follow an earlier protocol that involved additional steps (Protocol B, Figure 2.7). Variations in the protocols are addressed here as we outline the procedures of our liposomal AfBPP. Experimental results from the updated protocol will appear with 'Protocol A' in the Figure legend. Experimental results that follow the original protocol will appear with 'Protocol B' in the Figure legend.

The principal difference in Protocol B experiments was that more lipid content was used and probes were incorporated at lower percentages than are specified by Protocol A (4% instead of 8% for lipomimetic studies). Another key difference was that Protocol B samples were treated with 2-8 μL of 20% SDS detergent solution pre-click to accommodate the extra lipid content, as discussed in Section 2.3.

The click reagents for Protocol B were added separately in the order they are given in Figure 2.7. For Protocol A, a click mix was made using the same ingredients. Details for click enrichment are discussed in *Methods*, where Figure 2.20 tabulates concentrations and volumetric ratios of the click reagents for the Protocol A click mix. For alkynyl probes, the click reporter was Alexa-488 azide. For azido probes, the click reporter was Cy-3 alkyne or Alexa-488 alkyne for experiments done at The Scripps Research Institute (TSRI), which is noted in the text and Figure legends.

Protocol B also employed a solvent wash/precipitation to remove excess lipid content before gel loading. Any studies that follow Protocol A do not use the solvent wash/precipitation and all

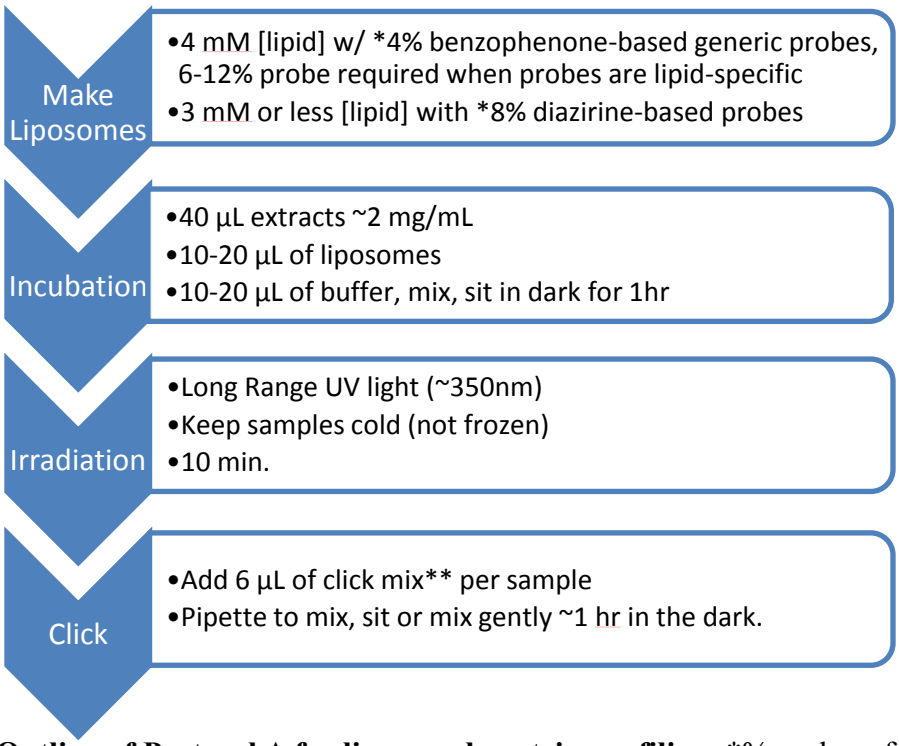

Figure 2.6: Outline of Protocol A for liposomal protein profiling. *% probe refers to molar percentage based on total molar lipid content. **click mix is 3:1:1:1, ligand:$CuSO_4$:TCEP:azide or alkyne reporter (Figure 2.8)

studies that follow Protocol B do. After the wash/precipitation the pellet was sometimes challenging to solvate in loading buffer. If this was the case, the pellets were briefly sonicated in loading buffer using a sonic probe with a perforated tip set to 20% power with 3 x 1s bursts. All experiments following Protocol B heated samples in loading buffer at 100 °C for 2 minutes before loading into gels, some experiments do not use sonication before heating and this is noted in Figure legends. Studies that follow Protocol A do not use any heat/sonication before loading.

Protocol B also added $CaCl_2$ to a final concentration of 1 mM to ensure there was ample cationic calcium to bridge certain DAG-binding proteins to anionic phospholipid cofactors. Protocol B also added protease inhibitor before incubation to minimize protein degradation during heated incubation. Updated Protocol A no longer uses heat and does not require addition of protease inhibitor. The Figure legends and Figures themselves will detail any other changes to the experimental procedures followed for that experiment.

The size of liposomes was also optimized and vesicles with 400-600 nm diameters afforded

liposomes 4-6mM [lipid]	Cell extracts ~2 mg/mL [protein]	30 mM $CaCl_2$	25% SDS	10 mM TCEP	1.7 mM Ligand	300 mM $CuSO_4$	5 mM Fluo-N_3	Protease inhibitor
30-40 µL	40 µL	2 µL	2-8 µL	2 µL	12 µL	2 µL	2 µL	8 µL
in 1X PBS uniform diameter of ~200nm	Pure proteins screened at ~200 µg/ml	in milliQ water	in pure water, different systems require varying amounts, start low.	in milliQ water, made fresh and kept from light	Stock solution in 4:1 tBuOH/ DMSO	in milliQ water, made fresh and kept from light	in DMSO, Any click reporter works	1 Pierce™ mini-pellet in 2 mL of milliQ water

Figure 2.7: Protocol B volumes and reagents for liposomal protein profiling. Details of the original protocol that was later optimized into Protocol A. Key changes were the reduction of lipid content to 10-20 µL of 3 mM liposomes, the redaction of $CaCl_2$ and protease inhibitor, as well as the removal of the SDS treatment.

the best results. Protocol A uses these larger vesicles and multiple means of preparation are discussed in Section 2.3. Protocol B used 100-200 nm vesicles and the preparation of liposomes in this size range is also discussed in detail in section **2.3**, along with cell lysate preparation and all other experimental protocols for the labeling studies presented herein.

Controls

Controls have been implemented to verify that labeling depended on the probe being present in the membrane and to verify probe photocrosslinking functionality. During proof of concept experiments, and in later experiments, liposomes that resembled study groups but lacked the probe molecules in their bilayer constituents were used to test for background labeling due to nonspecific protein-dye interactions. Experimental groups that don't receive irradiation are also employed to make sure the photosensitive crosslinking moieties are functioning.

For lipospecific studies, the generic probes serve as controls to weed out protein hits that are not specific to the headgroups of lipid-specific probes. For lipomimetic studies, probe liposomes that only contain bulk lipids and/or cofactors serve as controls to isolate protein hits that are dependent on chase lipid presence in the membrane. The complexity of our experimental platform means many variables could skew our results, particularly when using the generic probes. To

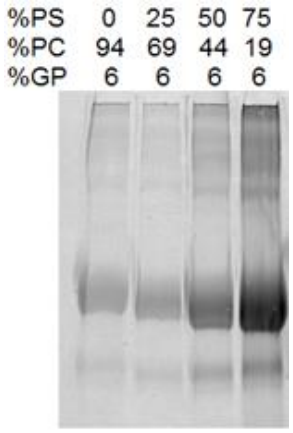

Figure 2.8: **A PS-Annexin lipomimetic proof of concept experiment.** Liposomes with 6% of GP **5** (Figure 2.3) are used to screen Annexin V affinity as a function of PS content. Protocol B. No sonication.

ensure the accuracy of our lipomimetic approach we conducted competition studies where no-probe liposomes with or without the chase lipid were pre-incubated with extracts before performing our normal labeling experiment. Competition liposomes with the chase lipid should compete for the protein more effectively than competition liposomes that lack the chase lipid, and thus competition-based reduction of intensity will be lipid-specific for bands with chase lipid-dependent labeling.

2.2: Results

Validation using known protein targets

We began with proof-of-concept assays (Figures 2.8, 2.9) to test if our protocol could illustrate the known affinity that Annexin V protein has for PS. Protocol B was applied to these studies and Figure 2.10 contains the volumes and concentration of incubation materials and click reagents. We observed predictable labeling that was dependent on PS content alongside reasonable background labeling to zwitterionic PC with equal probe content (6% of **5**). This preliminary study was early support for the validity of our lipomimetic platform.

No-probe liposomes were tested as well (CO, C4, C8, Figure 2.9) during proof-of-concept studies to be sure that labeling depended on the functionality of our probes. Gels were stained with

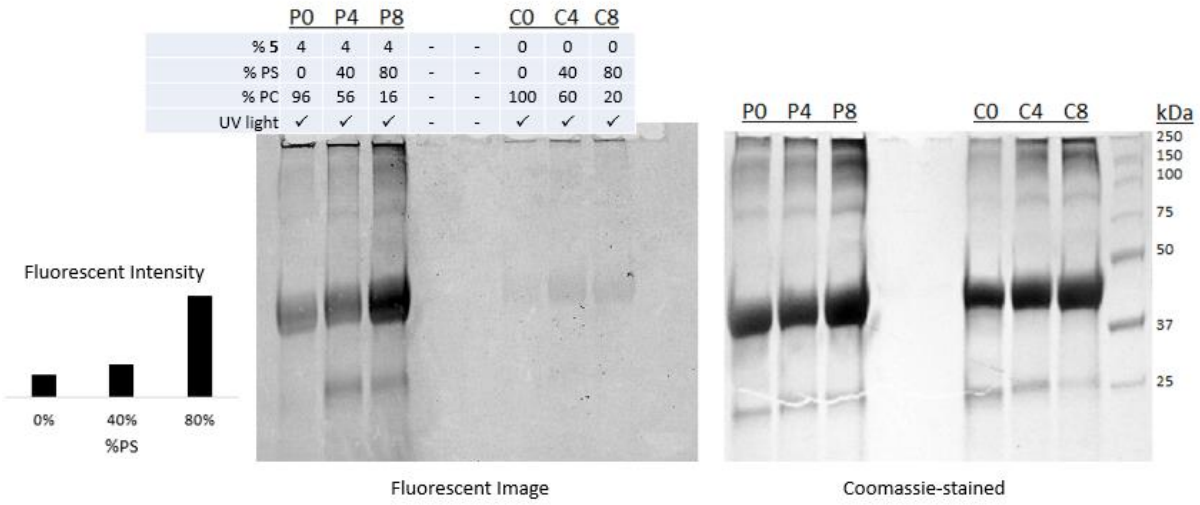

Figure 2.9: A lipomimetic proof of concept SDS-PAGE experiment. GP **5** was used at 4% to screen Annexin V affinity as a function of PS content. Fluorescence intensity is quantified (to the left) for PO, P4 and P8 samples. No-probe controls confirm probe functionality and coomassie-stained gels confirm equitable protein content. Protocol B, no sonication

Coomassie blue to be sure we had equitable protein content in each lane and that increased fluorescence was not attributed to increased protein retention. Quantification, such as can be seen in Figure 2.9, used imageJ software and suggested labeling in the case of PS-Annexin V might have a threshold-type increase when PS composes most of the membrane. Most importantly, the results in Figures 2.8 and 2.9 show that labeling is dependent on both our probe and the presence of target lipids. We built upon this proof-of-concept study by screening the HIV capsid protein CA, of which significantly less is known than Annexin V, with our lipomimetic assay.

CA protein was generously prepared by members of Dr. Francisco Barrera's research group, prepared under the supervision of Dr. Daiane Alves (T24 human cancer cell extracts were also prepared by Dr. Alves as described in section **2.3**). It has been established that CA requires interaction with lipid membranes to fold properly[237] and self-assemble into capsid structures, with specific affinity for anionic lipids such as PA.[238] We tested CA in the same manner as Annexin V experiments, the details for which are presented in Figure 2.10 and generally follow Protocol B.

Again, lipomimetic studies with CA suggested that our assay worked to qualify the lipid affinities of proteins, as can be seen in Figure 2.11. When PA is present in the membrane without probe **5**, or when probe **5** is present in the membrane without PA, minimal background labeling is

Lipo-somes 5 mM	protein 200 µg/ml	15 mM $CaCl_2$	10% SDS in 1X PBS	5 mM TCEP	1.7 mM Ligand	50 mM $CuSO_4$	3 mM Rh-N_3
40 µL	40 µL	4 µL	8 µL	3.5 µL	12 µL	12 µL	4 µL

Figure 2.10: **Volumes of incubation ingredients and click reagents for lipomimetic studies in isolated proteins**

observed. When we combine our probe and our chase lipid, however, CA is recruited to the membrane by PA where it may then be labeled by nonspecific probe **5**. Additional results from lipomimetic assays with CA and Annexin-V are presented in section **2.3.b:** *Additional experimental data*.

DAG-based labeling in lipomimetic studies using generic probe 7

The lipomimetic approach with diazirine probe **7** achieved selective labeling that depends on the percent of DAG incorporated into the liposomes. This work was aided by Kenneth Lum of the Cravatt lab at TSRI. Our work at TSRI was the culmination of numerous experiments to optimize our protocol. DAG-specific proteins were visualized by fluorescent SDS-PAGE experiment (Figure 2.12) in which we screened soluble membrane fractions of human embryonic kidney cells 293 (Hek) lysates. All liposomes, including controls, contain 10% PS as a binding cofactor for DAG. A few bands representing ~20 kDa proteins are labeled intensely by membrane-bound probe **7** when there is 16% natural DAG in the membrane. These DAG-specific bands vary in intensity when DAG concentration drops to 8% and continue to do so at or below 4% DAG, all but

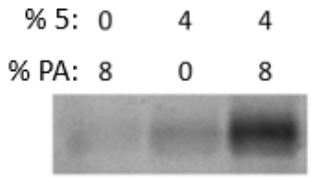

Figure 2.11: **Fluorescent image of a lipomimetic PA study screening the HIV-1 capsid protein CA.** CA protein binds to liposomes preferentially in the presence of PA. Concentrations of natural PA and **5** are indicated, and the remainder of the liposomes are composed of PC. Protocol B, no sonication

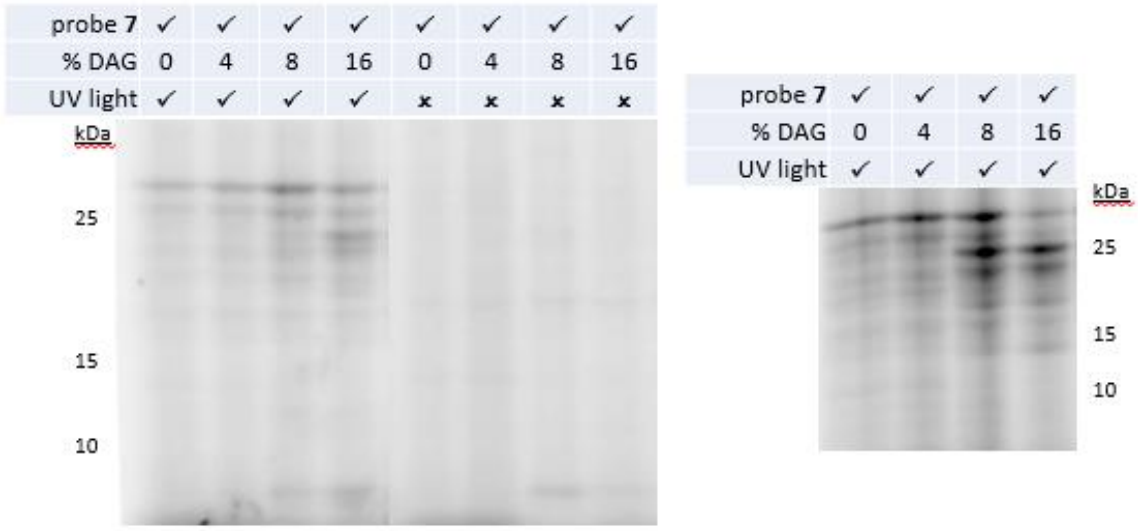

Figure 2.12: **A lipomimetic DAG study in Hek cell extracts with DAG-specific protein labeling.** Fluorescent image of experimentation performed at TSRI. UV+ samples shown in duplicate. Natural DAG preferentially recruited low kDa proteins from the soluble fraction of Hek extracts. Probe **7** present at 8% in the liposomal membranes. Entire gel images can be found under Experimental data. Protocol A.

disappearing at 0% DAG. Controls that lacked UV irradiation showed that the labeling depended on photoactivation of the diazirine group, the no-DAG control in the far-left lane of Figure 2.12 shows that labeling was not due to nonspecific dye interactions in irradiated samples.

We proceeded to see if DAG probe **3** (Figure 2.2) would label similar bands to non-specific probe **7** when DAG was present in the membrane. DAG probe **3** was also subjected to competitor liposomes that contained no probe. Competition liposomes with DAG competed away labeling more readily than competition liposomes without DAG, as can be seen in Figure 2.13. Figure 2.13 also shows the reproducibility of the selective labeling as lipomimetic treatment groups elevate their DAG content. Again, all liposomes including the competition samples contain 10% PS. These studies were also performed at TSRI and entire gel images are presented in the Experimental data section.

Lipomimetic labeling with other chase lipids

The lipomimetic approach used to investigate DAG has demonstrated specificity in complex mixtures of proteins only with diazirine-based probe **7**. Lipomimetic results using benzophenone crosslinking non-specific probes, such as **5** or **6**, are promising but inconsistent. Increases in

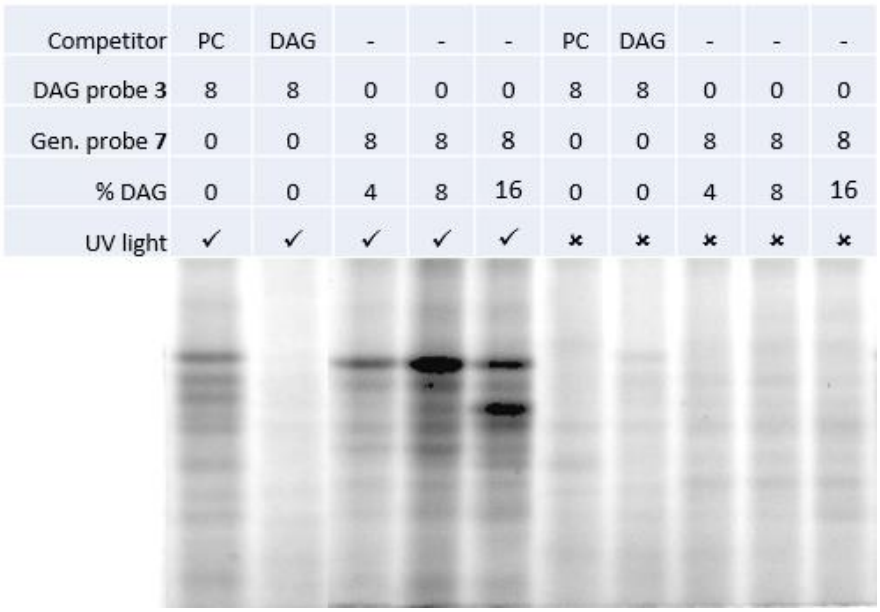

Figure 2.13: **A lipomimetic and competitive lipospecific DAG study in Hek cell extracts with DAG-specific protein labeling.** Fluorescent image of an experiment performed at TSRI in Hek cell lysates. The lipomimetic trend observed in Figure 2.12 is replicated here. Results of the lipospecific competition study suggest some of the proteins labeled by our DAG probe are attracted to natural DAG as well. Full gel study, in duplicate, is included in section **2.3.b**. Protocol A

labeling are either indiscriminate or the bands are not well enough resolved for this assay to be quantitative using these particular probes. However, we may draw the qualitative conclusion that signaling lipids such as DAG, PS or PA generally increase protein recruitment to liposomal membranes.

Figure 2.14, for example, shows an early lipomimetic SDS-PAGE experiment where the increase in labeling observed with the addition of PA was nearly proteome-wide when screening t24 human cancer cell extracts. A PIP_3 lipid was also used to screen t24 extracts, as seen in Figure 2.15, and in this case the labeling was dose-dependent and maxed out at only 2% PIP_3, which is consistent with PIP_3's presence at very low abundancies in natural membranes. In general, when choosing percentages at which to screen different chase lipids, we considered their natural abundance in addition to their tolerable percentages in terms of forming stable bilayers. Replicates of the study represented in Figure 2.14 were also clicked to a biotin for identification via mass spectrometry (MS). However, sample preparation was made challenging by the increased lipid

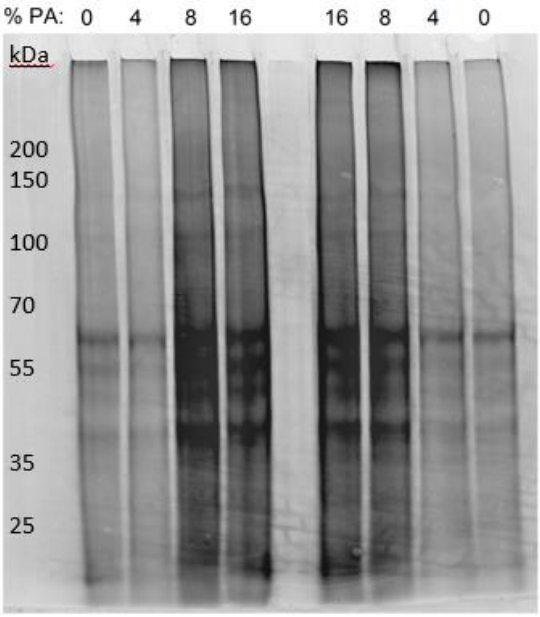

Figure 2.14: **A lipomimetic PA study in t24 cancer cell extracts.** Fluorescent image shown of study in duplicate. 4% of probe **5** used in all liposomes/lanes, PA as indicated, and the remainder of the liposomes comprised of PC. The increase in labeling is indiscriminate and appears threshold-based, Extracts are from t24 human cancer cells. Protocol B, no sonication

content in our system and protein hits were below significant levels as a result. The current state of experiments that culminate in MS is discussed in Section 2.4: *Future Work*.

Lipospecific studies with diazirine DAG probe 3

Figure 2.16 shows selective labeling with diazirine DAG probe **3** when compared with GP **7**, which has a similar architecture. benzophenone-based DAG probes have thus far proven unsuccessful—or inconsistent—at labeling proteins in a liposomal context. We have observed a ~175 kDa protein that was selectively labeled by **3** but not by corresponding generic probe **7**, as can be seen in Figure 2.16 where a narrow band fluoresces near the top of the gel only in the lanes where T24 extracts were treated with DAG probe **3**. Probe **20**, which is a crosslinking only probe described later in 'Future work' was included in this experiment, which used size exclusion columns (SECs) to purify samples after crosslinking but before click enrichment.

SECs selectively enrich large molecules or vesicles by trapping small molecules and salts in the pores of the column media: Sephadex™ beads. Size-exclusion based liposomal protein extraction

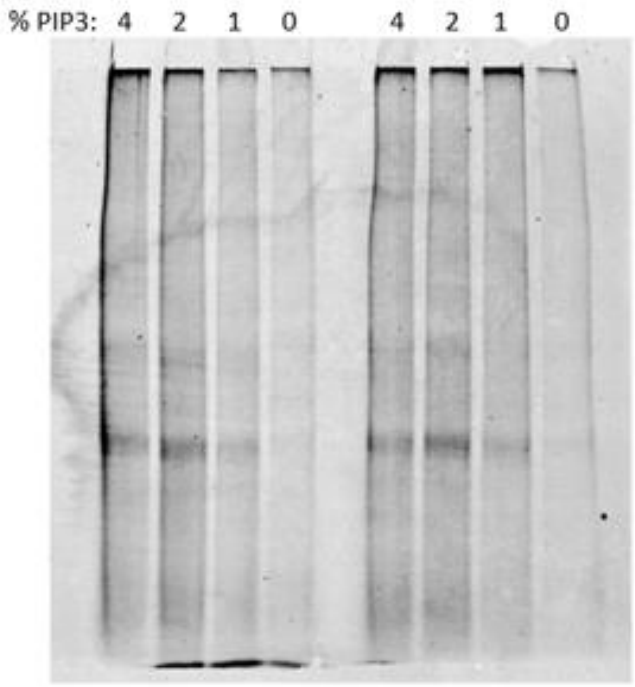

Figure 2.15: **A lipomimetic PIP_3 study in t24 extracts.** Fluorescent image shown of study in duplicate. 4% of probe **5** used in all lanes, PIP_3 lipid as indicated with the remainder PC. Quantification of intensity of the darker band was done using imageJ software and error bars are standard error based on the two replicates shown. Protocol B, no sonication

(SELPE) isolates membrane-bound proteins via their dramatically increased size when tethered to liposomes following photocrosslinking. When applying the lipomimetic or lipospecific platorm, SELPE experiments may selectively enrich DAG-binding proteins by trapping them on to large vesicles and carrying them through the SEC when natural DAG or DAG probes are used (Figure 2.16). SDS-PAGE followed by staining could test for preferential enrichment based on the presence of photoaffinity tags and chase lipids, potentially eliminating the need for click enrichment and fluorescent imaging. SELPE is a nascent platform, mentioned here to qualify Figure 2.16, and will be touched on again in *future work*. The experimental results in Figure 2.16 represent an early attempt to test SEC for its potential use in our unique liposomal chemical biology platforms. Interestingly, the band labeled by DAG probe **3** in Figure 2.16 was not labeled by PA probe **4**. We repeated this study with **4** and results are presented on the next page in Figure 2.17. This time, the SEC step was taken out to be sure that the regular protocol could produce the same result. Labeling by **3** was faint, but the same band was again labeled, which was definitively

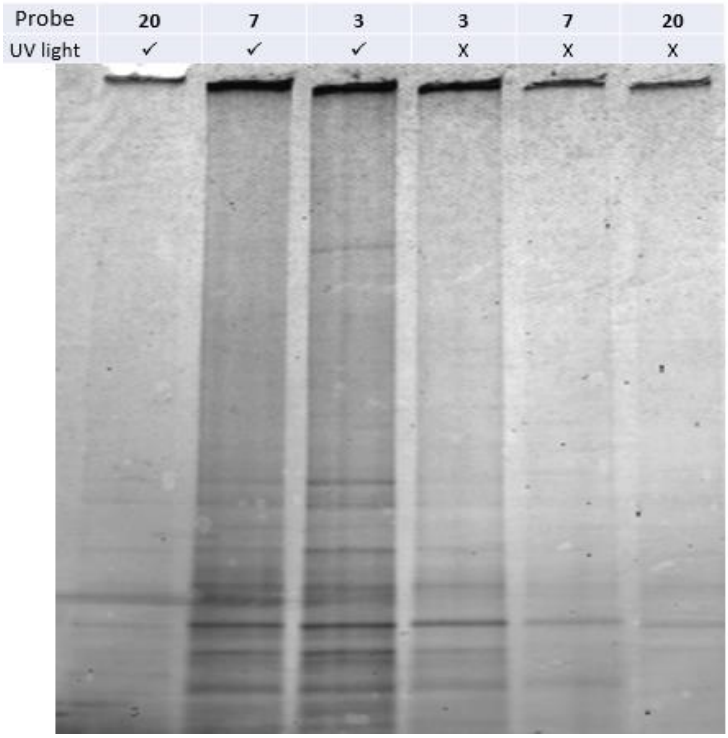

Figure 2.16: **A lipospecific DAG experiment in T24 cancer cell extracts using size exclusion column enrichment (SEC) pre-click.** Fluorescent image of a lipospecific DAG experiment in T24 extracts is hown. A crosslinking only probe was also screened and samples were enriched via SEC pre-click. No-UV controls show zero background for the band of interest (175 kDa). Protocol A, SEC details can be found in section 2.4: *Future Work*

not present in the lanes treated with the other probes. The experiment in Figure 2.17 also made use of competition liposomes with PA, DAG or only PC (all competitor liposomes contain 10% PS) to see if probe-specific bands could be competed off by the corresponding natural lipid. Some DAG probe-specific labeling was also observed in the low kDa area where selective lipomimetic labeling was observed in Hek cell lysates (Figure 2.12). Ultimately, the labeling in Figure 2.17 is too faint to draw any conclusions from the competition assay. Nevertheless, the same high kDa band labeled by **3** but not **7** is again observed. It bears repeating that at this point we continued to observe labeling increases that were protein specific rather than proteome-wide when employing Protocol A. Moreover, the labeling was repeatable with or without the SELPE addendum. Thus, SELPE remains a promising avenue for future work using our liposomal protein labeling platforms.

Lipospecific studies with PA probes

Amide-linked versions (instead of triazole) of probes **1** and **2** were synthesized but showed no labeling (see section **2.3.b**). PA probe **2**, Figure 2.2, required incorporation at 15% or more of the liposomal membrane to label selectively over generic probe controls in yeast extracts. Labeling was faint and we were unable to confirm that it was PA-specific. In T24 extracts, labeling was non-existent until we also added natural PA to the membrane as can be seen in Figure 2.18 (next page). In this case, we observed a less intense proteome-wide increase in labeling, similar to lipomimetic studies that used PA as the chase lipid with a much lower percentage of generic probe **5**. Treatment liposomes demanded incorporation of probes at high percentages to bring about labeling when screening extracts of the yeast cell line *saccharomyces cerevisiae*. Figure 2.19 (page after next) demonstrates this where 20% incorporation of a PA probe into treatment liposomes brought about labeling of an entirely different band (band 1) than seen in the lipomimetic PA experiment ran on the same gel that only labeled band 2.

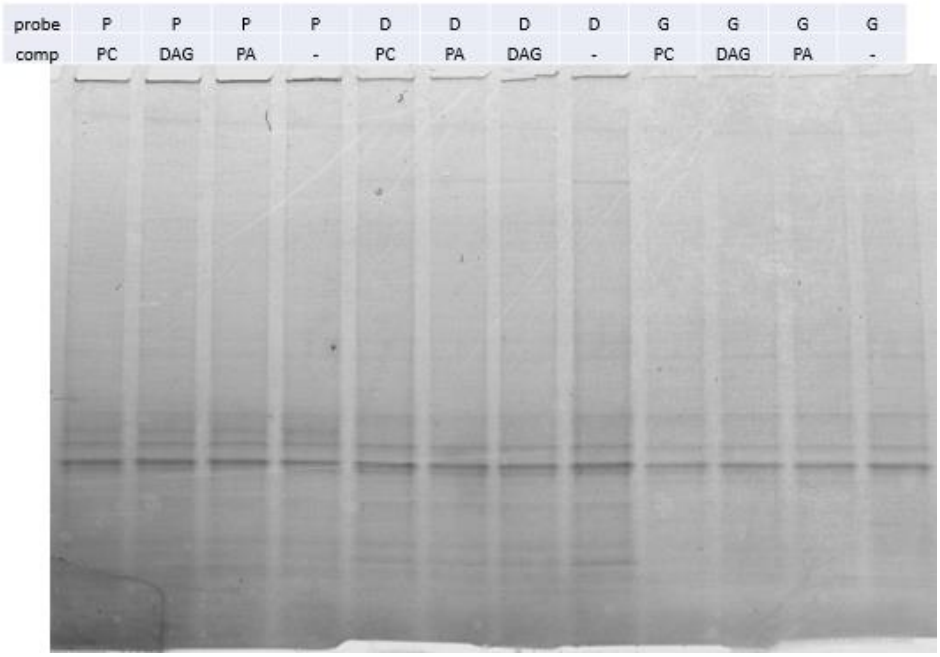

Figure 2.17: **A competitive lipospecific DAG/PA experiment.** Fluorescent image of a study in t24 extracts using PA probe (P) **4**, DAG probe (D) **3** and generic probe (G) **7**. Low kDa proteins are labeled by **3** in a similar region to those labeled in lipomimetic DAG experiments (Figure 2.10) and a high kDa protein is labeled by **3** (5th lane from right).

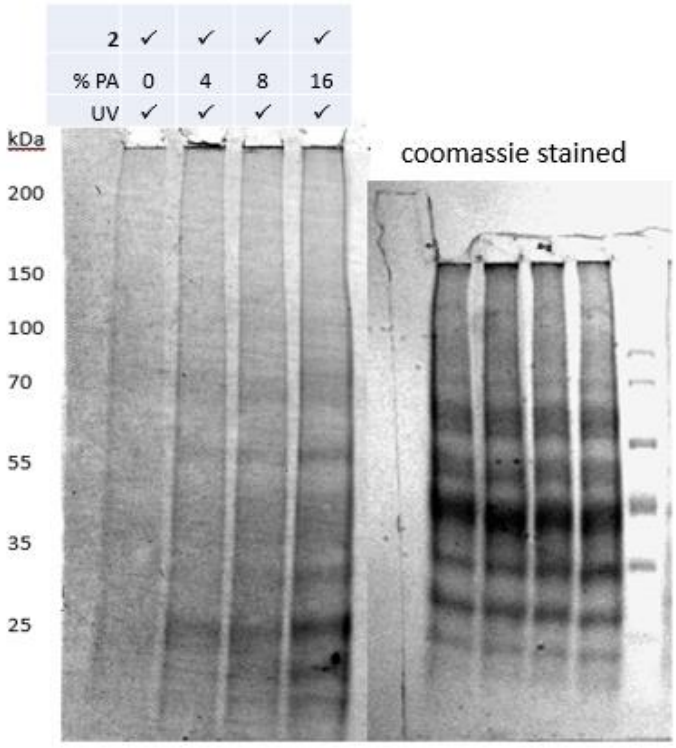

Figure 2.18: **A lipospecific PA study in t24 extracts.** Fluorescent and stained images of a study using 15% of PA probe **2**. Liposomes have gradient amounts of PA and the remainder is PC. The stained gel shows equitable protein content in all lanes. Protocol B, no sonication.

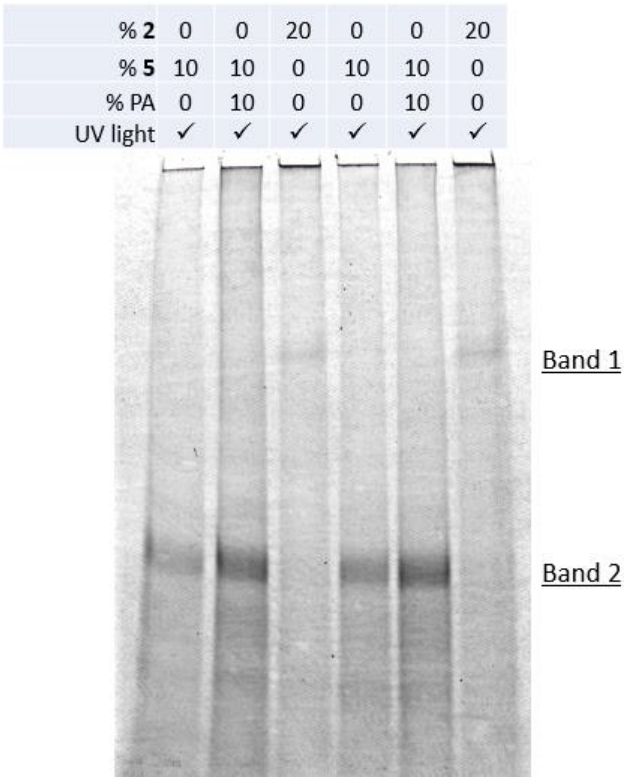

Figure 2.19: **A lipospecific PA study in yeast cell extracts.** *S. cerevisiae* yeast extracts are screened, image is a fluorescent scan of the study in duplicate. This study also tests a lipospecific PA probe (**2**) with a similar architecture to the lipomimetic generic probe **5**. Liposomes with **5** and PA label more intensely than probe only liposomes. The PA specific probe, however, labeled a solitary separate protein with no overlapping background. All liposomes contain 10% PS and the remainder is PC. Protocol B, no sonication

Conclusion

We have developed a robust platform for discovering protein-lipid interactions in a biomimetic membrane context. Assays that make use of large clickable benzophenone crosslinking headgroups can qualify the proteomic impact of DAG content, as well as other signaling lipids, but lack precision. Probes that make use of smaller diazirine crosslinking headgroups with discreet clickable tails are capable of more precise identification of protein-lipid binding interactions. Lipomimetic experiments have isolated low kDa proteins that appear to be labeled as a function of natural DAG content in the liposomes. Lipospecific experiments have isolated a high kDa protein band that selectively binds liposomes incorporating a DAG-based probe. The lipomimetic DAG studies represented in Figure 2.12 were repeated at TSRI with the clicking of a biotin-alkyne instead of a fluorophore-alkyne. These samples were then enriched via avidin chromatography, followed by digestion and MS—all performed by Kenneth Lum according to previously reported protocols.[215] Preliminary results are promising and we are currently awaiting more thorough analysis by Mr. Lum to determine if our lipomimetic studies identified known and/or novel DAG-binding PMPs. These MS studies are addressed in more detail in Section 2.4**:** *Future work*.

2.3: Materials, methods and optimization

Solvents and reagents were purchased from Sigma-Aldrich, Acros Organic or Fisher Scientific and used as received. Dry solvents were obtained using an Innovative Technology, Inc. Pure Solv delivery system and stored on molecular sieves. Column chromatography was done on 230-400 mesh silica gel from Sorbent Technologies. Characterization by nuclear magnetic resonance (NMR) was performed on Varian Mercury 300 MHz or Varian VNMRS 500 MHz spectrometers. High resolution mass spectrometry (HRMS) characterization was done on either a JEOL DART AccuTOF spectrometer (HRMS-DART) or an Exactive Quadrupole-Orbitrap spectrometer (HRMS- Orbi).

Synthesis of key intermediate 15 (Figure 2.4)

Syntheses of compounds **10**, **11**, and **12** were adapted from a previously reported procedure,[178] which used an acetonide protecting group in place of the cyclopentyl acetal used here.

Diethyl (2*R*,3*R*)-1,4-dioxaspiro[4.4]nonane-2,3-dicarboxylate (10)

Diethyl-L-tartrate (8.08 mL, 39.2 mmol) was added to 150 mL of toluene while stirring in a flame-dried round-bottom flask, followed by cyclopentanone (16.59 mL, 196 mmol) and then *para*-toluenesulfonic acid (*p*-TSOH, 744 mg, 4.32 mmol). The reaction mixture was heated to 135 °C under reflux with a Dean-Stark trap. After cooling to room temperature (rt), sodium carbonate (659 mg, 7.82 mmol) was added and stirring was continued for 10 min. Next, magnesium sulfate ($MgSO_4$) was added until no clumping was observed (~100 mg) followed by another 5 minutes of mixing. The solution was filtered, concentrated by rotary evaporation and then left under vacuum overnight and reduced to diol **11** without further purification. To confirm the formation of **10**, the crude was solvated in dichloromethane (DCM) for column chromatography on silica gel using 0-20% ethyl acetate (EtOAc) in hexanes (hex). **10** is collected as a yellow oil. ^{1}H NMR (300 MHz $CDCl_3$) δ 4.67 (s, 2H), 4.22 (q, *J* = 7.1 Hz, 4H), 2.01-1.74 (m, 4H), 1.74-1.61 (m, 4H), 1.26 (t, *J* = 7.1 Hz, 6H). ^{13}C NMR (126 MHz $CDCl_3$) δ 169.63, 123.31, 76.99, 61.84, 36.58, 23.44, 14.10. HRMS-DART: [M+H]+ calculated for $C_{13}H_{20}O_6$: 272.1260, found: 272.1285

((2*S*,3*S*)-1,4-Dioxaspiro[4.4]nonane-2,3-diyl)dimethanol (11)

Lithium aluminum hydride (4.460g, 117.6 mmol) was added to 0 °C anhydrous tetrahydrofuran (THF, 100 mL) with stirring in a flame-dried, three-neck round bottom flask. The suspension was kept in a dry N_2 atmosphere. Crude diester **10** (10.2 g, ~39.2 mmol) was dissolved in 100 mL of anhydrous THF and added dropwise to the reaction over 30 min. The reaction mixture was stirred at 0 °C for 2 h, then at room temperature for 2 h, before cooling back to 0 °C. The reaction mixture was then quenched carefully with 5 mL water, 5 mL of 10% NaOH, and 15 mL more of water. Stirring continued for 30 min while the quenched mixture warmed to rt. To dry the reaction, anhydrous $MgSO_4$ was added with stirring until clumping was no longer observed. The mixture was filtered to remove particulates and then concentrated by rotary evaporation. The crude was solvated in DCM for column chromatography with silica gel packed with hex and the following eluents: 50/50 EtOAc/hex, 75/25 EtOAc/hex, 100% EtOAc, 10% methanol (MeOH) in EtOAc. Compound **11** was isolated as a clear oil (3.833g, 53% yield over two steps). ^{1}H NMR (500 MHz $CDCl_3$) δ 3.89-3.84 (m, 2H), 3.71-3.66 (m, 4H), 3.36 (br.s, 2H), 1.84-1.71 (m, 4H), 1.70-1.557 (m, 4H). ^{13}C NMR (126 MHz $CDCl_3$) δ 119.31, 78.34, 62.42, 37.25, 23.37. HRMS-DART: [M+H]+

calculated for $C_9H_{16}O_4$: 189.1048, found: 189.1079

((2*S*,3*S*)-3-(Azidomethyl)-1,4-dioxaspiro[4.4]nonan-2-yl)methanol (12)

Diol **11** (3.8332g, 20.4 mmol) was solvated in 100 mL of anhydrous DCM. While stirring, silver (I) oxide (Ag_2O, 7.09 g, 30.6 mmol), tosyl chloride (4.28 g, 22.44 mmol), and finely crushed potassium iodide (.339 g, 2.04 mmol) were added in succession to create a mono-tosylated intermediate. The reaction was stirred at rt for 2 h and then filtered through a silica plug using DCM to be concentrated on rotary evaporator. The concentrated filtrate was dissolved in anhydrous dimethylformamide (DMF, 100 mL) and, with stirring, sodium azide (NaN_3, 3.32 g, 51.07 mmol) was added. The reaction was stirred at 85 °C overnight and then cooled to rt, extracted with EtOAc, dried with $MgSO_4$, and then concentrated under rotary evaporation. Crude **12** was resolvated in $CHCl_3$, washed 4 x with 100 mL water and 1 x with 100 mL brine before being dried with $MgSO_4$, concentrated by rotary evaporation and then resolvated in DCM for flash chromatography on silica gel packed with hex and eluted with 50/50 EtOAc/hex. Compound **12** was collected as an impure yellow oil and used without further purification. Beforehand, ^{1}H NMR was used to confirm that diastereotopic glyceroprotons emerge and resolve as doublets of doublets, and MS further confirmed the presence of our target compound: ^{1}H NMR (300 MHz $CDCl_3$) δ 4.07-3.98 (m, 1H), 3.96-3.89 (m, 1H), 3.78 (dd, *J* = 3.9 Hz, 8.1 Hz, 1H), 3.65 dd, *J* = 3.8 Hz, 7.3 Hz, 1H), 3.51 (dd, *J* = 4.6 Hz, 8.8 Hz 1H), 3.35 (dd, *J* = 4.6 Hz, 7.8 Hz, 1H), 2.09 (br. s, 1H), 1.91-1.76 (m, 4H), 1.76-1.60 (m, 4H). HRMS-DART: [M-N_2+H] + calculated for $C_9H_{15}N_3O_3$: 186.1052, found: 186.1085

(2*S*,3*S*)-2-(Azidomethyl)-3-(((4-methoxybenzyl)oxy)methyl)-1,4-dioxaspiro[4.4]nonane (13)

Crude **12** (4.28g, 20.07 mmols) was stirred in 100 mL of 0 °C anhydrous DMF under N_2. Sodium hydride (NaH, .9633g, 40.14 mmol) was added carefully. The solution was stirred at 0 °C for 1.5 h, exchanging the atmosphere for N_2 several times while H_2 gas escaped. *Para*-methoxybenzyl (PMB) chloride (6.286g, 40.14 mmol) was added and the reaction progressed at rt for 3.5 h. The mixture was quenched with 5 mL of methanol. The solvent was removed by rotary evaporation and the concentrated crude was then solvated with EtOAc (250 mL) and washed with 100 mL of ammonium chloride, 100 mL of brine, and then 150 mL of water. The organic layer was dried by

$MgSO_4$, filtered and concentrated to yield the crude product **13**. Some impurities were removed by column chromatography on silica gel pecked with hex and gradient EtOAc/hex elutions up to 75% EtOAc. Impure **13** was used for the next reaction without further purification. Before moving on, ^{13}C NMR and MS were used to confirm successful PMB protection. ^{13}C NMR (126 MHz $CDCl_3$) δ 159.29, 129.32, 119.89, 113.81, 77.90, 76.59, 73.23, 71.43, 69.93, 55.26, 52.30, 37.31, 23.45. HRMS-DART: $[M-N_2+H]+$ calculated for $C_{17}H_{23}N_3O_4$: 306.1627, found: 306.1656

(2*S*,3*S*)-1-Azido-4-((4-methoxybenzyl)oxy)butane-2,3-diol (14)

Impure **13** was re-dissolved in 20 mL of MeOH, followed by the addition of 2 g of *p*-TSOH (10% w/v) and mixing for 24 h. The reaction mixture was concentrated by rotary evaporation, solvated in 150 mL of EtOAc and washed with 150 mL of water (x 2) and 100 mL of brine (x 1). The organic layer was dried by $MgSO_4$, filtered and concentrated to yield crude **14**. Pure product was isolated as a colorless oil by column chromatography on silica gel packed with hex and eluted with 60-80% EtOAc/hexanes (1.77 g, 32% over 3 steps). ^1H NMR (300 MHz $CDCl_3$) δ 7.21 (d, J = 8.6 Hz, 2H), 6.83 (d, J = 8.7 Hz, 2H), 4.40 (s, 2H), 4.00 (br. s, 2H) 3.88-3.76 (m, 2H), 3.73 (s, 3H), 3.62-3.54 (m, 1H) 3.53-3.44 (m, 1H), 3.41 (d, J = 4.9 Hz, 2H). ^{13}C NMR (126 MHz $CDCl_3$) δ 159.23, 129.88, 129.48, 113.80, 73.02, 71.22, 70.92, 63.88, 55.20. HRMS-DART: $[M-N_2+H]+$ calculated for $C_{12}H_{17}N_3O_4$: 240.1158, found: 240.1189

1-(((2*S*,3*S*)-4-Azido-2,3-bis(hexadecyloxy)butoxy)methyl)-4-methoxybenzene (15)

Diol **14** (59.9 mg, 0.224 mmol) was mixed in 20 mL of dry DMF at 0 °C under N_2 atmosphere. While stirring, 40 mg of NaH (1.67 mmol) was added slowly. The solution was stirred at 0 °C for 1.5 h, exchanging the atmosphere for N_2 several times while H_2 gas escaped. 1-bromohexadecane (.24 mL) was added along with 80 mg of TBAI and the reaction was stirred at rt over night before being quenched with 2 mL of MeOH and then extracted with 100 mL of EtOAc. The organic solution was washed with water and brine, dried by $MgSO_4$, filtered and concentrated by rotary evaporation. The crude was solvated in DCM for Column chromatography on silica gel packed with hex and eluted with 0-10% EtOAc/hex to yield the pure product as a white powder (109.1 mg, 68%). ^1H NMR (300 MHz $CDCl_3$) δ 7.25 (d, J = 8.3 Hz, 2H), 6.88 (d, J = 8.3 Hz, 2H), 4.46 (s, 2H), 3.81 (s, 3H) 3.66-3.60 (m, 2H), 3.60-3.55 (m, 2H), 3.55-3.51 (m, 2H) 3.51-3.48 (m, 1H),

3.47-3.43 (m, 1H), 3.37-3.29 (m, 2H), 1.61-1.52 (m, 4H), 1.36-1.21 (m, 52H), 0.88 (t, *J* = 6.4 Hz, 6H). ^{13}C NMR (126 MHz $CDCl_3$) δ 159.23, 130.17, 129.26, 113.75, 78.97, 78.51, 73.07, 71.84, 71.44, 68.70, 55.23, 51.29, 31.91, 30.08, 29.69, 29.67, 29.64, 29.62, 29.49, 29.35, 26.10, 26.06, 22.67, 14.10. HRMS-DART: [M-N_2+H]+ calculated for $C_{44}H_{81}N_3O_4$: 688.6243, found: 688.6275

Synthesis of single azide-tail benzophenone probe 8 (Figure 2.5)

11-Azidoundecan-1-ol (17)

The starting material, 11-bromoundecanol (3 g, 11.94 mmol) was added to a flame dried round bottom flask and then taken up in 60 mL of dry DMF and stirred under argon gas while NaN_3 was added (1.553 g, 4.396 mmol). The reaction mixture was stirred for 3 h at 85°C. After cooling to room temperature, the reaction was diluted with DCM, washed with water, brine, and then 0.1 M HCl. The organic layer was collected and then dried with $MgSO_4$, filtered and concentrated by rotary evaporation to yield the pure product as a clear oil (2.7588 g, 92%). ^{1}H NMR (300 MHz $CDCl_3$) δ 3.64 (t, *J* = 6.6 Hz, 2H), 3.39 (t, *J* = 6.9 Hz, 2H), 1.90-1.79 (m, 2H), 1.61-1.52 (m, 2H), 1.45-1.24 (m, 14H). ^{13}C NMR (126 MHz $CDCl_3$) δ 62.95, 51.45, 32.64, 29.51, 29.41, 29.37, 29.10, 28.79, 26.67, 25.7.

11-Azidoundecyl methanesulfonate (18)

Starting material **17** (1.6617 g, 6.6164 mmol) was added to a flame dried round bottom flask and then taken up in 20 mL of dry DCM and stirred under N_2 gas at 0 °C. Pyridine was added (1.08 mL, 13.233 mmol) while mixing, followed by mesyl chloride (512 uL, 6.6164 mmol). The reaction mixture was stirred overnight at rt before washing with 20 mL of water and 1 mL of saturated ammonium chloride and extracting with DCM. The organic layer was concentrated by rotary evaporation and cleaned by flash chromatography using silica gel packed with hex and 10% EtOAc in hex as the eluent. The product was collected as a slightly impure yellow oil and used for the next reaction without further purification. ^{1}H NMR (300 MHz $CDCl_3$) δ 4.21 (t, *J* = 6.6 Hz, 2H), 3.25 (t, *J* = 7.9 Hz, 2H), 2.99 (s, 3H), 1.78-1.68 (m, 2H), 1.63-1.53 (m, 2H), 1.43-1.24 (m, 14H) HRMS-Orbi: [M+H]+ calculated for $C_{12}H_{25}N_3O_3S$: 292.1694, found: 292.196

1-Azido-11-iodoundecane (19)

Starting material **18** (194.2 mg, 0.6664 mmol) was added to a flame dried round bottom flask and then taken up in 15 mL of dry THF and stirred under argon gas while sodium iodide (NaI, 119.9 mg, 0.7997 mmol) was added. The reaction was refluxed at 60 °C overnight. After cooling to rt, the reaction was extracted with 8 mL of 6% sodium sulfate ($NaSO_4$), followed by 3 mL of $NaSO_4$. 20 mL of hex were added and the mixture was washed again with 10% $NaSO_4$ (5 mL) before the organic layer was collected and dried with $MgSO_4$ followed by filtration and concentration by rotary evaporation. Impurities were left behind by reverse trituration where hexanes were gently swirled over the dried crude product to selectively solvate and remove pure **19** as a clear oil (162.1 mg, 75% from **17**). ^{1}H NMR (300 MHz $CDCl_3$) δ 3.25 (t, *J* = 6.9 Hz, 2H), 3.22 (t, *J* = 7.0 Hz, 2H), 1.87-1.76 (m, 2H), 1.65-1.54 (m, 2H), 1.44-1.21 (m, 14H). ^{13}C NMR (126 MHz $CDCl_3$) δ 51.41, 33.53, 30.47, 29.39, 29.34, 29.11, 28.82, 28.50, 26.69, 7.28. HRMS-DART: $[M-N_2+H]+$ calculated for $C_{11}H_{22}IN_3$: 296.0797, found: 296.0794

(4-((11-Azidoundecyl)oxy)phenyl)(phenyl)methanone (8)

p-Hydroxybenzophenol (3.1 mg, 0.02 mmol) was added to a flame dried flask under argon atmosphere. 1 mL of dry DMSO was added followed by potassium bicarbonate (K_2CO_3, 5.0 mg, 0.02 mmol) and mixing for 5 min. TBAI (6.0 mg, 0.02 mmol) was added followed by mixing for 20 min. Compound **19** (6.0 mg, 0.02 mmol) was added next and the reaction was mixed at rt under argon for 4 h. The solvent was then removed by rotary evaporation and the crude was resolvated in 35% EtOAc/hex and purified by column chromatography using silica gel packed with hex and eluted with a gradient solvent system of 10% to 35% EtOAc/hex. Compound **8** was isolated as a white resin (4.3 mg, 71%). ^{1}H NMR (300 MHz $CDCl_3$) δ 7.81(d, *J* = 8.9 Hz, 2H), 7.75 (d, *J* = 7.0 Hz, 2H), 7.56 (t, *J* = 7.4 Hz, 1H), 7.47 (t, *J* = 7.7 Hz, 1H), 6.95 (d, *J* = 8.9 Hz, 2H), 4.03 (t, *J* = 6.6 Hz, 2H), 3.26 (t, *J* = 7.0 Hz, 2H), 1.85-1.78 (m, 2H), 1.63-1.58 (m, 2H), 1.51-1.44 (m, 2H), 1.40-1.27 (m, 12H). ^{13}C NMR (126 MHz $CDCl_3$) δ 195.56, 162.84, 138.34, 132.54, 131.80, 129.88, 129.69, 128.14, 113.98, 68.25, 51.47, 29.68, 29.48, 29.43, 29.31, 29.12, 29.10, 28.82, 26.69, 25.97. HRMS-Orbi: $[M+H]+$ calculated for $C_{24}H_{31}N_3O_2$: 394.2416, found: 394.25

General procedures for liposomal AfBPP

Liposome preparation

All lipids, apart from our synthetic probes, came from Avanti polar lipids. An Avestin lipofast-mini extrusion system was used for most Protocol B studies. We also tested T&T scientific Nanosizers™ and Avanti mini-extruders, the pros and cons of each are discussed herein. Detailed procedural guidelines for liposome formation are followed by a discussion of liposome preparation techniques.

The first step of liposome formation is the formation of lipid films. Stock solutions of bulk lipids, probe lipids, chase lipid and occasionally membrane binding cofactors (cholesterol or other chase lipids) in choloroform ($CHCl_3$) and/or methanol MeOH are combined. For our bulk lipid, PC, we used Egg-PC (mixed isomers). The DAG species we used was 1,2-dipalmitoyl-sn-glycerol. The PS and PA we used in our studies were batches of mixed isomers from porcine brain tissue and eggs, respectively. Below are the types of liposomes that would be formed for a lipomimetic experiment using a generic probe with DAG as the chase lipid.

- Control liposomes: 8% probe, 10% PS, 10% cholesterol and 72% PC (no DAG)
- Three sets of study liposomes: 4, 8 or 16% DAG (8% probe, 10% PS and 10% cholesterol in all) with 68, 64, and 56% PC respectively

To form such liposomes, stock solutions in $CHCl_3$ of PC (12.7 mM), PS (10 mM), DAG (5 mM) and a non-specific probe (5 mM) were formed in 1 dram glass vials, stored at -20 to -80 °C and used cold. A spreadsheet calculator (Figure 2.20) was created that outputs the volumes to be added from each stock solution to create each batch of liposomes. The spreadsheet takes stock concentrations, membrane composition by molar percentages, total desired moles of lipid, and final concentration of lipid molecules in solution to formulate both volumes of organic lipid stock solutions to be added to form lipid films, and the volume of aqueous media to be used for hydration. Following the example spreadsheet in Figure 2.20, the second column from the left has the amounts of stock solutions that would be combined to form lipid films for this particular liposomal treatment group.

Aliquots of each stock solution are added using pipet tips approved for use with non-fluorinated organic solvents, the solution is mixed thoroughly and then the solvent is removed by rotary evaporation. Solvent may be removed under a stream of nitrogen, however the added mixing by.

8GPC	uL	[mM]	nmols	% PC	% PS	% xx	% nL	% Probe	%Chol	
PC	17.0	12.7	216.0	72.0	10.0	0.0	0.0	8.0	10.0	
PS	3.0	10.0	30.0							
xx	0.0	5.0	0.0		nmols:	300.0		mM [Lipid]	3	
nL	0.0	5.0	0.0		uL Buffer:	100.0		mM [probe	0.24	
Probe	4.8	5.0	24.0					effective mM [probe]:		**0.12**
Chol	3.0	10.0	30.0					uM [probe] w/ 10 uL tx		**12**

Figure 2.20: **A spreadsheet to output stock solution volumes for lipid film formation.** The spreadsheet in this example has been modified to also output effective concentrations during treatment (tx).

rotary evaporation helps to insure homogenized films are formed. Samples are kept away from UV light as much as possible to avoid premature excitation of crosslinking species. Once visible $CHCl_3$ is gone, residual solvent is removed under vacuum for at least 1 h or up to 24 hHydration in phosphate buffered saline (PBS), is done by adding the specified volume (100 µL in the example in Figure 2.20) directly to the vial and vortexing thoroughly. Next, heating and mixing at 60 °C for 40 min (or 40 °C for 1 h) allows for the formation of giant multilamellar vesicles (GMVs). Freezing at least once at this point to disrupt multilamellarity is always done. If sonicating to size the liposomes, one freeze is sufficient. The number of freeze-thaw cycles should be adjusted for desired size, as discussed shortly. For freeze thaw cycles, a dry ice/acetone bath in a Dewar flask and a water bath set to 40-60 °C are used. The samples are cycled back and forth using adapters that allow for pressure change to avoid cracking of the glass vials without splashing of acetone or water when moving samples between baths. To freeze-thaw up to 7 samples at once using separate vial adapters for each, I fabricated a rudimentary device using 1 dram vial lids and a metal-capped mason jar. Lids were screwed to the metal cap and holes were drilled through the lids and cap. This device works well but must have empty vials placed on any of the vial lids not occupied by sample to be sure that acetone or water does not splash into the mason jar and drip into samples during freeze-thaw cycles.

When sonicating using liposomal formulations such as those described in the example on the previous page, DLS data has suggested that 1 minute of bath sonication yields 800 nM vesicles with wide polydispersity indices (PDIs). 3 to 5 min of sonication yields 600 to 400 nM vesicles respectively with consistent results and PDIs around 0.2. It should be noted that the samples were

always frozen directly before sonication to avoid over-heating in the sonic bath. Experimentation to test results of sonication should be done for each instrument and repeated periodically.

Extrusion is done after the last thaw, samples have been kept frozen for up to a week after the final thaw before extrusion. Using disposable 3D printed Nanosizer™ extruders from T&T Scientific, as few as one extrusion gives fantastic results when analyzing by DLS. Using traditional extrusion techniques, such as the Lipofast mini extruder from Avestin there is a tradeoff between the PDI, which gets better with more extrusion, and the functional size of the vesicles, which deviates as the disposable filter warps with each pass through the extruder. I find that with the Avesti Lipofast-mini extrusion system 7-11 passes is optimal depending on the concentration of the sample and the filter size. With the Avanti Mini-extruder, I find that up to 19 passes is fine with no diminishing returns in terms of size consistency. This may be due to their added filter supports, which prevent warping of the disposable carbon filters. Liposomes are stored cold, but not frozen, and used within 48 hours after extrusion.

For Protocol B, hydration was followed by 10 freeze-thaw cycles to form unilamellar liposomes around 150nm in diameter, and finished by extrusion to ensure uniform diameters of between samples. Protocol A uses liposomes in the ~500nm diameter range formed as described above by one freeze-thaw followed bath sonication for 5 minutes. For sonication, DLS data began to indicate giant vesicles in the 3-4 μm range in varying amounts between samples. This was attributed to the waning vitality of the sonic bath at our disposal and we returned to freeze-thaw and extrusion. Protocol A now uses 2 freeze-thaws followed by extrusion to 800nm using the Avestin extruder system which produces uniform vesicles around 600 nm in diameter.

Preparing cell lysates

Human embryonic kidney cells 293 (Hek) lysates were prepared at TSRI by Kenneth Lum and normalized to 2 mg/mL protein content. T24 cell lysates were prepared from human bladder cancer tissue cultures by Daiane Santana Alves of the Barrera research group at the University of Tennessee and were also used at 2 mg/mL protein content. Cell lysates were stored at -80 °C until use. Previously reported methods for preparation of human cell lysates[239] were used and are outlined below.

Cells are grown to 80% confluency in appropriate media including 10% fetal calf serum (FCS).

After harvesting and sonicating the cells, Dounce homogenization in phosphate buffer is followed by 45 min of centrifugation at 1000,000 x g. The supernatant then contains the soluble fraction where the proteome should include the PMP targets of our liposomal AfBPP. If protease inhibitors are used they must be ethylenediaminetetraacetic acid (EDTA)-free to prevent chelation of copper, which undermines click reporting down the line.

Saccharomyces cerevisiae yeast cell lysates were prepared in house using a procedure adapted from previously reported protocols.[240] Dounce homogenizers are not used and we instead use 1 mL of glass beads for lysis of ~1g cell pellets in 3 mL of lysis buffer (50 mM potassium phosphate dibasic, 0.5 mM Na_2SO_3 and 1 tablet of EDTA-free protease inhibitor (Pierce™ mini-tablet) per 10 mL of lysis buffer). After adding the glass beads, samples are vortexed for 30 seconds followed by 30 seconds on ice (x8) and then centrifuged for 3 min at 2500 rpm. The supernatant is then aliquoted out and normalized to 2 mg/mL [protein] by running a Bradford content assay and diluting with 1x PBS.

General incubation procedure

In a clear 96-well plate, 10 μL of 4 °C liposomes are first added (followed by other incubation ingredients if following Protocol B). Cell extracts (~2 mg/mL) or proteins (~150 μg/mL) also at 4 °C, are added next followed by pipetting up and down to mix. If buffer is added last (Protocol A) then mixing is done after addition 1x PBS. The plate is covered and for Protocol A the samples sit in the dark for 1 h, for Protocol B the samples shake gently at 37 °C for 45 min. For competition assays, competitor liposomes (or buffer, for controls) are added first and incubated for half the duration, then treatment liposomes are added for the second half of incubation.

Photocrosslinking

After incubation, the samples are placed on ice and irradiated under long-range UV light (365 nm) for 10 min. Protocol A uses a Rayonet with two 8 watt UV lamps or, for experiments at TSRI (noted in text and Figures), a Stratagene, UV Stratalinker™ 1800 Crosslinker with 4 x 8-watt UV bulbs. Protocol B used a 4 watt benchtop UV lamp at 365 nm. Early studies began with 1 h of irradiation on ice. Based on consultation with experts Natalie Sadler and Aaron Wright at Pacific Northwest National Lab (PNNL), we determined this was unnecessarily long and likely

Reagent	Concentration	Mix Ratio
Ligand	1.7 mM	3
$CuSO_4$	50 mM	1
Click Reporter	5 mM	1
TCEP	50 mM	1

Figure 2.21: **Optimal click reagent concentrations and corresponding volumetric ratios.** To determine the volume of click mix to add to each sample, use a final ligand concentration of 50-100 uM.

deleterious. We shortened our incubation time to 10 minutes and increased protein retention with no decrease in labeling.

Click enrichment

After photocrosslinking, Protocol A samples are enriched with a click mix given in Figure 2.21. According to Protocol A, 6 μL should be added which gives us a final ligand concentration of 60 μM. A 100 μM final ligand concentration can also be used, and the slightly lower volume was chosen as part of our efforts to reduce background labeling by dye molecules. Samples are mixed and then sit at room temperature for at least one hour, after which they are stored at 4 °C until they are ready to be separated by SDS-PAGE.

For Protocol B, click is preceded by an SDS treatment, which is described in the optimization discussion shortly. After the SDS treatment, click proceeds as directed by Figure 2.7. Reagents are added in the order they appear in Figure 2.7: TCEP, click ligand, $CuSO_4$, click reporter (azide or alkyne) and the samples are mixed at room temperature for at least 1 hour. Once the click reaction is done, Protocol B proceeds to the solvent wash/precipitation. Solvent wash/precipitation and the gel-loading of the resultant pellets are also detailed in the upcoming optimization section. As mentioned, solvating the pellets in loading buffers was difficult at times and Protocol B made use of tip sonication to get the pellets into loading buffer solution, as needed. Experiments that did not sonicate the pellets are noted in their Figure legends. Tip sonication, when used, was done at 20% power with two 1 s bursts. Sample occasionally shot up the sides of the tubes, when this happened all samples were briefly centrifuged at low speed to move the liquid back to the bottom of the

tubes.

Gel loading/running

Clicked Protocol A samples proceed directly to gel loading by adding 30 µL of 4x gel loading buffer. Our 4X loading buffer is traditional for an SDS-PAGE experiment and the ingredients are as follows: 4 mL 100% glycerol, 2.4 mL 1M Tris/HCl pH 6.8, 0.8 g SDS, 4 mg bromophenol blue, 0.5 mL beta-mercaptoethanol, 3.1 mL H_2O. After adding buffer, samples are mixed and then sat at room temperature for at least 10 minutes (no heating). If there is need to delay gel running it is preferable to chill the samples rather than freeze to prevent protein precipitation.

Any SDS-PAGE system capable of separating proteins between 200 and 10 kDa will work well to culminate our experiments. We have used multiple systems with success and find gradient gels are ideal but fixed percentages at or near 10% also work well. Homemade extra-large 10% polyacrylamide gels were used for experiments at TSRI and loading was done by Presently, we are using Invitrogen™ Novex™ 8-16% Tris-Glycine Midi Protein Gels.

Fluorescent imaging and staining

Our imaging needs were met by a Typhoon fluorescent imager (General Electric) located in the University of Tennessee genomics hub headed by Sujata Argarwal. The Typhoon settings depend on the reporter dye being used, namely excitation/emission settings. The photo-multiplication tube (PMT) was left at 600 nm by default but adjusted as needed (lowered to account for excess intensity or raised if labeling was faint). A pixel size of 100 microns gave sufficient resolution when the sensitivity was set to normal. A multipurpose Biorad gel-doc station with a light table was used to capture pictures of stained gels. Experiments at TSRI made use of a similar Biorad Chemidoc® documentation station with fluorescent capabilities.

Staining was always done using Pageblue protein staining solution (coomassie) by soaking gels overnight and then destaining overnight in pure water followed by several rinses. Coomassie stain was recycled and used three times before discarding. Image editing for clarity was minimal and always linear. Stained gel images were occasionally obtained using free-standing light tables and mobile phone cameras. However, all stained images presented here were taken on the aformentioned Biorad gel-doc station.

Optimizing labeling studies

A major challenge in liposomal AfBPP is finding an appropriate amount of lipid content such that we may introduce our probes in a membrane context without interfering with the in-gel imaging that culminates our experiments. We began with 200 μL of 5.5 mM [lipid] content incubated with 100 μL of cell extracts. Coomassie staining revealed early on that proteins were not entering the gels and we attributed this to two possible causes. Either the lipids were hogging the SDS such that not enough remained to surround our proteins and impart the requisite charge for gel movement. Or, intact liposomes with covalently trapped proteins were too large to enter the gel. Large blobs of fluorescence as well as stained protein content were observed at the top of the gels to evidence this theory. After more experimentation, we settled on 40 μL of liposomes for treatment. We also found that using 40 μL of 2 mg/mL cell extracts gave us ample protein signal as judged by stained gels.

SDS treatment

An SDS treatment step was introduced to disrupt the membranes before the click reaction and to ensure the lipid content was occupied with SDS to allow for proper solvation of proteins in gel loading buffers following the click reaction. This allowed proteins to enter the gel, as confirmed by staining, but excess SDS was likely killing the click reaction and no labeling was observed. We optimized the amount of SDS and found 5-10 μL of a 20% w/v solution of SDS allowed click reporting and protein separation in gel (total SDS not to exceed 1.5% w/v). This SDS treatment helped keep protein content consistent in gel experiments when using 40 μL of 5 mM [lipid] liposomes to label proteins. When using this volume/concentration of liposomes, it was possible to label proteins with a little as 2% probe in the membrane.

After adding 20% w/v SDS solution, samples are heated to 70 °C for 10 minutes, followed by thorough mixing and sitting in a sonic bath for another 10 minutes. Samples proceed directly to click. The SDS treatment step enabled some early success with our Protocol And was still a part of our experimental procedures for some of the gel experiment results already presented, as noted in the Figure legends, including experimentation with Annexin V and CA proteins. Studies appearing in the additional experimental data later in this chapter made use of the SDS treatment.

Problems with consistency and repeatability remained so we sought advice from the Cravatt lab

at TSRI, as previously mentioned, and decided to increase probe concentration in the membrane to 8% and decrease the volume/concentration of liposomes drastically. This allowed us to go back to no SDS treatment given the significant reduction in overall lipid content. We had previously tested probe concentrations this high and knew we could form stable liposomes and label proteins intensely if not selectively. The concurrent reduction in the abundance of liposomes was predicted to afford more selectivity to our system by decreasing the amount of non-specific labeling. We discovered that 10 μL of 3 mM liposomes with 8% probe could allow for consistent labeling with trends that were DAG-dependent in lipomimetic studies. The volumes and concentrations we chose for optimal Protocol A are far from arbitrary. Rather, they were chosen based off observations of all previous liposomal AfBPP studies and manipulated to match the final probe concentration of successful non-liposomal ABPP experiments reported by the Cravatt group.[215]

Other incubation ingredients

For Protocol B we added $CaCl_2$ to a total of 1 mM (not counting calcium content of PBS or cell extracts.) Early successes came when the added $CaCl_2$ was a part of our experimental procedures. However, when we removed the added calcium, we observed no change in labeling. Calcium content of the extracts and/or PBS buffer was sufficient for our studies but future studies based around varied labeling based on ionic concentration would be interesting. Our system often incorporates anionic phospholipids such as PA or PS, so there was a risk of creating fusion between vesicles if calcium content was too high.[241] We now rely on the calcium present in our PBS buffer and cell extracts to support any C_1-DAG interactions in both lipomimetic and lipospecific experiments where DAG is the chase lipid.

Protocol B also used protease inhibitor (Pierce™ mini-tablets, EDTA free) to prevent protein degradation while liposomes and cell extracts incubated at 37 °C. Now that we incubate at room temperature we do not use protease inhibitor. Protease inhibitor, incidentally, may also have interfered with click reporting during early experiments that used cell extracts with EDTA-containing buffers. Natalie Sadler and Aaron Wright brought this to our attention through collaboration at PNNL, and we are grateful for The Wright Group's expert advice during the inception of this protocol. Presently, the incubation that has proven most successful is that which appears in Figure 2.6.

Click enrichment

Click reactions to enrich tagged proteins with dye molecules is another aspect of this protocol that underwent significant changes during optimization of these experiments. Initially, we were adding each reagent individually in the following order: tris (2-carboxyethyl) phosphine (TCEP) was added first followed by the $CuSO_4$, the click ligand and finally the azide or alkyne reporter. TCEP has two purposes. It reduces the copper II present in copper sulfate ($CuSO_4$) to copper (I) and also reduces disulfide bonds in proteins allowing them to unfold. It is possible that when we were clicking in this order the TCEP was being used by the proteins and not available in sufficient quantities to reduce the copper to its catalytic form.

Presently, we make a click mix where the ligand, which is tris(benzyltriazolylmethyl)amine (TBTA, Figure 2.22) predominates the volumetric ratio at ½ of the mix, as can be seen in Figure 2.8. In our system, it is particularly important to use an organic soluble probe in a 4:1 ratio of tetrabutyl alcohol (tBuOH) and dimethylsulfoxide (DMSO). The amount of the click mix to add to each sample is calculated based on a final ligand concentration of 100 uM. This ensures there is enough organic media to help solvate the lipid material, freeing the lipidic click tag for reaction with the reporter, which is also in organic media (DMSO). This was confirmed by switching to an aqueous click ligand, tris(3-hydroxypropyltriazolylmethyl)amine (THPTA), which was unable to catalyze the click reaction and we observed a general decrease in labeling when using THPTA in water, presumably due to an inefficient click reaction.

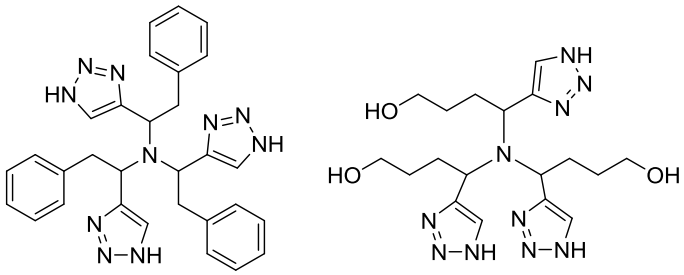

Figure 2.22: S**tructures of click ligands.** Left, tris(benzyltriazolylmethyl)-amine (TBTA). Right, tris (3-hydroxypropyl-triazolylmethyl) amine. (THPTA)

After the click mix is added, the samples are mixed and then sit in darkness for at least one hour. It is possible to delay moving to the gel running portion of the experimental procedure by chilling the samples or quenching with gel loading buffer. If the samples are to be chilled, they should not be frozen as this may cause labeled proteins to crash out of solution as the complex of protein with lipid probe and clicked dye is highly organic and the media is still predominantly aqueous. Best results are achieved by running immediately after clicking. If delay is necessary, better results are observed when samples are stored cold but not frozen between click and gel running. The simplification of the click portion of our protocol mirrors the general theme of our optimization efforts to circle back to the least complicated iteration of the protocol.

Precipitation/wash

A solvent wash/protein precipitation was used for all experiments that followed Protocol B. It allowed us to accomplish two goals: concentrate the protein content of our samples to amplify the signal of labeled PMPs, and remove lipid content allowing the SDS to do its job and usher protein content into PAGE for separation. Ultimately, the wash/precipitation proved unnecessary when only 10-20 μL of 3 mM [lipid] treatment liposomes are added to 40 μL of 2 mg/mL [protein] cell extracts with an additional 30-20 μL of PBS so that total protein concentration is 1 mg/mL and lipid concentration is below .75 mM with final click concentrations are based off of 50-100 μM ligand.

During optimization, however, the solvent wash and precipitation allowed us to clean up the samples, reduce background and produce less noisy gel images. The procedure generally included the addition of methanol, followed by vortex and light centrifugation, then chloroform followed by vortex and light centrifugation, and then water followed by vortex and longer centrifugation followed by removal of the upper phase. Another methanol wash and supernatant removal ended this clean up step. A step-by-step description of the solvent wash/precipitation with more details is as follows:

- add 200 μL MeOH, vortex, centrifuge at 9000XG for 30 sec
- add 150 μL $CHCl_3$, vortex, centrifuge at 9000XG for 30 sec
- Add 200 μL pure H_20, vortex, centrifuge for 3 min at 9000XG
- Remove upper phase, careful not to disturb interphase/bottom phase (leave the chunky

stuff in the middle alone, even if it means you don't get all of the upper phase out.)

- Optional: repeat this water wash
- Add 250 µL MeOH, vortex, centrifuge for 3 min at 9000XG
- Remove supernatant, don't disturb pellet
- Optional: Add 150 µL MeOH, vortex, centrifuge
- Remove supernatant, don't disturb pellet, you should be able to use a smaller pipet tip to remove the supernatant at this point (20-200, set) making it easier to leave the pellet unperturbed
- Let samples sit until solvent dries off (anywhere from 20 minutes to 2 hours, in the back of a hood), if you are in a hurry you can dry under a gentle nitrogen stream for ~10 minutes. Be careful not to blow the pellet out of the eppie, this is easy to do, it is safer to dry passively.)

Of the two optional steps above, the extra wash with water appeared, at first, to be the more effective at reducing background labeling. However, upon staining gel studies that employ an extra aqueous sample cleaning, we discovered unequal protein lane to lane. Figure 2.23, on the following page, depicts a lipomimetic study that employed a second water wash. The gel image is clean and we do see increased labeling at higher concentrations of natural DAG and PA, but the stained gel shows inequitable protein content between samples.

While the solvent wash was in place we felt it necessary to stain every gel experiment to be sure labeling was a product of preferential recruitment of proteins to the membrane and not preferential enrichment after click. We still use gel staining to confirm equitable protein content with each new experiment but as there is no longer experimental variation with propensity to vary protein total concentration there is no longer any variation between lanes of stained gels. As such, we have moved on to rely more on no-UV controls to ensure experimental accuracy and UV (-) controls are used in each replicate of every study.

Volumetric ratios of solvents and water were changed experimentally to see if we could retain the wash/precipitation without the inconsistencies. The volumes/ratios given above demonstrated the most promising results, however selectivity of the resultant gel experiments was not achieved until we decreased the lipid content and removed the wash/precipitation step from our experimental protocol. This simplification proved instrumental to allowing us to achieve

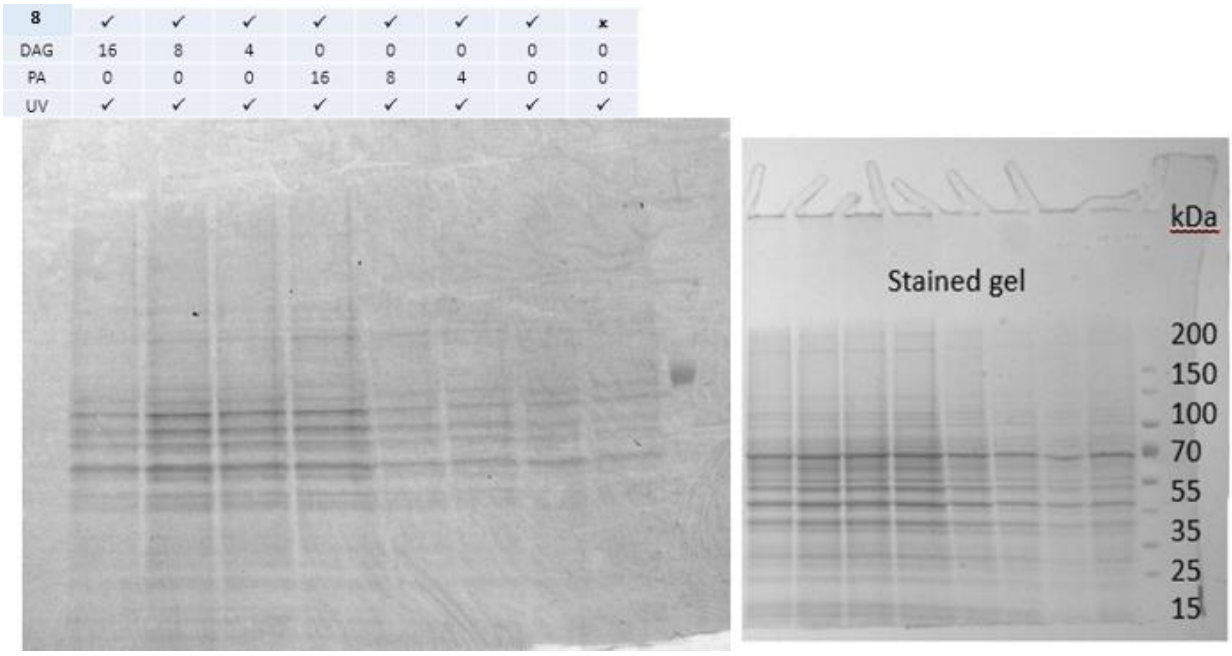

Figure 2.23: **A lipomimetic study performed using single tail benzophenone probe 8 with the solvent wash/precipitation step with an extra water wash and top phase removal.** Selective labeling appears when chase-lipids are added, however this experiment should protein inequities as evidenced by the control lanes to the right in the stained gel image (right). Protocol A.

reproducible selective labeling in lipospecific and lipomimetic studies, as presented earlier.

There are a few viable explanations as to why the wash/precipitation was ineffective. In principal, it is a delicate task to clean up our samples using any type of solvent wash without introducing intervening variables. This is because crosslinking indubitably introduces variable lipophilicity to labeled proteins and the added lipid character of labeled proteins may have caused labeled proteins—depending on the number of crosslinked probe molecules—to favor the organic layer during the solvent wash.

Gel loading procedure for Protocol B

The gel loading was also more complicated when our system employed the solvent wash/precipitation and reduced samples to a pellet. With the optimized system, there is no sonication or heating necessary before gel loading. Beforehand, solvating the dried pellets in loading buffer was sometimes challenging so sonication and heating were employed to ensure consistent protein loading. The general procedure with gel loading buffer ingredients is as follows:

- Add 25 µL of **buffer 1** (4 % SDS, 50 mM triethanolamine, pH 7.4, 150 mM NaCl), 15µL of **buffer 2** (50 % glycerol, 250 mM tris/HCl, pH 6.8, 10 % SDS, 0.03 % bromo phenol blue), **2 µL of B-mercaptoethanol**, vortex thoroughly, centrifuge lightly/quickly.
- Three 1s bursts with a probe sonicater on 20% power
- Heat at 100°C for 2 minutes, gently shake down to room temp and then load into gel

2.3.b: Additional experimental data

As it stands, this project has demonstrated that gel-based liposomal AfBPP is a viable strategy for qualifying lipid-protein interactions. We have shown that bifunctional lipidic ABPP probes may be presented liposomaly, but by doing discovered that the introduction of liposomes by Protocol B necessitates augmentation of mass spec protocols. We were unable to identify labeled proteins by click-derivatization with biotin for pull down mass spectrometry experiments to identify proteins when using Protocol B. Protocol A experiments that culminate in biotin reporting and mass spectrometry to quantify our protein hits will be useful not only for the raw information

provided but also to confirm the repeatability of our liposomal AfBPP platform. Along the way, we have observed interesting SDS-PAGE results in addition to those already presented, some of which are presented in this section.

Lipospecific DAG probe results

We found that probe architectures with triazole linkages, such as lipid-specific probes **1** and **2** performed better than probes with amide linkages to the glycerol backbone. However, corresponding generic probes **5** and **6** perform significantly better than their lipid-specific counterparts with bifunctional headgroups. The click reaction that resulted in the triazole linkage also eliminated the need for an additional synthetic step to reduce the azide at that position before conjugating to a carboxylic acid As alluded to earlier, we observed no labeling when probes **1** and **2** were linked to their bifunctional headgroups by an amide bond, as can be seen in Figure 2.24, compound **1a**. DAG probe **1a** was unable to label proteins even at 16% incorporation into the membrane, as can be seen in Figure 2.25. While the triazole-linked iterations of these probes showed labeling promise, they did not inspire confidence in their biomimetic capabilities. In retrospect, the bifunctional headgroup is very large, which may impede upon the probe's ability to naturally qualify lipid-specific protein-headgroup interactions.

Additionally, DAG probe **1** showed faint labeling and required incorporation at high percentages to bring the labeling up to appreciable levels, as can be seen in Figure 2.26. The incorporation of PA along with **1** did indeed potentiate labeling (**1** alone showed extremely faint labeling without the incorporation of PA). The increase in fluorescence was indiscriminate, like the results of lipomimetic PA studies with generic ester lipid probe **5** (Figure 2.15) and lipospecific studies with PA probe **2** (Figure 2.19)**.** This suggested to us that while **1** was capable of labeling proteins it was relatively nonspecific and had little to do with the hydroxyl headgroup meant to imitate natural DAG.

Lipomimetic DAG and PA studies using benzophenone probe 5

Much of the optimization efforts were with early probes that made use of benzophenone crosslinking headgroups, with click tags also included in the headgroups. Problems with nonspecific labeling, as discussed already, continued to undermine the utility of ester/ether linked

% gen. probe **5**	0	4	4	0	0	4	4	0
% DAG probe **1a**	0	0	0	4	0	0	0	4
% nat. DAG	4	0	4	0	4	0	4	0
% PC	96	96	92	96	96	96	92	96
UV light	✓	✓	✓	✓	-	✓	✓	✓

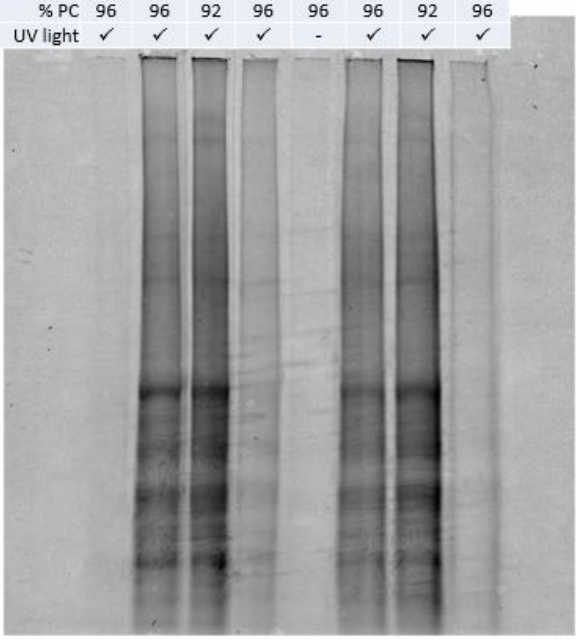

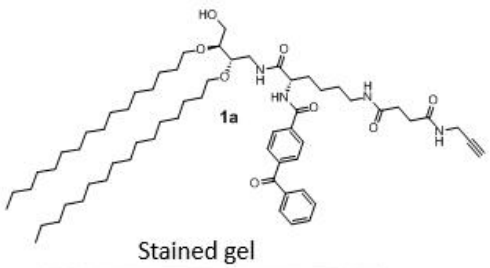

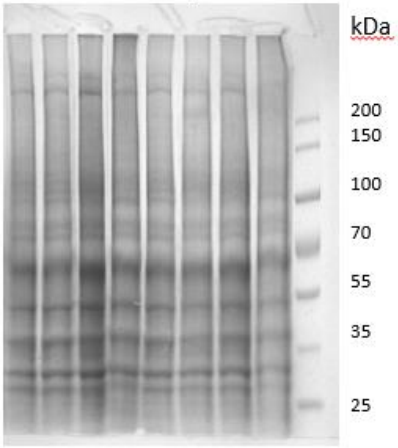

Figure 2.24: A gel experiment comparing lipospecific use of an amide-linked bifunctional DAG probe with a lipomimetic DAG study. We were hopeful that DAG probe **1a** with an amide linked bifunctional headgroup could selectively label proteins in a lipospecific manner. As can be seen, the amide linked DAG probed was unable to crosslink and enrich PMPs. Protocol B.

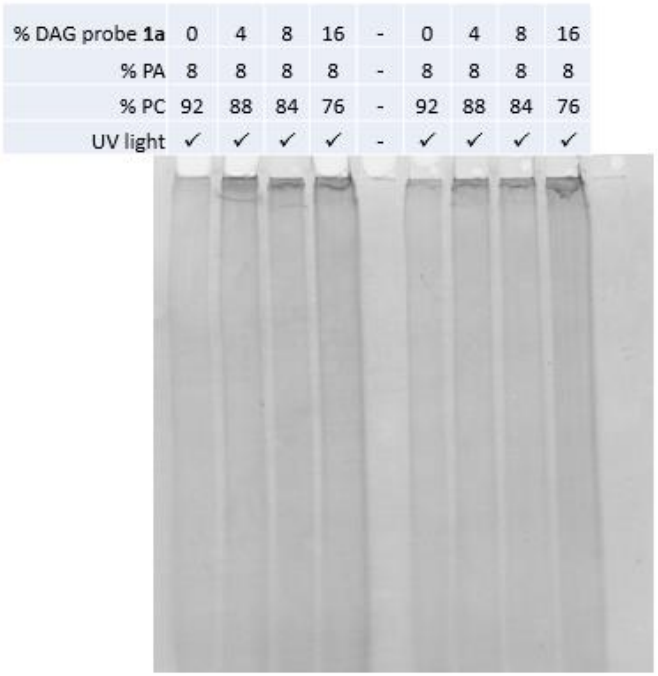

Figure 2.25: **Fluorescent image of a lipospecific study using amide-linked DAG probe 1a.** PA was used as an anionic binding cofactor. No labeling was observed. Protocol B.

benzophenone probe **5** even when we went back and applied optimal experimental conditions, as can be seen by the gel study represented in Figure 2.26.

Lipomimetic studies comparing the lipid affinities of HIV capsid protein (CA)

CA self-assembly is crucial for integrity of the HIV virus.[242] Recent AFM experiments have suggested that protein-lipid interactions between the capsid proteins and the viral envelope control the assembly of CA,[237] while earlier studies had already suggested CA has affinity for anionic lipids such as PA and PS.[238] In Figure 2.27 we have one of our early CA studies using PS before we implemented the SDS treatment step. Uneven protein loading lane to lane can be observed in the stained gel image. Least protein content is present in the lane with treatment liposomes containing the most PS (P8), despite this the labeling by these liposomes was most intense.

We optimized CA studies using PA. PA is cheaper than PS and exerts its effects at lower natural percentages than PS, therefore PA was a logical choice for a chase lipid in optimization studies. We began with 2 μL of SDS during the SDS treatment, by the time we increased it to 6 μL we

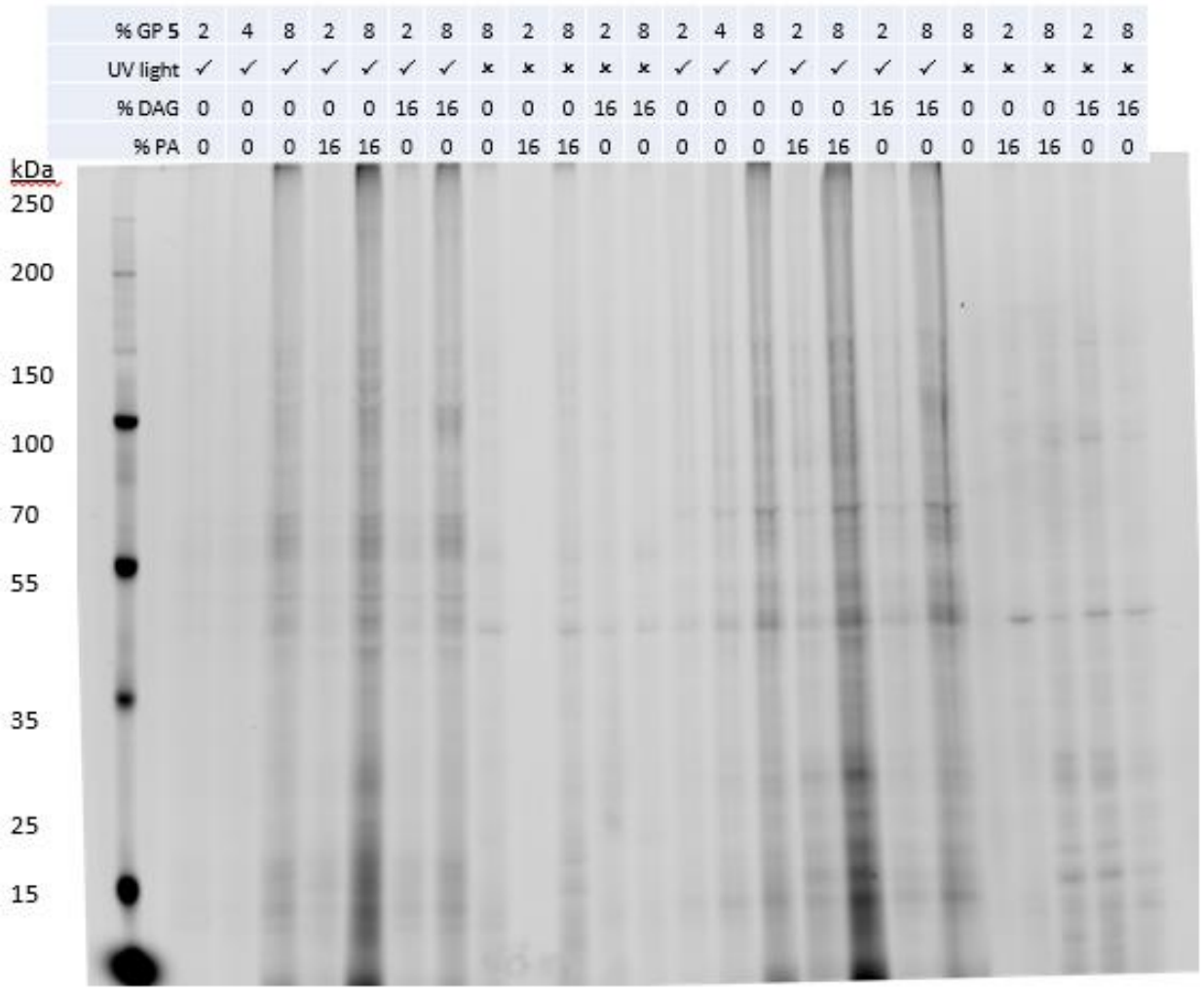

Figure 2.26: **Fluorescent image of a lipomimetic study using GP 5.** This study was in duplicate with **5** at 2, 4 and 8 % of the membrane (no chase lipid) and at 2 and 4 % with chase lipids (DAG or PA at 15%). Results are like those from Protocol B studies where labeling does occur but seems to be indiscriminate, bands are broad and difficult to define and introduction of anionic chase lipids (i.e. PA) lead to lane-darkening. Experimentation performed at TSRI. Protocol A.

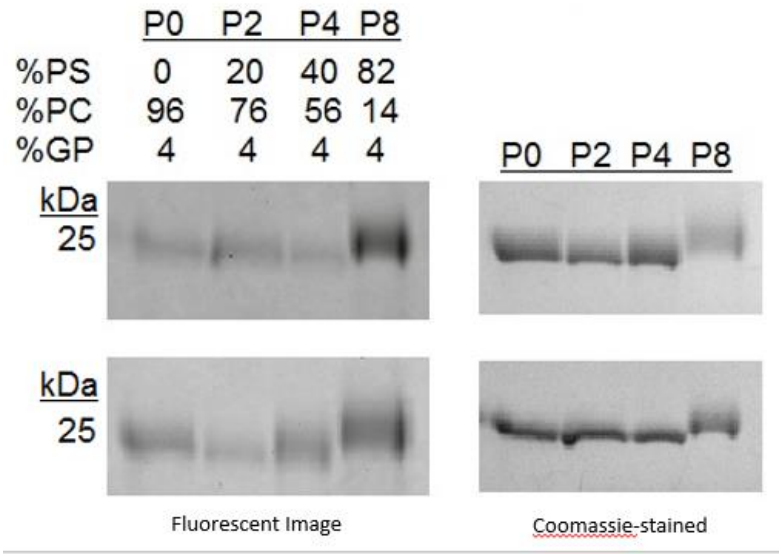

Figure 2.27: L**ipomimetic PS study of CA protein.** A pre-optimized Protocol B experiment is shown with generic probe **5** to screen CA affinities. P8 (80% PS) intensity is significantly higher despite less protein entering the gel as can be seen in the coomassie-stained images to the right of the fluorescent images. Protocol B. No sonication.

were pleased to have fixed the uneven protein loading observed in Figure 2.27.

CA demonstrated a much more predictable and repeatable affinity for PA (Figure 2.28) than it did for PS, which was confirmed when we repeated our CA studies with PS under more optimal conditions (Figure 2.29). Because PA is more anionic than PS, this is easily reconciled with what was previously understood about the HIV viral capsid.[238]

It was suspected that CA's affinity for PA and PS was due to electrostatics. To test this, we screened CA for DAG affinity, as DAG carries no charge at physiological pH. Indeed, as seen in Figure 2.30, DAG did not seem to increase or decrease CA's affinity for liposomes incorporated with natural DAG. This can be justified not only by electrostatics, but also by the different cone angles of PA and DAG, given that PA-binding proteins have demonstrated curvature dependent membrane docking.[9] Lipid-specific perturbations to membrane geometries are a crucial natural phenomena in terms of lipid signaling and lipid-dependent vesicular communications in biological contexts. The lipomimetic approach likely produces protein hits that vary not only because of the headgroups present, but also because of membrane topography and shape.

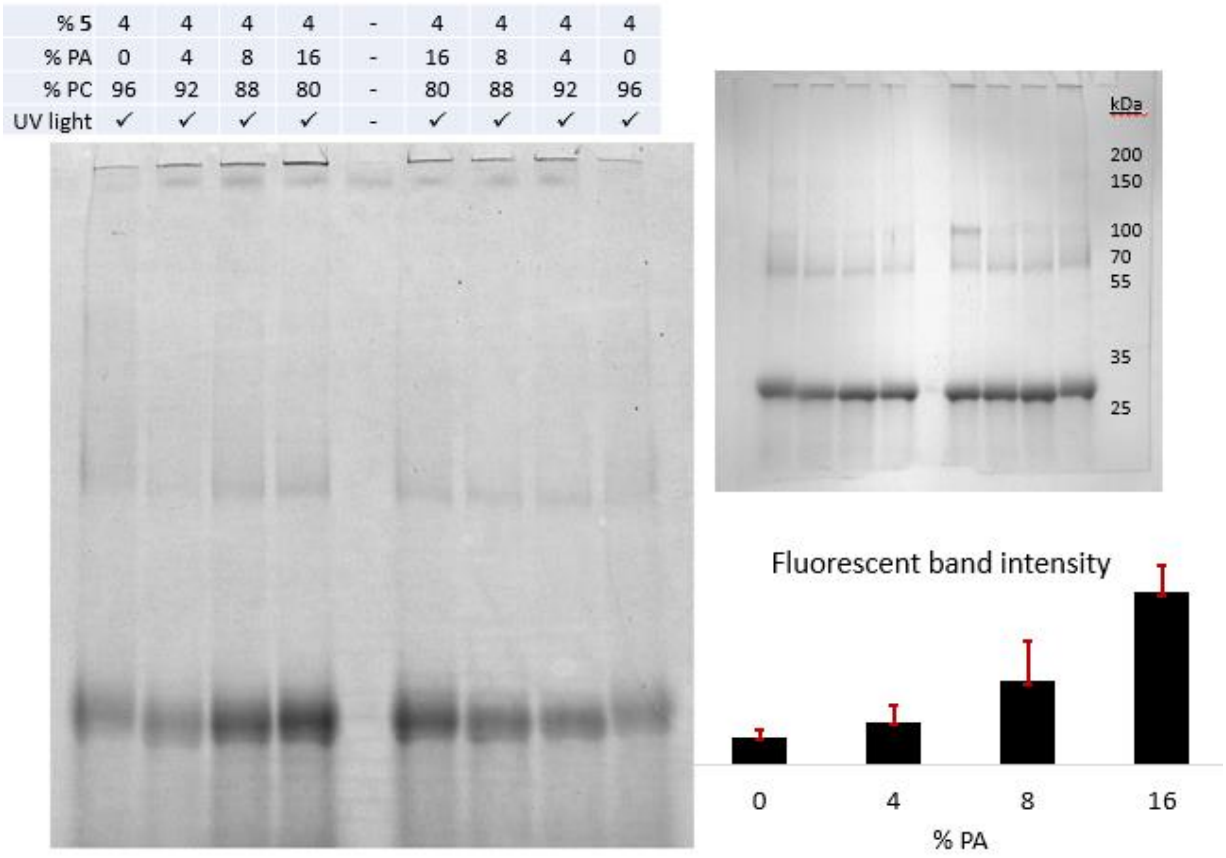

Figure 2.28: **Lipomimetic PA study of CA protein.** HIV capsid protein CA is recruited to liposomal membranes more intensely as PA composition rises from 0 to 16%. Florescent band intensity was measured using imageJ software and error bars are standard error for the two replicates shown. Protocol B. No sonication

% 5	4	4	4	4	-	-	4	4	4	4
% PS	0	18	37	72	-	-	72	37	18	0
% PC	96	78	59	24	-	-	24	59	78	96
UV light	✓	✓	✓	✓	-	-	✓	✓	✓	✓

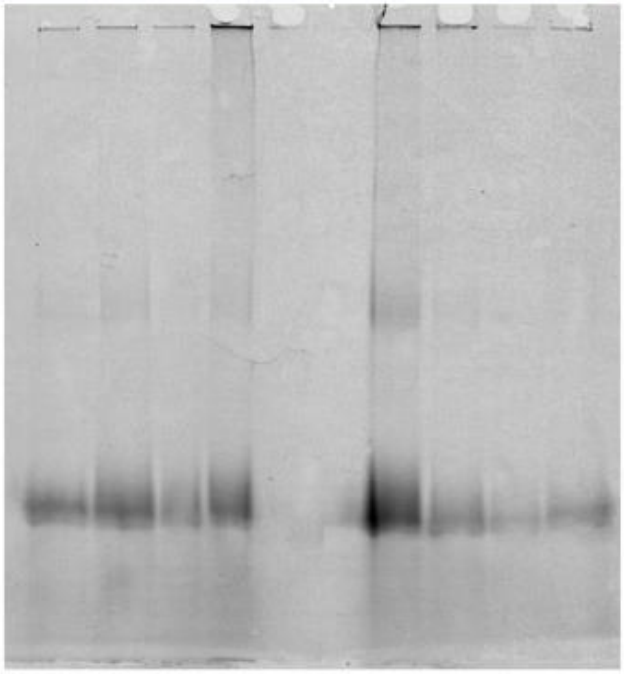

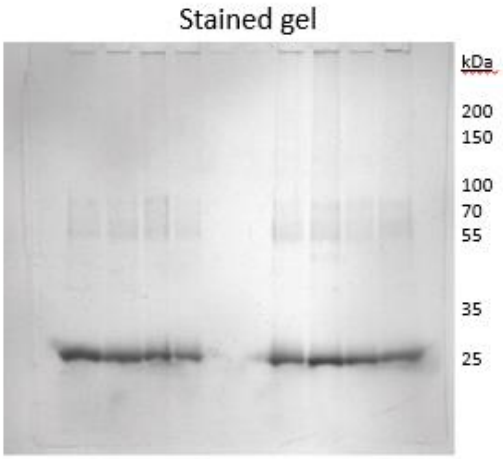

Figure 2.29: **A lipomimetic PS study with CA protein.** In the fluorescent image (left), replicates to the right indicate CA affinity for PS while replicates to the left show inconsistent PS-recruitment of CA to the membrane. Protocol B. No sonication

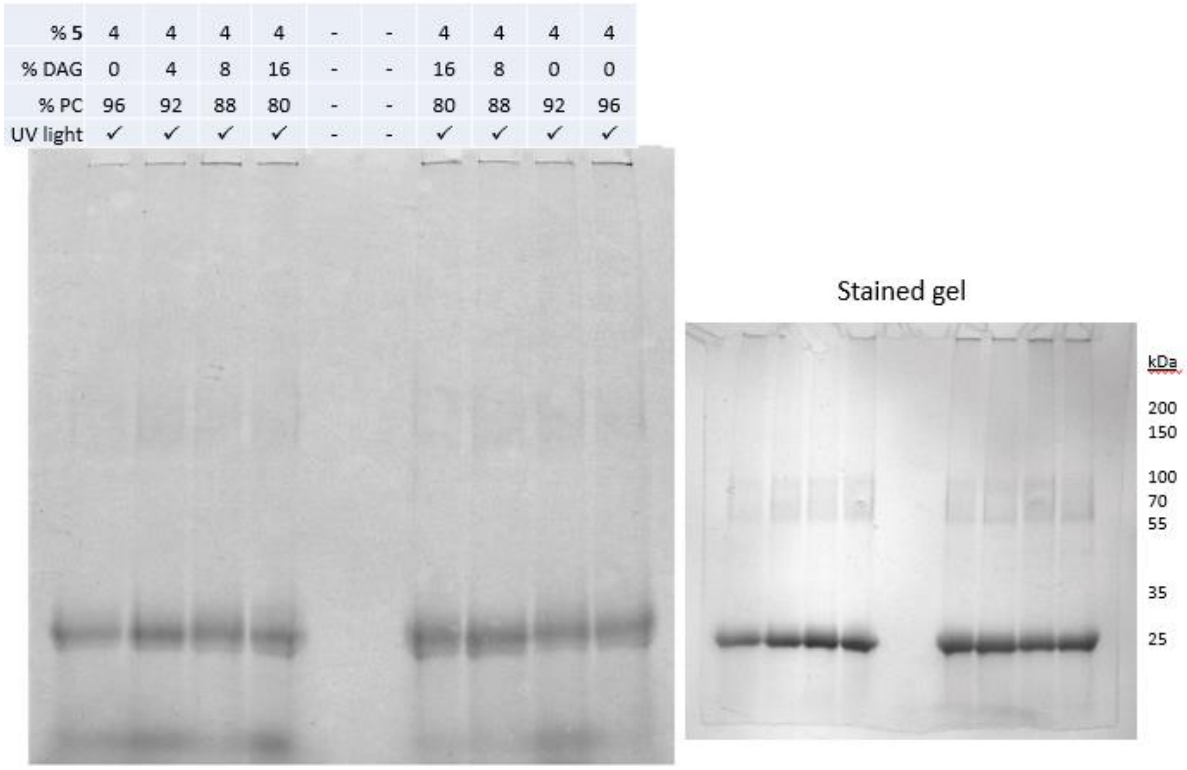

Figure 2.30: **A lipomimetic DAG study with CA protein.** As can be seen in the fluorescent image on the left, DAG had no effect on CA recruitment, a significant departure from the results of PS and PA experiments screening CA affinity. Protocol B. No sonication

2.4: Future work

Our initial goal was to discover new protein-lipid binding interactions. As such, liposomal AfBPP culminating with MS to identify selectively labeled bands will be the ultimate application of our platform. Protocol A experiments that finished with biotin click reporting at TSRI and passed to Kenneth Lum for avidin-based purification and analysis by MS. These studies generated data with enough protein hits to warrant analysis. Pending Mr. Lum's analysis, replicate MS studies will commence to complete this project. During the MS studies at TSRI, we aliquot a portion of the sample and click to a fluorophore to separate by SDS-PAGE. Figure 2.32 contains the fluorescent gel image representative of the MS data being processed at TSRI. Liposomal samples went up to 8% DAG, based on previous data (Figure 2.12) suggesting this biologically-relevant DAG concentration was sufficient to bring about lipid-specific labeling. Probes are incorporated at 8%, including DAG probe **3**, which can be seen in the left lane labeling roughly the same bands as corresponding generic probe **7**. This suggests the lipospecific studies in these Hek cell lysates are not nearly as effective as the lipomimetic study. In Figure 2.31, 'H' indicates heavy cells that are isotopically labeled so that labeled proteins in UV-positive samples may be distinguished from light cells ('L') used for the UV-negative samples. The use of H and L cells creates resolution on the MS chromatograph that insures only probe-specific labeling is identified. Best Group member Adam Carr also tested his probes administered non-liposomally in corresponding MS experiments with aliquots also represented in the fluorescent gel image in Figure 2.31. To get his probes into solution, Mr. Carr required probe-specific combinations of DMSO, alcohols and water. Interestingly, the ionically-charged PA probe **4** did not label nearly as intensely as DAG probe **3**, and **3** exhibited significantly more labeling than in the background lane of generic probe **7**. This result differs from the liposomal application of these lipid-specific probes, implying that free-probe administration is indeed a much different experimental platform. The membrane-context and consistency of probe solvation-conditions is an attractive feature of the liposomal application, however the use of these probes non-liposomally can also be considered an avenue for future work. During our time at TSRI, Mr. Carr and Mr. Lum had success feeding free-probes to live cells. However, I observed no labeling in tandem liposomal live cell AfBPP studies. Our current perspective is that protein discovery in cell lysates is the ideal application of the

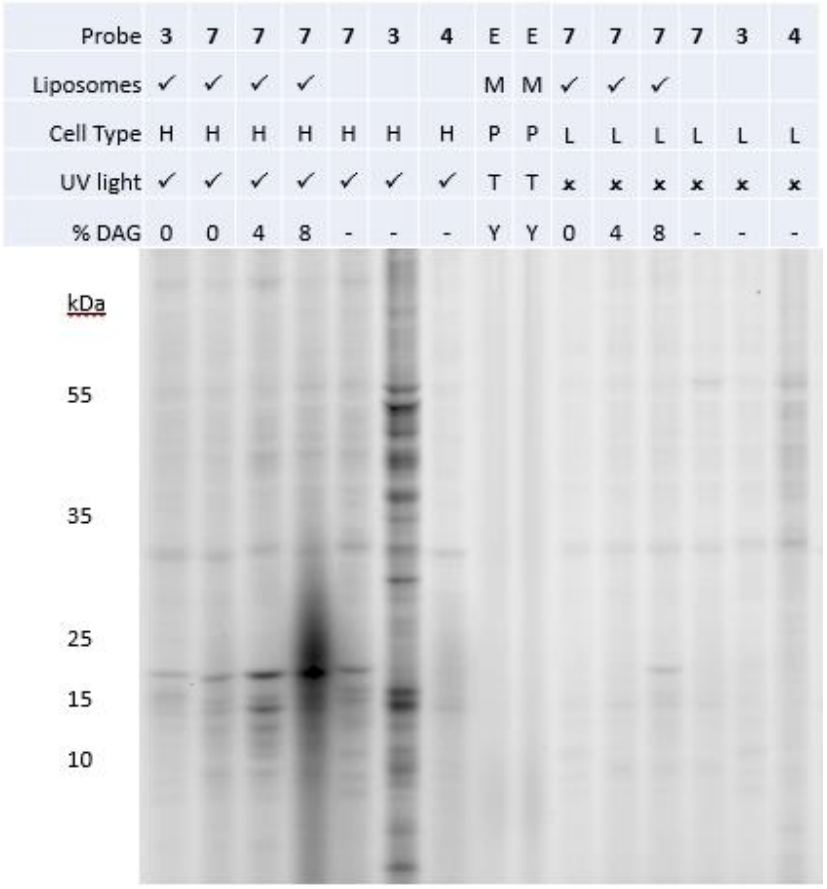

Figure 2.31: **Fluorescently labeled aliquots from MS studies at TSRI.** Liposomal treatments are indicated, as well as heavy (H) and light (L) cells. Dark smear due to over-abundant signal in the 8% DAG lipomimetic lane. Protocol A.

liposomal platform, however optimizing conditions for live-cell studies is yet another potential direction of liposomal AfBPP.

In regards to liposomal AfBPP MS experiments that followed Protocol B. Natalie Sadler at PNNL did the avidin purification for these samples and reported solvation issues that translated to too few protein hits, rendering the data insignificant. We reasoned this was a result of either excess lipid content or residual detergent from the SDS-treatment. Either way, this was something we overcame by switching to Protocol A, which raises probe concentration slightly to lower total lipid content considerably.

We have relied on the expertise and instrument-access of other labs for the mass spec portion of this project. Using heavy and light cells in biotin pull-down experiments helps to avoid false positives, but it also limits the capacity for this platform to be high-throughput. Currently, we are adding a step after the photocrosslinking where samples are passed through a size exclusion column (SEC) so that only proteins bound to the membrane are carried through. SEC makes use of polymeric dextran gels called sephadex that elute vesicles immediately, fractionates macromolecules, and traps small molecules in the column media. Fractionation depends on the size of the sephadex gel media, which ranges from g-10 to g-200 with larger numbers representing larger pore sizes and retention or fractionation of larger molecules.

SELPE

SEC-based liposomal protein extraction (SELPE) was conceived to create meaningful data from MS instruments at our immediate disposal. SELPE allows us to isolate resolved protein fractions unique to each liposomal treatment type. If successful, this will expedite protein discovery by illuminating avidin purification and allowing more accessible instruments to analyze our samples.

Theoretically, crosslinked proteins are bound because they adhere to a stable membrane surface, thus the crosslinking reaction should not result in additional membrane perturbation. Before the disruption of the liposomes (by adding the highly organic click mixture in Protocol A or the SDS treatment in Protocol B), the labeled proteins are a part of the larger liposomal superstructure. Thus, they may be separated by size from non-bound proteins. SEC is an established means to separate liposomes from smaller aqueous components of the extraliposomal matrix, which we have used prevoiusly.[148] Isolated SEC fractions are desalted and free of click-reactants and non-labeled

proteins. If proteins are indeed recruited to the membrane based on liposomal treatment type, then we may digest these fractions directly and test them by mass spec to see which proteins are selectively enriched (based on the protein content in background fractions). In lipomimetic studies, this would be done by subtracting protein hits of generic probe-only liposomes from the protein hits from probe liposomes with chase lipids. For lipospecific studies, this would involve subtracting the protein hits from generic probe-only liposomes from lipid-specific probe liposomes. An aliquot of tested fractions is saved for click-enrichment and visualization in gel. For SELPE applications, visualization may use clickable probes and fluorophores, or non-clickable (crosslinking only) probes and gel staining since SELPE relies on inequitable protein content to qualify labeling.

Figure 2.16 shows successful Protocol A application of SELPE using sephadex g-200 beads swelled in 1x PBS and pre-treated with PC-only liposomes to prevent liposome retention. During this trail run liposomes were formed to 600 nm using 1 freeze-thaw and sonication. Since then, we have experimented with 10 and 5 freeze thaws and in both instances the labeling disappears. DLS confirmed that these liposomes were 150 nm and 300 nm respectively, and thus liposomal-protein complexes were not large enough to elute through the relatively large sephadex 200 medium. SELPE conditions are still under optimization, more experimentation with larger liposomes and smaller sephadex beads will determine how best to apply this promising addendum to our liposomal AfBPP. To aid in SELPE development, crosslinking-only probe **20** was synthesized via the facile scheme presented in Figure 2.32.

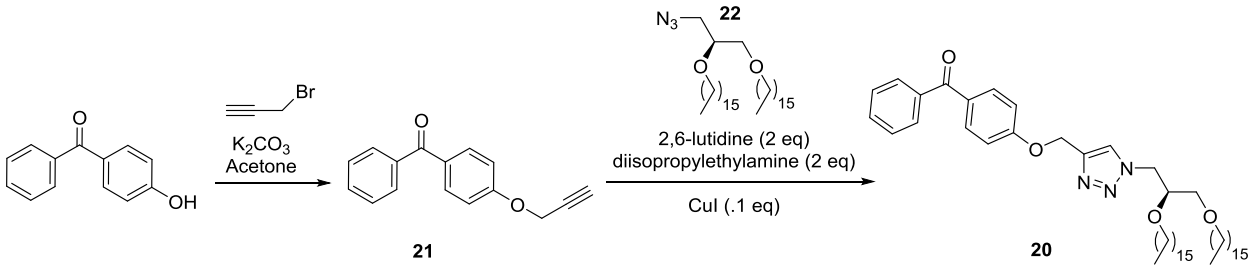

Figure 2.32: **Synthesis of crosslinking-only benzophenone lipid 20.** This simple functional lipid is being used to optimize SELPE conditions. Data not shown.

Our first SELPE studies made use of **20** to liposomally screen t24 human carcinoma cell extracts and protein content of fractions was determined by Bradford assay. Figure 2.33 has an example of one such optimization study, where the amount of protein eluted in fraction 2 was amplified by the presence of crosslinking lipid **20**. This study used g-70 medium and SUVs created by sonicating for 20 minutes. Later fractions from the study in Figure 2.33 began to fractionate proteins too large to be retained on the the g-70 media, demonstrating the ability of liposomes to usher through captured membrane proteins before the sephadex gel begins to separate proteins based on inherent size.

We will continue to optimize SELPE as it is envisioned to be an elegant extension of the liposomal protein profiling platform presented herein. As such, SELPE may one day be applied to any of the other possible applications of our platform. Such applications include the study of other signaling lipids or combinations thereof, as well as the anchoring of peptides, carbohydrates or other molecules on our liposomes to screen protein interactions and/or gauge the feasibility of LDS targeting moieties.

Discussion

As it stands, this liposomal AfBPP platform could translate well to biochemical investigations of molecular membrane partitioning, the study of biomedically engineered liposomes tailored to clinical applications, or any other number of relevant studies geared at assessing bilayer behaviors and interactions. Variations in natural membrane context will also be interesting to investigate by the lipospecific approach to determine if more labeled bands are produced by DAG probe **3** with the addition of binding cofactors other than PS, such as PA, SM, or additional calcium content. It will also be interesting to see if GUVs label differently than the LUVs we have studied thus far. Once confident MS protein hits are garnered via our collaboration with the Cravatt Lab at TSRI, or by SELPE, the promise already demonstrated by this platform will grow considerably.

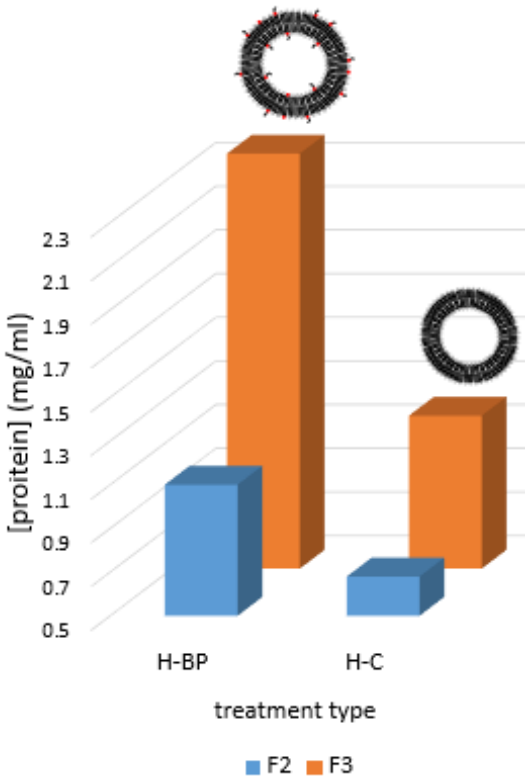

Figure 2.33: **SELPE data.** Protein content from fractions 2 and 3 (F2, F3) from SECs following incubation and crosslinking in T24 human cancer cells (H) using benzophenone probe at 4% (BP) or 0% (C) of PC SUVs. G-70 media was used and swelled in 1x PBS augmented with C liposomes to .5 mM [lipid]. Elution used 1x PBS through 2 mL of g-70 beads in glass mini-columns with .8 cm diameters, collecting 100 µL fractions.

CHAPTER 3: TARGETING NANODRUGS USING NATURAL SIGNALING LIPIDS

3.1: Introduction

This project was made possible by a collaboration with the vascular research lab (VRL) of Dr. Deidre Mountain at the University of Tennessee Graduate School of Medicine in Knoxville. The principal aim of the experimentation described in this chapter is to specifically increase the cell association and subsequent cargo delivery of an LDS using DAG and/or PS. Our collaboration with the VRL began with development of a novel liposomal nanocarrier to treat the cyclic degeneration of arterial tissue following vascular injury.[144] The VRL's original project was headed by Trey Fisher and is described as background for this chapter's titular project.

Figure 3.1 represents what we have gleaned from this project thus far, which is that DAG and/or PS potentiate the cell association of a PEGylated lipoparticle (PLP) already functionalized with a stearyl octa-arginine, (stearyl-R8) cell penetrating peptide (CPP). Cell association refers to the retention of liposomes either by adhering to cell surfaces or entering the cells, such that treatment liposomes are not washed away after incubation. Differential lipid expression is well-established in cells and based on observations from work described in chapter 2, we posit that signaling lipids present a simple solution to the complex problem of actively targeting LDSs. Nonetheless, tailoring the natural signaling lipid content of liposomes to generate specificity and increase delivery efficacy remains largely unexplored.

Some studies have broached this concept, such as experimentation with raft-like LDSs for HIV-1 treatment.[137] DAG and PS have both been widely studied for their ability to promote fusion between vesicles.[23, 241] Added fusogenic tendencies could be an ancillary benefit to incorporating DAG and/or PS in LDS architectures. PS is envisioned to work electrostatically, given its negative charge, while DAG is known to be a key factor in promoting vesicular communications that require fission and fusion of smaller lipid vesicles sent intra/extracellularly or at synaptic gaps.[20, 22, 69] At the least, increased fusogenic behavior of liposomes with elevated DAG/PS content should be considered a contributing variable to the cell association studies described herein. However, increased fusogenic properties inherent to the liposomes cannot account for cell-type specific trends in association. Lipid-protein and lipid-lipid interactions between liposomes and cell surfaces

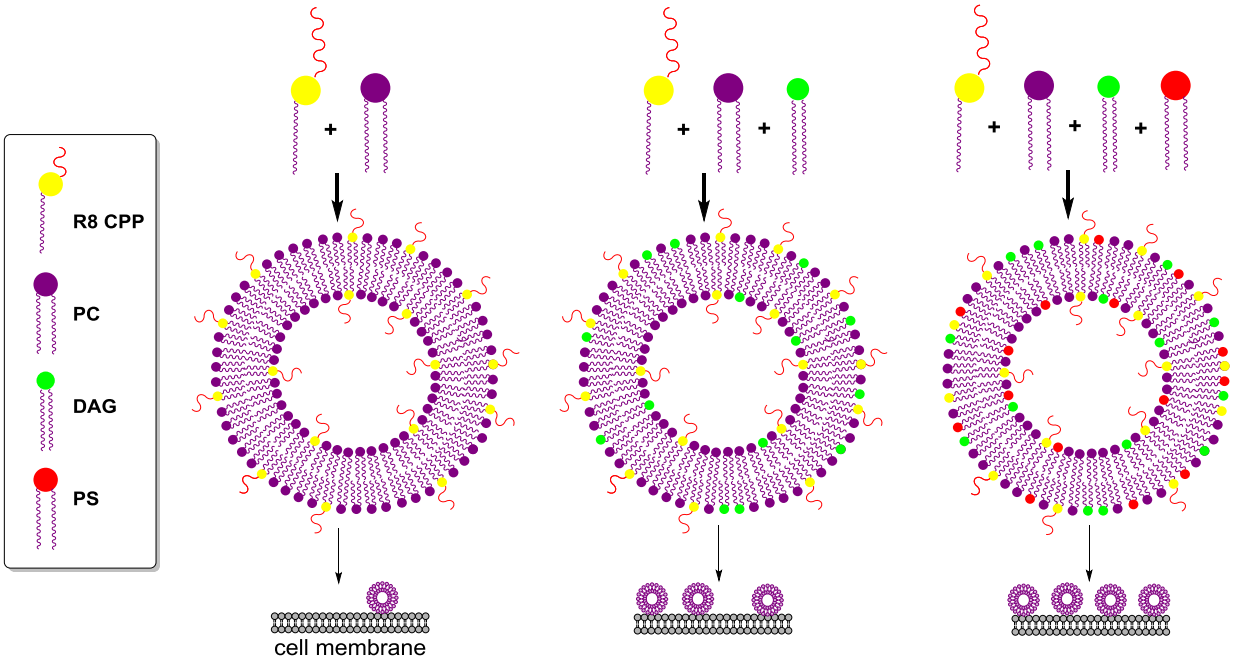

Figure 3.1: **A schematic representation of how the addition of DAG and/or PS potentiates the cellular association of an octa-arginine (R8) cell penetrating peptide (CPP)-functionalized liposome.** Gray membranes (bottom of image) represent cell surfaces.

are the leading hypotheses to explicate the dose-dependent increases in association of DAG and/or PS-containing liposomes that occur disparately between types of cells/LDS formulations.

Before delving more deeply in-to the experimental design and results of lipid modifications to the R8-PLP, we will first present the requisite background. A brief review of active targeting will be followed by a summary of the VRL's previous work to develop the R8-PLP delivery system before lipid modification.

Actively targeting nanocarriers to specific cell types

Active targeting involves rationally engineering nanocarriers to control cell preferences. LDSs may display small molecules or peptides on their surfaces that home them to target tissues. This is accomplished by exploiting abnormalities unique to diseased tissues, most commonly tumor microdomains. Other target tissues with specific cellular affinities may be targeted, such as the liver. For example, the asialoglycoprotein receptor is a glycoprotein found only on mammalian hepatocytes that binds selectively to galactose residues, and this relationship has been exploited by liver-targeted galactose-decorated nanoparticles.[243] Carcinomas remain the most commonly targeted types of diseased cells due to aberrant expression of certain cell surface receptors and expression of modified proteins unique to cancerous cells.[244] Active targeting molecules include monoclonal antibodies, antibody fragments, single chain variable fragments, aptamers, proteins, peptides, aptides, vitamins, carbohydrates, glycoproteins and other small molecules.[7]

Proteins are the most commonly used active targeting tools. For example, the cyclic arginine-glycine-aspartic acid peptide (cRGD) is a commonly used targeting motif that increases nanocarrier delivery to tumors.[245] Breast cancer cells are among the most studied targets of functionalized nanodrugs and significant research has gone into the active targeting of breast cancers. A few examples include progesterone, HER2 antibodies and estrogen, which have all been used to target cell surface receptors that are overexpressed or unique to breast cancer tissues.[246] Mucin-1 (MUC-1), a DAG-binding protein mentioned in chapter 1, is overexpressed in breast cancers as well and can be targeted using a monoclonal antibody called hCTM01,[247] as well as other MUC-1 specific aptamers.[248] Breast cancers also present abnormally high numbers of estrogen receptors on their membrane surfaces, which may be targeted by tamoxifen.[249] Tamoxifen is closer in size to sterol hormone targeting groups (progesterone and estrogen) than it is to protein

targeting molecules.

Sterol hormones used to target LDSs are technically examples of lipids used in active targeting. This general distinction does not support the glycerophospholipid-based strategy we explore herein, however, the ability of small molecules to impart selectivity to bilayer-based nanodelivery does. Folic acid (FA) is a common example of a small molecule targeting entity,[250] folate receptors are overexpressed in many tumor types (including breast cancer) due to their need to grow rapidly.[251] Sigma-1 and Sigma-2 receptors, which may be targeted by anisamide (a small molecule with affinity for sigma receptors),[252] are overabundant on rapidly spreading cells such as metastatic tumors.[253] The success of relatively small targeting entities like anisamide and FA lends credence to the hypothesis that if the headgroups of lipid constituents within LDS bilayers are varied, then cell association of said LDSs will vary as well, dependent on cell type.

There are many other active targeting strategies, several of which have been inspired by the integrin family of proteins;[162, 250] αβ integrins are transmembrane glycoproteins observed in greater abundance in the membranes of tumor cells. Tumor abnormalities are not the only means by which we target cancer cells. The vasculature around target sites may also be targeted by LDSs. E-selectin, an adhesion molecule selectively expressed by inflamed or cancerous blood vessels, has demonstrated promise as a target for controlling metastasis of cancer cells through nanotherapies.[254] Inflamed vasculature sites have also been targeted by a peptide recognized by vascular cell adhesion molecule-1 (VCAM-1). VCAM-1 is an often-targeted receptor unique to activated endothelial cells, which may be exploited to deliver drugs that inhibit endothelial cell adhesion and function.[255]

PS is the lone example of a rationally selected natural lipid to build actively targeted liposomal architectures. PS can be used to target liposomes to macrophages,[256] which are drawn to PS when flipped to outer-leaflets of apoptotic cells. Apart from this example, lipid signaling has not been used to target LDSs, to our knowledge. Altering bilayer lipid profiles to selectively increase ligandability to target cells is an intuitive strategy since many cell-surface proteins are associated with specific arrays of lipids, as detailed in chapter 1. Historically, lipid profiles of LDSs are varied only to maximize stability, increase circulation time and, in doing so, potentiate passive targeting.

Examples of successful deviations from traditional PC-vesicles include the inclusion of PG, PE and the cationic lipid dioleoyloxypropyltrimethylammonium (DOTAP).[159] DOTAP is essentially

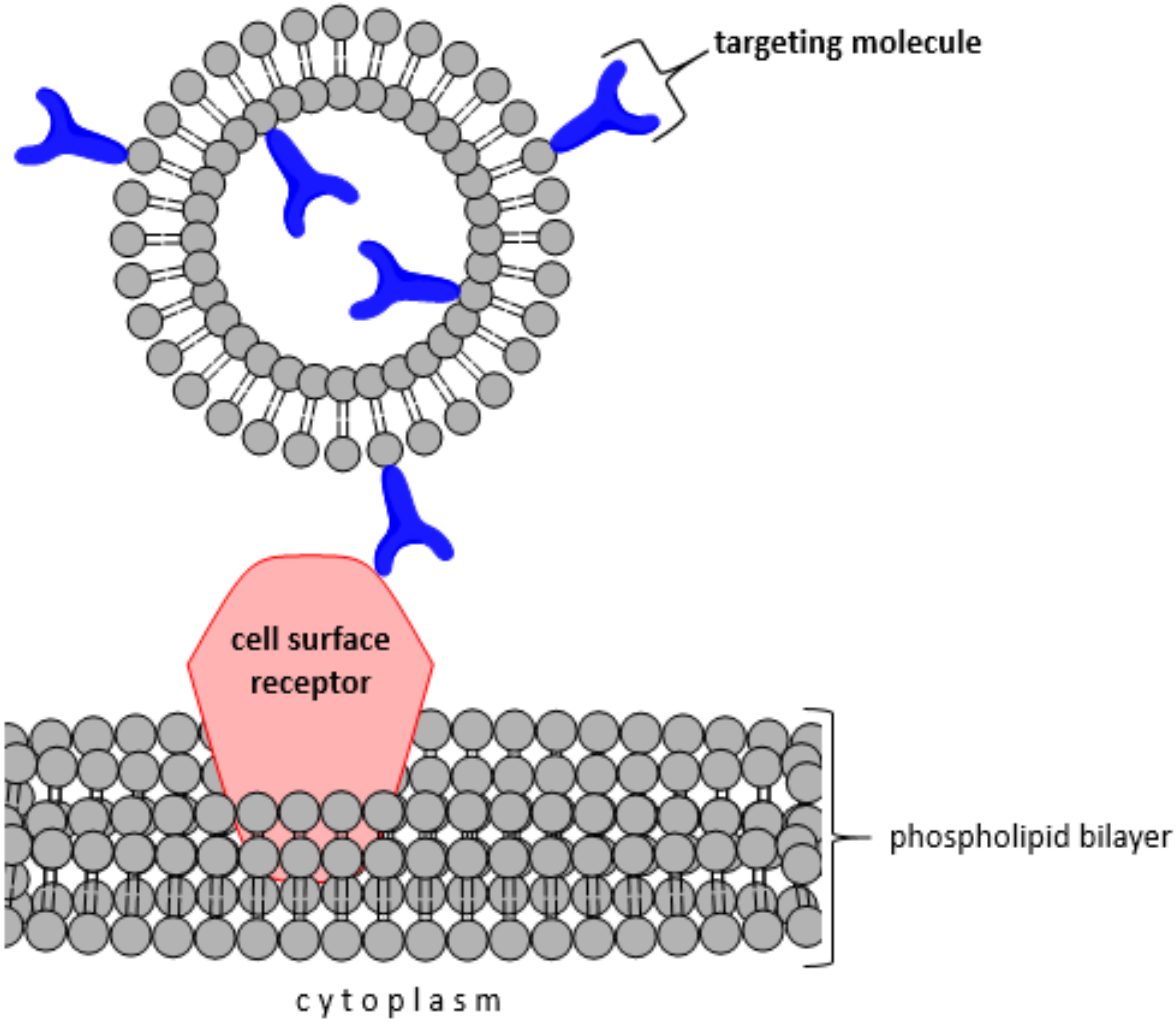

Figure 3.2: **A cartoon depiction of active targeting.** A liposome displays a targeting molecule (blue) with preference for a cell surface receptor (red) overexpressed at the target cite.

dioleoyl PC, without the phosphate group, but rather a cationic trimethyl ammonium at its *sn*-1 position. SM may also be exchanged for PC to create SM + cholesterol liposomes, termed Optisomes®,[257] which are well-established alternatives to PEG-PC liposomes for extended circulation, evasion of the RES, and passive delivery of drug cargo.[167] Other lipid add-ins to LDSs include fatty glycerides such as triolein or tricaprylin, which afford opportunities to control LDS stability for specific applications.[170-171] PG, PE and triglycerides are similarly incorporated as favorable structural components,[166, 168] but not for their abilities to increase cellular association of LDSs. To our knowledge, DAG species are unexplored as structural or functional components of liposomal nanodrugs.

Active targeting, as defined here, refers to the exploitation of molecular relationships to add specificity. Liposomal nanocarriers may also increase their efficacy in other ways. Modifications to promote release will be discussed in chapter 4, along with fusogenic liposomes. LDSs can be imbued with virus-like fusogenic capabilities by melding regular liposomes with viral particles, creating nanodrugs that can target and fuse with tumor cells, increasing delivery efficacy.[258] In fact, the protein-driven mechanisms of viral adhesion and cellular entry were the impetuses for CPP-use in nanocarriers. CPPs can be conceived as active targeting in some instances. However, as active targeting has evolved to create unprecedented specificity, CPPs are not always discriminate enough to be considered as such. Nonetheless, the viral-like cell-entry properties they bestow upon LDSs provide a crucial advantage for emerging nanotherapies.

Cell penetrating peptides

Trans-activating transcriptional activator (TAT) was discovered in 1988 from HIV-1 and is the original CPP.[259] CPPs are cationic and small (40 or fewer amino acids) and are occasionally called membrane translocating sequences, protein transduction domains, or Trojan peptides. Arginine and lysine are the most common amino acid links in CPP chains.[260] Arginine's guanidinium moiety is crucial to the ability of cationic CPPs to bore through the plasma membrane and drag their nanocarriers into the cytoplasm.[261] Extracellular alkalinity exposes deprotonated fatty acids on the outer leaflet of cell membranes, which attract the guanidiniums. This ionic binding triggers bilayer insertion, thereby creating a temporary toroidal pore. Peptide diffusion on the surface of the pore ushers it to the acidic cytosolic matrix where protonation of fatty acids allows release of the CPP,

and the vessel.[261] This is but one possible mechanism of CPP entry and, although this mechanism fits with the CPP used in the work described in this chapter, it should be noted that there are 1,000+ CPPs with a litany of possible cell entry mechanisms. Other entry mechanisms may center on the nanodrug system or target cell, rather than the peptide itself.[262, 263] Mechanisms aside, CPPs are useful for allowing LDSs to cross membranes and achieve intracellular delivery with reduced endosomal escape.

The research described in this chapter makes use of a cationic polyarginine CPP called octa-arginine (R8) with a lipid anchor (stearic acid) for anchoring to our LDS membrane. Stearyl R8, presented in Figure 3.3, has increased the efficacy of several nanotherapies in addition to the LDS already reported by the VRL,[144] discussed next. For instance, R8 has been applied to increase delivery of a viral-like lipid/polymer hybrid genetic nanotherapy to mammalian neurons.[264] Because polyarginine CPPs are not discriminate, much research has gone into finding out ways to increase the selectivity of CPP-guided nanocarriers.[265]

An R8-LDS for treating vascular disease through gene silencing

The VRL has developed a novel genetic nanotechnology for the attenuation of peripheral vascular disease (PVD) through RNA interference (RNAi).[144] Endovascular interventions are widely employed and effective at treating PVD.[266] However, intimal hyperplasia (IH) is a common occurrence following these treatments and can induce restenosis (narrowing of the blood vessel), which demands a follow-up endovascular intervention.[267] Secondary endovascular interventions

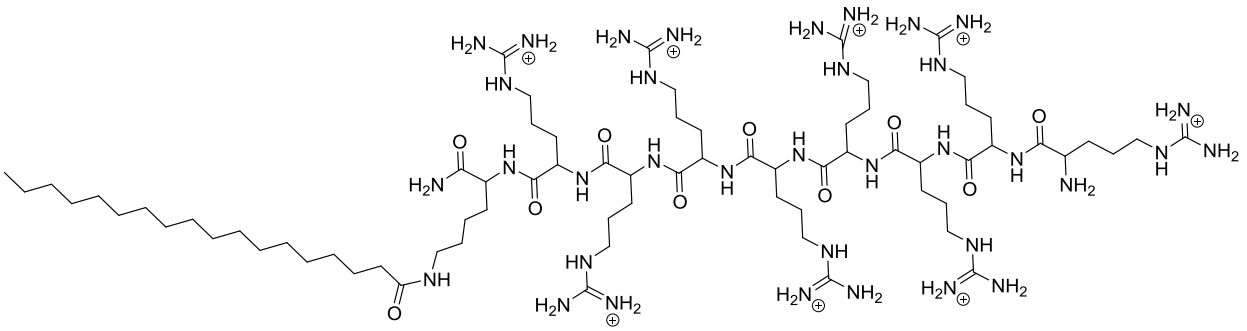

Figure 3.3: **A stearyl octa-arginine (R8) CPP**

have significantly lower rates of success and higher mortality risks.[268] There are more than 200 million PVD cases worldwide[269] and this number increases as populations continue to age. Increasing efficacy of the principal endovascular interventions and developing non-invasive treatments of IH would improve quality of life for millions of patients and substantially lower healthcare costs.

Dysfunctional vascular smooth muscle cells and endothelial cells (VSMCs and VECs) are at the root of IH. Specifically, over-active VSMCs proliferate and cause restenosis while indolent VECs exhibit delayed recovery at the site of injury. To treat IH, the VRL chose short-interfacing RNA (siRNA) due to its therapeutic promise as a gene-silencing agent capable of switching off the cyclic degeneration of vascular tissue when delivered by a nanocarrier.[270] RNAi using siRNA affords the opportunity to silence specific genes, effecting a phenotypic response that ameliorates pathological cellular behavior such as unchecked growth and cyclic inflammation by 'turning off' responsible upregulated proteins.[271] siRNA therapies have already been explored for the treatment of vascular disease and show promise therein.[272] Previously, the VRL investigated and characterized cellular pathways to IH.[273-274] Dr. Mountain's team has studied the role of matrix metalloproteases (MMPs) in the progression of IH[275] and thus settled on siRNA cargo to silence MMP-2 operation in VSMCs as the target for their genetic liposomal nanotherapy.

Using liposomes as the delivery mechanism for their genetic cargo was an obvious choice as cationic liposomes (CLs) have had success *in vitro* shuttling siRNA to target sites to control gene expression.[276] The biocompatibility of CLs (which make use of cationic DOTAP lipids) is suspect, however, and to advance the clinical viability of liposomal genetic therapies the VRL chose to test natural PC-based vesicles functionalized with PEG camouflage and a lipid-anchored CPP. The highly cationic octa-arginine CPP (R8) imbues the LDS with some of the same electrostatic benefits of CLs while maintaining biocompatibility within the liposomal architecture. The R8 peptide is useful for increasing both adhesion and cellular uptake; it is an effective means to potentiate passive targeting. R8 is not discriminate enough to be considered an active targeting agent. Nonetheless, it does increase delivery efficacy substantially.[144] There is ample literature precedent to suggest that siRNA gene silencing liposomes are a viable drug-delivery strategy. At least four different liposomal siRNA-loaded liposomes have made it to clinical trials over the last

few years.[277] Stable nucleic acid lipid particles (SNALPS) commonly employ cationic and fusogenic lipids as nanodrug components. Additionally, dual-functionalized nucleic acid-delivering liposomes have been reported that bear both a CPP and a targeting peptide with affinity to a metalloprotease present in certain tumor types.[278]

Our research group has experience preparing and characterizing liposomes and because of this we were approached by the VRL to help develop an experimental design that allowed them to form a multifunctional PEGylated liposome that maintained high encapsulation efficiency of their siRNA cargo. Mr. Fisher and Dr. Mountain's lab quickly advanced the project independently and our research group remained involved to consult on chemical aspects of their project and to characterize membrane-derivatization products using matrix assisted laser desorption ionization (MALDI).

The VRL compared CLs, PEG-only DOPC/cholesterol liposomes (PLP), and PLPs formed with the stearyl-R8 CPP (R8-PLP). Their work showed that the R8 CPP increased cell association steadily and dramatically at 10%. Additionally, R8 addition to PLP increased encapsulation efficiency (EE) of siRNA such that it was the same as CLs. CLs demonstrated significant cytotoxicity while the R8-PLP and PLP did not.

The R8-PLP delivered siRNA and achieved transfection. Significant silencing was observed of glyceraldehyde 3-phosphate dehydrogenase (GAPDH) as determined by qualitative polymerase chain reaction (qPCR). GAPDH, known as a quintessential cytosolic glycolytic protein, has come under scrutiny for its aberrant expression in certain tumors and is suspected to aid in the proliferation of atherosclerotic plaques.[279] Ultimately, Dr. Mountain's team developed a promising new genetic nanotherapy using PC liposomes. The VRL's next goal is to actively target their liposomes such that siRNA may be selectively targeted to VSMCs with the potential to usher other therapeutic cargo to VECs.

Many small peptides are capable of targeting liposomes to specific cell types, as exemplified in Figure 3.2 and discussed in the introduction. This strategy is being pursued by the VRL and has the potential for potent specificity, although it presents many challenges. The R8-PLP, for example, already comes equipped with 10% PE-anchored PEG and 10% stearyl-R8 peptide (the remaining 80% is composed of a 7:3 mixture of DOPC and Cholesterol). Liposomal modifications that include PEG or peptide headgroups can lead to lateral dispersion on the membrane surface,

which creates bilayer instability. 20% of total lipid content is already on the high-end of literature precedent of PEG/lipopeptide content for stable liposomal nanocarriers. To go beyond this could compromise morphology, consistency and encapsulation efficiency. Another option is to decrease the R8/PEG content to accommodate additional lipopeptides for active targeting, however this could decrease circulation time and/or functionality. Additionally, peptide-peptide interactions between the R8 and potential targeting moieties could jeopardize the system.

Therefore, we were curious to see if lipids such as DAG and/or PS could be used to potentiate the activity of the R8-PLP. DAG and PS have been formed into stable membranes as high 25%[23] and they do not present bulky headgroups that aggravate the membrane with lateral dispersion forces. The body uses lysosomes and lipidic vesicles to communicate and shuttle cargo both intercellularly and intracellularly and DAG is crucial to these operations.[33, 51] Moreover, tight control of signaling lipid abundance seems to be crucial for smooth muscle cell function,[45, 123] and there is evidence to suggest that cell-specific proteomes will have preference for certain membrane compositions.[12, 280] By taking cues from biology, this strategy aims to make the LDS more attractive to the target cells.

Experimental design

To test the hypothesis that signaling lipids can be incorporated into LDS architectures to increase the efficacy of liposomal theranostics, we devised a three-tiered project as outlined in Figure 3.4. The propensity of DAG and/or PS to increase the association of an R8-PLP to either VSMCs or VECs was tested first at gradient percentages of individual lipids at 5, 10, 15 and 20% of LDS membranes. Based on these results, we devised combinatorial LDS formulations that screened for optimal DAG content when PS content was fixed at 10% PS among all lipid-modified LDS treatment groups. Prior to combinatorial cell association studies, we tested these mixed lipid LDS architectures for their ability to efficiently encapsulate siRNA. Finally, qualitative polymerase chain reaction experiments will assess gene-silencing to quantify delivery of siRNA by DAG/PS-modified LDSs.

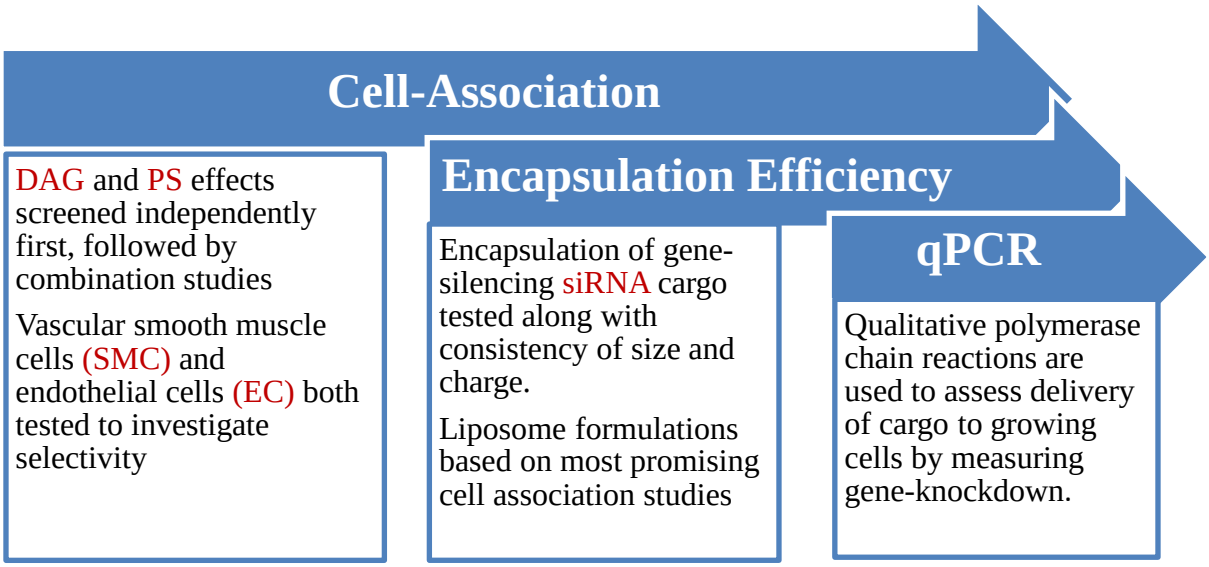

Figure 3.4: **Experimental design to test the ability of DAG and/or PS to increase delivery efficacy of an CPP liposomal nanocarrier (R8-PLP)**

Controls

For the first round of cell association studies—before combining DAG and PS into one liposomes—we included PLP controls which neither had the R8 CPP nor any DAG/PS content. This was done as an additional confirmation that our results were consistent with the VRL's previously reported data suggesting the R8 increased cell association when present at 10% of total membrane composition. Figure 3.4 presents flow chart for studying the effects of liposome composition on delivery. Figure3.5 has the molecular structures of all lipids used. Data were charted as fold increases above liposomes containing R8-stearate but lacking DAG/PS. Each assay used not only a new batch of cells but also a fresh batch of liposomes to control for variations in liposome preparation, if present. Negative controls were employed upon treatment whereby cells received starvation media only (no liposomes). Controls which had signaling lipids but lacked the R8 peptide were also used to check if the lipids could increase cell association without the presence of the CPP. Additionally, the VRL has adopted protocols to insure consistent liposomal concentrations between treatment groups, as detailed in the Methods section.

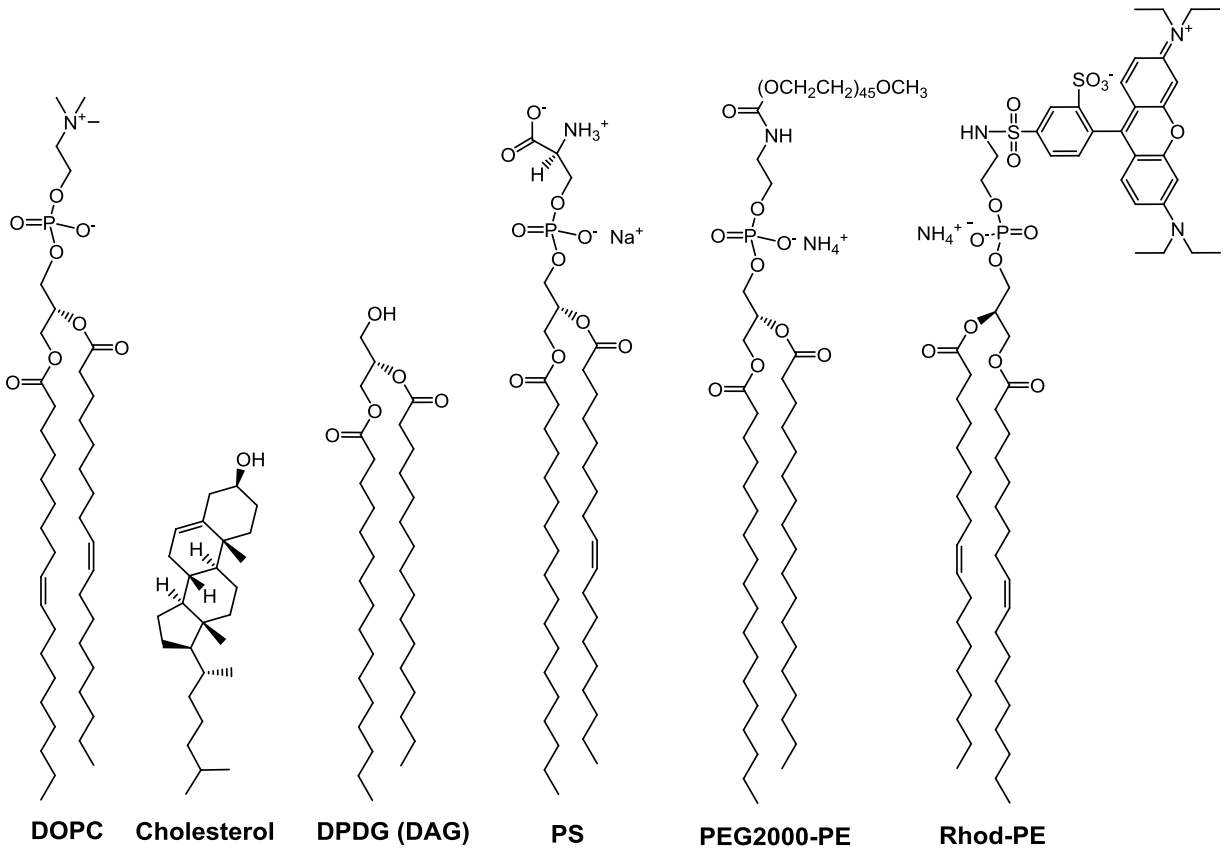

Figure 3.5: **Structures of lipid constituents used for in LDS formulations.** 1,2-Dioleoyl-*sn*-glycero-3-phosphocholine (DOPC) is our bulk lipid. Dipalmitoyl DAG and PEG-PE were used. PS was derived naturally from porcine brain tissue and its most abundant form is shown with one palmitic and one oleic tail. Rhodamine-PE (Rhod-PE) is dioleoyl. Stearyl-R8 is shown in Figure 3.3.

LDS formulations

Figure 3.5 contains all lipid structures used in these experiments. Liposomes were formed by thin film hydration, ethanol injection and dialysis. Details of liposomal preparation and characterization are described in Section 3.3, *Methods*, along with cell culture, association and encapsulation efficiency assays, and other procedural details. Figure 3.6 contains a table of LDS compositions tested in our first cell association assays. Combinatorial formulations are presented in Figure 3.13 alongside the results from their experimentation.

3.2: Results

When natural DAG and/or PS were incorporated at incrementally higher percentages within the architecture of an LDS with fixed R8, repeatable and dose-dependent responses of increased association to VSMCs and VECs with trends unique to each lipid and cell type were observed. DLS data confirm that our liposomes have consistent integrity at 37 °C when they are formed with encapsulated siRNA cargo. DLS and zeta potential characterization for liposomal formulations are presented later when discussing the results of our encapsulation studies, as these formulations contain the genetic therapeutic cargo. siRNA is costly so to conserve resources the cell association experiments presented first do not incorporate the cargo.

The fluorescent images of VSMCs in Figures 3.7 are consistent with the results of initial cell association assays (Figures 3.8, 3.9). Encapsulation efficiency experiments proved that our DAG/PS-modified LDSs retain their ability to secure genetic cargo for therapeutic applications (Figure 3.12).

DAG-potentiated cell association to VSMCs

As % DAG increases from the R8-only treatment group to R8+20% DAG (D20), an exponential increase in cell association is observed, as can be seen in Figure 3.8. These results were remarkably consistent and suggest DAG incorporation into nanocarrier architectures is a worthwhile strategy for potentiating cellular association. When LDS formulations with potent cell association are fed to cells at higher molar treatment percentages, there is observable cell damage (data not shown), which is why we treat with 0.1 mM [lipid] rather than the previously reported 0.2 mM [lipid] in cell association experiments.[144]

	% PEG-2000-PE	% R8	% Rhod-PE	% DAG	% PS	% PC/Chol (7:3)
PLP	10	0	0.1	0	0	89.9
R8	10	10	0.1	0	0	79.9
D5	10	10	0.1	5	0	74.9
D10	10	10	0.1	10	0	69.9
D15	10	10	0.1	15	0	64.9
D20	10	10	0.1	20	0	59.9
P5	10	10	0.1	0	5	74.9
P10	10	10	0.1	0	10	69.9
P15	10	10	0.1	0	15	64.9
P20	10	10	0.1	0	20	59.9
P20N	10	0	0.1	0	20	69.9

Figure 3.6: **Lipid compositions of LDS formulations for initial cell association assays.** These treatment types were selected to incrementally screen the ability of DAG and PS to increase the cell association of R8-PLPs.

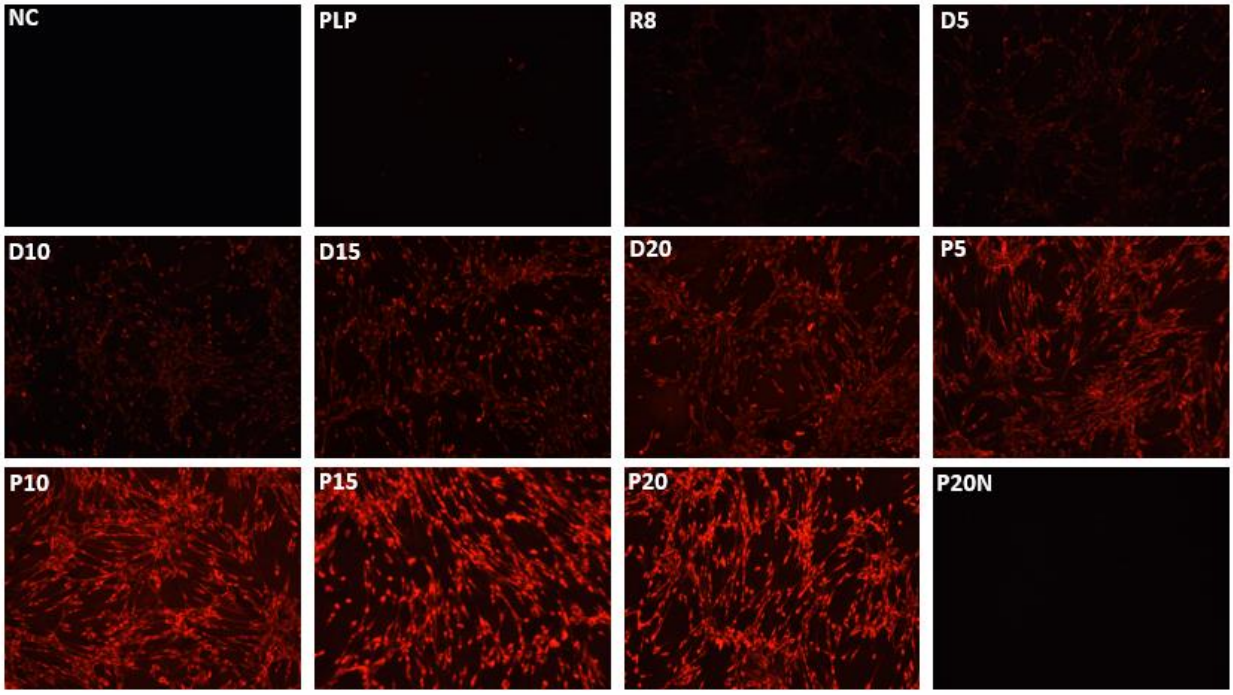

Figure 3.7: **Fluorescent microscopy images showing increased cell association of liposomes as signaling lipid content goes up.** Refer to Figure 3.6 for detailed composition of each treatment type.

Cellular integrity is equitable between negative controls, which are treated with buffer only, and liposomal treatment groups when treating with 0.1 mM [lipid]—as confirmed by bright field microscopy. However, when we moved to combinatorial studies, as discussed later, we observed morphological changes in cell membranes in treatment groups with very high associations. A possible explanation could be that the increased uptake of DAG/PS LDSs leads to incorporation of DAG and PS into the cell membranes, altering bilayer shape.

PS-potentiated cell association to VSMCs

As the percentage of PS increases from R8 only to 15% PS (P15) a linear increase in cell association is observed (Figure 3.9). However, at 20% PS the cell association begins to drop back down. The disparity of these results when compared with DAG treatment groups is intriguing, and suggests that signaling lipids could present strategic opportunities to tune the associations of LDSs. An additional control with 20% PS and no R8 (P20N) demonstrated occasional increases in cell association between replicates, as can be seen by the large error bars for that treatment group.

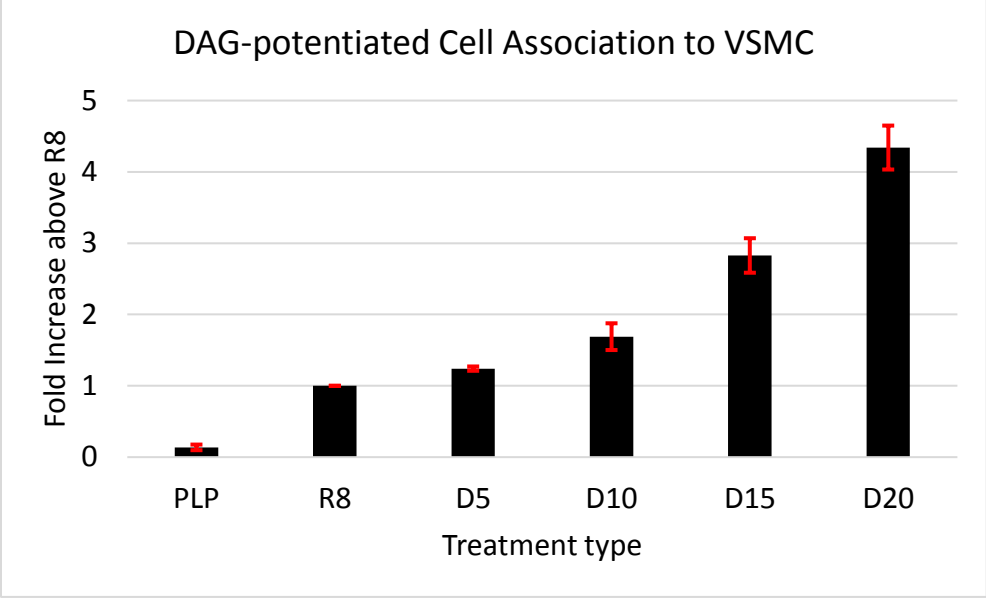

Figure 3.8: **Quantified cell association data from DAG-VSMC experiments.** DAG content increases cell association of R8-PLP liposomes in a repeatable, dose dependent manner that appears exponential if R8 is treated as zero. Error bars are standard error based on at least 3 replicates.

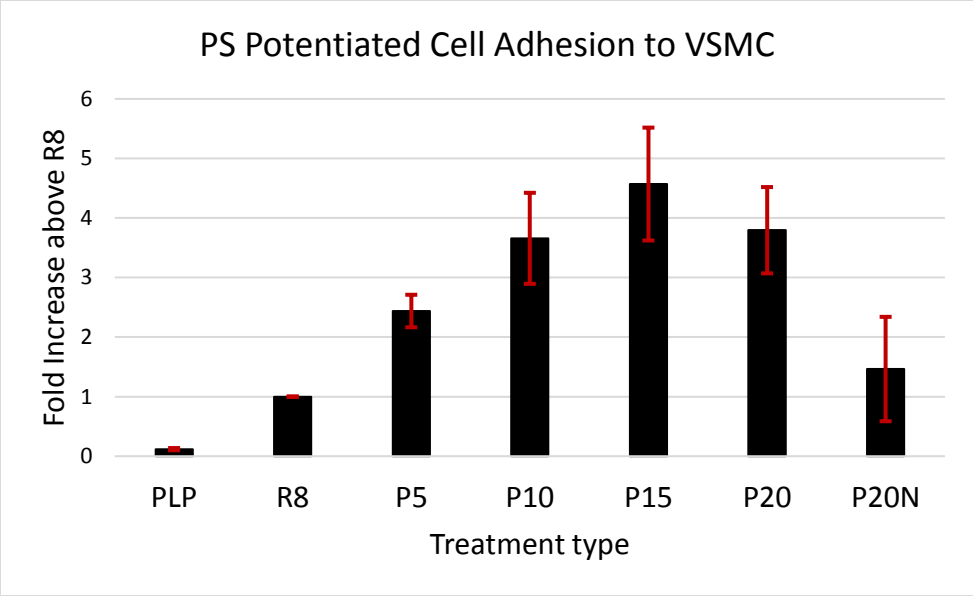

Figure 3.9: **Quantified cell association data from PS-VSMC experiments.** PS content increases cell association of R8-PLP liposomes in a linear manner to 15% with diminished returns at 20 %PS. Error bars are standard error based on at least 3 replicates.

Overall, the results of PS studies in VSMCs were less consistent than DAG studies. This may imply different mechanisms of increased association between DAG and PS. In any case, the consistency of DAG-promoted association is an attractive feature when considering the clinical translatability of this strategy.

DAG-potentiated cell association to VEC

Results presented here are based on only two replicates thus far. Thus, it is too soon to confidently ascertain quantifiable information from these studies. We can qualitatively state that the DAG-potentiated cell association in VECs (Figure 3.10) is more like the threshold type trend we observe up to 15% PS in VSMCs (Figure 3.9), rather than the consistent trend we observed in VSMCs when treating with DAG (Figure 3.8). The changes in association are less consistent between the first two VECs replicates than observed with VSMCs studies, however the inconsistency does not belie the fact that VECs also have some clear sensitivity to DAG inclusion, especially at 20% DAG.

The data so far suggest that DAG has positive effect on LDS association in both cell types.

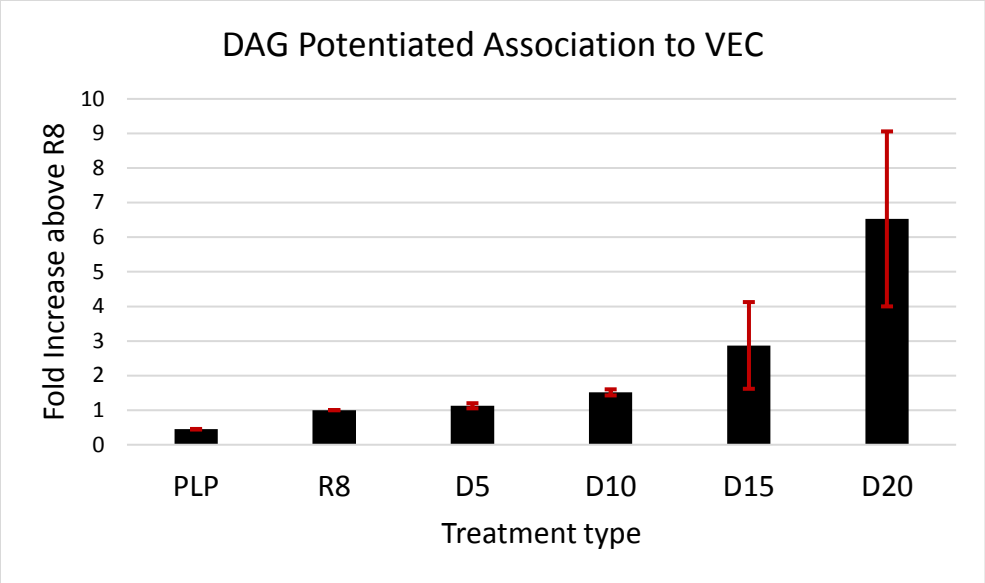

Figure 3.10: **Quantified cell association data from DAG-VEC experiments.** DAG content induces a much different response than observed in VSMC. Error bars are standard error based on 2 replicates.

Discriminate increases would be ideal for our applications, but the utility of DAG in nanodrug architectures to provide universal increases in delivery efficacy is still a worthwhile discovery. If the mechanisms of increased association do indeed vary between these cell types, DAG (at certain percentages) could afford opportunities for active targeting. Ideally, DAG/PS will eventually present opportunities to selectively usher gene silencing material to VSMCs to prevent restenosis, while leaving VECs free to convalesce until they can return to healthy function. More studies are needed in VECs to determine if DAG alone or DAG/PS can be used to selectively target one cell type over the other.

PS-potentiated association to VEC

As can be seen in Figure 3.11, PS has already shown more consistency in its ability to potentiate association of the R8-PLP to VEC, although only two replicates are presented. This is markedly different than the response DAG elicits from VECs thus far. Moreover, it is disparate from the response elicited by PS in VSMCs, especially the P20 sample that saw a decrease in association when compared with the trend up to the P15 treatment group in VSMCs (Figure 3.9). In VEC,

however, the P20 treatment group continues the steady increase observed as % PS increases (Figure 3.11).

Here, the data again suggest that PS and DAG are capable of imbuing LDSs with tunable targeting capabilities. In the case of vascular injury, the opportunity to stimulate languid VECs while silencing MMP-2 in proliferating VSMCs could greatly increase the treatment efficacies of IH following PVD interventions. Again, more studies are required, but there appear to be disparate trends between DAG and PS as we move from VSMCs to VECs. However, the possibility has yet to emerge where a PS-LDS could selectively target only one cell type while a DAG-LDS could target the other. The differences we have observed thus far between cell types is in consistency; we have yet to demonstrate the selectivity we aim to achieve. Nonetheless, the utility of these lipids to increase treatment efficacies is already apparent, even at this early stage of experimentation, and the results so far suggest that continued exploration of lipid-guided LDSs could uncover formulations that can indeed target one cell type over the other with consistency. Moreover, batch-to-batch consistency among LDS formulations is a major hurdle for establishing

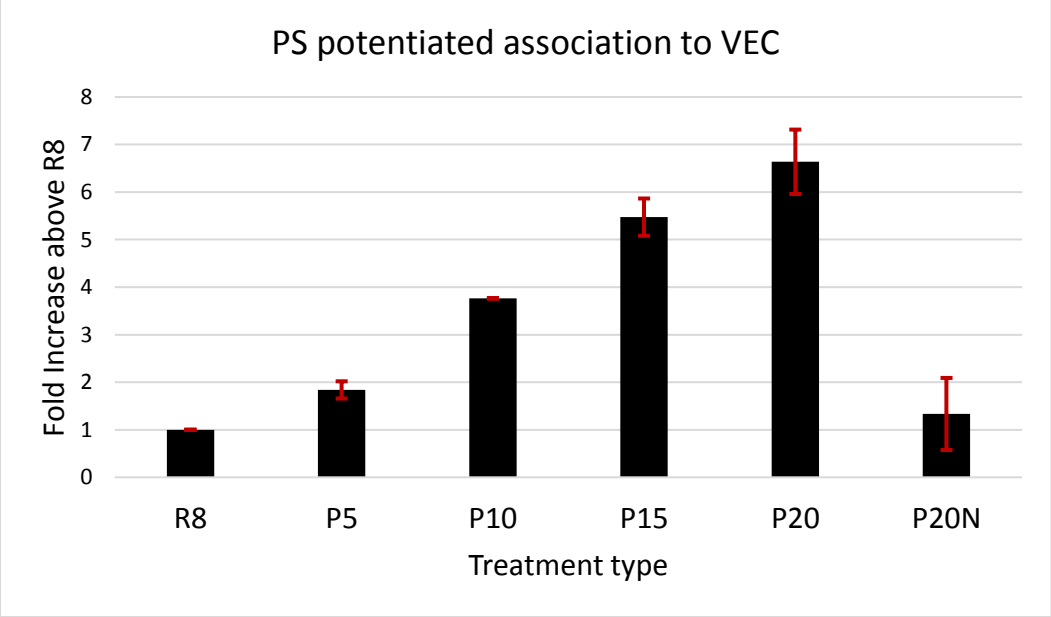

Figure 3.11: **Quantified cell association data from PS-VEC experiments.** Increases in association appear more consistent than with PS treatments in VSMC, and more pronounced than DAG treatments in VEC. Error bars are standard error based on 2 replicates.

a clinically viable nanodrug. With this in mind, we have shown that PS is a more appropriate targeting lipid for VECs, while DAG demonstrates more clinical potential for applications for LDSs targeted to VSMCs.

Encapsulation efficiency of optimal DAG/PS liposomes

The demonstrable increases in association of our vesicles by adding DAG and/or PS was a promising result at the outset of our project, however the R8-PLP must retain its ability to encapsulate genetic cargo when the signaling lipids are added, if they are to be a clinically viable active targeting strategy. Therefore, encapsulation efficiency studies were performed on the following liposomal formulations: D10P10, D15P10, D20P10, D20, P10 and R8 (Figure 3.12). The details of liposome composition are provided in Figure 3.13. When we moved on to combinatorial cell association studies we incorporated a formulation with 20% DAG, 10% PS and no stearyl-R8, termed DPN (Figure 3.13). Encapsulation efficiency was measured by including siRNA cargo in the buffer used for ethanol injection during liposome formation, followed by dialysis to remove unencapsulated siRNA. Then, liposomes were ruptured using detergent and siRNA content was quantified. Detailed experimental procedures are included in Section 3.3: *Methods*.

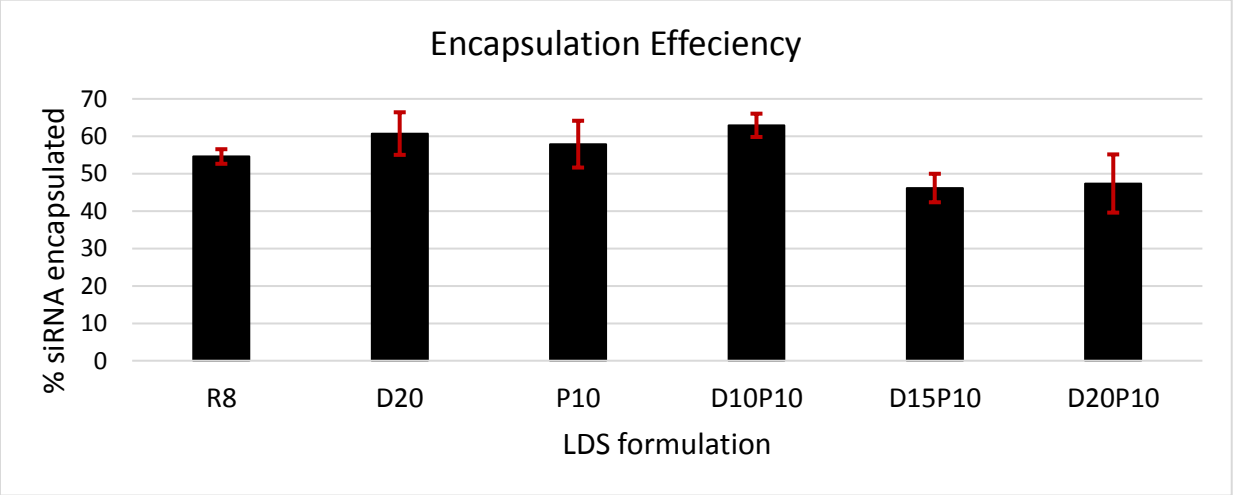

Figure 3.12: **Encapsulation efficiency results.** Combinatorial formulations as well as D20 and P10 retain acceptable encapsulation efficiencies when compared with the R8-PLP (R8).

As can be seen in Figure 3.12, we found that with PS constant at 10% there was no reduction in encapsulation efficiency up to 10% DAG and minimal, inconsistent reductions at 15% and 20% DAG. Moreover, the D10P10 liposomes encapsulated the siRNA more efficiently than the R8 liposomes while D20 and P10 had insignificant increases coupled with less consistent results.

DLS size and zeta potential studies of optimal DAG/PS formulations

Liposomes screened for encapsulation efficiency were also tested by DLS to measure average size, polydispersity index (PDI) and zeta potential. Figure 3.14 shows that our liposomes have consistent size profiles around 50-70 nm in diameter. Interestingly, 20% DAG appears to be more tolerable when PS occupies 10% of the membrane as well. Sizes and PDI rise with the addition of DAG and/or PS, diameter reliability is within tolerable ranges for such a complex LDS. Moving forward, it may be worthwhile to lower the percent of PEG or R8 to decrease nonbilayer membrane content, and test such formulations for cell association and encapsulation efficiency.

Combinatorial cell association studies in VSMCs using DAG and PS

Once we confirmed that our combinatorial DAG/PS LDS formulations encapsulated cargo well

	% PEG-2000-PE	% R8	% Rhod-PE	% DAG	% PS	% PC/Chol (7:3)
R8	10	10	0.1	0	0	79.9
D5P10	10	10	0.1	5	10	64.9
D10P10	10	10	0.1	10	10	59.9
D15P10	10	10	0.1	15	10	54.9
D20P10	10	10	0.1	20	10	49.9
P10	10	10	0.1	0	10	69.9
D20	10	10	0.1	20	0	59.9
DPN	10	0	0.1	20	10	59.9

Figure 3.13: Combinatorial LDS treatment groups. All formulations except the DPN control group and D5P10 were screened for encapsulation efficiency, size, and zeta potential before moving on to combinatorial cell association assays

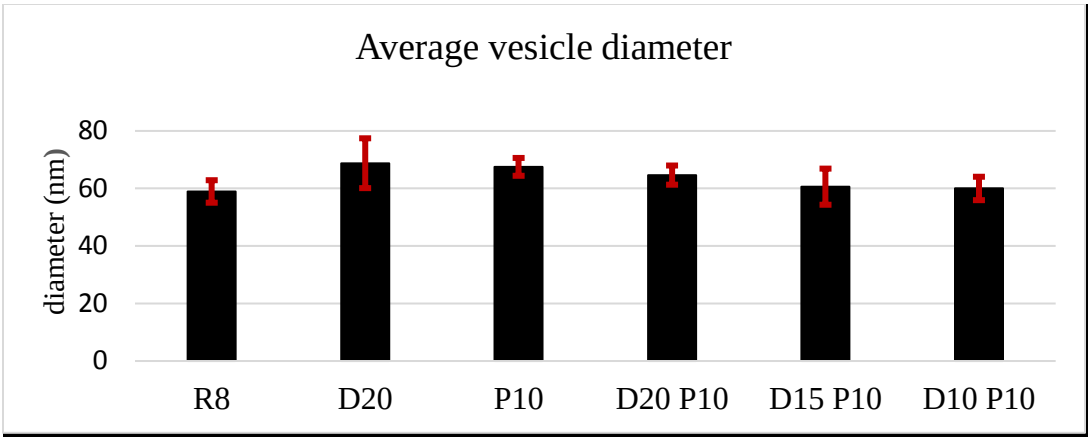

Figure 3.14: **Average diameter of DAG/PS LDS formulations**. Error bars are standard error from at least 3 replicates

and had acceptable zeta potentials and size consistencies, we moved on to test these formulations using the same cell association procedure described previously. Figure 3.16 shows that the D5P10 formulation yields a remarkable increase in cell association above the R8 only formulation when compared to previous cell association assays. Cell association drops with D10P10 but then continues to go up and peak where we expected it to with the D20P10 formulation.

D5P10 liposomes have a PDI consistently below 0.2 (Figure 3.14), which is also an attractive feature of this formulation. Furthermore, fluorescence microscopy demonstrated some cell damage with combinatorial formulations high in DAG (Figure 3.17). Therefore, the D5P10 liposomes are a very exciting treatment group to carry forward with to qPCR studies as we can achieve significant increases by incorporating low percentages of our type 1 signaling lipid, DAG.

Future work: Cargo delivery profiles by qPCR & cytotoxicity assays

This project has not yet progressed to studying the ability of our formulations to deliver siRNA cargo, achieve transfection, and silence MMP-2 activity in VSMC. These studies are imminent, and we are excited to proceed with this project and present our findings so that liposomal nanodrug architectures for various applications can begin to test the effect of incorporating signaling lipids. Based on previous work by the VRL and correlations between cell association and gene transfection, we anticipate that our novel LDS formulations will achieve significantly higher deliver profiles than R8-only controls.

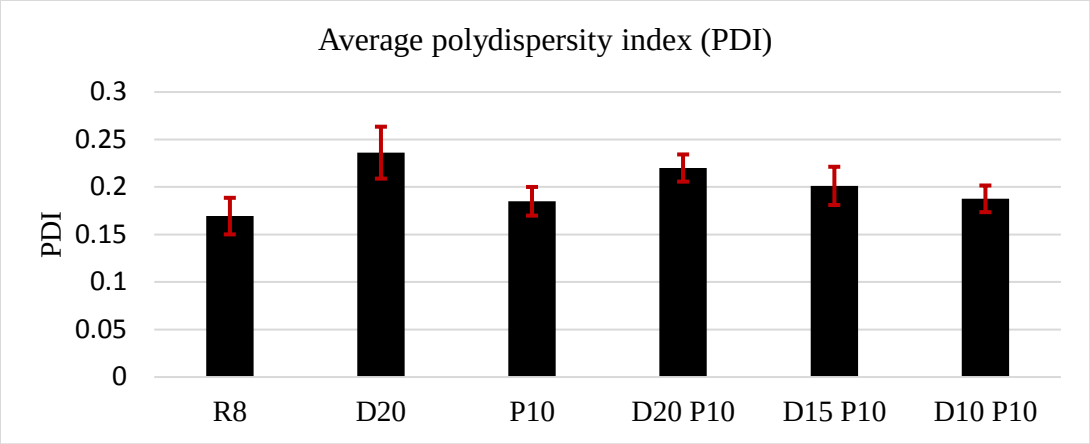

Figure 3.15: **Average PDI of DAG/PS liposome formulations.** Error bars are standard error based off at least 3 replicates.

Additional future work includes cytotoxicity assays to confirm that our LDSs do not kill cells. Based on microscopy evidence, we are confident they will not. Cells are checked under a bight field microscope consistently during growth and treatment and appear healthy. VECs will also continue to be subjected to cell association assays with the initial LDS formulations in Figure 3.6, and once that is complete they will be screened with the combinatorial formulations found in Figure 3.13, just as VSMCs were.

Discussion

As alluded to previously, the idea that DAG and other signaling lipids could be used in liposomal architectures to increase nanocarrier efficacy was conceived during the work described in Chapter 2. The literature review in Chapter 1 lays out various roles that DAG plays in pathological cells. This raises the possibility that DAG's mechanism of increased cellular association may involve active targeting of overly abundant proteins selectively expressed in the injured human aortic cells that have been studied. However, more experimentation in a variety of tissue types is required to confidently assert that the increased association we have observed is due to intermolecular activity beyond DAG's mechanical impact on supramolecular assemblages. If DAG was found to have little or no impact on the cell association of LDSs when treating healthy

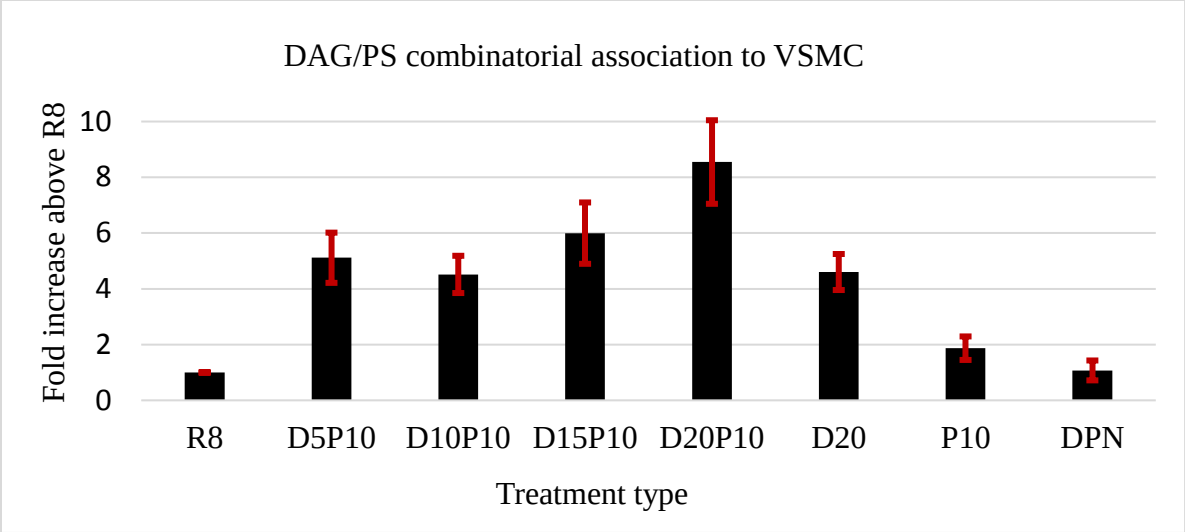

Figure 3.16: **Cell association data using combinatorial formulations of DAG/PS.** Error bars are standard error based on at least 3 replicates.

tissues from other parts of the body, this would support the notion that DAG's protein affinities were at play in the results we presented here. If the experimental trends presented above are indeed due to membrane perturbations brought about by DAG's type 1 lipid geometry, this project still demonstrates that DAG, PS, and other signaling lipids present solutions to increasing the cellular association of liposomal nanocarriers.

3.3: Methods

Liposome formation and characterization

Lipids (Figure 3.5) were purchased from Avanti Polar Lipids (Alabaster, AL), stearyl-R8 was purchased from LifeTein LLC (Somerset, NJ). Lipids were combined as indicated in Figures 3.6 and 3.12 by dissolving in chloroform and mixing in 1 dram glass vials and then removing solvents under a stream of nitrogen to create lipid films. Liposomes were then formed by ethanol injection as previously reported.[281] Lipid films were resuspended in 200 µL of pure molecular grade ethanol and mixed for 30 minutes at 40 °C . Ethanolic lipid solutions were then injected dropwise into 10 nmM tris-HCl (pH 8) under constant vortexing. Liposomes were then purified from ethanol via overnight dialysis in pure water at 4 °C using 1 mL 300 kD Float-A-Lyzer™ G2 dialysis devices

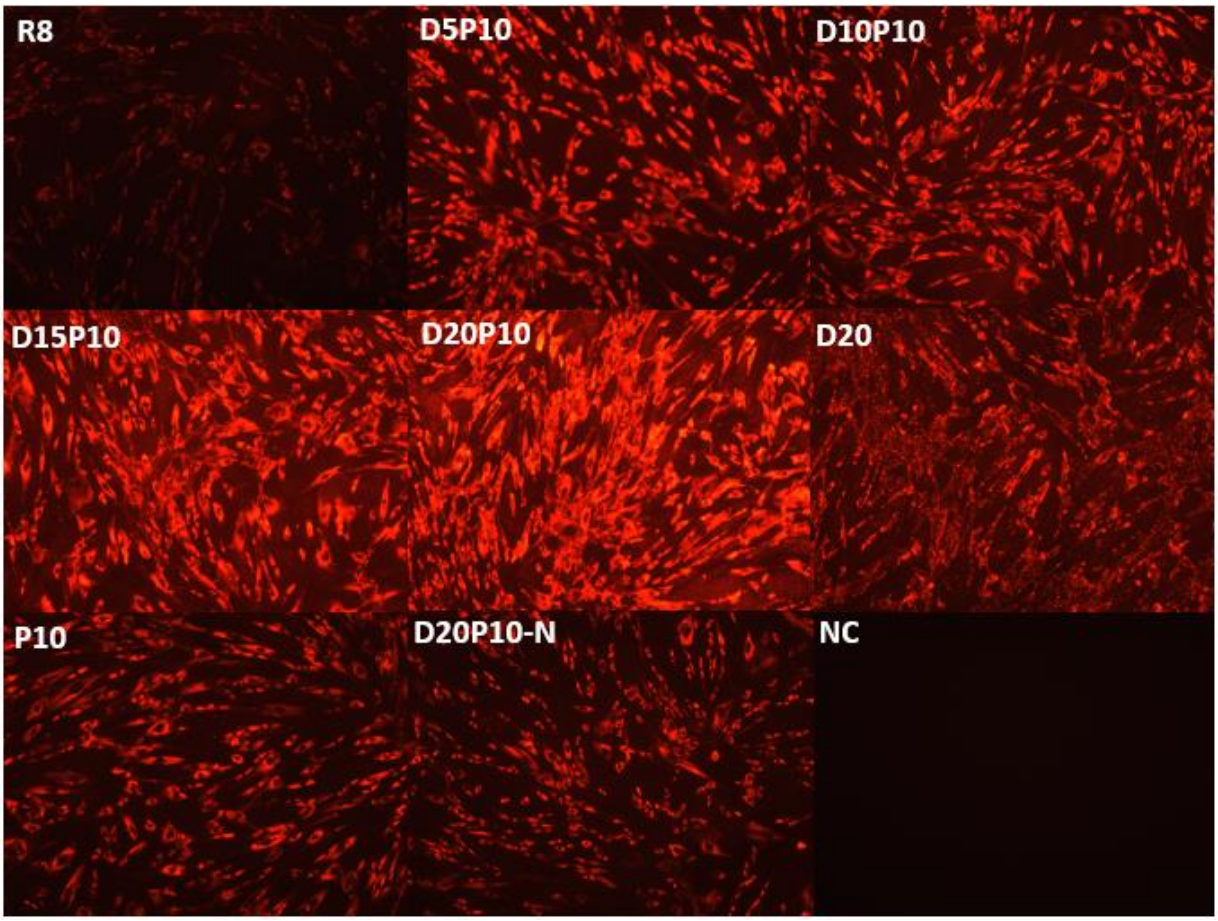

Figure 3.17: **Representative fluorescent images from combinatorial DAG/PS cell association assays in VSMC**

(Spectrum labs, Rancho Dominguez, CA). A single pure water exchange midway through dialysis ensured efficient purification from residual ethanol. After dialysis, the final volume was measured and used to determine treatment volumes for cell association assays such that all samples received equimolar lipid content. Liposomes were extruded to 100 nm using polycarbonate membranes Nanosizers™ (T&T scientific, Knoxville, TN), stored at 4 °C and used within 48 hours.

Average size, PDI and zeta potential for of every LDS treatment type was measured in triplicate by dynamic light scattering (DLS) and electrophoretic mobility on the Zetaizer Nano ZS instrument (Malvern Instruments Ltd, Worchestershire, UK).

Cell culture

Cryopreserved 49-year-old male tissue samples were purchased from LifeLine Cell Technology (Walkersville, MD) for culturing of human aortic smooth muscle cells (HASMCs). Cells were grown in T75 flasks and then plated at 1.5×10^5 cells per well (6-well plate) for cell association experiments. Cells were grown to ~80% confluency in VascuLife growth medium composed with VascuLife Basal Medium and VascuLife smooth muscle cell supplement kit with gentamicin and amphotericin (LifeLine Cell Technology). Incubation was performed at 37 °C under 5% CO_2 with 95% humidity until cells reached ~80% confluency. Before liposomal treatment, cells were made quiescent by treating overnight with Dulbecco's Modified Eagle Medium (DMEM, Thermofisher Scientific) with gentamicin and amphotericin.

Measuring cell association

Lipid-dependent cell association was measured using a set of standard procedures previously adapted by the VRL to confirm R8-dependent cell association. The assay involves the formation of liposomes with 0.1% rhodamine-PE, 10% PEG and 10% R8 among positive controls with the addition of signaling lipids accompanied by a reduction in PC/Chol content, as depicted in Figures 3.6 and 3.12. 80% confluent cells were treated with 0.1 mM [lipid] liposomes in DMEM. After 24 h treatment, cells were washed three times in PBS, lysed with 1 mL of 1% Triton X-100, and centrifuged at 12,000 RPM for 5 min at 4 °C to remove debris. Cell lysates (200 μL) were plated in triplicate in 96-well plates, carefully so as not to contaminate samples with debris. Fluorometric analysis using a Glomax multi microplate reader by Promega with a 575 nm filter determined

average fluorescence units for each sample, minus baseline fluorescence of nontreated controls receiving no rhodamine source within each experimental replicate. Samples were normalized to the R8-only liposomes to judge fold increase in association as a function of DAG/PS content. Replicate studies always used fresh batches of liposomes. Fluorescence microscopy made use of a Texas Red fluorescent filter at 400X with 400 ms exposure across all groups.

Measuring encapsulation efficiency

To encapsulate siRNA, liposomes were prepared precisely the same as described previously but the tris buffer (used during EtOH injection) also contained 50 μg of siRNA (Thermofisher Scientific, Waltham, MA) and 10 mM $CaCl_2$. Dialysis also included an additional media exchange (two total) to ensure that all unencapsulated siRNA was removed.

Retention of siRNA after ethanol injection, dialysis and extrusion was quantified using a Quant-iT RiboGreen RNA Assay Kit (Thermofisher Scientific). 10 μL of liposomes were digested in 1% Triton X-100 at 37 °C for 15 min to release siRNA from their aqueous cores. Samples were then mixed 1:1 with RiboGreen reagent that labels siRNA with fluorescence, and emission was then measured at 525 nm. A standard curve of siRNA in 1% Triton X-100 was created to qualify the arbitrary fluorescence units of siRNA released from digested liposomes and thus determine siRNA concentration. Encapsulation efficiency was then calculated for each LDS formulation as (μg siRNA encapsulate/50 μg total siRNA) × 100.

Acknowledgments

This work was performed at the VRL within the University of Tennessee Medical Center (UTMC) in Knoxville, TN. Significant assistance and direction came from Dr. Mountain, Trey Fisher, Conner West and others at the VRL. The Best Lab is grateful for their ongoing support.

CHAPTER 4: USING SYNTHETIC LIPIDS TO ACHIEVE LIPOSOMAL FUSION AND CARGO RELEASE

4.1: Introduction

Collectively, a few of the other projects I assisted with during my graduate career fall under the umbrella of controlled—or 'triggered'—release. Lipids engineered to respond to target cells or external stimuli may be incorporated into LDS to create stimuli sensitive nanoparticles (SSNs). SSN technology, a field the Best Lab strives to be at the forefront of, will be briefly reviewed in this chapter's introduction. The review in section 4.1 will include mention of two Best Lab projects: a photoactivatable lipid trigger activated by UV light to stimulate liposomal release, and promoting fusion between membranes via synthetic clickable lipids. Section 4.2 will detail how we confirmed the mixing of aqueous contents as part of our investigation of click-promoted fusion.

Figure 4.1 shows the general strategy of how functional lipids can promote release of aqueous cargo. Lipophilic cargo can also be encapsulated within bilayers and be selectively released in this

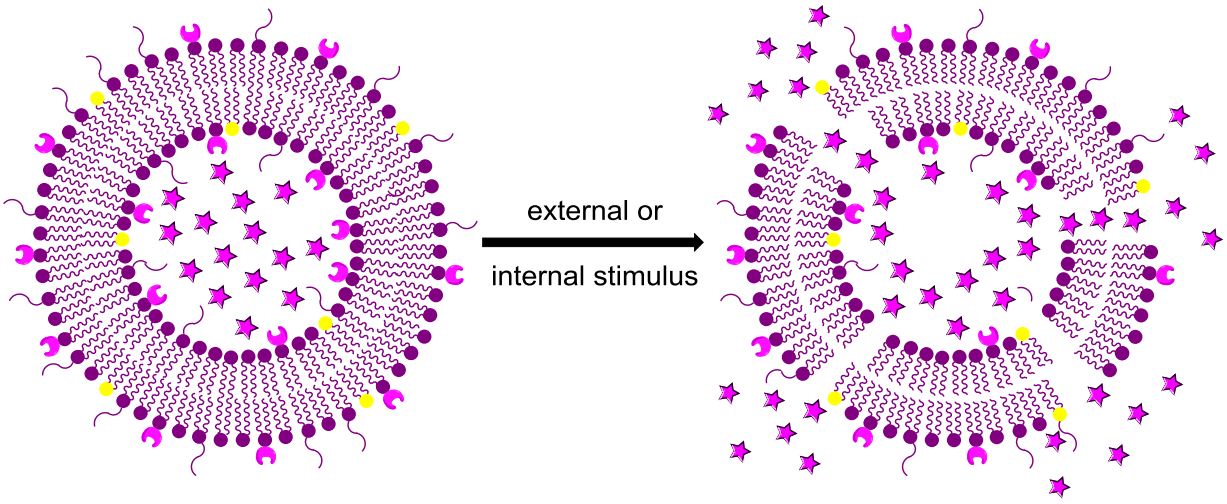

Figure 4.1: **A cartoon of triggered release from SSNs.** A synthetic lipid (yellow headgroup) is shown reacting to a stimulus to perturb its membrane environment, allowing for release of aqueous cargo (star shape).

way. Just like the active targeting strategies reviewed earlier, very few SSNs make it to clinical testing and as yet none have passed. Section **4.3** will discuss the future directions of SSNs, including strategies that take cues from biology for more clinically viable triggered release platforms.

Existing strategies for controlling liposomal release

Advances towards active targeting are for naught if liposomes succumb to cellular endocytic pathways or if cargo is degraded lysosomaly prior to being released into the cytosol. To ensure delivery of encapsulated drug, triggered release strategies have developed two distinct modes of operation. Passive release makes use of unique cell pathologies at target cites, just like active targeting. Active release involves engineering SSNs that respond to external stimuli to control release. Both of these strategies are referred to as forms of 'smart delivery'.[7]

Passive release liposomes are triggered to release their contents in the presence of abnormal pH, temperature, oxidative conditions or other traits characteristic of target tissues, such as unusual enzymatic activities at tumors. Aberrant enzymatic activity harnessed by passive release strategies includes the matrix metalloproteases,[282] which are the therapeutic targets addressed in the previous chapter. Passive release stimuli are inherent to the target site, such as the lowered pH[283] and increased redox potentials of tumors and inflamed tissue.[284] Research to capitalize on these intrinsic differences has created a plethora of responsive liposomes, including pH-sensitive sheddable PEG coatings so that LDSs drop their camouflage upon reaching target cites with higher acidity, increasing cellular uptake.[285] However, intrinsic differences such as acidity are often slight, making these strategies promising but challenging to actuate.

Active release platforms, on the other hand, respond to external stimuli. This affords more control over the location of release. However, reaching the vessels with the stimulus can be challenging once they have entered the body and accumulated at target sites. External stimuli for active release include applied heat,[286] ultrasound,[287] light[288] or electromagnetic fields.[289] Demarcations between active release strategies are often blurred. For instance, inductive magnetic heating[290] or ultrasound[291] can be used to achieve hyperthermic release. No matter the heating mechanism (be it superparamagnetic, echogenic, or simply applied heat), SSNs exhibiting hyperthermic release are called thermosensitive liposomes.

A common thermosensitive strategy among SSN formulations involves tailoring liposomal architectures with lyso lipids to lower their transition temperatures to heighten heat-sensitivity.[292] Lysolipid thermally sensitive liposomes (LTSL) incorporate mixtures of monoacyl and diacyl PC to create SSNs that respond to thermal ablation brought about by microwave, radiofrequency or aforementioned heating mechanisms.[293] Currently, a thermosensitive SSN, ThermoDox®, has reached phase 3 clinical trials. ThermoDox® is a LTSL administered with radiofrequency ablation to stimulate release, but it is also sensitized to microwave or ultrasound heating.[294] ThermoDox® is the only SSN currently under clinicial trials.[159]

Visudyne®, which was developed well over a decade ago, is a commercially available LDS that delivers a photodynamic therapy (PDT), which in this case is a light-absorbing synthetic porphyrin called verteporfin.[295] Although IR light triggers the therapeutic agent in this case, the liposomes (as a delivery vessel) are not being triggered to unload their cargo by the administered light. In terms of commercially available SSNs that respond to light, there are technically still none. The promise of light-mediated liposomal release technologies remains unrealized clinically. In general, the dearth of commercially available SSNs highlights the need for developing more tools for triggering liposomal release.[159]

The complex, interdisciplinary nature of SSN development can be a barrier towards their implementation. Careful biophysical tuning of trigger molecules must coincide with rationally chosen, well-vetted bilayer counterparts for biomedically engineered responsive LDSs. Moreover, these endeavors often rely on inorganic, polymer, or synthetic organic chemistry to afford nanodrug developers the tools they need to control liposomal release. As an example, we will discuss a synthetic photoactivated lipid developed by the Best Lab.

A photocleavable PC-analog for controlled release of liposomal cargo

This was the principal project of former Best Lab member Dr. Andrew Bayer. I aided his synthesis of an intermediate compound (full tail acid **4.6**, Figure 4.2) used by Dr. Bayer to complete his lipid nitrobenzyl PC trigger (NB-PC), which displayed promising release characteristics.[150] The synthesis in Figure 4.2 was devised by Dr. Best and Dr. Bayer. They chose PC as the trigger analog for its strong bilayer properties and formed stable bilayer vesicles with 100% NB-PC. Full tail acid **4.6** was engineered to have a nitrobenzyl entity that is stimulated by UV light to undergo

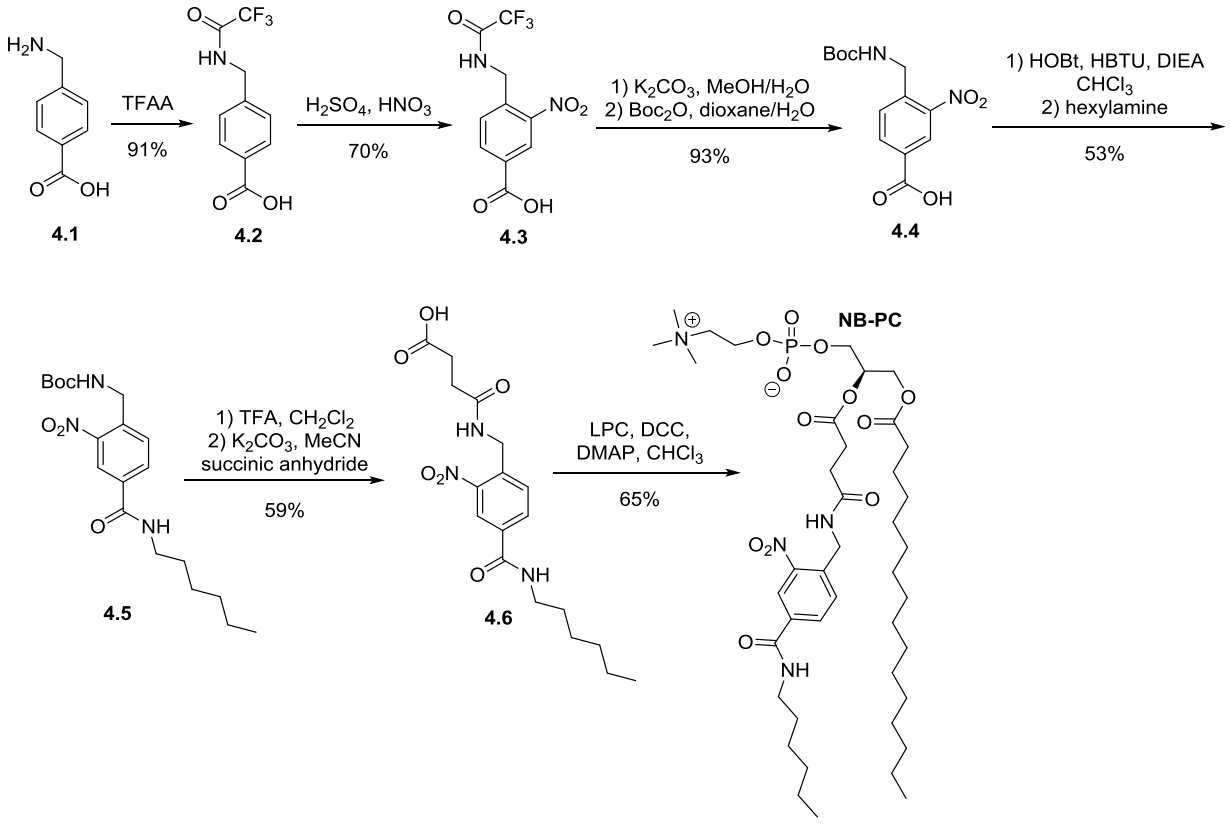

Figure 4.2: **Synthesis of a photocleavable release trigger.** NB-PC, synthesized by Andrew Bayer of the Best Lab, was used to create an SSN triggered by UV light to release bilayer cargo. NB-PC exemplifies how synthetic organic chemistry creates tools to break new ground for LDS functionality.

cleavage. By coupling **4.6** to LPC, Dr. Bayer created a PC analog that is triggered to turn itself back into an LPC analog. LPC has strong non-bilayer tendencies. Thus, tail cleavage destabilizes the membrane substantially, releasing bilayer cargo.

Cleavage of the full tail acid occurs as follows: the nitrobenzyl group absorbs a ~365 nm photon, exciting the nitro oxygen proximal to its *ortho*-benzyl neighbor, and causing to react with the benzylic carbon, promoting cleavage of the bond between the benzyl carbon and the amide-LPC leaving group. The resultant cleaved tail exists as benzaldehyde with an *ortho*-nitroso (the *para*-*N*-hexyl-phenylamide at the bottom of the tail is unaffected.) Dr. Bayer found that the NB-PC trigger began to promote release when it was incorporated at as low as 10% of PC vesicles, with steady increases in release profiles as percent NB-PC went up. Importantly, release controlled by exposure to UV light, with no background release observed in samples kept in the dark.

To access full tail acid **4.6**, we began by capping the amine of 4-(aminomethyl)benzoic acid (**4.1**) with trifluoraceticanhydride (TFAA) to create **4.2**. We then nitrated the benzene ring using standard electrophilic aromatic nitration conditions; the slow addition of sulfuric acid combined with nitric acid created nitrobenzyl **4.3**. The amine was freed from its trifluoro acetamide cap using potassium bicarbonate, and then reprotected with a Boc group to form **4.4**. We then coupled the carboxylic acid to a hexylamine tail to form the bottom of our full tail acid as seen in compound **4.5**. The top portion of the full tail acid **4.6** came in the form of an opened succinic anhydride molecule by first removing the Boc group using trifluoracetic acid (TFA) and then treating with potassium bicarbonate and succinic anhydride. Dr. Bayer finished the synthesis by coupling **4.6** to LPC to create NB-PC trigger. Full experimental procedures and characterizations for the synthesis of full tail acid **4.6** and **NB-PC** have been reported previously[150] and are omitted from this dissertation.

To measure release of membrane-bound cargo, the Best Lab utilized a nile red-based fluorescence release assay. Nile red, Figure 4.3, is only fluorescent in aqueous solution when solvated in a membrane context, and thus can be used to study membrane behavior. Nile red's utility is also born if its inherent similarity in structure to hydrophobic drug molecules such as camptothecin (CPT), as can be seen in Figure 4.3. CPT is a chemotherapy commonly used in development nanoparticle delivery of cancer drugs.[296] The NB-PC photo-trigger demonstrated highly predictable release properties based on reduction in Nile red signal, which was released

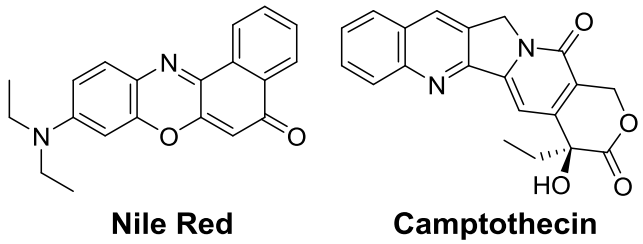

Figure 4.3: **Structures of Nile red dye and the cancer drug Camptothecin are compared.** Nile red was used as a hydrophobic drug mimic to confirm the ability of NB-PC (Figure 4.2) to promote release from SSNs upon exposure to UV light.

from the membrane only in response to UV light, only when NB-PC was incorporated into the membrane.

Clearly, active release strategies have the potential to impart a degree of control beyond that of passive targeting. While these two strategies strive to achieve similar goals, passive release is an extension of active targeting and takes its cues from biological phenomena that enable release. Active release hinges upon external, bioorthogonal stimuli that selectively motivate SSNs to expel their contents. A related field of controlled release that draws inspiration from both passive and active release platforms is liposomal fusion.

Inducing membrane fusion using clickable lipids

Ever since artificial membranes were first developed as functional nanoparticles, vesicle fusion has been explored in relation to liposomal technologies. In biology, lipophilic SNARE proteins dictate when and how membranes fuse.[297] A variety of functional liposomes have emerged that make use of complementary molecular interactions or electrostatics to promote vesicle conglomeration, adhesion, and fusion.[298] Significant research has gone into unraveling the degree of fusion and multicompartmental vesicle formation that takes place given various fusion strategies. However, for fusion technologies to develop clinically viable applications, bioorthoganality is paramount. Here, we return yet again to click chemistry to discuss an offshoot of active release where SPAAC can be used to spontaneously fuse liposomes respectively decorated with clickable azide and alkyne moieties.

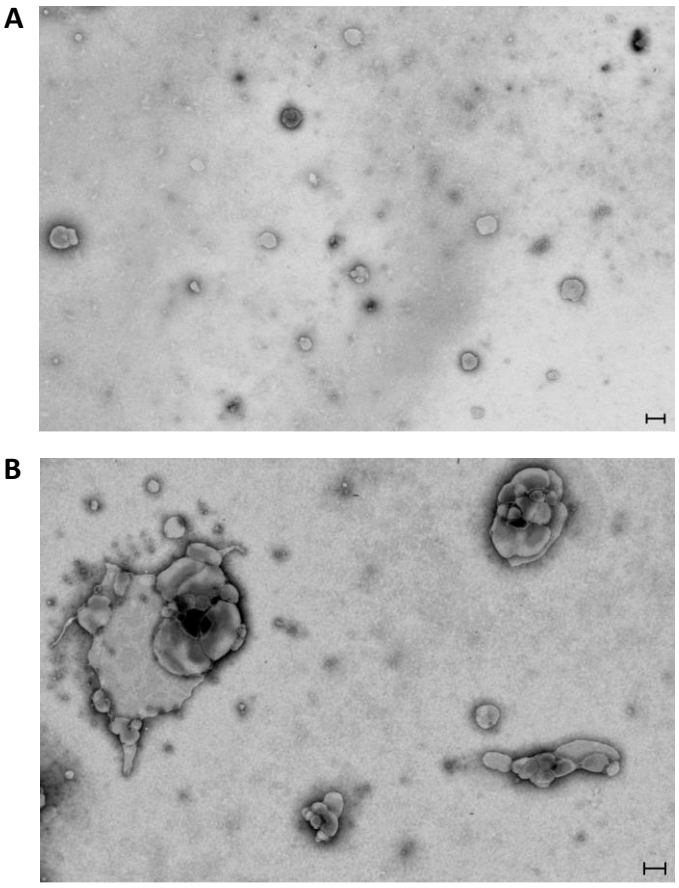

Figure 4.4: STEM images of azido liposomes before and after incubation with cyclooctyne liposomes.[148] Image A shows ~100-200 nm liposomes bearing a lipid-anchored, concentric circles within membranes indicate collapse of unilamellar vesicles under the stain used for contrast, occasional aggregation was observed. Image B shows GMV formations only present when azide and cyclooctyne liposomes are mixed. Aggregation and fusion are readily observed.

Click chemistry, as discussed in Chapter 1, is a robust platform for the derivatization and manipulation of liposomes. Dr. Best and former Best Lab member, Dr. Stuart Whitehead, devised a scheme whereby fluorescent dilution experiments and electron microscopy were used to confirm SPAAC-driven fusion between azido and cyclooctyne liposomes.[148] Clickable liposomes were formed using synthetic phospholipids with either azide or cyclooctyne moieties anchored to their surfaces. Clickable liposomes where also pre-formed with lipidic dye molecules to enable Förster Resonance Energy Transfer (FRET) assays for qualifying intermixing of sibling membranes. Initially, I advised and aided in liposome formation, DLS and (scanning) transition electron microscopy (STEM/TEM) to help probe for photographic evidence (Figure 4.4) of increased vesicle aggregation/fusion in the presence of Dr. Whitehead's clickable synthetic lipids.

4.2: Verifying mixing of aqueous cargo between fused liposomes

Dr. Whitehead's FRET and STEM results evidenced fusion events that occurred only when azido and cyclooctyne liposomes were incubated together. However, said experiments did not preclude the possibility that inner leaflets were still intact and aqueous cargo was not being delivered. If a pseudo-fusion event such as this was occurring, covalent linkages between clickable liposome membranes would have resulted in multivesicular formations with discrete aqueous compartments. Thus, the possibility remained that Dr. Whitehead's synthetic clickable lipids had achieved covalent conglomeration rather than full fusion. Conveniently, content mixing assays can be performed that verify the rupture of aqueous liposomal cores.[241]

We suspected full fusion was occurring, as the STEM images in Figure 4.4 suggested the presence of larger, non-spherical vesicles. Moreover, the four-tailed linked-lipid species formed upon inter-vesicle click reactions would instantly create exponentially larger headgroups for each reacting lipid. This would theoretically increase lateral dispersion immensely for each membrane, destabilizing the bilayers and exposing inner-leaflets. We reasoned that if clickable groups on inner-leaflets become exposed, the cascade of membrane dissociations would lead to amphiphilic reorganization into fused vesicles with some degree of multilamellarity and/or multivesicularity. These vesicles would likely be bilayer liposomes, since at least 50% of our formulations were bilayer-forming PC, with mixed aqueous cargos. This mechanism could be justified by FRET and

STEM, but not confirmed. Thus, we applied additional experimentation to test for internal compartment disruption, which was necessary to be confident that click-promoted fusion could be applied to the delivery of both hydrophobic and hydrophilic cargo.

The terbium-trichloride ($TbCl_3$)-dipicolinic acid (DPA) content mixing assay

$TbCl_3$ and DPA, Figure 4.5, have negligible inherent fluorescence on their own. When these two compounds are mixed, however, an exponential increase in fluorescence is observed. In the study group, clickable sibling liposomes were each filled with one of these dye partners and incubated with another and then probed for changes in fluorescence as compared to control groups. Control groups contained the appropriate dye partner but lacked the clickable lipids to promote fusion. If our system was simply inducing aggregation and/or multivesicular conglomeration, control and study groups would produce similar data. If, however, we were inducing fusion between our clickable liposomes, a predictable and repeatable increase in fluorescence should be observed in the study group that should be significantly higher than background leakage observed in the control groups. Moreover, fluorescence would be increased in both samples in non-specific vesicle leakage was occurring.

Results

We observed significantly greater increases in fluorescence intensity when liposomes displayed their clickable lipids, as can be seen in Figure 4.6.[148] This was attributed to fusion events that resulted in the mixing of aqueous cargo to form the fluorescent Tb-DPA complex.

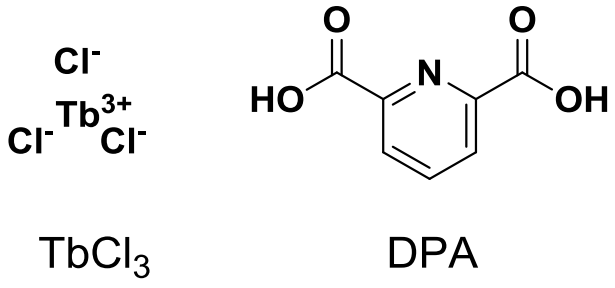

Figure 4.5: Structures of DPA and $TbCl_3$

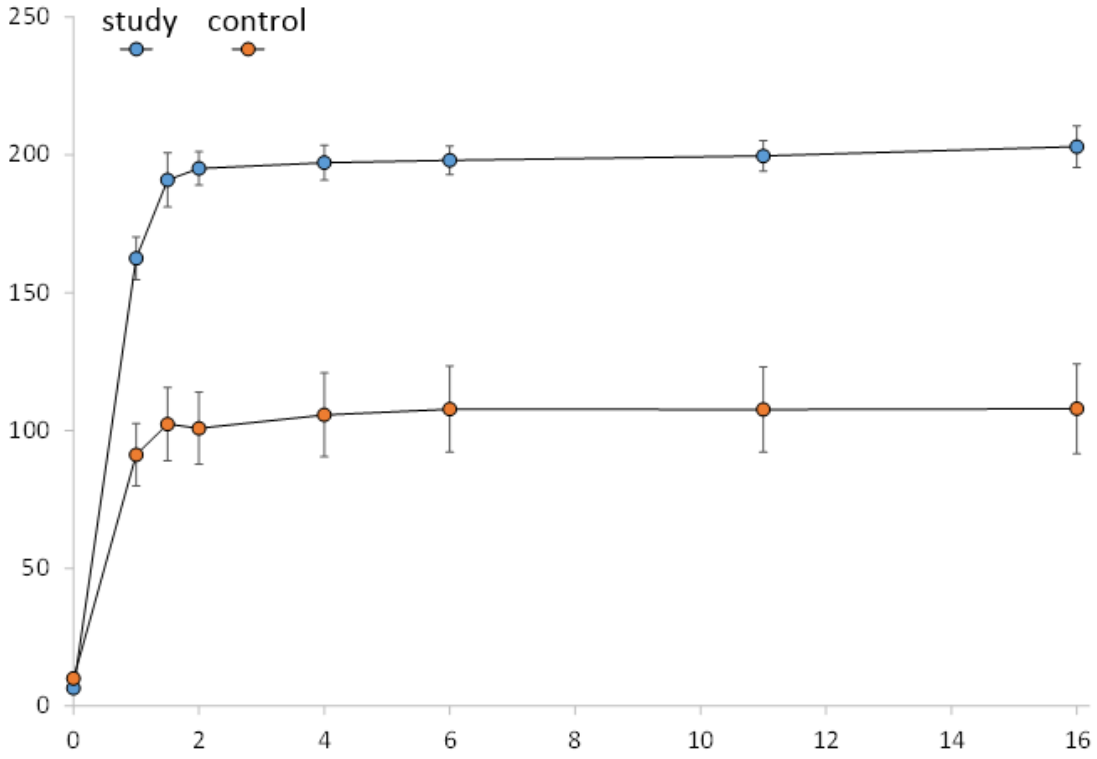

Figure 4.6: Results of the DPA and $TbCl_3$ content mixing assay.[148] Fluorescent signal of the terbium-DPA complex is detected at 489 nm to determine mixing of aqueous cargo. Change in intensity is charted as a function of incubation time in minutes. A significant increase in the mixing of aqueous cargo is observed in the study liposomes (46/46/8 PC/PE/cyclootyne lipid encapsulating DPA + 46/46/8 PC/PE/azido lipid encapsulating $TbCl_3$). Change in intensity of control liposomes (54/46 PC/PE encapsulating DPA + 54/46 PC/PE encapsulating $TbCl_3$) is due to osmotic leakage of aqueous cargo. Error bars are standard error based on at least three replicates.

To achieve these results, we experimented with reverse phase evaporation (REV) liposome formation to increase encapsulation efficiency of DPA and $TbCl_3$. Ultimately, we settled upon standard thin-film hydration followed by freeze-thaw and extrusion, finishing with SEC to remove unencapsulated dye molecules. Various other parameters of the content mixing assay were optimized to yield consistent fluorescent data that we could confidently attribute to mixed aqueous cargo. Procedural details are presented next in *Methods*.

Methods

ODIBO lipid (**OL**, Figure 4.7) was synthesized by Dr. Whitehead[148] and an azido lipid (**AL**, Figure 4.7) was previously synthesized by the Best Lab.[299] All other lipids were purchased from Avanti Polar lipids. Solvents, reagents and other materials were purchased from Acros, Aldrich or Fisher Scientific and used as received. Liposome extrusion was done with a LiposoFast-Basic extruder (Avestin). Fluorescence experiments were done in a PerkinElmer LS-55 luminescence spectrometer with a 100 μL microcuvette using a scan rate of 100 nm/min, a 5.0 nm excitation slit, and a 7.5 nm emission slit. Excitation was at 278 nm, emission was measured using an average of 3 scans and maximum emission was observed at 489 nm. SEC protocols and content mixing assay buffer ingredients were adapted from a previously reported protocol,[241] as described below.

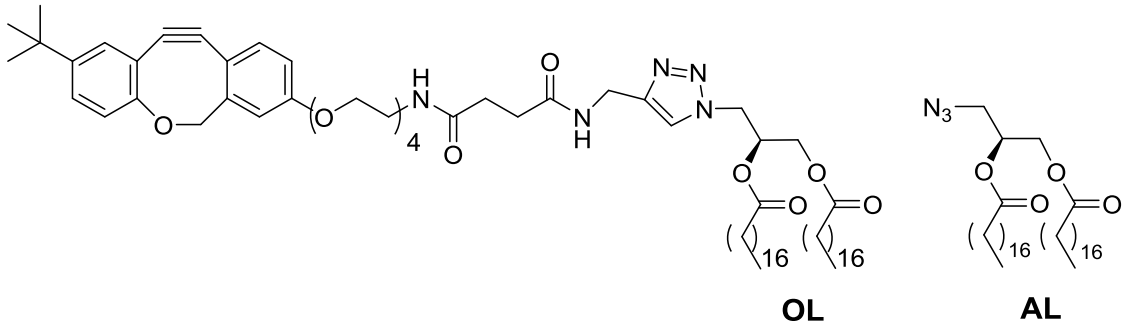

Figure 4.7: Synthetic clickable lipids used. Clickable lipids of the ODIBO (OL) and Azide (AL) variety were immobilized in respective liposomes used to promote liposomal fusion between click-sibling vesicles. Both lipids were synthesized by Dr. Whitehead[148] and other members of the Best Lab.[299]

Liposomes were formed by making stock solutions from dry PC (65 mM), OL(1.3 mM), and AL (1.3 mM) solvated in $CHCl_3$. PE which was purchased in $CHCl_3$ at 13.9 mM and used as is. Lipid films of three different compositions were formed ('**O**', '**A**', and '**C**') by combining appropriate volumes of stock solutions (with a total of 4 mM of lipids when rehydrated in 1 mL of aqueous buffer) to make: **O** 46:46:8 (PC:PE:**OL**), **A** 46:46:8 (PC:PE:**AL**), **C** 54:46 (PC:PE). **C** was made in duplicate. Film formation culminated with solvent removal using rotary evaporation followed by sitting overnight under vacuum. Two distinct hydration buffers were formed and kept away from light: buffer **T** contained 15 mM $TbCl_3$ while buffer **D** contained 50 mM DPA. The remainder of both buffers was comprised of 2 mM L-(–)-histidine and 2 mM N-[Tris(hydroxymethyl)methyl]-2-aminoethanesulfonic acid sodium salt (TES). Hydration consisted of adding 1 mL of buffer, vortexing thoroughly, heating for 1 h at 50 ^{o}C with intermittent vortexing. Film **O** was hydrated in 1 mL buffer **D** to create study group **OD**. Film **A** was hydrated in buffer **T** to create study group **AT**. One **C** film was hydrated in buffer **T** and the other in buffer **D** to create **CT** and **CD** control groups. 10 freeze/thaw cycles to disrupt multilamellarity were done after hydration. To ensure consistent diameters between samples, liposome solutions were extruded 11 times using a 100 nm polycarbonate membrane. The final extrusion was followed directly by SEC to remove unencapsulated dye molecules. 60 mL of SEC buffer was prepared with ultrapure water using the following reagents: 2 mM TES (N-[tris(hydroxymethyl)methyl]-2-aminoethanesulfonic acid), 2 mM histidine, 100 mM NaCl and 1 mM EDTA. SEC buffer was used to swell 1.2 g of Sephadex^{TM} G-50 Medium (GE Healthcare) for 3 hours with occasional mixing. The bead slurry was gravity packed into lass microcolumns with 8 mm diameters with 5 cm of the swelled Sephadex^{TM} media. Each liposome type was eluded through its own column using SEC buffer. 1 mL fractions were collected, kept 4 °C, and used directly or within 1 day. Liposomes eluded in the second fractions, from which aliquots were taken for fluorescence studies. For the study group: **O** (300 uL) were added first scanned alone, followed by **A** (300 uL), a brief mix, and another scan applying heat. The cuvette was sealed and placed in a 40 °C water bath followed by 5 s of vortexing. Heating times between measurements were as follows: 30 s, 30 s, 2 min, 2 min, 5 min, 5 min, 10 min, 15 min, 20 min for a total of 1 hour. Control experiments were done in precisely the same manner with **CD** added first and scanned alone in place of **O**, and **CT** added subsequently.

4.3: The future of triggered release

Active targeting and passive release demonstrate how developing nanoparticles can add specificity to nanodrugs by tailoring targeting groups and trigger types to whatever tumor, disease or infection is to be attacked. Our work in Chapter 3 demonstrates that rationally designed lipid architectures may also add specificity to liposomal nanoparticles. To date, commercially available LDSs are still lacking for many intuitive applications. Bacterial infections, for example, are good targets for future nanodrugs. The EPR effect, which is responsible for the passive targeting that makes nanodrugs more selective/effective than free drugs, can also be exploited for the nanoparticular treatment of bacterial infections. A 2013 review on the matter suggested that not only is increased vascular permeability a conserved trait of human bacterial pathogens, but sites of infection exhibit EPR similarly to tumors and other neoplasms.[300]

Given the similarity in size between nanoparticles and infectious agents, it is a reasonable assertion that EPR could also be applied to the obfuscation of bacteria in circulation, particularly in their granular 'cystic' form. Furthermore, research has suggested that the cystic form of a certain bacteria may be the source of pathogenesis of the bacteria that causes lyme disease.[301-302] Given that the fenestrations accompanying tumors also accompany bacterial infections, liposomal antibiotics are an outstanding opportunity to advance antibacterial drugs.

Regarding triggered release, let us continue with the causal agent of Lyme disease, the spirochete bacteria B. burgdorferi, as an example. The differential environments of spirochetes and their hosts could be a tactical advantage of nanocarriers developed for spirochete hunting. A manganese-based localization strategy in the form of a cationic recognition site with lipophilic appendages is particularly intriguing for treating Lyme. Part of B. burgdorferi's survivability comes from its ability to function without iron.[303] The bacteria's outer membrane instead consists of manganese (Mn^{2+}) metalloproteins.[304] An interesting caveat of metalloproteins that chelate and fold about low-abundance cations such as Mn^{2+} is that the metals do not compete for the proteins, but rather the proteins have their preference and compete with other molecules for the metals.[305]

In addition to Mn^{2+}, dysregulation of metal cations is a conserved trait of many diseases. Calcium overabundance is linked to Alzheimer's disease,[306-308] and many other serious conditions[309-310] including amyotrophic lateral sclerosis (ALS),[311-314] ischemic stroke,[315-318] and

malaria.[319-321] Potassium is another ion crucial to cellular function[322] and potassium ion channel proteins are the most diverse class of transmembrane ion transporters whose overexpression has been conclusively linked to cancer, particularly metastasizing cells.[323] Ion channels in general make up a significant portion of drug targets.[324] Zinc would be another interesting environmental trigger for passive release. Overabundant zinc is lethal, and correlated to brain diseases and injuries,[325-329] several cancers,[330-336] and Alzheimer's disease.[337-346] Moreover, zinc deprivation[347-349] and zinc sensors[350-352] have been successfully tested to inhibit progression of diseased cells. The metalloproteases targeted by the nanodrugs developed in Chapter 3 further evidence that cation dysregulation is a promising future strategy for developing triggered release platforms. The future of controlled liposomal release hinges upon our understanding of the pathologies we aim to treat, and our ability to generate lipidic tools with which we may capitalize upon newly uncovered pathological proclivities.

EPILOGUE

To gain a more complete understanding of how the lipidomes and proteomes of our cells interact, it can be advantageous to step back from a purely biophysical perspective. Lipid-protein signaling operations are, ultimately, consequences of chemical proclivities and the contextual view of these events incorporates an impossible number of variables that reform said chemical proclivities based on environmental cofactors and membrane mechanics. This macroscopic perspective is often lost among laboratory chemists and promising nanotechnologies developed under their guise often lack clinical viability as a result.[172] Conversely, I have observed a general skepticism among clinicians when presented with promising new treatment strategies as a result of the general dearth of novel therapies that progress to human clinical trials after testing in animal models. This observation came through my work as a clinical intern at the Pat Summitt Alzheimer's Clinic, formerly known as the Cole Neuroscience Clinic. In between patient interviews, my conversations with care providers would often range to science and discussions about what excited medical doctors versus what excited research doctors. Lab-based therapeutic development often isolates molecular protein interactions. When it doesn't, it is usually limited to cells growing in a dish or humanized animal models. What kills cancer cells in a dish rarely kills tumors in humans and what reverses Alzheimer's plaques in rodents rarely does so in humans.

The disparity between model systems is naturally the reason for this lack of translatability, but fortunately scientists now have yet another means to control for these differences: the liposome. If a cancer drug is too toxic to administer, liposomal drug delivery may be a solution. If a powerful AD treatment fails to cross the BBB in humans, again a liposomal shuttling system could overcome this hurdle. It is challenging to think of a drug that would not benefit from liposomal administration. Liposomal delivery of common medications like ibuprofen and antibiotics could have great impact. New applications of simple LDSs warrant as much investigation as sophisticated multifunctional iterations of existing cancer nanodrugs. If chemists and biologists thought more like physicians while developing nanodelivery systems, several more nanodrugs would be FDA approved. On the other hand, if physicians thought more like lab scientists while considering new treatment options for clinical trials, then they would be much more excited about liposomal therapies.

Liposomes, like other surface sciences and nanotechnologies, bridge fields like engineering, biophysics, analytical and organic chemistry, chemical and cellular biology, and beyond. Applications continue to arise and will ideally narrow the gap between clinicians and chemists. Many scientific tools such as toxic reagents and expensive nonrenewable materials have applicability despite themselves. Liposomes on the other hand are nontoxic, biodegradable, highly tunable and enable technologies that may otherwise not exist. Liposomes have opened up new doors in regenerative medicine,[4] renewable energy,[353] and many other fields.

Within this dissertation is a road map, of sorts, towards bringing LDSs closer to their vast clinical applicability. Chapter 1 underscores the crucial role that low-abundance signaling lipids such as DAG play in cellular pathologies, while Chapter 2 illustrates the utility of liposomes in adding to the well of signaling lipid knowledge. Additionally, studies such as those described in Chapter 2 could be used to characterize the affinities of target tissues and membranes of pathogenic bacteria and viruses to better inform upon ideal liposomal formulations for nanoparticle-based treatments. The potential to find simple, natural solutions to increasing LDS efficacy can be found in lipids such as DAG and PS, as illustrated by the work in Chapter 3. Finally, Chapter 4 presented cutting-edge technologies that creep closer to commercial availability with each passing year. The rapid expanse of liposomes is accelerated not only by imaginative new technologies, but also by investigations into the protein interactions and membrane characteristics of lipids like DAG.

REFERENCES

1. Lehrer, J. *Proust was a Neuroscientist*; Houghton Mifflin Co: Boston, 2007.
2. Sud, M.; Fahy, E.; Cotter, D.; Brown, A.; Dennis, E. A.; Glass, C. K.; Merrill, A. H. Jr.; Murphy, R. C.; Raetz, C. R.; Russell, D. W.; Subramaniam, S. LMSD: lipid maps structure database. *Nucleic Acids Res* **2007,** *35* (Database issue), D527-532.
3. Escriba, P. V.; Gonzalez-Ros, J. M.; Goni, F. M.; Kinnunen, P. K.; Vigh, L.; Sanchez-Magraner, L.; Fernandez, A. M.; Busquets, X.; Horvath, I.; Barcelo-Coblijn, G. Membranes: a meeting point for lipids, proteins and therapies. *J Cell Mol Med* **2008,** *12* (3), 829-875.
4. Monteiro, N.; Martins, A.; Reis, R. L.; Neves, N. M. Liposomes in tissue engineering and regenerative medicine. *J. Royal Soc. Interface* **2014,** *11* (101).
5. Cullis, P. R.; de Kruijff, B. Lipid polymorphism and the functional roles of lipids in biological membranes. *Biochim Biophys Acta* **1979,** *559* (4), 399-420.
6. van Meer, G.; Voelker, D. R.; Feigenson, G. W. Membrane lipids: where they are and how they behave. *Nat. Rev. Mol. Cell Biol.* **2008,** *9* (2), 112-124.
7. Alam, S.; Mattern-Schain, S. I.; Best, M. D. Targeting and Triggered Release Using Lipid-Based Supramolecular Assemblies as Medicinal Nanocarriers. In *Reference Module in Chemistry, Molecular Sciences and Chemical Engineering*, Elsevier: 2016.
8. Ruiz, M. Self-assembled phospholipid structures. https://commons.wikimedia.org (accessed June 27, 2017).
9. Putta, P.; Rankenberg, J.; Korver, R. A.; van Wijk, R.; Munnik, T.; Testerink, C.; Kooijman, E. E. Phosphatidic acid binding proteins display differential binding as a function of membrane curvature stress and chemical properties. *Biochim Biophys Acta* **2016,** *1858* (11), 2709-2716.
10. Bell, R. M.; Ballas, L. M.; Coleman, R. A. Lipid topogenesis. *J Lipid Res* **1981,** *22* (3), 391-403.
11. Chauhan, N.; Farine, L.; Pandey, K.; Menon, A. K.; Bütikofer, P. Lipid topogenesis – 35 years on. *Biochim Biophys Acta* **2016,** *1861* (8 Pt B), 757-766.
12. Cho, W.; Stahelin, R. V. Membrane-protein interactions in cell signaling and membrane trafficking. *Annu Rev Biophys Biomol Struct* **2005,** *34*, 119-51.
13. Fukushima, K.; Takahashi, K.; Yamasaki, E.; Onishi, Y.; Fukushima, N.; Honoki, K.; Tsujiuchi, T. Lysophosphatidic acid signaling via LPA1 and LPA3 regulates cellular functions during tumor progression in pancreatic cancer cells. *Exp Cell Res* **2017,** *352* (1), 139-145.
14. Antal, C. E.; Hudson, A. M.; Kang, E.; Zanca, C.; Wirth, C.; Stephenson, N. L.; Trotter, E. W.; Gallegos, L. L.; Miller, C. J.; Furnari, F. B.; Hunter, T.; Brognard, J.; Newton, A. C. Cancer-associated protein kinase C mutations reveal kinase's role as tumor suppressor. *Cell* **2015,** *160* (3), 489-502.
15. Bruntz, R. C.; Lindsley, C. W.; Brown, H. A. Phospholipase D signaling pathways and phosphatidic acid as therapeutic targets in cancer. *Pharmacol Rev* **2014,** *66* (4), 1033-79.
16. Griner, E. M.; Kazanietz, M. G. Protein kinase C and other diacylglycerol effectors in cancer. *Nat Rev Cancer* **2007,** *7* (4), 281-294.
17. Wood, P. L.; Medicherla, S.; Sheikh, N.; Terry, B.; Phillipps, A.; Kaye, J. A.; Quinn, J. F.; Woltjer, R. L. Targeted Lipidomics of Fontal Cortex and Plasma Diacylglycerols (DAG) in Mild Cognitive Impairment (MCI) and Alzheimer's Disease: Validation of DAG Accumulation Early in the Pathophysiology of Alzheimer's Disease. *J. Alzheimers dis* **2015,** *48* (2), 537-546.
18. Escriba, P. V.; Sanchez-Dominguez, J. M.; Alemany, R.; Perona, J. S.; Ruiz-Gutierrez,

V. Alteration of lipids, G proteins, and PKC in cell membranes of elderly hypertensives. *Hypertension* **2003,** *41* (1), 176-182.
19. Kuhajda, F. P. Fatty acid synthase and cancer: new application of an old pathway. *Cancer Res* **2006,** *66* (12), 5977-5980.
20. Spitaler, M.; Emslie, E.; Wood, C. D.; Cantrell, D. Diacylglycerol and protein kinase D localization during T lymphocyte activation. *Immunity* **2006,** *24* (5), 535-546.
21. Topham, M. K. Signaling roles of diacylglycerol kinases. *J Cell Biochem* **2006,** *97* (3), 474-484.
22. Sarri, E.; Sicart, A.; Lazaro-Dieguez, F.; Egea, G. Phospholipid synthesis participates in the regulation of diacylglycerol required for membrane trafficking at the Golgi complex. *J Biol Chem* **2011,** *286* (32).
23. Goldberg, E. M.; Lester, D. S.; Borchardt, D. B.; Zidovetzki, R. Effects of diacylglycerols and Ca2+ on structure of phosphatidylcholine/phosphatidylserine bilayers. *Biophys J.* **1994,** *66* (2 Pt 1), 382-393.
24. Luostarinen, R.; Boberg, M.; Saldeen, T. Fatty acid composition in total phospholipids of human coronary arteries in sudden cardiac death. *Atherosclerosis* **1993,** *99* (2), 187-193.
25. Pessin, M. S.; Raben, D. M. Molecular species analysis of 1,2-diglycerides stimulated by alpha-thrombin in cultured fibroblasts. *J Biol Chem* **1989,** *264* (15), 8729-8738.
26. Nadler, A.; Reither, G.; Feng, S.; Stein, F.; Reither, S.; Muller, R.; Schultz, C. The fatty acid composition of diacylglycerols determines local signaling patterns. *Angew Chem Int Ed Engl* **2013,** *52* (24), 6330-6334.
27. Marignani, P. A.; Epand, R. M.; Sebaldt, R. J. Acyl chain dependence of diacylglycerol activation of protein kinase C activity in vitro. *Biochem Biophys Res Commun* **1996,** *225* (2), 469-473.
28. Lodish H, B. A. Zipursky SL, et al. Membrane Proteins. In *Molecular Cell Biology*, 4th ed.; Freeman, W. H. Ed. New York, 2000.
29. Ben-Tal, N.; Honig, B.; Miller, C.; McLaughlin, S. Electrostatic binding of proteins to membranes. Theoretical predictions and experimental results with charybdotoxin and phospholipid vesicles. *Biophys J.* **1997,** *73* (4), 1717-1727.
30. Goni, F. M. Non-permanent proteins in membranes: when proteins come as visitors (Review). *Mol Membr Biol* **2002,** *19* (4), 237-245.
31. Guda, P.; Chittur, S. V.; Guda, C. Comparative Analysis of Protein-Protein Interactions in Cancer-Associated Genes. *Genomics, Proteomics & Bioinformatics* **2009,** *7* (1-2), 25-36.
32. Johnson, J. E.; Cornell, R. B. Amphitropic proteins: regulation by reversible membrane interactions (review). *Mol Membr Biol* **1999,** *16* (3), 217-235.
33. Augustin, I.; Korte, S.; Rickmann, M.; Kretzschmar, H. A.; Südhof, T. C.; Herms, J. W.; Brose, N. The Cerebellum-Specific Munc13 Isoform Munc13-3 Regulates Cerebellar Synaptic Transmission and Motor Learning in Mice. *J. Neurosci* **2001,** *21* (1), 10.
34. Chauveau, A.; Le Floc'h, A.; Bantilan, N. S.; Koretzky, G. A.; Huse, M. Diacylglycerol kinase alpha establishes T cell polarity by shaping diacylglycerol accumulation at the immunological synapse. *Sci Signal* **2014,** *7* (340), ra82.
35. Alenghat, F. J.; Golan, D. E. Membrane Protein Dynamics and Functional Implications in Mammalian Cells. *Current topics in membranes* **2013,** *72*, 89-120.
36. Aloulou, A.; Ali, Y. B.; Bezzine, S.; Gargouri, Y.; Gelb, M. H. Phospholipases: an

overview. *Methods Mol Biol* **2012,** *861*, 63-85.
37. Zhao, J. Phospholipase D and phosphatidic acid in plant defence response: from protein–protein and lipid–protein interactions to hormone signalling. *J. Exp. Bot.* **2015,** *66* (7), 1721-1736.
38. Matin, A.; Jung, S. Y. Phospholipase activities in clinical and environmental isolates of Acanthamoeba. *Korean J Parasitol* **2011,** *49* (1), 1-8.
39. Tyutyunnykova, A.; Telegeev, G.; Dubrovska, A. The controversial role of phospholipase C epsilon (PLCε) in cancer development and progression. *Cancer* **2017,** *8* (5), 716-729.
40. Sezgin, E.; Levental, I.; Mayor, S.; Eggeling, C. The mystery of membrane organization: composition, regulation and roles of lipid rafts. *Nat Rev Mol Cell Biol* **2017,** *18* (6), 361-374.
41. Gorter, E.; Grendel, F. On bimolecular layers of lipoids on the chromocytes of the blood. *J Exp Med* **1925,** *41* (4), 439-443.
42. M. H. F. Wilkins. Bilayer Structure in Membranes. *Nature New Biology* **1971,** *230*, 72-76.
43. Singer, S. J.; Nicolson, G. L. The fluid mosaic model of the structure of cell membranes. *Science* **1972,** *175* (4023), 720-731.
44. Mehdizadeh, A.; Bonyadi, M.; Darabi, M.; Rahbarghazi, R.; Montazersaheb, S.; Velaei, K.; Shaaker, M.; Somi, M. H. Common chemotherapeutic agents modulate fatty acid distribution in human hepatocellular carcinoma and colorectal cancer cells. *Bioimpacts* **2017,** *7* (1), 31-39.
45. Ohanian, J.; Liu, G.; Ohanian, V.; Heagerty, A. M. Lipid second messengers derived from glycerolipids and sphingolipids, and their role in smooth muscle function. *Acta Physiol Scand* **1998,** *164* (4), 533-548.
46. Balasubramanian, K.; Schroit, A. J. Aminophospholipid asymmetry: A matter of life and death. *Annu Rev Physiol* **2003,** *65*, 701-734.
47. Zwaal, R. F.; Comfurius, P.; Bevers, E. M. Surface exposure of phosphatidylserine in pathological cells. *Cell Mol Life Sci* **2005,** *62* (9), 971-88.
48. Baenke, F.; Peck, B.; Miess, H.; Schulze, A. Hooked on fat: the role of lipid synthesis in cancer metabolism and tumour development. *Dis Model Mech* **2013,** *6* (6), 1353-63.
49. Palsdottir, H.; Hunte, C. Lipids in membrane protein structures. *Biochim Biophys Acta* **2004,** *1666* (1-2), 2-18.
50. Pierce, K. L.; Premont, R. T.; Lefkowitz, R. J. Seven-transmembrane receptors. *Nat Rev Mol Cell Biol* **2002,** *3* (9), 639-50.
51. Johnson, Joanne E.; Goulding, Rebecca E.; Ding, Z.; Partovi, A.; Anthony, Kira V.; Beaulieu, N.; Tazmini, G.; Cornell, Rosemary B.; Kay, Robert J. Differential membrane binding and diacylglycerol recognition by C1 domains of RasGRPs. *The Biochemical Journal* **2007,** *406* (Pt 2), 223-236.
52. Shen, N.; Guryev, O.; Rizo, J. Intramolecular occlusion of the diacylglycerol-binding site in the C1 domain of munc13-1. *Biochemistry* **2005,** *44* (4), 1089-96.
53. Hommel, U.; Zurini, M.; Luyten, M. Solution structure of a cysteine rich domain of rat protein kinase C. *Nat Struct Biol* **1994,** *1* (6), 383-7.
54. Yang, C.; Kazanietz, M. G. Divergence and complexities in DAG signaling: looking beyond PKC. *Trends Pharmacol Sci* **2003,** *24* (11), 602-608.
55. Emerit, I.; Cerutti, P. A. Tumour promoter phorbol-12-myristate-13-acetate induces chromosomal damage via indirect action. *Nature* **1981,** *293* (5828), 144-146.

56. Wang, H. B.; Wang, X. Y.; Liu, L. P.; Qin, G. W.; Kang, T. G. Tigliane diterpenoids from the Euphorbiaceae and Thymelaeaceae families. *Chem Rev* **2015,** *115* (9), 2975-3011.
57. Stahelin, R. V.; Wang, J.; Blatner, N. R.; Rafter, J. D.; Murray, D.; Cho, W. The origin of C1A-C2 interdomain interactions in protein kinase Calpha. *J Biol Chem* **2005,** *280* (43), 36452-36463.
58. Steinberg, S. F. Structural basis of protein kinase C isoform function. *Physiol Rev* **2008,** *88* (4), 1341-1378.
59. Moravcevic, K.; Oxley, C. L.; Lemmon, M. A. Conditional peripheral membrane proteins: facing up to limited specificity. *Structure* **2012,** *20* (1), 15-27.
60. Huang, L.; Liu, Y.; Jin, W.; Ji, X.; Dong, Z. Ketamine potentiates hippocampal neurodegeneration and persistent learning and memory impairment through the PKCgamma-ERK signaling pathway in the developing brain. *Brain Res* **2012,** *1476*, 164-171.
61. Cijsouw, T.; Weber, J. P.; Broeke, J. H.; Broek, J. A.; Schut, D.; Kroon, T.; Saarloos, I.; Verhage, M.; Toonen, R. F. Munc18-1 redistributes in nerve terminals in an activity- and PKC-dependent manner. *J Cell Biol* **2014,** *204* (5), 759-775.
62. Strachan-Whaley, M. R.; Reilly, K.; Dobson, J.; Kalisch, B. E. Map kinase and PKC signaling pathways modulate NGF-mediated apoE transcription. *Neurosci Lett* **2015,** *595*, 54-59.
63. Chen, X.; Egly, C.; Riley, A. M.; Li, W.; Tewson, P.; Hughes, T. E.; Quinn, A. M.; Obukhov, A. G. PKC-dependent Phosphorylation of the H1 Histamine Receptor Modulates TRPC6 Activity. *Cells* **2014,** *3* (2), 247-257.
64. Wang, Q. J. PKD at the crossroads of DAG and PKC signaling. *Trends Pharmacol Sci* **2006,** *27* (6), 317-323.
65. Chou, E. C.; Capello, S. A.; Levin, R. M.; Longhurst, P. A. Excitatory alpha1-adrenergic receptors predominate over inhibitory beta-receptors in rabbit dorsal detrusor. *J Urol* **2003,** *170* (6 Pt 1), 2503-2507.
66. Singh, J.; Rattan, S. Role of PKC and RhoA/ROCK pathways in the spontaneous phasic activity in the rectal smooth muscle. *Am J Physiol Gastrointest Liver Physiol* **2013,** *304* (8), G723-31.
67. Muro, E.; Atilla-Gokcumen, G. E.; Eggert, U. S. Lipids in cell biology: how can we understand them better? *Molecular Biology of the Cell* **2014,** *25* (12), 1819-1823.
68. Baldanzi, G.; Mitola, S.; Cutrupi, S.; Filigheddu, N.; van Blitterswijk, W. J.; Sinigaglia, F.; Bussolino, F.; Graziani, A. Activation of diacylglycerol kinase alpha is required for VEGF-induced angiogenic signaling in vitro. *Oncogene* **2004,** *23* (28), 4828-4838.
69. Quann, E. J.; Merino, E.; Furuta, T.; Huse, M. Localized diacylglycerol drives the polarization of the microtubule-organizing center in T cells. *Nat Immunol* **2009,** *10* (6), 627-35.
70. Chan, R. B.; Oliveira, T. G.; Cortes, E. P.; Honig, L. S.; Duff, K. E.; Small, S. A.; Wenk, M. R.; Shui, G.; Di Paolo, G. Comparative lipidomic analysis of mouse and human brain with Alzheimer disease. *J Biol Chem* **2012,** *287* (4), 2678-88.
71. Kang, L.; He, Z.; Xu, P.; Fan, J.; Betz, A.; Brose, N.; Xu, T. Munc13-1 is required for the sustained release of insulin from pancreatic beta cells. *Cell Metab* **2006,** *3* (6), 463-8.
72. Gioia, D. A.; Alexander, N. J.; McCool, B. A. Differential Expression of Munc13-2 Produces Unique Synaptic Phenotypes in the Basolateral Amygdala of C57BL/6J and DBA/2J Mice. *J. Neurosci* **2016,** *36* (43), 10964-10977.
73. Gorden, D. L.; Ivanova, P. T.; Myers, D. S.; McIntyre, J. O.; VanSaun, M. N.; Wright, J.

K.; Matrisian, L. M.; Brown, H. A. Increased diacylglycerols characterize hepatic lipid changes in progression of human nonalcoholic fatty liver disease; comparison to a murine model. *PLoS One* **2011,** *6* (8), e22775.
74. Kawaguchi, M.; Valencia, J. C.; Namiki, T.; Suzuki, T.; Hearing, V. J. Diacylglycerol kinase regulates tyrosinase expression and function in human melanocytes. *J Invest Dermatol* **2012,** *132* (12), 2791-9.
75. Carman, G. M.; Han, G.-S. Phosphatidic Acid Phosphatase, a Key Enzyme in the Regulation of Lipid Synthesis. *J. Biol. Chem* **2009,** *284* (5), 2593-2597.
76. Guo, L.; Mishra, G.; Taylor, K.; Wang, X. Phosphatidic Acid Binds and Stimulates Arabidopsis Sphingosine Kinases. *J. Biol. Chem* **2011,** *286* (15), 13336-13345.
77. Liu, H.; Chakravarty, D.; Maceyka, M.; Milstien, S.; Spiegel, S. Sphingosine kinases: a novel family of lipid kinases. *Prog Nucleic Acid Res Mol Biol* **2002,** *71*, 493-511.
78. Strub, G. M.; Maceyka, M.; Hait, N. C.; Milstien, S.; Spiegel, S. Extracellular and Intracellular Actions of Sphingosine-1-Phosphate. *Advances in experimental medicine and biology* **2010,** *688*, 141-155.
79. Ghosh, S.; Bell, R. M. Regulation of Raf-1 kinase by interaction with the lipid second messenger, phosphatidic acid. *Biochem Soc Trans* **1997,** *25* (2), 561-5.
80. Ghosh, S.; Strum, J. C.; Sciorra, V. A.; Daniel, L.; Bell, R. M. Raf-1 kinase possesses distinct binding domains for phosphatidylserine and phosphatidic acid. Phosphatidic acid regulates the translocation of Raf-1 in 12-O-tetradecanoylphorbol-13-acetate-stimulated Madin-Darby canine kidney cells. *J Biol Chem* **1996,** *271* (14), 8472-80.
81. Morkel, M.; Riemer, P.; Bläker, H.; Sers, C. Similar but different: distinct roles for KRAS and BRAF oncogenes in colorectal cancer development and therapy resistance. *Oncotarget* **2015,** *6* (25), 20785-20800.
82. Hatzivassiliou, G.; Song, K.; Yen, I.; Brandhuber, B. J.; Anderson, D. J.; Alvarado, R.; Ludlam, M. J.; Stokoe, D.; Gloor, S. L.; Vigers, G.; Morales, T.; Aliagas, I.; Liu, B.; Sideris, S.; Hoeflich, K. P.; Jaiswal, B. S.; Seshagiri, S.; Koeppen, H.; Belvin, M.; Friedman, L. S.; Malek, S. RAF inhibitors prime wild-type RAF to activate the MAPK pathway and enhance growth. *Nature* **2010,** *464* (7287), 431-5.
83. Testerink, C.; Larsen, P. B.; van der Does, D.; van Himbergen, J. A.; Munnik, T. Phosphatidic acid binds to and inhibits the activity of Arabidopsis CTR1. *J Exp Bot* **2007,** *58* (14), 3905-14.
84. Amin, S.; Kumar, A.; Nilchi, L.; Wright, K.; Kozlowski, M. Breast cancer cells proliferation is regulated by tyrosine phosphatase SHP1 through c-jun N-terminal kinase and cooperative induction of RFX-1 and AP-4 transcription factors. *Mol Cancer Res* **2011,** *9* (8), 1112-25.
85. Roy Choudhury, S.; Pandey, S. Phosphatidic acid binding inhibits RGS1 activity to affect specific signaling pathways in Arabidopsis. *Plant J* **2017,** *90* (3), 466-477.
86. Foster, D. A. Phosphatidic acid signaling to mTOR: Signals for the survival of human cancer cells. *Biochim Biophys Acta* **2009,** *1791* (9), 949-955.
87. Menon, D.; Salloum, D.; Bernfeld, E.; Gorodetsky, E.; Akselrod, A.; Frias, M. A.; Sudderth, J.; Chen, P. H.; DeBerardinis, R.; Foster, D. A. Lipid sensing by mTOR complexes via de novo synthesis of phosphatidic acid. *J Biol Chem* **2017,** *292* (15), 6303-6311.
88. Chalfant, C. E.; Kishikawa, K.; Mumby, M. C.; Kamibayashi, C.; Bielawska, A.;

Hannun, Y. A. Long chain ceramides activate protein phosphatase-1 and protein phosphatase-2A. Activation is stereospecific and regulated by phosphatidic acid. *J Biol Chem* **1999,** *274* (29), 20313-7.
89. Tyagi, M.; Iordanskiy, S.; Ammosova, T.; Kumari, N.; Smith, K.; Breuer, D.; Ilatovskiy, A. V.; Kont, Y. S.; Ivanov, A.; Uren, A.; Kovalskyy, D.; Petukhov, M.; Kashanchi, F.; Nekhai, S. Reactivation of latent HIV-1 provirus via targeting protein phosphatase-1. *Retrovirology* **2015,** *12*, 63.
90. Qin, X.; Wang, Y.; Paudel, H. K. Inhibition of Early Growth Response 1 in the Hippocampus Alleviates Neuropathology and Improves Cognition in an Alzheimer Model with Plaques and Tangles. *Am J Pathol* **2017**.
91. Zhang, C.; Tang, J.; Xie, J.; Zhang, H.; Li, Y.; Zhang, J.; Verpooten, D.; He, B.; Cao, Y. A conserved domain of herpes simplex virus ICP34.5 regulates protein phosphatase complex in mammalian cells. *FEBS Lett* **2008,** *582* (2), 171-6.
92. Yao, H.; Wang, G.; Wang, X. Nuclear translocation of proteins and the effect of phosphatidic acid. *Plant Signal Behave.* **2014,** *9* (12), e977711.
93. Zhang, W.; Qin, C.; Zhao, J.; Wang, X. Phospholipase Dα1-derived phosphatidic acid interacts with ABI1 phosphatase 2C and regulates abscisic acid signaling. *PLoS* **2004,** *101* (25), 9508-9513.
94. Sun, Y.; Kim, N. H.; Ji, L.; Kim, S. H.; Lee, J.; Rhee, H. J. Lysophosphatidic acid activates beta-catenin/T cell factor signaling, which contributes to the suppression of apoptosis in H19-7 cells. *Mol Med Rep* **2013,** *8* (6), 1729-33.
95. Katso, R.; Okkenhaug, K.; Ahmadi, K.; White, S.; Timms, J.; Waterfield, M. D. Cellular function of phosphoinositide 3-kinases: implications for development, homeostasis, and cancer. *Annu Rev Cell Dev Biol* **2001,** *17*, 615-75.
96. Best, M. D. Global approaches for the elucidation of phosphoinositide-binding proteins. *Chem Phys Lipids* **2014,** *182*, 19-28.
97. Rowland, M. M.; Gong, D.; Bostic, H. E.; Lucas, N.; Cho, W.; Best, M. D. Microarray analysis of Akt PH domain binding employing synthetic biotinylated analogs of all seven phosphoinositide headgroup isomers. *Chem Phys Lipids* **2012,** *165* (2), 207-15.
98. Yeung, T.; Gilbert, G. E.; Shi, J.; Silvius, J.; Kapus, A.; Grinstein, S. Membrane phosphatidylserine regulates surface charge and protein localization. *Science* **2008,** *319* (5860), 210-3.
99. Huang, B. X.; Akbar, M.; Kevala, K.; Kim, H. Y. Phosphatidylserine is a critical modulator for Akt activation. *J Cell Biol* **2011,** *192* (6), 979-92.
100. Stahelin, R. V.; Scott, J. L.; Frick, C. T. Cellular and molecular interactions of phosphoinositides and peripheral proteins. *Chem Phys Lipids* **2014,** *182*, 3-18.
101. Chen, Z.; Mao, Y.; Yang, J.; Zhang, T.; Zhao, L.; Yu, K.; Zheng, M.; Jiang, H.; Yang, H. Characterizing the binding of annexin V to a lipid bilayer using molecular dynamics simulations. *Proteins* **2014,** *82* (2), 312-22.
102. Lizarbe, M. A.; Barrasa, J. I.; Olmo, N.; Gavilanes, F.; Turnay, J. Annexin-Phospholipid Interactions. Functional Implications. *Int. J. Mol. Sci* **2013,** *14* (2), 2652-2683.
103. Lladó, V.; López, D. J.; Ibarguren, M.; Alonso, M.; Soriano, J. B.; Escribá, P. V.; Busquets, X. Regulation of the cancer cell membrane lipid composition by NaCHOleate: Effects on cell signaling and therapeutical relevance in glioma. *Biochim Biophys Acta - Biomembranes*

2014, *1838* (6), 1619-1627.
104. Krishna, S.; Zhong, X. Regulation of Lipid Signaling by Diacylglycerol Kinases during T Cell Development and Function. *Front Immunol* **2013**, 178 (4), 178.
105. Downward, J. Targeting RAS signalling pathways in cancer therapy. *Nat Rev Cancer* **2003,** *3* (1), 11-22.
106. Rajalingam, K.; Schreck, R.; Rapp, U. R.; Albert, Š. Ras oncogenes and their downstream targets. *Biochim Biophys Acta - Molecular Cell Research* **2007,** *1773* (8), 1177-1195.
107. Bos, J. L. ras oncogenes in human cancer: a review. *Cancer Res* **1989,** *49* (17), 4682-9.
108. Roose, J. P.; Mollenauer, M.; Gupta, V. A.; Stone, J.; Weiss, A. A Diacylglycerol-Protein Kinase C-RasGRP1 Pathway Directs Ras Activation upon Antigen Receptor Stimulation of T Cells. *Molecular and Cellular Biology* **2005,** *25* (11), 4426-4441.
109. Durand, N.; Borges, S.; Storz, P. Protein Kinase D Enzymes as Regulators of EMT and Cancer Cell Invasion. *J Clin Med* **2016,** *5* (2).
110. Bruinsma, S. P.; Cagan, R. L.; Baranski, T. J. Chimaerin and Rac regulate cell number, adherens junctions, and ERK MAP kinase signaling in the Drosophila eye. *Proc Natl Acad Sci U S A* **2007,** *104* (17), 7098-103.
111. Yang, C.; Liu, Y.; Leskow, F. C.; Weaver, V. M.; Kazanietz, M. G. Rac-GAP-dependent inhibition of breast cancer cell proliferation by {beta}2-chimerin. *J Biol Chem* **2005,** *280* (26), 24363-70.
112. Vial, E.; Sahai, E.; Marshall, C. J. ERK-MAPK signaling coordinately regulates activity of Rac1 and RhoA for tumor cell motility. *Cancer Cell* **2003,** *4* (1), 67-79.
113. Yang, C.; Liu, Y.; Lemmon, M. A.; Kazanietz, M. G. Essential role for Rac in heregulin beta1 mitogenic signaling: a mechanism that involves epidermal growth factor receptor and is independent of ErbB4. *Mol Cell Biol* **2006,** *26* (3), 831-42.
114. Dominguez, C. L.; Floyd, D. H.; Xiao, A.; Mullins, G. R.; Kefas, B. A.; Xin, W.; Yacur, M. N.; Abounader, R.; Lee, J. K.; Wilson, G. M.; Harris, T. E.; Purow, B. W. Diacylglycerol kinase alpha is a critical signaling node and novel therapeutic target in glioblastoma and other cancers. *Cancer Discov* **2013,** *3* (7), 782-97.
115. Yanagisawa, K.; Yasuda, S.; Kai, M.; Imai, S.; Yamada, K.; Yamashita, T.; Jimbow, K.; Kanoh, H.; Sakane, F. Diacylglycerol kinase alpha suppresses tumor necrosis factor-alpha-induced apoptosis of human melanoma cells through NF-kappaB activation. *Biochim Biophys Acta* **2007,** *1771* (4), 462-74.
116. Azordegan, N.; Fraser, V.; Le, K.; Hillyer, L. M.; Ma, D. W.; Fischer, G.; Moghadasian, M. H. Carcinogenesis alters fatty acid profile in breast tissue. *Mol Cell Biochem* **2013,** *374* (1-2), 223-32.
117. Hofmann, J. Modulation of protein kinase C in antitumor treatment. *Rev Physiol Biochem Pharmacol* **2001,** *142*, 1-96.
118. Akinaga, S.; Gomi, K.; Morimoto, M.; Tamaoki, T.; Okabe, M. Antitumor Activity of UCN-01, a Selective Inhibitor of Protein Kinase C, in Murine and Human Tumor Models. *Cancer Research* **1991,** *51* (18), 4888-4892.
119. Comet, N. R.; Aguilo, J. I.; Rathore, M. G.; Catalan, E.; Garaude, J.; Uze, G.; Naval, J.; Pardo, J.; Villalba, M.; Anel, A. IFNalpha signaling through PKC-theta is essential for antitumor NK cell function. *Oncoimmunology* **2014,** *3* (8), e948705.

120. Ackerman, D.; Simon, M. C. Hypoxia, lipids, and cancer: surviving the harsh tumor microenvironment. *Trends Cell Biol* **2014,** *24* (8), 472-8.
121. Brown, D. A.; London, E. Structure and function of sphingolipid- and cholesterol-rich membrane rafts. *J Biol Chem* **2000,** *275* (23), 17221-4.
122. Ibarguren, M.; Lopez, D. J.; Encinar, J. A.; Gonzalez-Ros, J. M.; Busquets, X.; Escriba, P. V. Partitioning of liquid-ordered/liquid-disordered membrane microdomains induced by the fluidifying effect of 2-hydroxylated fatty acid derivatives. *Biochim Biophys Acta* **2013,** *1828* (11), 2553-63.
123. Mason, R. P.; Jacob, R. F. Membrane microdomains and vascular biology: emerging role in atherogenesis. *Circulation* **2003,** *107* (17), 2270-3.
124. Baumgart, T.; Hess, S. T.; Webb, W. W. Imaging coexisting fluid domains in biomembrane models coupling curvature and line tension. *Nature* **2003,** *425* (6960), 821-4.
125. Sharma, P.; Varma, R.; Sarasij, R. C.; Ira; Gousset, K.; Krishnamoorthy, G.; Rao, M.; Mayor, S. Nanoscale organization of multiple GPI-anchored proteins in living cell membranes. *Cell* **2004,** *116* (4), 577-89.
126. Yethiraj, A.; Weisshaar, J. C. Why Are Lipid Rafts Not Observed In Vivo? *Biophys J.* **2007,** *93* (9), 3113-3119.
127. Nickels, J. D.; Chatterjee, S.; Stanley, C. B.; Qian, S.; Cheng, X.; Myles, D. A. A.; Standaert, R. F.; Elkins, J. G.; Katsaras, J. The in vivo structure of biological membranes and evidence for lipid domains. *PLoS Biol* **2017,** *15* (5), e2002214.
128. Marsh, D.; Horváth, L. I. Structure, dynamics and composition of the lipid-protein interface. Perspectives from spin-labelling. *Biochim Biophys Acta - Reviews on Biomembranes* **1998,** *1376* (3), 267-296.
129. Niemela, P. S.; Miettinen, M. S.; Monticelli, L.; Hammaren, H.; Bjelkmar, P.; Murtola, T.; Lindahl, E.; Vattulainen, I. Membrane proteins diffuse as dynamic complexes with lipids. *J Am Chem Soc* **2010,** *132* (22), 7574-7575.
130. Sevcsik, E.; Brameshuber, M.; Folser, M.; Weghuber, J.; Honigmann, A.; Schutz, G. J. GPI-anchored proteins do not reside in ordered domains in the live cell plasma membrane. *Nat Commun* **2015,** *6*, 6969.
131. Sanchez, S. A.; Tricerri, M. A.; Gratton, E. Laurdan generalized polarization fluctuations measures membrane packing micro-heterogeneity in vivo. *Proc Natl Acad Sci U S A* **2012,** *109* (19), 7314-9.
132. Owen, D. M.; Williamson, D. J.; Magenau, A.; Gaus, K. Sub-resolution lipid domains exist in the plasma membrane and regulate protein diffusion and distribution. *Nat Commun* **2012,** *3*, 1256.
133. Eggeling, C.; Ringemann, C.; Medda, R.; Schwarzmann, G.; Sandhoff, K.; Polyakova, S.; Belov, V. N.; Hein, B.; von Middendorff, C.; Schonle, A.; Hell, S. W. Direct observation of the nanoscale dynamics of membrane lipids in a living cell. *Nature* **2009,** *457* (7233), 1159-62.
134. Jiang, Y.; Pryse, K. M.; Melnykov, A.; Genin, G. M.; Elson, E. L. Investigation of Nanoscopic Phase Separations in Lipid Membranes Using Inverse FCS. *Biophys J* **2017,** *112* (11), 2367-2376.
135. Risselada, H. J. Membrane Fusion Stalks and Lipid Rafts: A Love-Hate Relationship. *Biophys J* **2017,** *112* (12), 2475-2478.
136. Peetla, C.; Bhave, R.; Vijayaraghavalu, S.; Stine, A.; Kooijman, E.; Labhasetwar, V.

Drug Resistance in Breast Cancer Cells: Biophysical Characterization of and Doxorubicin Interactions with Membrane Lipids. *Molecular pharmaceutics* **2010,** *7* (6), 2334-2348.
137. Gomara, M. J.; Perez-Pomeda, I.; Gatell, J. M.; Sanchez-Merino, V.; Yuste, E.; Haro, I. Lipid raft-like liposomes used for targeted delivery of a chimeric entry-inhibitor peptide with anti-HIV-1 activity. *Nanomedicine* **2017,** *13* (2), 601-609.
138. Simons, K.; Ehehalt, R. Cholesterol, lipid rafts, and disease. *J Clin Invest* **2002,** *110* (5), 597-603.
139. Belt, W. D. The origin of adrenal cortical mitochondria and liposomes: a preliminary report. *J Biophys Biochem Cytol* **1958,** *4* (3), 337-40.
140. Horne, R. W.; Bangham, A. D.; Whittaker, V. P. NEGATIVELY STAINED LIPOPROTEIN MEMBRANES. *Nature* **1963,** *200*, 1340.
141. Sessa, G.; Weissmann, G. Phospholipid spherules (liposomes) as a model for biological membranes. *J Lipid Res* **1968,** *9* (3), 310-8.
142. Barenholz, Y. Doxil(R)--the first FDA-approved nano-drug: lessons learned. *J Control Release* **2012,** *160* (2), 117-34.
143. Accardo, A.; Morelli, G. Review peptide-targeted liposomes for selective drug delivery: Advantages and problematic issues. *Biopolymers* **2015,** *104* (5), 462-79.
144. Mountain, D.; Fisher, R.; K. Mattern-Schain, S. I.; Best, M. D. Kirkpatrick, S. S.; Freeman, M. B.; Grandas, O. H. Improving the efficacy of liposomal-mediated vascular gene therapy via lipid surface modifications. *J Surg Res* **2017**.
145. Arnhold, J.; Deev, A. I. A simple procedure for preparation of REV-liposomes. *Pharmazie* **1985,** *40* (11), 808-9.
146. Fritze, A.; Hens, F.; Kimpfler, A.; Schubert, R.; Peschka-Süss, R. Remote loading of doxorubicin into liposomes driven by a transmembrane phosphate gradient. *Biochim Biophys Acta - Biomembranes* **2006,** *1758* (10), 1633-1640.
147. Alves, N. J.; Cusick, W.; Stefanick, J. F.; Ashley, J. D.; Handlogten, M. W.; Bilgicer, B. Functionalized liposome purification via Liposome Extruder Purification (LEP). *Analyst* **2013,** *138* (17), 4746-4751.
148. Whitehead, S. A.; McNitt, C. D.; Mattern-Schain, S. I.; Carr, A. J.; Alam, S.; Popik, V. V.; Best, M. D. Artificial Membrane Fusion Triggered by Strain-Promoted Alkyne-Azide Cycloaddition. *Bioconjug Chem* **2017,** *28* (4), 923-932.
149. Panahi, Y.; Farshbaf, M.; Mohammadhosseini, M.; Mirahadi, M.; Khalilov, R.; Saghfi, S.; Akbarzadeh, A. Recent advances on liposomal nanoparticles: synthesis, characterization and biomedical applications. *Artif Cells Nanomed Biotechnol* **2017,** *45* (4), 788-799.
150. Bayer, A. M.; Alam, S.; Mattern-Schain, S. I.; Best, M. D. Triggered Liposomal Release through a Synthetic Phosphatidylcholine Analogue Bearing a Photocleavable Moiety Embedded within the sn-2 Acyl Chain. *Chem. Eur. J* **2014,** *20* (12), 3350-3357.
151. Huynh, N. T.; Passirani, C.; Saulnier, P.; Benoit, J. P. Lipid nanocapsules: a new platform for nanomedicine. *Int J Pharm* **2009,** *379* (2), 201-9.
152. Maeda, H.; Sawa, T.; Konno, T. Mechanism of tumor-targeted delivery of macromolecular drugs, including the EPR effect in solid tumor and clinical overview of the prototype polymeric drug SMANCS. *J Control Release* **2001,** *74* (1-3), 47-61.
153. Dos Santos, N.; Allen, C.; Doppen, A. M.; Anantha, M.; Cox, K. A.; Gallagher, R. C.; Karlsson, G.; Edwards, K.; Kenner, G.; Samuels, L.; Webb, M. S.; Bally, M. B. Influence of

poly(ethylene glycol) grafting density and polymer length on liposomes: relating plasma circulation lifetimes to protein binding. *Biochim Biophys Acta* **2007,** *1768* (6), 1367-77.
154. Leonard, R. C.; Williams, S.; Tulpule, A.; Levine, A. M.; Oliveros, S. Improving the therapeutic index of anthracycline chemotherapy: focus on liposomal doxorubicin (Myocet). *Breast* **2009,** *18* (4), 218-24.
155. Michalek, S. M.; Childers, N. K.; Katz, J.; Dertzbaugh, M.; Zhang, S.; Russell, M. W.; Macrina, F. L.; Jackson, S.; Mestecky, J. Liposomes and conjugate vaccines for antigen delivery and induction of mucosal immune responses. *Adv Exp Med Biol* **1992,** *327*, 191-8.
156. Azzopardi, E. A.; Ferguson, E. L.; Thomas, D. W. The enhanced permeability retention effect: a new paradigm for drug targeting in infection. *J Antimicrob Chemother* **2013,** *68* (2), 257-74.
157. Allen, T. M.; Cullis, P. R. Liposomal drug delivery systems: from concept to clinical applications. *Adv Drug Deliv Rev* **2013,** *65* (1), 36-48.
158. Petros, R. A.; DeSimone, J. M. Strategies in the design of nanoparticles for therapeutic applications. *Nat Rev Drug Discov* **2010,** *9* (8), 615-27.
159. Bulbake, U.; Doppalapudi, S.; Kommineni, N.; Khan, W. Liposomal Formulations in Clinical Use: An Updated Review. *Pharmaceutics* **2017,** *9* (2).
160. Vail, D. M.; MacEwen, E. G.; Kurzman, I. D.; Dubielzig, R. R.; Helfand, S. C.; Kisseberth, W. C.; London, C. A.; Obradovich, J. E.; Madewell, B. R.; Rodriguez, C. O. Jr.; et al. Liposome-encapsulated muramyl tripeptide phosphatidylethanolamine adjuvant immunotherapy for splenic hemangiosarcoma in the dog: a randomized multi-institutional clinical trial. *Clin Cancer Res* **1995,** *1* (10), 1165-70.
161. Kreuter, J. Nanoparticulate systems for brain delivery of drugs. *Adv Drug Deliv Rev* **2001,** *47* (1), 65-81.
162. Noble, G. T.; Stefanick, J. F.; Ashley, J. D.; Kiziltepe, T.; Bilgicer, B. Ligand-targeted liposome design: challenges and fundamental considerations. *Trends Biotechnol* **2014,** *32* (1), 32-45.
163. Kanapathipillai, M.; Brock, A.; Ingber, D. E. Nanoparticle targeting of anti-cancer drugs that alter intracellular signaling or influence the tumor microenvironment. *Adv Drug Deliv Rev* **2014,** *79-80*, 107-18.
164. Uehara, T.; Fujiwara, T.; Takeda, K.; Kunisada, T.; Ozaki, T.; Udono, H. Immunotherapy for Bone and Soft Tissue Sarcomas. *Biomed Res Int* **2015,** *2015*, 820813.
165. Palekar, R. U.; Myerson, J. W.; Schlesinger, P. H.; Sadler, J. E.; Pan, H.; Wickline, S. A. Thrombin-targeted liposomes establish a sustained localized anticlotting barrier against acute thrombosis. *Mol Pharm* **2013,** *10* (11), 4168-75.
166. Walsh, T. J.; Hiemenz, J. W.; Seibel, N. L.; Perfect, J. R.; Horwith, G.; Lee, L.; Silber, J. L.; DiNubile, M. J.; Reboli, A.; Bow, E.; Lister, J.; Anaissie, E. J. Amphotericin B lipid complex for invasive fungal infections: analysis of safety and efficacy in 556 cases. *Clin Infect Dis* **1998,** *26* (6), 1383-96.
167. Webb, M. S.; Harasym, T. O.; Masin, D.; Bally, M. B.; Mayer, L. D. Sphingomyelin-cholesterol liposomes significantly enhance the pharmacokinetic and therapeutic properties of vincristine in murine and human tumour models. *Br J Cancer* **1995,** *72* (4), 896-904.
168. Zylberberg, C.; Matosevic, S. Pharmaceutical liposomal drug delivery: a review of new delivery systems and a look at the regulatory landscape. *Drug Deliv* **2016,** *23* (9), 3319-3329.

169. Zhong, H.; Deng, Y.; Wang, X.; Yang, B. Multivesicular liposome formulation for the sustained delivery of breviscapine. *Int J Pharm* **2005,** *301* (1-2), 15-24.
170. Gluck, R.; Metcalfe, I. C. New technology platforms in the development of vaccines for the future. *Vaccine* **2002,** *20 Suppl 5*, B10-6.
171. Hartrick, C. T.; Hartrick, K. A. Extended-release epidural morphine (DepoDur): review and safety analysis. *Expert Rev Neurother* **2008,** *8* (11), 1641-8.
172. Landesman-Milo, D.; Peer, D. Transforming Nanomedicines From Lab Scale Production to Novel Clinical Modality. *Bioconjugate Chemistry* **2016,** *27* (4), 855-862.
173. Speers, A. E.; Cravatt, B. F. A tandem orthogonal proteolysis strategy for high-content chemical proteomics. *J Am Chem Soc* **2005,** *127* (28), 10018-9.
174. Cravatt, B. F.; Wright, A. T.; Kozarich, J. W. Activity-based protein profiling: from enzyme chemistry to proteomic chemistry. *Annu Rev Biochem* **2008,** *77*, 383-414.
175. Best, M. D. Click chemistry and bioorthogonal reactions: unprecedented selectivity in the labeling of biological molecules. *Biochemistry* **2009,** *48* (28), 6571-84.
176. Sletten, E. M.; Bertozzi, C. R. Bioorthogonal chemistry: fishing for selectivity in a sea of functionality. *Angew Chem Int Ed Engl* **2009,** *48* (38), 6974-98.
177. Rostovtsev, V. V.; Green, L. G.; Fokin, V. V.; Sharpless, K. B. A stepwise huisgen cycloaddition process: copper(I)-catalyzed regioselective "ligation" of azides and terminal alkynes. *Angew Chem Int Ed Engl* **2002,** *41* (14), 2596-9.
178. Smith, M. D.; Gong, D.; Sudhahar, C. G.; Reno, J. C.; Stahelin, R. V.; Best, M. D. Synthesis and convenient functionalization of azide-labeled diacylglycerol analogues for modular access to biologically active lipid probes. *Bioconjug Chem* **2008,** *19* (9), 1855-63.
179. Smith, M. D.; Sudhahar, C. G.; Gong, D.; Stahelin, R. V.; Best, M. D. Modular synthesis of biologically active phosphatidic acid probes using click chemistry. *Mol Biosyst* **2009,** *5* (9), 962-72.
180. Blackman, M. L.; Royzen, M.; Fox, J. M. Tetrazine ligation: fast bioconjugation based on inverse-electron-demand Diels-Alder reactivity. *J Am Chem Soc* **2008,** *130* (41), 13518-9.
181. Emmetiere, F.; Irwin, C.; Viola-Villegas, N. T.; Longo, V.; Cheal, S. M.; Zanzonico, P.; Pillarsetty, N.; Weber, W. A.; Lewis, J. S.; Reiner, T. (18)F-labeled-bioorthogonal liposomes for in vivo targeting. *Bioconjug Chem* **2013,** *24* (11), 1784-9.
182. Reshetnyak, Y. K.; Segala, M.; Andreev, O. A.; Engelman, D. M. A monomeric membrane peptide that lives in three worlds: in solution, attached to, and inserted across lipid bilayers. *Biophys J* **2007,** *93* (7), 2363-72.
183. Vavere, A. L.; Biddlecombe, G. B.; Spees, W. M.; Garbow, J. R.; Wijesinghe, D.; Andreev, O. A.; Engelman, D. M.; Reshetnyak, Y. K.; Lewis, J. S. A novel technology for the imaging of acidic prostate tumors by positron emission tomography. *Cancer Res* **2009,** *69* (10), 4510-6.
184. Devaraj, N. K.; Thurber, G. M.; Keliher, E. J.; Marinelli, B.; Weissleder, R. Reactive polymer enables efficient in vivo bioorthogonal chemistry. *Proc Natl Acad Sci U S A* **2012,** *109* (13), 4762-7.
185. Rossin, R.; van Duijnhoven, S. M.; Lappchen, T.; van den Bosch, S. M.; Robillard, M. S. Trans-cyclooctene tag with improved properties for tumor pretargeting with the diels-alder reaction. *Mol Pharm* **2014,** *11* (9), 3090-6.
186. Spanedda, M. V.; De Giorgi, M.; Hassane, F. S.; Schuber, F.; Bourel-Bonnet, L.; Frisch,

B. Coupling of Ligands to the Liposome Surface by Click Chemistry. *Methods Mol Biol* **2017,** *1522*, 93-106.
188. van Lengerich, B.; Rawle, R. J.; Boxer, S. G. Covalent attachment of lipid vesicles to a fluid-supported bilayer allows observation of DNA-mediated vesicle interactions. *Langmuir* **2010,** *26* (11), 8666-72.
189. Kumar, A.; Erasquin, U. J.; Qin, G.; Li, K.; Cai, C. "Clickable", polymerized liposomes as a versatile and stable platform for rapid optimization of their peripheral compositions. *Chem Commun (Camb)* **2010,** *46* (31), 5746-8.
190. Tarallo, R.; Accardo, A.; Falanga, A.; Guarnieri, D.; Vitiello, G.; Netti, P.; D'Errico, G.; Morelli, G.; Galdiero, S. Clickable functionalization of liposomes with the gH625 peptide from Herpes simplex virus type I for intracellular drug delivery. *Chemistry* **2011,** *17* (45), 12659-68.
191. Salome, C.; Spanedda, M. V.; Hilbold, B.; Berner, E.; Heurtault, B.; Fournel, S.; Frisch, B.; Bourel-Bonnet, L. Smart tools and orthogonal click-like reactions onto small unilamellar vesicles. *Chem Phys Lipids* **2015,** *188*, 27-36.
192. Bostic, H. E.; Smith, M. D.; Poloukhtine, A. A.; Popik, V. V.; Best, M. D. Membrane labeling and immobilization via copper-free click chemistry. *Chem Commun (Camb)* **2012,** *48* (10), 1431-3.
193. Oude Blenke, E.; Klaasse, G.; Merten, H.; Pluckthun, A.; Mastrobattista, E.; Martin, N. I. Liposome functionalization with copper-free "click chemistry". *J Control Release* **2015,** *202*, 14-20.
194. Zhang, H.; Ma, Y.; Sun, X. L. Chemically-selective surface glyco-functionalization of liposomes through Staudinger ligation. *Chem Commun (Camb)* **2009,** (21), 3032-4.
195. Best, M. D.; Rowland, M. M.; Bostic, H. E. Exploiting bioorthogonal chemistry to elucidate protein-lipid binding interactions and other biological roles of phospholipids. *Acc Chem Res* **2011,** *44* (9), 686-98.
196. Best, M. D. The Development and Application of Clickable Lipid Analogs for Elucidating and Harnessing Lipid Functions. In *Click Chemistry in Glycoscience*, John Wiley & Sons, Inc.: 2013; pp 77-105.
197. Accardo, A.; Ringhieri, P.; Tesauro, D.; Morelli, G. Liposomes derivatized with tetrabranched neurotensin peptides via click chemistry reactions. *New J Chem* **2013,** *37* (11), 3528-3534.
198. Zhang, H.; Weingart, J.; Jiang, R.; Peng, J.; Wu, Q.; Sun, X. L. Bio-inspired liposomal thrombomodulin conjugate through bio-orthogonal chemistry. *Bioconjug Chem* **2013,** *24* (4), 550-9.
199. Saka, S. K.; Honigmann, A.; Eggeling, C.; Hell, S. W.; Lang, T.; Rizzoli, S. O. Multi-protein assemblies underlie the mesoscale organization of the plasma membrane. *Nat Commun* **2014,** *5*, 4509.
200. Berger, A. B.; Vitorino, P. M.; Bogyo, M. Activity-based protein profiling: applications to biomarker discovery, in vivo imaging and drug discovery. *Am J Pharmacogenomics* **2004,** *4* (6), 371-81.
201. Nomura, D. K.; Dix, M. M.; Cravatt, B. F. Activity-based protein profiling for biochemical pathway discovery in cancer. *Nat Rev Cancer* **2010,** *10* (9), 630-8.
202. Hatanaka, Y.; Sadakane, Y. Photoaffinity labeling in drug discovery and developments: chemical gateway for entering proteomic frontier. *Curr Top Med Chem* **2002,** *2* (3), 271-88.

203. Dorman, G.; Prestwich, G. D. Using photolabile ligands in drug discovery and development. *Trends Biotechnol* **2000,** *18* (2), 64-77.
204. Tully, S. E.; Cravatt, B. F. Activity-based probes that target functional subclasses of phospholipases in proteomes. *J Am Chem Soc* **2010,** *132* (10), 3264-5.
205. Benjamin, D. I.; Cravatt, B. F.; Nomura, D. K. Global profiling strategies for mapping dysregulated metabolic pathways in cancer. *Cell Metab* **2012,** *16* (5), 565-77.
206. Kadry, A. M.; Okereke, C. S.; Abdel-Rahman, M. S.; Friedman, M. A.; Davis, R. A. Pharmacokinetics of benzophenone-3 after oral exposure in male rats. *J Appl Toxicol* **1995,** *15* (2), 97-102.
207. Heurung, A. R.; Raju, S. I.; Warshaw, E. M. Benzophenones. *Dermatitis* **2014,** *25* (1), 3-10.
208. Kleiner, P.; Heydenreuter, W.; Stahl, M.; Korotkov, V. S.; Sieber, S. A. A Whole Proteome Inventory of Background Photocrosslinker Binding. *Angewandte Chemie International Edition* **2017,** *56* (5), 1396-1401.
209. Best, M. D.; Zhang, H.; Prestwich, G. D. Inositol polyphosphates, diphosphoinositol polyphosphates and phosphatidylinositol polyphosphate lipids: structure, synthesis, and development of probes for studying biological activity. *Nat Prod Rep* **2010,** *27* (10), 1403-30.
210. Gubbens, J.; de Kroon, A. I. Proteome-wide detection of phospholipid-protein interactions in mitochondria by photocrosslinking and click chemistry. *Mol Biosyst* **2010,** *6* (10), 1751-9.
211. Haberkant, P.; Raijmakers, R.; Wildwater, M.; Sachsenheimer, T.; Brugger, B.; Maeda, K.; Houweling, M.; Gavin, A. C.; Schultz, C.; van Meer, G.; Heck, A. J.; Holthuis, J. C. In vivo profiling and visualization of cellular protein-lipid interactions using bifunctional fatty acids. *Angew Chem Int Ed Engl* **2013,** *52* (14), 4033-4038.
212. Saario, S. M.; McKinney, M. K.; Speers, A. E.; Wang, C.; Cravatt, B. F. Clickable, photoreactive inhibitors to probe the active site microenvironment of fatty acid amide hydrolase(). *Chem Sci* **2012,** *3* (1), 77-83.
213. Haberkant, P.; Stein, F.; Hoglinger, D.; Gerl, M. J.; Brugger, B.; Van Veldhoven, P. P.; Krijgsveld, J.; Gavin, A. C.; Schultz, C. Bifunctional Sphingosine for Cell-Based Analysis of Protein-Sphingolipid Interactions. *ACS Chem Biol* **2016,** *11* (1), 222-230.
214. Gu, X.; Huang, Y.; Levison, B. S.; Gerstenecker, G.; DiDonato, A. J.; Hazen, L. B.; Lee, J.; Gogonea, V.; DiDonato, J. A.; Hazen, S. L. Identification of Critical Paraoxonase 1 Residues Involved in High Density Lipoprotein Interaction. *J Biol Chem* **2016,** *291* (4), 1890-1904.
215. Niphakis, M. J.; Lum, K. M.; Cognetta, A. B. III; Correia, B. E.; Ichu, T.-A.; Olucha, J.; Brown, S. J.; Kundu, S.; Piscitelli, F.; Rosen, H.; Cravatt, B. F. A global map of lipid-binding proteins and their ligandability in cells. *Cell* **2015,** *161* (7), 1668-1680.
216. Gubbens, J.; Ruijter, E.; de Fays, L. E.; Damen, J. M.; de Kruijff, B.; Slijper, M.; Rijkers, D. T.; Liskamp, R. M.; de Kroon, A. I. Photocrosslinking and click chemistry enable the specific detection of proteins interacting with phospholipids at the membrane interface. *Chem Biol* **2009,** *16* (1), 3-14.
217. Wang, D.; Du, S.; Cazenave-Gassiot, A.; Ge, J.; Lee, J. S.; Wenk, M. R.; Yao, S. Q. Global Mapping of Protein-Lipid Interactions by Using Modified Choline-Containing Phospholipids Metabolically Synthesized in Live Cells. *Angew Chem Int Ed Engl* **2017,** *56* (21), 5829-5833.

218. Gubbens, J.; Vader, P.; Damen, J. M.; O'Flaherty, M. C.; Slijper, M.; de Kruijff, B.; de Kroon, A. I. Probing the membrane interface-interacting proteome using photoactivatable lipid cross-linkers. *J Proteome Res* **2007,** *6* (5), 1951-62.
219. White, G. F.; Racher, K. I.; Lipski, A.; Hallett, F. R.; Wood, J. M. Physical properties of liposomes and proteoliposomes prepared from Escherichia coli polar lipids. *Biochim Biophys Acta* **2000,** *1468* (1-2), 175-86.
220. Jackman, J. A.; Yorulmaz Avsar, S.; Ferhan, A. R.; Li, D.; Park, J. H.; Zhdanov, V. P.; Cho, N. J. Quantitative Profiling of Nanoscale Liposome Deformation by a Localized Surface Plasmon Resonance Sensor. *Anal Chem* **2017,** *89* (2), 1102-1109.
221. Vermette, P.; Griesser, H. J.; Kambouris, P.; Meagher, L. Characterization of surface-immobilized layers of intact liposomes. *Biomacromolecules* **2004,** *5* (4), 1496-502.
222. Leung, S. J.; Romanowski, M. NIR-activated content release from plasmon resonant liposomes for probing single-cell responses. *ACS Nano* **2012,** *6* (11), 9383-91.
223. Sun, G.; Chung, T. S.; Jeyaseelan, K.; Armugam, A. Stabilization and immobilization of aquaporin reconstituted lipid vesicles for water purification. *Colloids Surf B Biointerfaces* **2013,** *102*, 466-71.
224. Carlred, L.; Gunnarsson, A.; Sole-Domenech, S.; Johansson, B.; Vukojevic, V.; Terenius, L.; Codita, A.; Winblad, B.; Schalling, M.; Hook, F.; Sjovall, P. Simultaneous imaging of amyloid-beta and lipids in brain tissue using antibody-coupled liposomes and time-of-flight secondary ion mass spectrometry. *J Am Chem Soc* **2014,** *136* (28), 9973-81.
225. Kanter, J. L.; Narayana, S.; Ho, P. P.; Catz, I.; Warren, K. G.; Sobel, R. A.; Steinman, L.; Robinson, W. H. Lipid microarrays identify key mediators of autoimmune brain inflammation. *Nat Med* **2006,** *12* (1), 138-43.
226. Gallego, O.; Betts, M. J.; Gvozdenovic-Jeremic, J.; Maeda, K.; Matetzki, C.; Aguilar-Gurrieri, C.; Beltran-Alvarez, P.; Bonn, S.; Fernandez-Tornero, C.; Jensen, L. J.; Kuhn, M.; Trott, J.; Rybin, V.; Muller, C. W.; Bork, P.; Kaksonen, M.; Russell, R. B.; Gavin, A. C. A systematic screen for protein-lipid interactions in Saccharomyces cerevisiae. *Mol Syst Biol* **2010,** *6*, 430.
227. Feng, L. Probing lipid-protein interactions using lipid microarrays. *Prostaglandins Other Lipid Mediat* **2005,** *77* (1-4), 158-167.
228. Smith, M. D.; Best, M. D. Characterization of protein-membrane binding interactions via a microplate assay employing whole liposome immobilization. *Methods Mol Biol* **2011,** *751*, 477-89.
229. Losey, E. A.; Smith, M. D.; Meng, M.; Best, M. D. Microplate-based analysis of protein-membrane binding interactions via immobilization of whole liposomes containing a biotinylated anchor. *Bioconjug Chem* **2009,** *20* (2), 376-383.
230. Saliba, A. E.; Vonkova, I.; Ceschia, S.; Findlay, G. M.; Maeda, K.; Tischer, C.; Deghou, S.; van Noort, V.; Bork, P.; Pawson, T.; Ellenberg, J.; Gavin, A. C. A quantitative liposome microarray to systematically characterize protein-lipid interactions. *Nat Methods* **2014,** *11* (1), 47-50.
231. Lu, K. Y.; Tao, S. C.; Yang, T. C.; Ho, Y. H.; Lee, C. H.; Lin, C. C.; Juan, H. F.; Huang, H. C.; Yang, C. Y.; Chen, M. S.; Lin, Y. Y.; Lu, J. Y.; Zhu, H.; Chen, C. S. Profiling lipid-protein interactions using nonquenched fluorescent liposomal nanovesicles and proteome microarrays. *Mol Cell Proteomics* **2012,** *11* (11), 1177-1190.

232. Kalyankar, N. D.; Sharma, M. K.; Vaidya, S. V.; Calhoun, D.; Maldarelli, C.; Couzis, A.; Gilchrist, L. Arraying of intact liposomes into chemically functionalized microwells. *Langmuir* **2006,** *22* (12), 5403-11.
233. Tsopelas, F.; Vallianatou, T.; Tsantili-Kakoulidou, A. Advances in immobilized artificial membrane (IAM) chromatography for novel drug discovery. *Expert Opin Drug Discov* **2016,** *11* (5), 473-488.
234. Yang, Q.; Liu, X.-Y.; Ajiki, S.-i.; Hara, M.; Lundahl, P.; Miyake, J. Avidin–biotin immobilization of unilamellar liposomes in gel beads for chromatographic analysis of drug–membrane partitioning. *J Chromatogr B Biomed Sci App* **1998,** *707* (1–2), 131-141.
235. Liu, X.; Yang, Q.; Nakamura, C.; Miyake, J. Avidin-biotin-immobilized liposome column for chromatographic fluorescence on-line analysis of solute-membrane interactions. *J Chromatogr B Biomed Sci Appl* **2001,** *750* (1), 51-60.
236. Ferguson, C. G.; James, R. D.; Bigman, C. S.; Shepard, D. A.; Abdiche, Y.; Katsamba, P. S.; Myszka, D. G.; Prestwich, G. D. Phosphoinositide-containing polymerized liposomes: stable membrane-mimetic vesicles for protein-lipid binding analysis. *Bioconjug Chem* **2005,** *16* (6), 1475-83.
237. Miles, P.; Frankel, D. Lipid directed assembly of the HIV capsid protein. *Soft Matter* **2014,** *10* (47), 9562-7.
238. Barrera, F. N.; Hurtado-Gomez, E.; Lidon-Moya, M. C.; Neira, J. L. Binding of the C-terminal domain of the HIV-1 capsid protein to lipid membranes: a biophysical characterization. *Biochem J* **2006,** *394* (Pt 1), 345-53.
239. Speers, A. E.; Cravatt, B. F. Profiling enzyme activities in vivo using click chemistry methods. *Chem Biol* **2004,** *11* (4), 535-546.
240. Sattlegger, E.; Chernova, T. A.; Gogoi, N. M.; Pillai, I. V.; Chernoff, Y. O.; Munn, A. L. Yeast studies reveal moonlighting functions of the ancient actin cytoskeleton. *IUBMB Life* **2014,** *66* (8), 538-45.
241. Wilschut, J.; Duzgunes, N.; Fraley, R.; Papahadjopoulos, D. Studies on the mechanism of membrane fusion: kinetics of calcium ion induced fusion of phosphatidylserine vesicles followed by a new assay for mixing of aqueous vesicle contents. *Biochemistry* **1980,** *19* (26), 6011-6021.
242. Mateu, M. G. The capsid protein of human immunodeficiency virus: intersubunit interactions during virus assembly. *Febs j* **2009,** *276* (21), 6098-109.
243. Zhang, H. L.; Ma, Y.; Sun, X. L. Recent Developments in Carbohydrate-Decorated Targeted Drug/Gene Delivery. *Med. Res. Rev.* **2010,** *30* (2), 270-289.
244. Saw, P. E.; Kim, S.; Lee, I. H.; Park, J.; Yu, M.; Lee, J.; Kim, J. I.; Jon, S. Aptide-conjugated liposome targeting tumor-associated fibronectin for glioma therapy. *J. Mat. Chem. B* **2013,** *1* (37), 4723-4726.
245. Dicheva, B. M.; ten Hagen, T. L. M.; Seynhaeve, A. L. B.; Amin, M.; Eggermont, A. M. M.; Koning, G. A. Enhanced Specificity and Drug Delivery in Tumors by cRGD - Anchoring Thermosensitive Liposomes. *Pharm. Res.* **2015,** *32* (12), 3862-3876.
246. Khan, D. R.; Webb, M. N.; Cadotte, T. H.; Gavette, M. N. Use of Targeted Liposome-based Chemotherapeutics to Treat Breast Cancer. *Breast cancer : basic and clinical research* **2015,** *9* (Suppl 2), 1-5.
247. Lozano, N.; Al-Ahmady, Z. S.; Beziere, N. S.; Ntziachristos, V.; Kostarelos, K. Monoclonal antibody-targeted PEGylated liposome-ICG encapsulating doxorubicin as a

potential theranostic agent. *Int J Pharm* **2015,** *482* (1-2), 2-10.
248. Du, W.; Yuan, Y.; Wang, L.; Cui, Y.; Wang, H.; Xu, H.; Liang, G. Multifunctional Bioconjugate for Cancer Cell-Targeted Theranostics. *Bioconjugate chemistry* **2015,** *26* (12), 2571-2578.
249. Jain, A. S.; Goel, P. N.; Shah, S. M.; Dhawan, V. V.; Nikam, Y.; Gude, R. P.; Nagarsenker, M. S. Tamoxifen guided liposomes for targeting encapsulated anticancer agent to estrogen receptor positive breast cancer cells: in vitro and in vivo evaluation. *Biomedicine & pharmacotherapy = Biomedecine & pharmacotherapie* **2014,** *68* (4), 429-38.
250. Deshpande, P. P.; Biswas, S.; Torchilin, V. P. Current trends in the use of liposomes for tumor targeting. *Nanomedicine* **2013,** *8* (9), 1509-1528.
251. Liechty, W. B.; Peppas, N. A. Expert opinion: Responsive polymer nanoparticles in cancer therapy. *Eur. J. Pharm. Biopharm.* **2012,** *80* (2), 241-246.
252. Banerjee, R.; Tyagi, P.; Li, S.; Huang, L. Anisamide-targeted stealth liposomes: A potent carrier for targeting doxorubicin to human prostate cancer cells. *Int. J. Cancer* **2004,** *112* (4), 693-700.
253. van Waarde, A.; Rybczynska, A. A.; Ramakrishnan, N. K.; Ishiwata, K.; Elsinga, P. H.; Dierckx, R. Potential applications for sigma receptor ligands in cancer diagnosis and therapy. *Biochim. Biophys. Acta-Biomembr.* **2015,** *1848* (10), 2703-2714.
254. Shamay, Y.; Raviv, L.; Golan, M.; Voronov, E.; Apte, R. N.; David, A. Inhibition of primary and metastatic tumors in mice by E-selectin-targeted polymer-drug conjugates. *J Control Release* **2015,** *217*, 102-112.
255. Calin, M.; Stan, D.; Schlesinger, M.; Simion, V.; Deleanu, M.; Constantinescu, C. A.; Gan, A. M.; Pirvulescu, M. M.; Butoi, E.; Manduteanu, I.; Bota, M.; Enachescu, M.; Borsig, L.; Bendas, G.; Simionescu, M. VCAM-1 directed target-sensitive liposomes carrying CCR2 antagonists bind to activated endothelium and reduce adhesion and transmigration of monocytes. *Eur. J. Pharm. Biopharm.* **2015,** *89*, 18-29.
256. Anderson, P. M.; Tomaras, M.; McConnell, K. Mifamurtide in osteosarcoma--a practical review. *Drugs Today (Barc)* **2010,** *46* (5), 327-37.
257. Pillai, G.; Ceballos-Coronel, M. L. Science and technology of the emerging nanomedicines in cancer therapy: A primer for physicians and pharmacists. *SAGE Open Medicine* **2013,** *1*, 2050312113513759.
258. Kunisawa, J.; Masuda, T.; Katayama, K.; Yoshikawa, T.; Tsutsumi, Y.; Akashi, M.; Mayumi, T.; Nakagawa, S. Fusogenic liposome delivers encapsulated nanoparticles for cytosolic controlled gene release. *J Control Release* **2005,** *105* (3), 344-353.
259. Wagstaff, K. M.; Jans, D. A. Protein transduction: Cell penetrating peptides and their therapeutic applications. *Curr. Med. Chem* **2006,** *13* (12), 1371-1387.
260. Vargas, J. R.; Stanzl, E. G.; Teng, N. N.; Wender, P. A. Cell-penetrating, guanidinium-rich molecular transporters for overcoming efflux-mediated multidrug resistance. *Molecular pharmaceutics* **2014,** *11* (8), 2553-65.
261. Herce, H. D.; Garcia, A. E.; Cardoso, M. C. Fundamental Molecular Mechanism for the Cellular Uptake of Guanidinium-Rich Molecules. *J. Am. Chem. Soc* **2014,** *136* (50), 17459-17467.
262. Kauffman, W. B.; Fuselier, T.; He, J.; Wimley, W. C. Mechanism Maters: A Taxonomy of Cell Penetrating Peptices. *Trends in Biochemical Sciences* **2015,** *40* (12), 749-764.

263. Koren, E.; Torchilin, V. P. Cell-penetrating peptides: breaking through to the other side. *Trends in Molecular Medicine* **2012,** *18* (7), 385-393.
264. Tönges, L.; Lingor, P.; Egle, R.; Dietz, G. P. H.; Fahr, A.; Bähr, M. Stearylated octaarginine and artificial virus-like particles for transfection of siRNA into primary rat neurons. *RNA* **2006,** *12* (7), 1431-1438.
265. Gao, H.; Zhang, Q.; Yu, Z.; He, Q. Cell-penetrating peptide-based intelligent liposomal systems for enhanced drug delivery. *Curr Pharm Biotechnol* **2014,** *15* (3), 210-9.
266. Fioole, B.; van de Rest, H. J. M.; Meijer, J. R. M.; van Leersum, M.; van Koeverden, S.; Moll, F. L.; van den Berg, J. C.; de Vries, J.-P. P. M. Percutaneous transluminal angioplasty and stenting as first-choice treatment in patients with chronic mesenteric ischemia. *J Vasc Surg* **2010,** *51* (2), 386-391.
267. Atkins, M. D.; Kwolek, C. J.; LaMuraglia, G. M.; Brewster, D. C.; Chung, T. K.; Cambria, R. P. Surgical revascularization versus endovascular therapy for chronic mesenteric ischemia: A comparative experience. *J Vasc Surg* **2007,** *45* (6), 1162-1171.
268. Klein, W. M.; van der Graaf, Y.; Seegers, J.; Moll, F. L.; Mali, W. P. Long-term cardiovascular morbidity, mortality, and reintervention after endovascular treatment in patients with iliac artery disease: The Dutch Iliac Stent Trial Study. *Radiology* **2004,** *232* (2), 491-8.
269. Fowkes, F. G. R.; Rudan, D.; Rudan, I.; Aboyans, V.; Denenberg, J. O.; McDermott, M. M.; Norman, P. E.; Sampson, U. K. A.; Williams, L. J.; Mensah, G. A.; Criqui, M. H. Comparison of global estimates of prevalence and risk factors for peripheral artery disease in 2000 and 2010: a systematic review and analysis. *The Lancet 382* (9901), 1329-1340.
270. Maheshwari, R.; Tekade, M.; Sharma, P. A.; Tekade, R. K. Nanocarriers Assisted siRNA Gene Therapy for the Management of Cardiovascular Disorders. *Curr Pharm Des* **2015,** *21* (30), 4427-40.
271. Dalby, B.; Cates, S.; Harris, A.; Ohki, E. C.; Tilkins, M. L.; Price, P. J.; Ciccarone, V. C. Advanced transfection with Lipofectamine 2000 reagent: primary neurons, siRNA, and high-throughput applications. *Methods* **2004,** *33* (2), 95-103.
272. Che, H. L.; Bae, I. H.; Lim, K. S.; Song, I. T.; Lee, H.; Muthiah, M.; Namgung, R.; Kim, W. J.; Kim, D. G.; Ahn, Y.; Jeong, M. H.; Park, I. K. Suppression of post-angioplasty restenosis with an Akt1 siRNA-embedded coronary stent in a rabbit model. *Biomaterials* **2012,** *33* (33), 8548-8556.
273. Freeman, B. M.; Univers, J.; Fisher, R. K.; Kirkpatrick, S. S.; Klein, F. A.; Freeman, M. B.; Mountain, D. J. H.; Grandas, O. H. Testosterone replacement attenuates intimal hyperplasia development in an androgen deficient model of vascular injury. *J Surg Res* **2017,** *207* (Supplement C), 53-62.
274. Grandas, O. H.; Mountain, D. J.; Kirkpatrick, S. S.; Rudrapatna, V. S.; Cassada, D. C.; Stevens, S. L.; Freeman, M. B.; Goldman, M. H. Effect of hormones on matrix metalloproteinases gene regulation in human aortic smooth muscle cells. *J Surg Res* **2008,** *148* (1), 94-9.
275. Mountain, D. J. H.; Freeman, B. M.; Kirkpatrick, S. S.; Beddies, J. W.; Arnold, J. D.; Freeman, M. B.; Goldman, M. H.; Stevens, S. L.; Klein, F. A.; Grandas, O. H. Androgens regulate MMPs and the cellular processes of intimal hyperplasia. *J Surg Res* **2013,** *184* (1), 619-627.
276. Ylä-Herttuala, S.; Martin, J. F. Cardiovascular gene therapy. *The Lancet* **2000,** *355*

(9199), 213-222.
277. Kanapathipillai, M.; Brock, A.; Ingber, D. E. Nanoparticle targeting of anti-cancer drugs that alter intracellular signaling or influence the tumor microenvironment. *Adv. Drug Deliv. Rev.* **2014,** *79–80*, 107-118.
278. Yang, Y.; Yang, Y. F.; Xie, X. Y.; Wang, Z. Y.; Gong, W.; Zhang, H.; Li, Y.; Yu, F. L.; Li, Z. P.; Mei, X. G. Dual-modified liposomes with a two-photon-sensitive cell penetrating peptide and NGR ligand for siRNA targeting delivery. *Biomaterials* **2015,** *48*, 84-96.
279. Perrotta, I.; Aquila, S.; Mazzulla, S. Expression profile and subcellular localization of GAPDH in the smooth muscle cells of human atherosclerotic plaque: an immunohistochemical and ultrastructural study with biological therapeutic perspectives. *Microsc Microanal* **2014,** *20* (4), 1145-57.
280. Niphakis, M. J.; Lum, K. M.; Cognetta, A. B. 3rd; Correia, B. E.; Ichu, T. A.; Olucha, J.; Brown, S. J.; Kundu, S.; Piscitelli, F.; Rosen, H.; Cravatt, B. F. A Global Map of Lipid-Binding Proteins and Their Ligandability in Cells. *Cell* **2015,** *161* (7), 1668-80.
281. Somiya, M.; Yamaguchi, K.; Liu, Q.; Niimi, T.; Maturana, A. D.; Iijima, M.; Yoshimoto, N.; Kuroda, S. i. One-step scalable preparation method for non-cationic liposomes with high siRNA content. *Int. J. Pharm.* **2015,** *490* (1), 316-323.
282. Zhu, L.; Kate, P.; Torchilin, V. P. Matrix metalloprotease 2-responsive multifunctional liposomal nanocarrier for enhanced tumor targeting. *ACS Nano* **2012,** *6* (4), 3491-8.
283. Gillies, R. J.; Liu, Z.; Bhujwalla, Z. 31P-MRS measurements of extracellular pH of tumors using 3-aminopropylphosphonate. *Am J Physiol* **1994,** *267* (1 Pt 1), C195-203.
284. Ong, W.; Yang, Y.; Cruciano, A. C.; McCarley, R. L. Redox-triggered contents release from liposomes. *J Am Chem Soc* **2008,** *130* (44), 14739-14744.
285. Kale, A. A.; Torchilin, V. P. Design, synthesis, and characterization of pH-sensitive PEG-PE conjugates for stimuli-sensitive pharmaceutical nanocarriers: the effect of substitutes at the hydrazone linkage on the ph stability of PEG-PE conjugates. *Bioconjug Chem* **2007,** *18* (2), 363-370.
286. Lopez-Noriega, A.; Ruiz-Hernandez, E.; Quinlan, E.; Storm, G.; Hennink, W. E.; O'Brien, F. J. Thermally triggered release of a pro-osteogenic peptide from a functionalized collagen-based scaffold using thermosensitive liposomes. *J Control Release* **2014,** *187*, 158-166.
287. Myhr, G. Multimodal ultrasound mediated drug release model in local cancer therapy. *Med Hypotheses* **2007,** *69* (6), 1325-33.
288. Puri, A. Phototriggerable liposomes: current research and future perspectives. *Pharmaceutics* **2013,** *6* (1), 1-25.
289. Yang, C.; Rait, A.; Pirollo, K. F.; Dagata, J. A.; Farkas, N.; Chang, E. H. Nanoimmunoliposome delivery of superparamagnetic iron oxide markedly enhances targeting and uptake in human cancer cells in vitro and in vivo. *Nanomedicine* **2008,** *4* (4), 318-329.
290. Hardiansyah, A.; Yang, M. C.; Liu, T. Y.; Kuo, C. Y.; Huang, L. Y.; Chan, T. Y. Hydrophobic Drug-Loaded PEGylated Magnetic Liposomes for Drug-Controlled Release. *Nanoscale Res Lett* **2017,** *12* (1), 355.
291. Ta, T.; Bartolak-Suki, E.; Park, E. J.; Karrobi, K.; McDannold, N. J.; Porter, T. M. Localized delivery of doxorubicin in vivo from polymer-modified thermosensitive liposomes with MR-guided focused ultrasound-mediated heating. *J Control Release* **2014,** *194*, 71-81.
292. Chen, J.; He, C. Q.; Lin, A. H.; Gu, W.; Chen, Z. P.; Li, W.; Cai, B. C. Thermosensitive

liposomes with higher phase transition temperature for targeted drug delivery to tumor. *Int J Pharm* **2014,** *475* (1-2), 408-415.
293. Ahmed, M.; Moussa, M.; Goldberg, S. N. Synergy in cancer treatment between liposomal chemotherapeutics and thermal ablation. *Chemistry and physics of lipids* **2012,** *165* (4), 424-437.
294. Mikhail, A. S.; Negussie, A. H.; Pritchard, W. F.; Haemmerich, D.; Woods, D.; Bakhutashvili, I.; Esparza-Trujillo, J.; Brancato, S. J.; Karanian, J.; Agarwal, P. K.; Wood, B. J. Lyso-thermosensitive liposomal doxorubicin for treatment of bladder cancer. *Int J Hyperthermia* **2017,** *33* (7), 733-740.
295. Bressler, N. M. Photodynamic therapy of subfoveal choroidal neovascularization in age-related macular degeneration with verteporfin: two-year results of 2 randomized clinical trials-tap report 2. *Arch Ophthalmol* **2001,** *119* (2), 198-207.
296. Cook, R. L.; Householder, K. T.; Chung, E. P.; Prakapenka, A. V.; DiPerna, D. M.; Sirianni, R. W. A critical evaluation of drug delivery from ligand modified nanoparticles: confounding small molecule distribution and efficacy in the central nervous system. *J Control Release* **2015,** *220* (0 0), 89-97.
297. Han, J.; Pluhackova, K.; Böckmann, R. A. The Multifaceted Role of SNARE Proteins in Membrane Fusion. *Frontiers in Physiology* **2017,** *8*, 5.
298. Paleos, C. M.; Tsiourvas, D.; Sideratou, Z. Interaction of vesicles: adhesion, fusion and multicompartment systems formation. *Chembiochem* **2011,** *12* (4), 510-21.
299. Alam, S.; Alves, D. S.; Whitehead, S. A.; Bayer, A. M.; McNitt, C. D.; Popik, V. V.; Barrera, F. N.; Best, M. D. A clickable and photocleavable lipid analogue for cell membrane delivery and release. *Bioconjug Chem* **2015,** *26* (6), 1021-31.
300. Azzopardi, E. A.; Ferguson, E. L.; Thomas, D. W. The enhanced permeability retention effect: a new paradigm for drug targeting in infection. *J. Antimicrob. Chemother* **2013,** *68* (2), 257-274.
301. Miklossy, J.; Kasas, S.; Zurn, A. D.; McCall, S.; Yu, S.; McGeer, P. L. Persisting atypical and cystic forms of Borrelia burgdorferi and local inflammation in Lyme neuroborreliosis. *J Neuroinflammation* **2008,** *5*.
302. MacDonald, A. B. Plaques of Alzheimer's disease originate from cysts of Borrelia burgdorferi, the Lyme disease spirochete. *Med Hypotheses* **2006,** *67*.
303. Posey, J. E.; Gherardini, F. C. Lack of a Role for Iron in the Lyme Disease Pathogen. *Science (New York, N.Y.)* **2000,** *288* (5471), 1651-1653.
304. Aguirre, J. D.; Clark, H. M.; McIlvin, M.; Vazquez, C.; Palmere, S. L.; Grab, D. J.; Seshu, J.; Hart, P. J.; Saito, M.; Culotta, V. C. A manganese-rich environment supports superoxide dismutase activity in a Lyme disease pathogen, Borrelia burgdorferi. *J Biol Chem* **2013,** *288* (12), 8468-78.
305. Waldron, K. J.; Rutherford, J. C.; Ford, D.; Robinson, N. J. Metalloproteins and metal sensing. *Nature* **2009,** *460* (7257), 823-830.
306. LaFerla, F. M. Calcium dyshomeostasis and intracellular signalling in Alzheimer's disease. *Nat. Rev. Neurosci.* **2002,** *3* (11), 862-872.
307. Stutzmann, G. E. The pathogenesis of Alzheimers disease - Is it a lifelong "Calciumopathy"? *Neuroscientist* **2007,** *13* (5), 546-559.
308. Bezprozvanny, I.; Mattson, M. P. Neuronal calcium mishandling and the pathogenesis of Alzheimer's disease. *Trends Neurosci.* **2008,** *31* (9), 454-463.

309. Stutzmann, G. E.; Mattson, M. P. Endoplasmic reticulum Ca2+ handling in excitable cells in health and disease. *Pharmacol. Rev.* **2011,** *63* (3), 700-727.
310. Verkhratsky, A. Physiology and pathophysiology of the calcium store in the endoplasmic reticulum of neurons. *Physiol. Rev.* **2005,** *85* (1), 201-279.
311. Kruman, II; Pedersen, W. A.; Springer, J. E.; Mattson, M. P. ALS-linked Cu/Zn-SOD mutation increases vulnerability of motor neurons to excitotoxicity by a mechanism involving increased oxidative stress and perturbed calcium homeostasis. *Exp.Neurol.* **1999,** *160* (1), 28-39.
312. Guo, Z. H.; Kindy, M. S.; Kruman, I.; Mattson, M. P. ALS-linked Cu/Zn-SOD mutation impairs cerebral synaptic glucose and glutamate transport and exacerbates ischemic brain injury. *J. Cer. Blood Flow Metab.* **2000,** *20* (3), 463-468.
313. DiBernardo, A. B.; Cudkowicz, M. E. Translating preclinical insights into effective human trials in ALS. *Biochim. Biophys. Acta* **2006,** *1762* (11-12), 1139-1149.
314. Leal, S. S.; Gomes, C. M. Calcium dysregulation links ALS defective proteins and motor neuron selective vulnerability. *Front. Cell. Neurosci.* **2015,** *9*.
315. Mattson, M. P.; Kroemer, G. Mitochondria in cell death: Novel targets for neuroprotection and cardioprotection. *Trends Molec. Med.* **2003,** *9* (5), 196-205.
316. Verkhratsky, A.; Toescu, E. C. Endoplasmic reticulum Ca2+ homeostasis and neuronal death. *J. Cell. Molec. Med.* **2003,** *7* (4), 351-361.
317. MacDonald, J. F.; Xiong, Z. G.; Jackson, M. F. Paradox of Ca2+ signaling, cell death and stroke. *Trends Neurosci.* **2006,** *29* (2), 75-81.
318. Mattson, M. P. Calcium and neurodegeneration. *Aging Cell* **2007,** *6* (3), 337-350.
319. Garcia, C. R. S. Calcium homeostasis and signaling in the blood-stage malaria parasite. *Parasitol.Today* **1999,** *15* (12), 488-491.
320. Gazarini, M. L.; Thomas, A. P.; Pozzan, T.; Garcia, C. R. S. Calcium signaling in a low calcium environment: how the intracellular malaria parasite solves the problem. *J. Cell Biol.* **2003,** *161* (1), 103-110.
321. Brochet, M.; Billker, O. Calcium signalling in malaria parasites. *Molec. Microbiol.* **2016,** *100* (3), 397-408.
322. DeCoursey, T. E.; Chandy, K. G.; Gupta, S.; Cahalan, M. D. Voltage-gated K+ channels in human T lymphocytes: a role in mitogenesis? *Nature* **1984,** *307* (5950), 465-8.
323. Huang, X.; Jan, L. Y. Targeting potassium channels in cancer. *J. CellBbio.* **2014,** *206* (2), 151-162.
324. Overington, J. P.; Al-Lazikani, B.; Hopkins, A. L. How many drug targets are there? *Nature reviews. Drug discovery* **2006,** *5* (12), 993-6.
325. Choi, D. W.; Koh, J. Y. Zinc and brain injury. *Annu. Rev. Neurosci.* **1998,** *21*, 347-375.
326. Cope, E. C.; Morris, D. R.; Levenson, C. W. Improving treatments and outcomes: an emerging role for zinc in traumatic brain injury. *Nutr. Rev.* **2012,** *70* (7), 410-413.
327. Lee, J. M.; Zipfel, G. J.; Park, K. H.; He, Y. Y.; Hsu, C. Y.; Choi, D. W. Zinc translocation accelerates infarction after mild transient focal ischemia. *Neuroscience* **2002,** *115* (3), 871-878.
328. Yin, H. Z.; Sensi, S. L.; Ogoshi, F.; Weiss, J. H. Blockade of Ca2+-permeable AMPA/kainate channels decreases oxygen-glucose deprivation-induced Zn2+ accumulation and neuronal loss in hippocampal pyramidal neurons. *J. Neurosci.* **2002,** *22* (4), 1273-1279.
329. Suh, S. W.; Garnier, P.; Aoyama, K.; Chen, Y. M.; Swanson, R. A. Zinc release

contributes to hypoglycemia-induced neuronal death. *Neurobiol. Dis.* **2004,** *16* (3), 538-545.
330. Grattan, B. J.; Freake, H. C. Zinc and cancer: Implications for LIV-1 in breast cancer. *Nutrients* **2012,** *4* (7), 648-675.
331. Frezza, M.; Hindo, S.; Chen, D.; Davenport, A.; Schmitt, S.; Tomco, D.; Dou, Q. P. Novel metals and metal complexes as platforms for cancer therapy. *Curr. Pharm. Des.* **2010,** *16* (16), 1813-1825.
332. Manning, D. L.; Robertson, J. F. R.; Ellis, I. O.; Elston, C. W.; McClelland, R. A.; Gee, J. M. W.; Jones, R. J.; Green, C. D.; Cannon, P.; Blamey, R. W.; Nicholson, R. I. Estrogen-regulared genes in breast-cancer-association of PLIV1 withlymph-node involvement *Eur. J. Cancer* **1994,** *30A* (5), 675-678.
333. Li, M.; Zhang, Y.; Liu, Z.; Bharadwaj, U.; Wang, H.; Wang, X.; Zhang, S.; Liuzzi, J. P.; Chang, S.-M.; Cousins, R. J.; Fisher, W. E.; Brunicardi, F. C.; Logsdon, C. D.; Chen, C.; Yao, Q. Aberrant expression of zinc transporter ZIP4 (SLC39A4) significantly contributes to human pancreatic cancer pathogenesis and progression. *Proc. Natl. Acad. Sci. U. S. A.* **2007,** *104* (47), 18636-18641.
334. Taylor, K. M.; Morgan, H. E.; Smart, K.; Zahari, N. M.; Pumford, S.; Ellis, I. O.; Robertson, J. F. R.; Nicholson, R. I. The emerging role of the LIV-1 subfamily of zinc transporters in breast cancer. *Mol. Med.* **2007,** *13* (7-8), 396-406.
335. Murakami, M.; Hirano, T. Intracellular zinc homeostasis and zinc signaling. *Cancer Sci.* **2008,** *99* (8), 1515-1522.
336. Franklin, R. B.; Costello, L. C. The important role of the apoptotic effects of zinc in the development of cancers. *J. Cell. Biochem.* **2009,** *106* (5), 750-757.
337. Bush, A. I.; Pettingell, W. H.; Multhaup, G.; Paradis, M. D.; Vonsattel, J. P.; Gusella, J. F.; Beyreuther, K.; Masters, C. L.; Tanzi, R. E. Rapid induction of Alzheimer A-beta amyloid formation by zinc. *Science* **1994,** *265* (5177), 1464-1467.
338. Bush, A. I.; Pettingell, W. H.; Paradis, M. D.; Tanzi, R. E. Modulation of A-beta adhesiveness and secretase site cleavage by zinc. *J. Biol. Chem.* **1994,** *269* (16), 12152-12158.
339. Ayton, S.; Lei, P.; Bush, A. I. Biometals and their therapeutic implications in Alzheimer's disease. *Neurotherapeutics* **2015,** *12* (1), 109-120.
340. Kulikova, A. A.; Makarov, A. A.; Kozin, S. A. Roles of zinc ions and structural polymorphism of beta-amyloid in the development of Alzheimer's disease. *Mol. Biol.* **2015,** *49* (2), 217-230.
341. Prakash, A.; Bharti, K.; Majeed, A. A. Zinc: indications in brain disorders. *Fund. Clin. Pharmacol.* **2015,** *29* (2), 131-149.
342. Khan, M. Z. A possible significant role of zinc and GPR39 zinc sensing receptor in Alzheimer disease and epilepsy. *Biomed. Pharmacotherapy* **2016,** *79*, 263-272.
343. Li, L. B.; Wang, Z. Y. Disruption of brain zinc homeostasis promotes the pathophysiological progress of Alzheimer's disease. *Histol. Histopathol.* **2016,** *31* (6), 623-627.
344. Bush, A. I. Metals and neuroscience. *Curr. Opin. Chem. Biol.* **2000,** *4* (2), 184-191.
345. Bush, A. I. The metallobiology of Alzheimer's disease. *Trends Neurosci.* **2003,** *26* (4), 207-214.
346. Barnham, K. J.; Bush, A. I. Biological metals and metal-targeting compounds in major neurodegenerative diseases. *Chem. Soc. Rev.* **2014,** *43* (19), 6727-6749.
347. Dewys, W.; Pories, W. J.; Richter, M. C.; Strain, W. H. Inhibition of walker 256

carcinosarcoma by dietary zinc deficiency. *Proc. Soc. Exp. Biol. Med.* **1970,** *135* (1), 17.
348. Pories, W. J.; DeWys, W. D.; Flynn, A.; Mansour, E. G.; Strain, W. H. Implications of the inhibition of animal tumors by dietary zinc deficiency. *Adv. Exp. Med. Biol.* **1977,** *91*, 243-57.
349. Mills, B. J.; Broghamer, W. L.; Higgins, P. J.; Lindeman, R. D. Inhibition of tumor-growth by zinc depletion of rats. *J. Nutr.* **1984,** *114* (4), 746-752.
350. Regland, B.; Lehmann, W.; Abedini, I.; Blennow, K.; Jonsson, M.; Karlsson, I.; Sjogren, M.; Wallin, A.; Xilinas, M.; Gottfries, C. G. Treatment of Alzheimer's disease with clioquinol. *Dem. Ger. Cog. Disorders* **2001,** *12* (6), 408-414.
351. Ritchie, C. W.; Bush, A. I.; Mackinnon, A.; Macfarlane, S.; Mastwyk, M.; MacGregor, L.; Kiers, L.; Cherny, R.; Li, Q. X.; Tammer, A.; Carrington, D.; Mavros, C.; Volitakis, I.; Xilinas, M.; Ames, D.; Davis, S.; Beyreuther, K.; Tanzi, R. E.; Masters, C. L. Metal-protein attenuation with iodochlorhydroxyquin (clioquinol) targeting A beta amyloid deposition and toxicity in Alzheimer disease - A pilot phase 2 clinical trial. *Arch. Neur.* **2003,** *60* (12), 1685-1691.
352. Dutta, A.; Schaller, M.; Franco, A. T.; Sankavaram, K.; Grattan, B. J.; Freake, H. C. Zinc retention differs between primary and transformed cells in response to zinc deprivation. *J. Nutr. Biochem.* **2010,** *21* (2), 162-170.
353. Niroomand, H.; Mukherjee, D.; Khomami, B. Tuning the photoexcitation response of cyanobacterial Photosystem I via reconstitution into Proteoliposomes. *Scientific Reports* **2017,** *7*, 2492.

APPENDIX

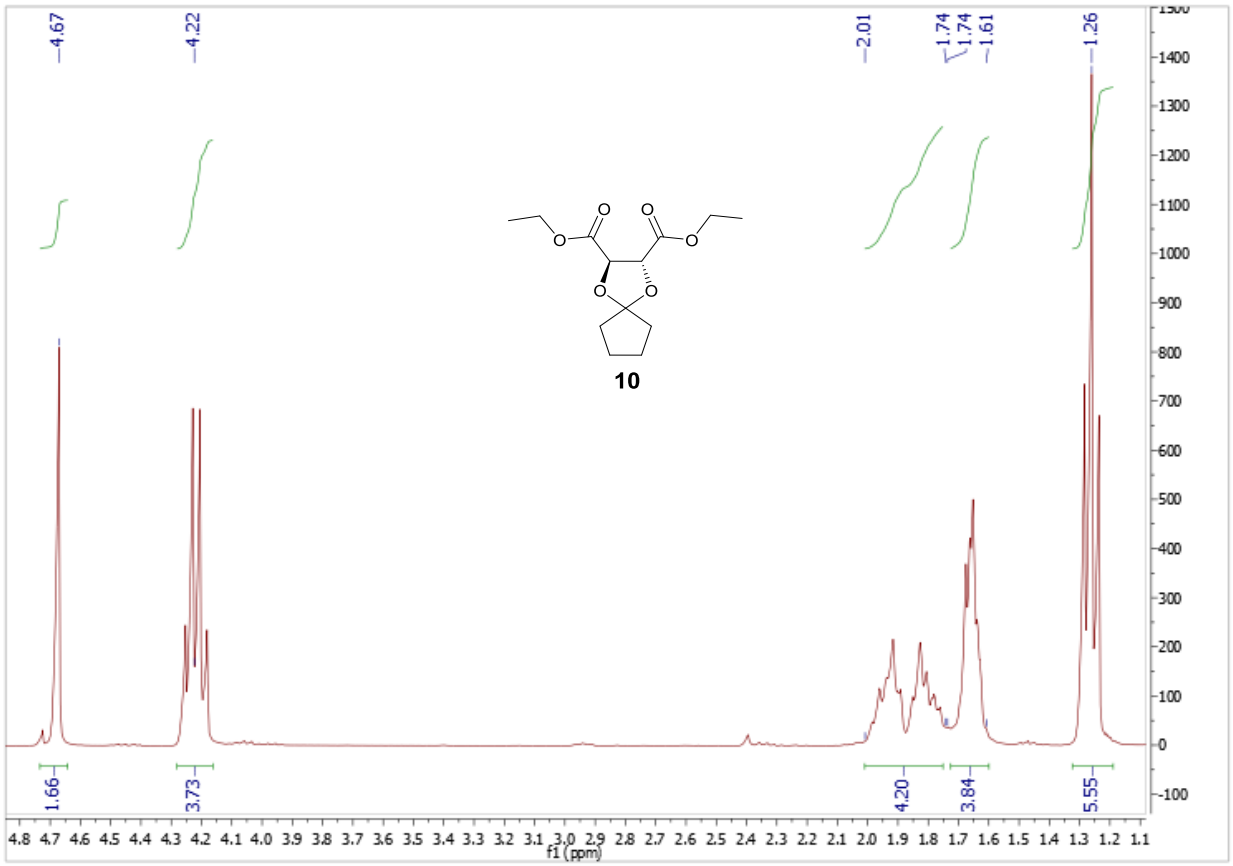
4.67
4.22
2.01
1.74
1.74
1.61
1.26
10
1.66
3.73
4.20
3.84
5.55
f1 (ppm)

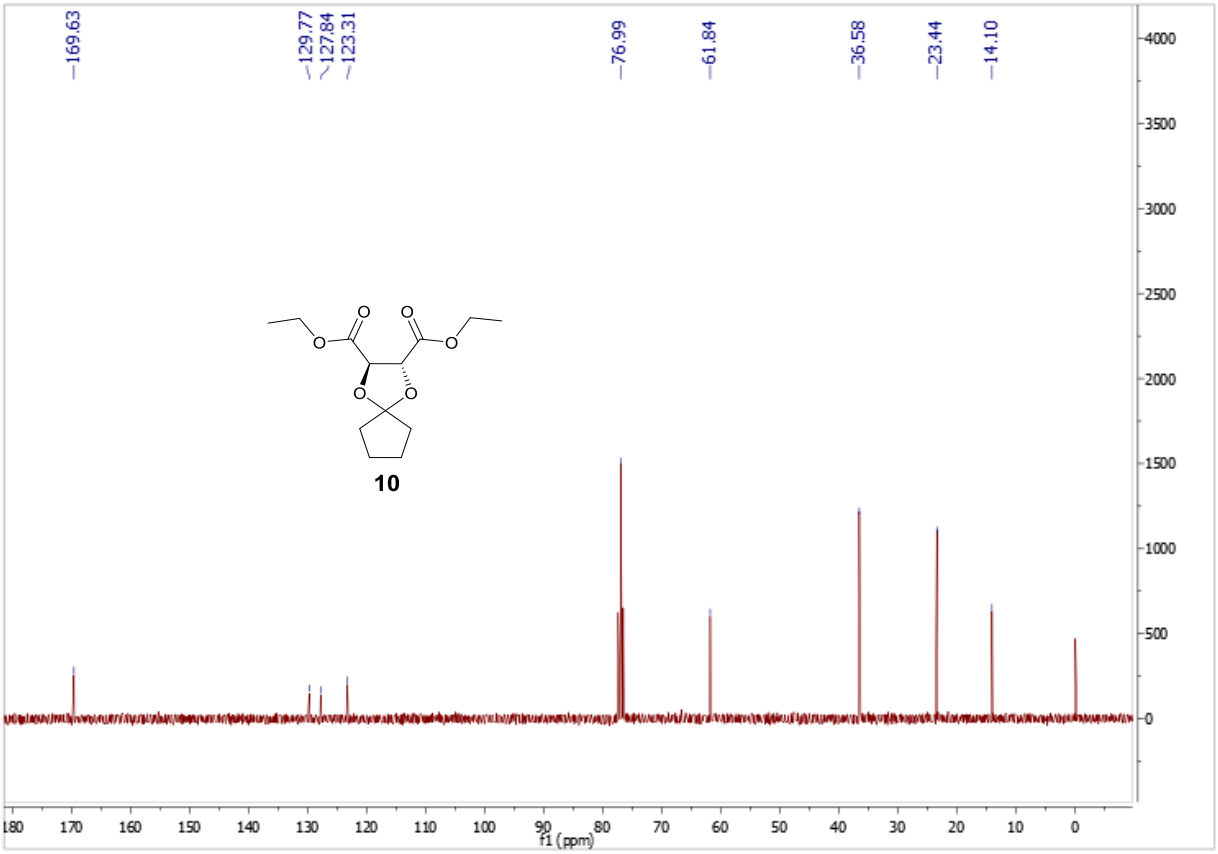
169.63
129.77
127.84
123.31
76.99
61.84
36.58
23.44
14.10
4000
3500
3000
2500
2000
1500
1000
500
0
180
170
160
150
140
130
120
110
100
90
80
70
60
50
40
30
20
10
0
f1 (ppm)
10

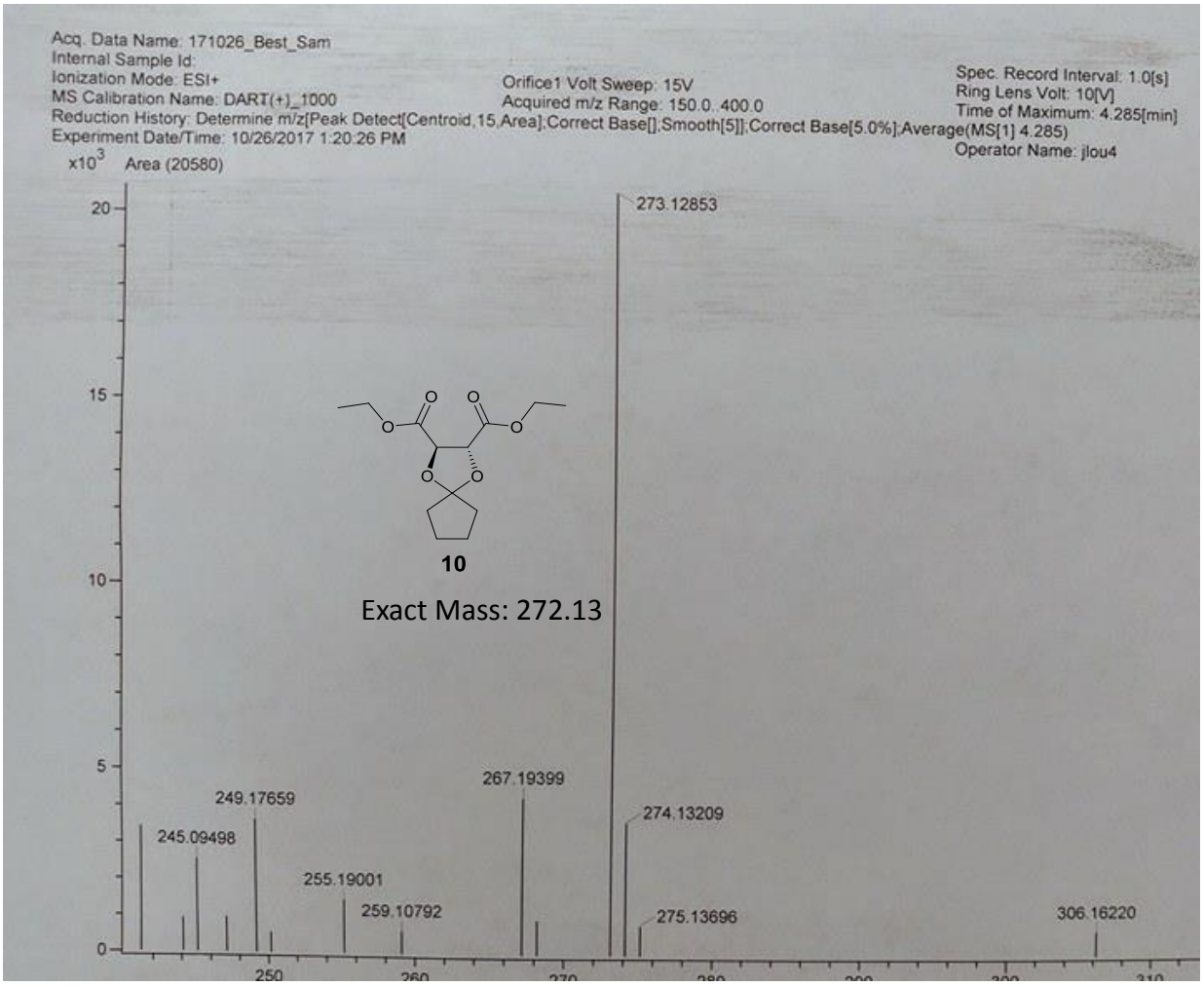
Acq. Data Name: 171026_Best_Sam
Internal Sample Id:
Ionization Mode: ESI+
MS Calibration Name: DART(+)_1000
Reduction History: Determine m/z[Peak Detect[Centroid,15,Area];Correct Base[];Smooth[5]];Correct Base[5.0%];Average(MS[1] 4.285)
Experiment Date/Time: 10/26/2017 1:20:26 PM
Orifice1 Volt Sweep: 15V
Acquired m/z Range: 150.0. 400.0
Spec. Record Interval: 1.0[s]
Ring Lens Volt: 10[V]
Time of Maximum: 4.285[min]
Operator Name: jlou4
x10^3 Area (20580)
20
15
10
5
0
273.12853
267.19399
249.17659
274.13209
245.09498
255.19001
259.10792
275.13696
306.16220
250
260
10
Exact Mass: 272.13

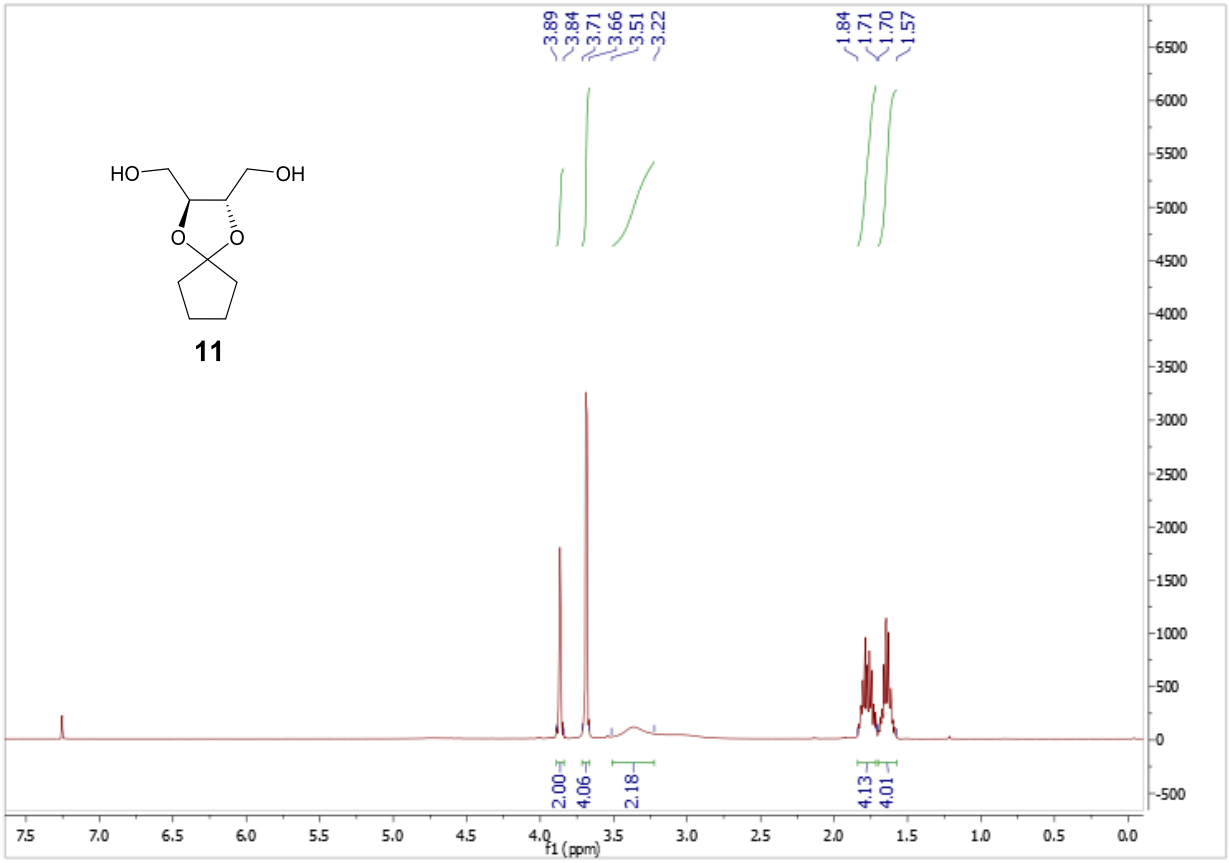
HO
OH
O
O
11
3.89
3.84
3.71
3.66
3.51
3.22
1.84
1.71
1.70
1.57
2.00
4.06
2.18
4.13
4.01
f1 (ppm)

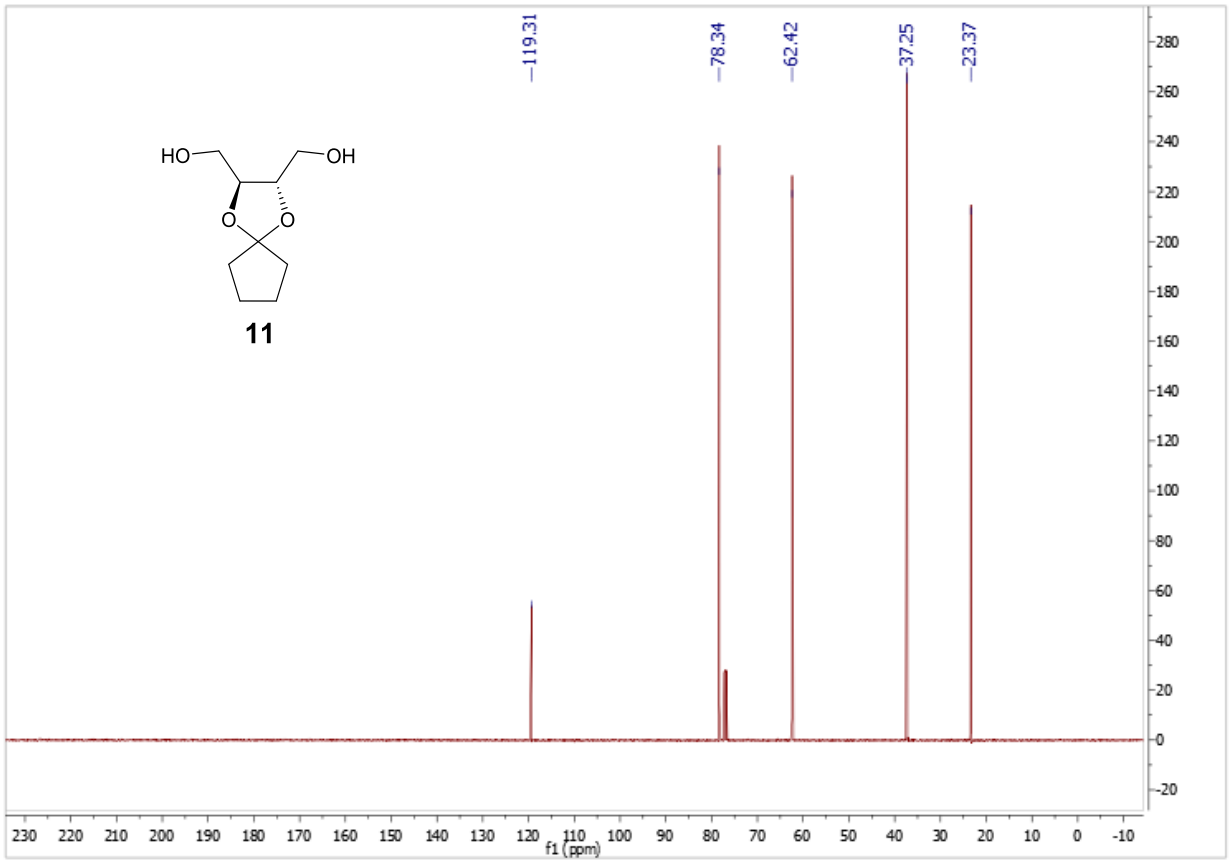
HO
OH
O
O
11
119.31
78.34
62.42
37.25
23.37
f1 (ppm)

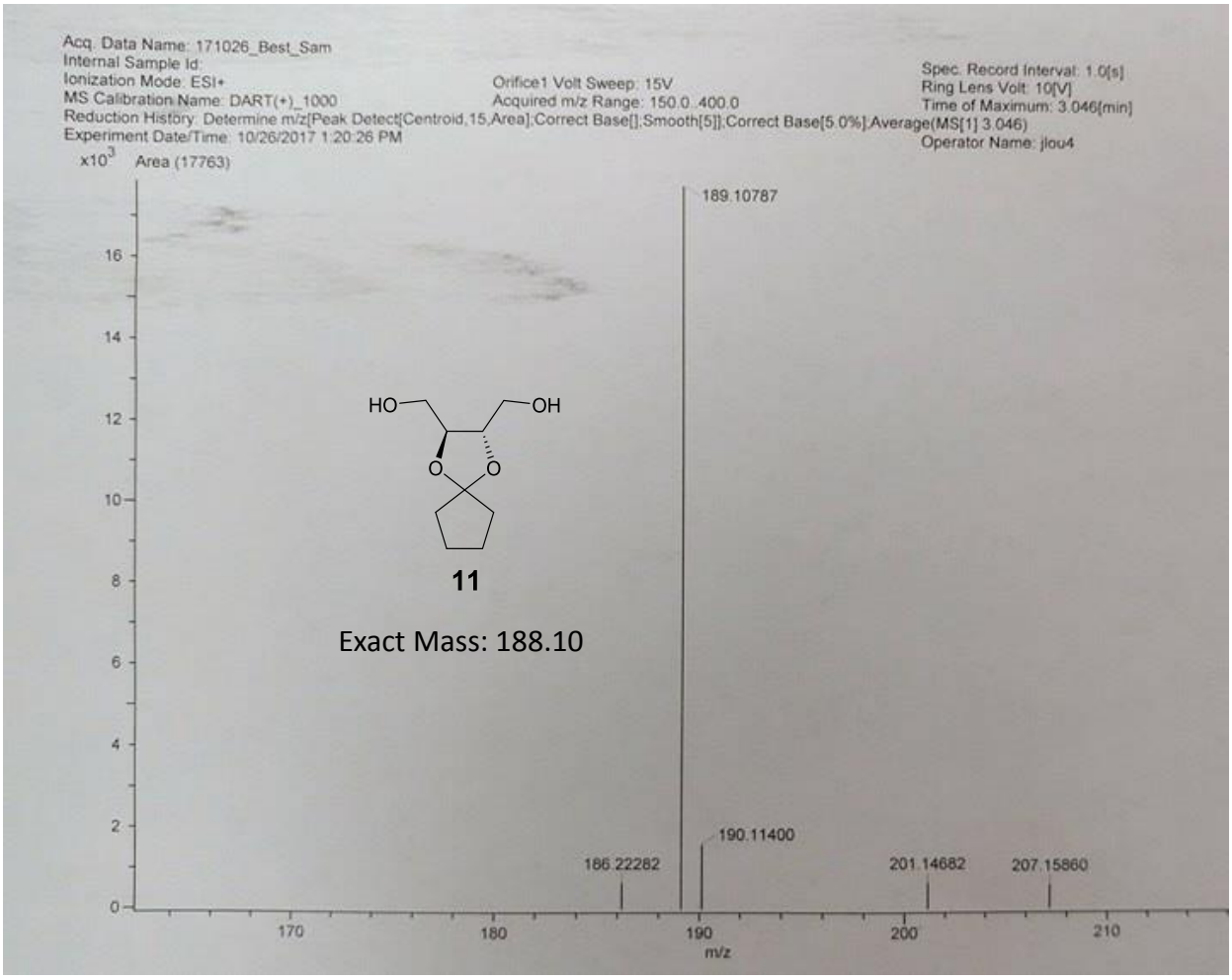
Acq. Data Name: 171026_Best_Sam
Internal Sample Id:
Ionization Mode: ESI+
MS Calibration Name: DART(+)_1000
Orifice1 Volt Sweep: 15V
Acquired m/z Range: 150.0..400.0
Spec. Record Interval: 1.0[s]
Ring Lens Volt: 10[V]
Time of Maximum: 3.046[min]
Reduction History: Determine m/z[Peak Detect[Centroid,15,Area],Correct Base[],Smooth[5]],Correct Base[5.0%],Average(MS[1] 3.046)
Experiment Date/Time: 10/26/2017 1:20:26 PM
Operator Name: jlou4
x10^3
Area (17763)
189.10787
190.11400
186.22282
201.14682
207.15860
HO
OH
O
O
11
Exact Mass: 188.10
m/z

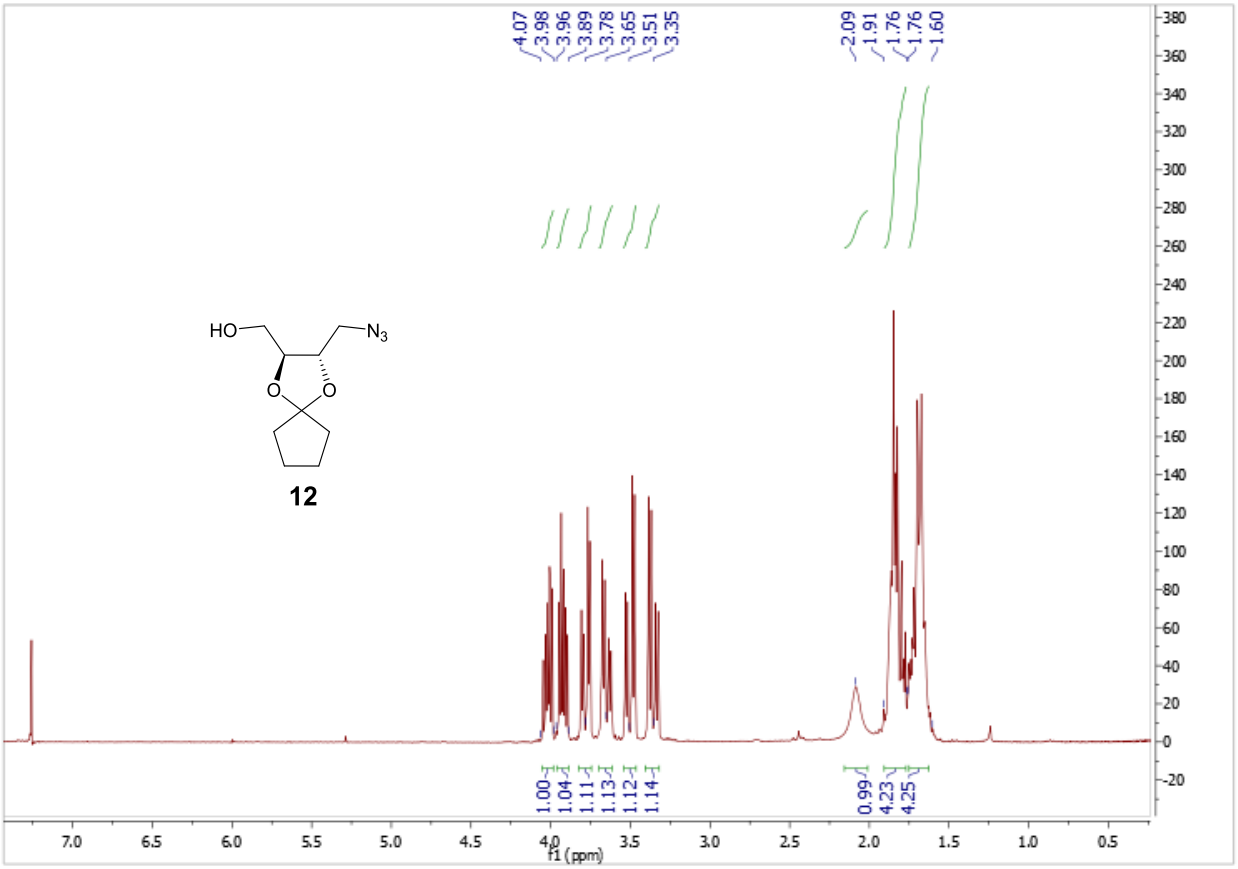
4.07
3.98
3.96
3.89
3.78
3.65
3.51
3.35
2.09
1.91
1.76
1.76
1.60
HO
N3
O
O
12
1.00
1.04
1.11
1.13
1.12
1.14
0.99
4.23
4.25
f1 (ppm)

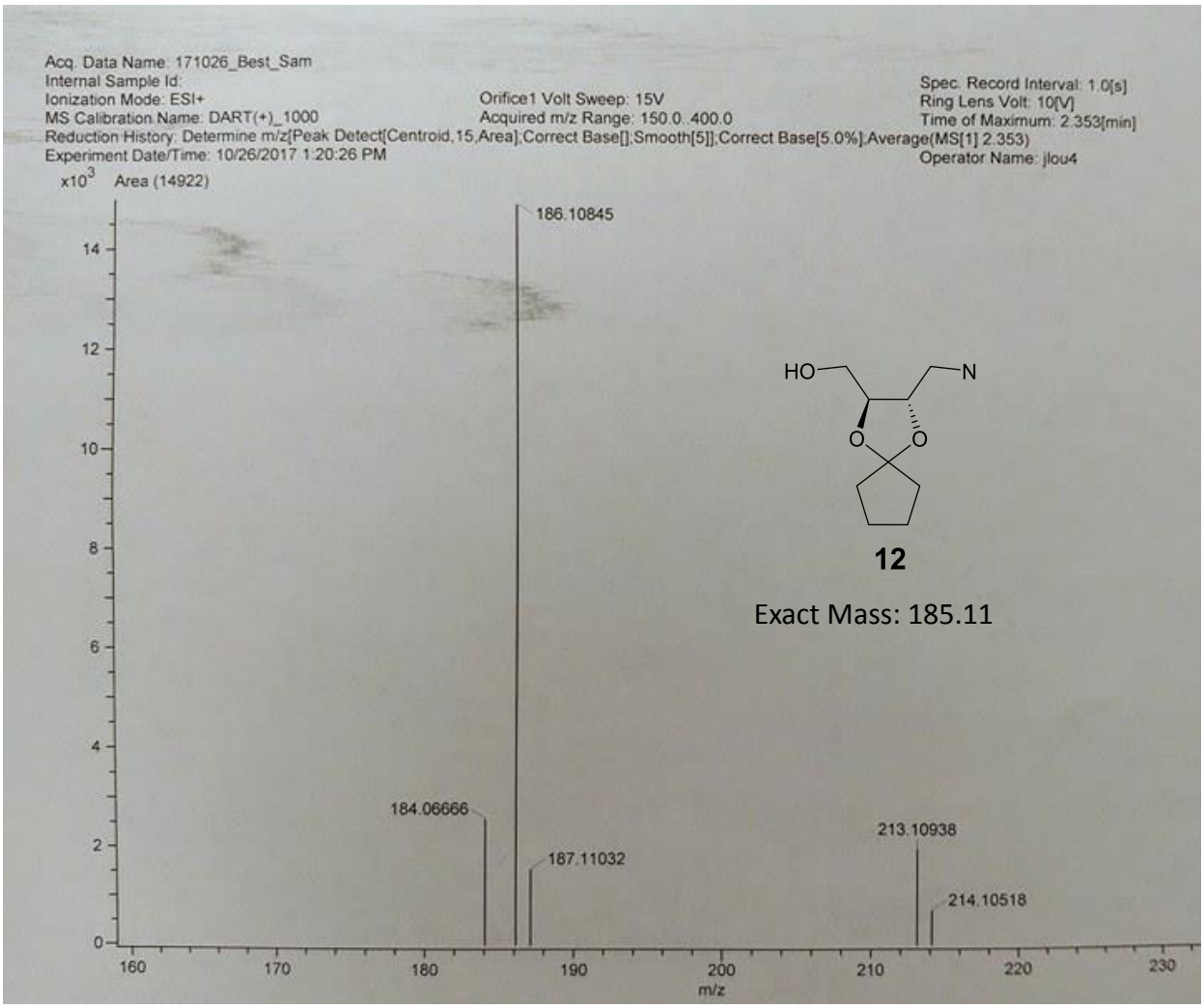
Acq. Data Name: 171026_Best_Sam
Internal Sample Id:
Ionization Mode: ESI+
MS Calibration Name: DART(+)_1000
Orifice1 Volt Sweep: 15V
Acquired m/z Range: 150.0..400.0
Spec. Record Interval: 1.0[s]
Ring Lens Volt: 10[V]
Time of Maximum: 2.353[min]
Reduction History: Determine m/z[Peak Detect[Centroid,15,Area];Correct Base[];Smooth[5]];Correct Base[5.0%];Average(MS[1] 2.353)
Experiment Date/Time: 10/26/2017 1:20:26 PM
Operator Name: jlou4
x10^3 Area (14922)
186.10845
184.06666
187.11032
213.10938
214.10518
m/z
HO
N
O
O
12
Exact Mass: 185.11

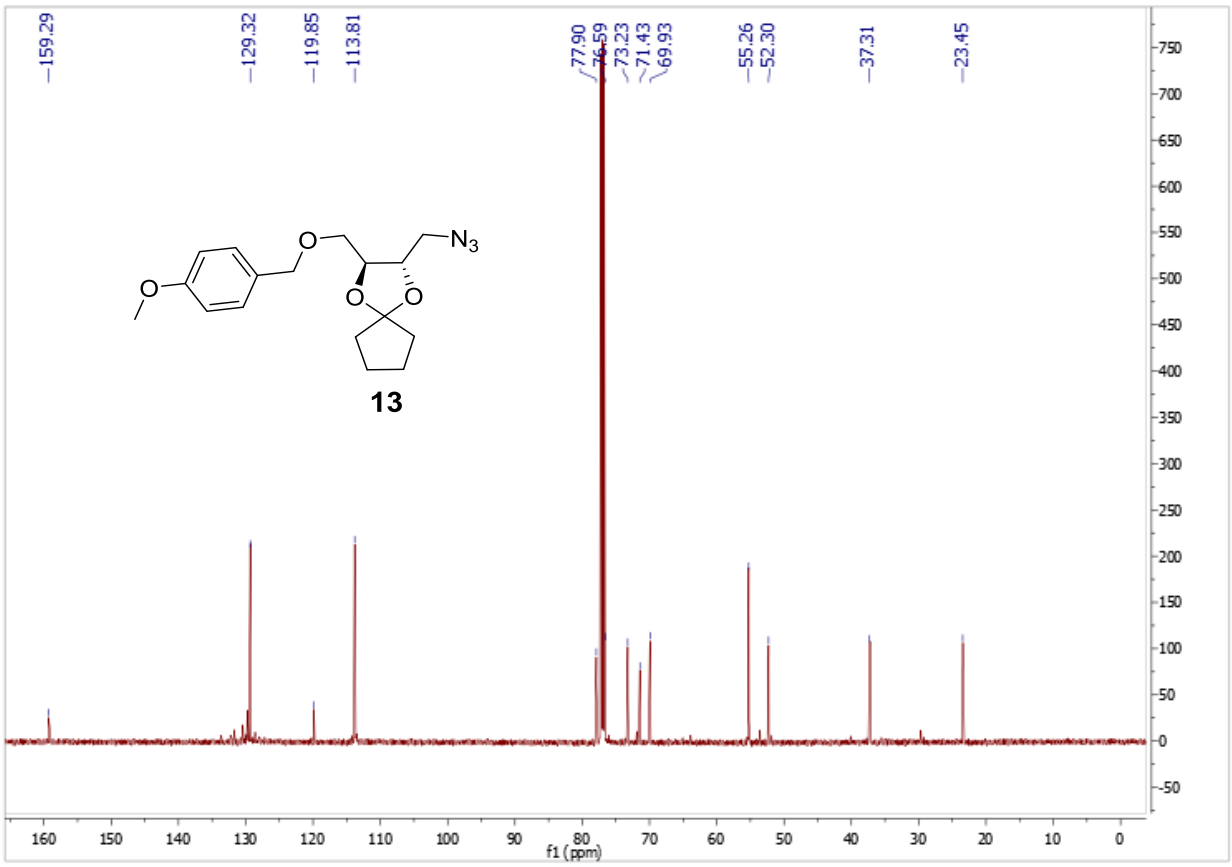
159.29
129.32
119.85
113.81
77.90
76.59
73.23
71.43
69.93
55.26
52.30
37.31
23.45
O
N3
O
O
O
13
f1 (ppm)

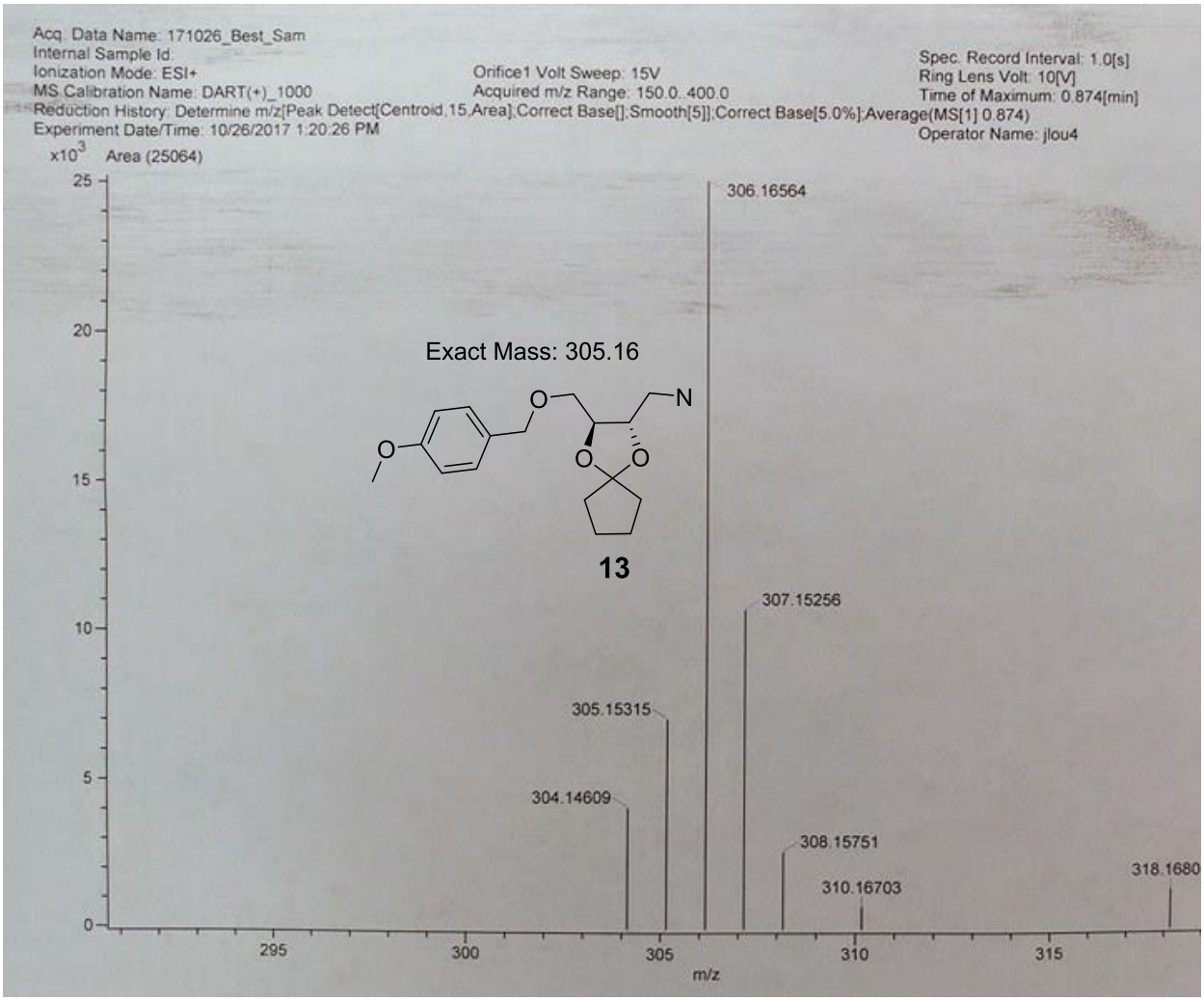
Acq. Data Name: 171026_Best_Sam
Internal Sample Id:
Ionization Mode: ESI+
MS Calibration Name: DART(+)_1000
Orifice1 Volt Sweep: 15V
Acquired m/z Range: 150.0..400.0
Spec. Record Interval: 1.0[s]
Ring Lens Volt: 10[V]
Time of Maximum: 0.874[min]
Reduction History: Determine m/z[Peak Detect[Centroid,15,Area];Correct Base[];Smooth[5]];Correct Base[5.0%];Average(MS[1] 0.874)
Experiment Date/Time: 10/26/2017 1:20:26 PM
Operator Name: jlou4
x10^3 Area (25064)
Exact Mass: 305.16
13
306.16564
307.15256
305.15315
304.14609
308.15751
310.16703
318.1680
m/z

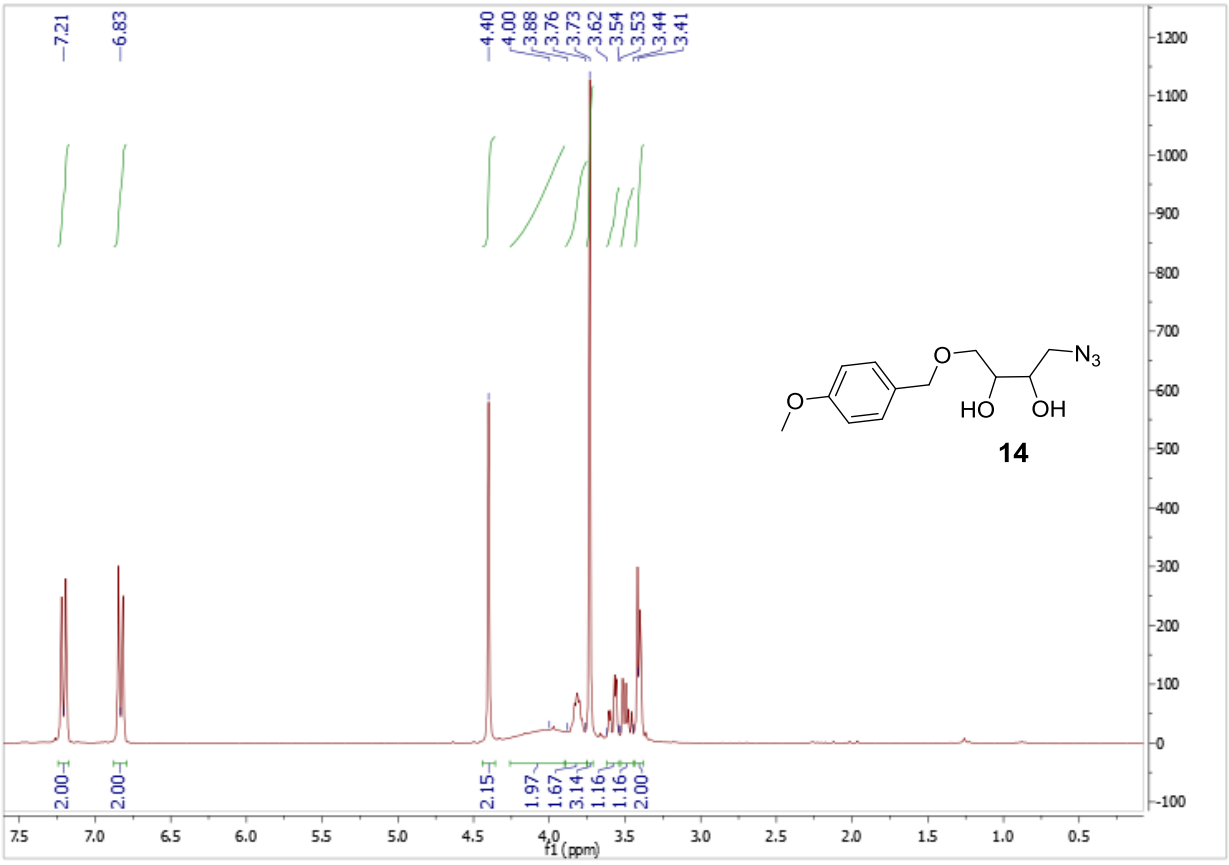
7.21
6.83
4.40
4.00
3.88
3.76
3.73
3.62
3.54
3.53
3.44
3.41
2.00
2.00
2.15
1.97
1.67
3.14
1.16
1.16
2.00
f1 (ppm)
O
N3
HO
OH
O
14

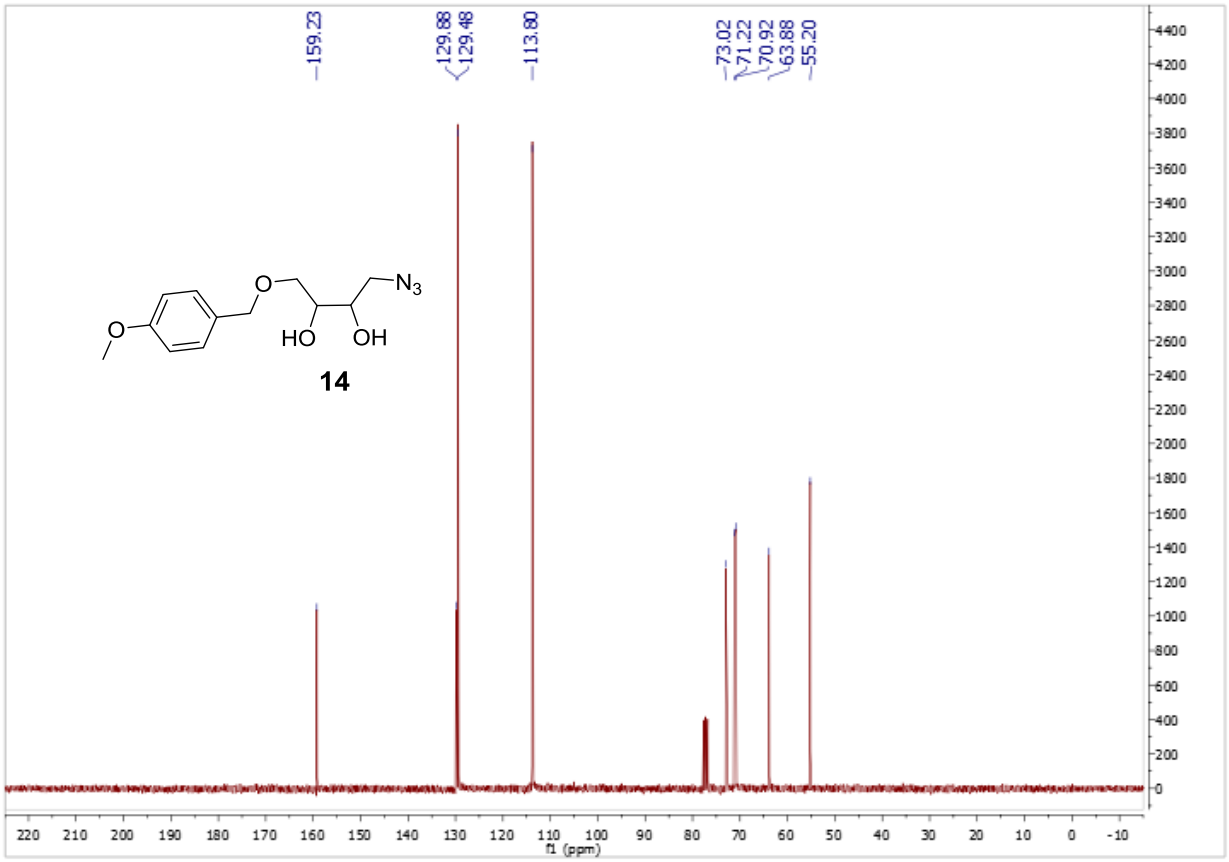
159.23
129.88
129.48
113.80
73.02
71.22
70.92
63.88
55.20
O
O
HO
OH
N_3
14
f1 (ppm)

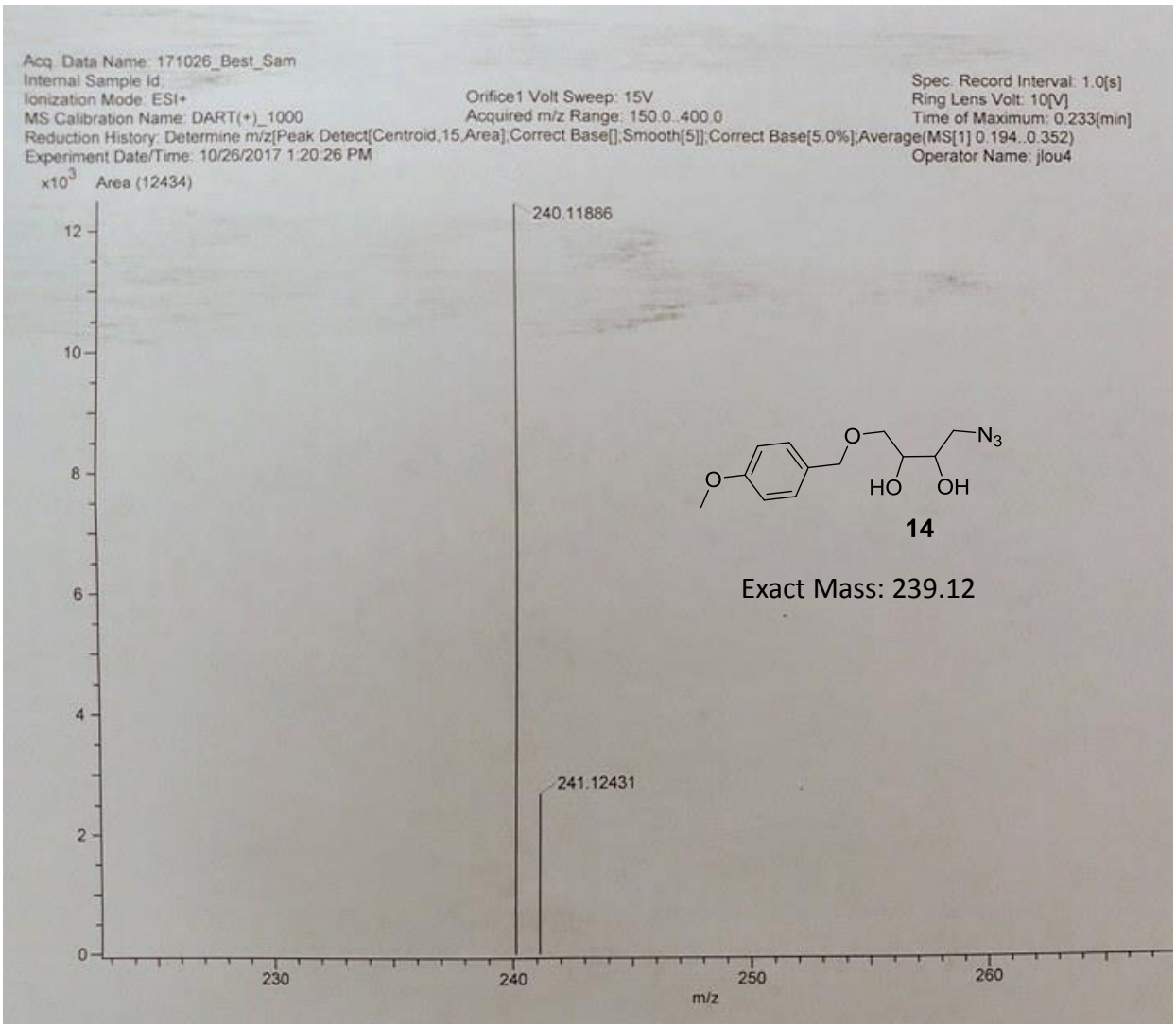

14

Exact Mass: 239.12

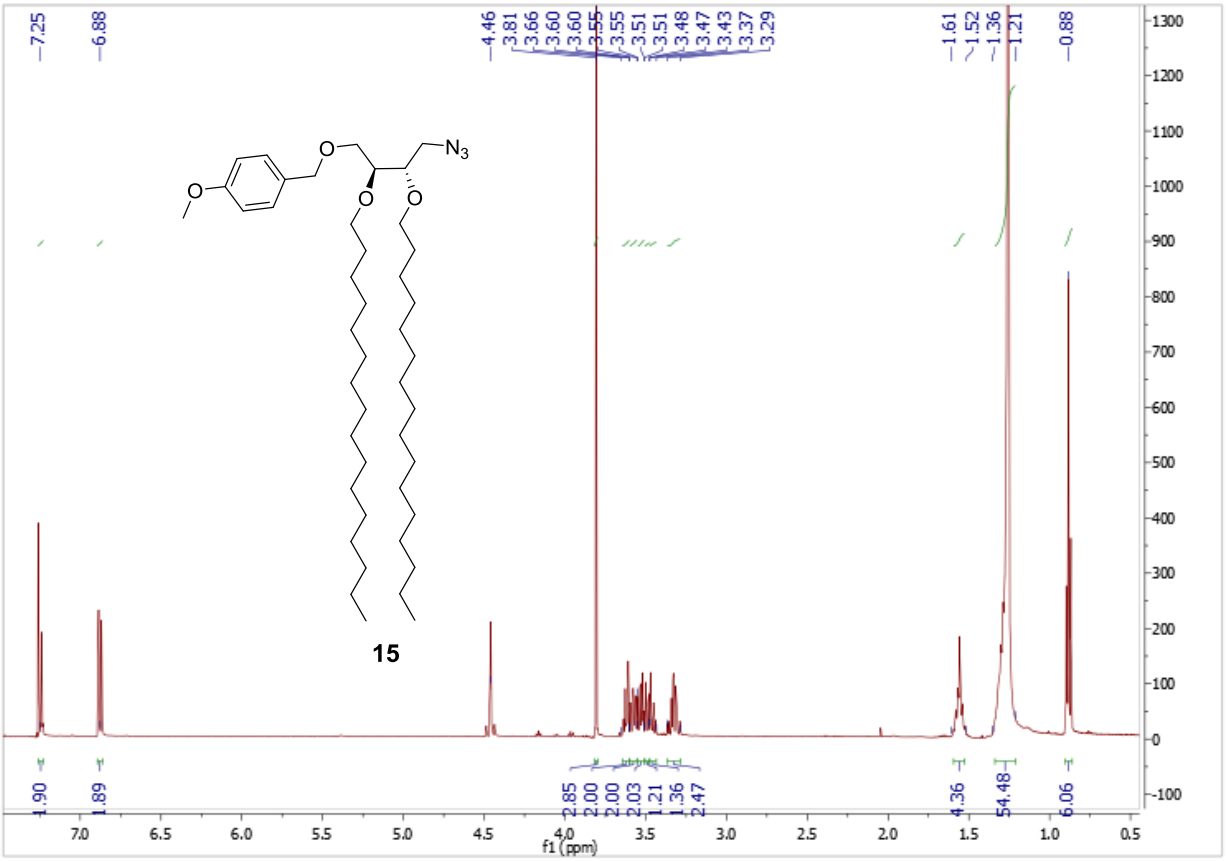
7.25
6.88
4.46
3.81
3.66
3.60
3.60
3.55
3.55
3.51
3.51
3.48
3.47
3.43
3.37
3.29
1.61
1.52
1.36
1.21
0.88
O
O
O
O
N3
15
1.90
1.89
2.85
2.00
2.00
2.03
1.21
1.36
2.47
4.36
54.48
6.06
f1 (ppm)

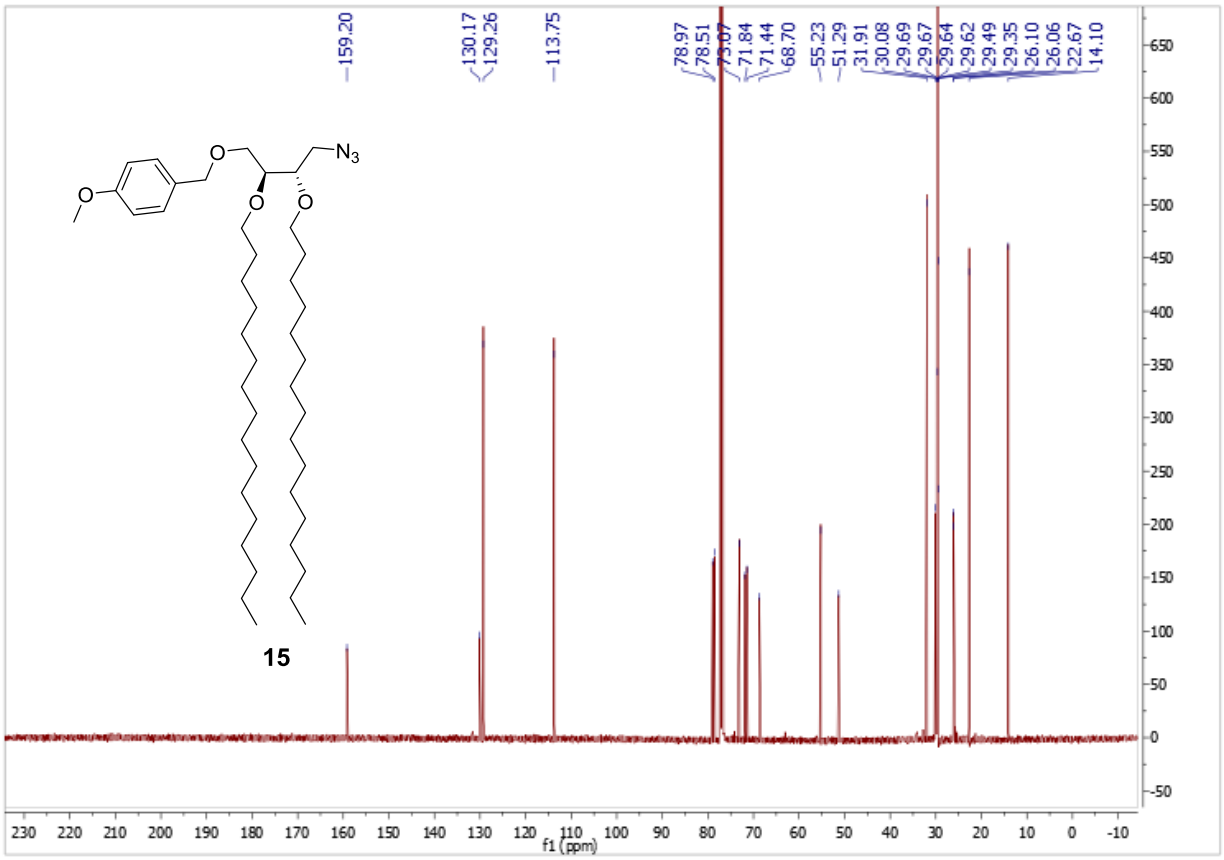
159.20
130.17
129.26
113.75
78.97
78.51
73.07
71.84
71.44
68.70
55.23
51.29
31.91
30.08
29.69
29.67
29.64
29.62
29.49
29.35
26.10
26.06
22.67
14.10
O
O
O
O
N3
15
f1 (ppm)

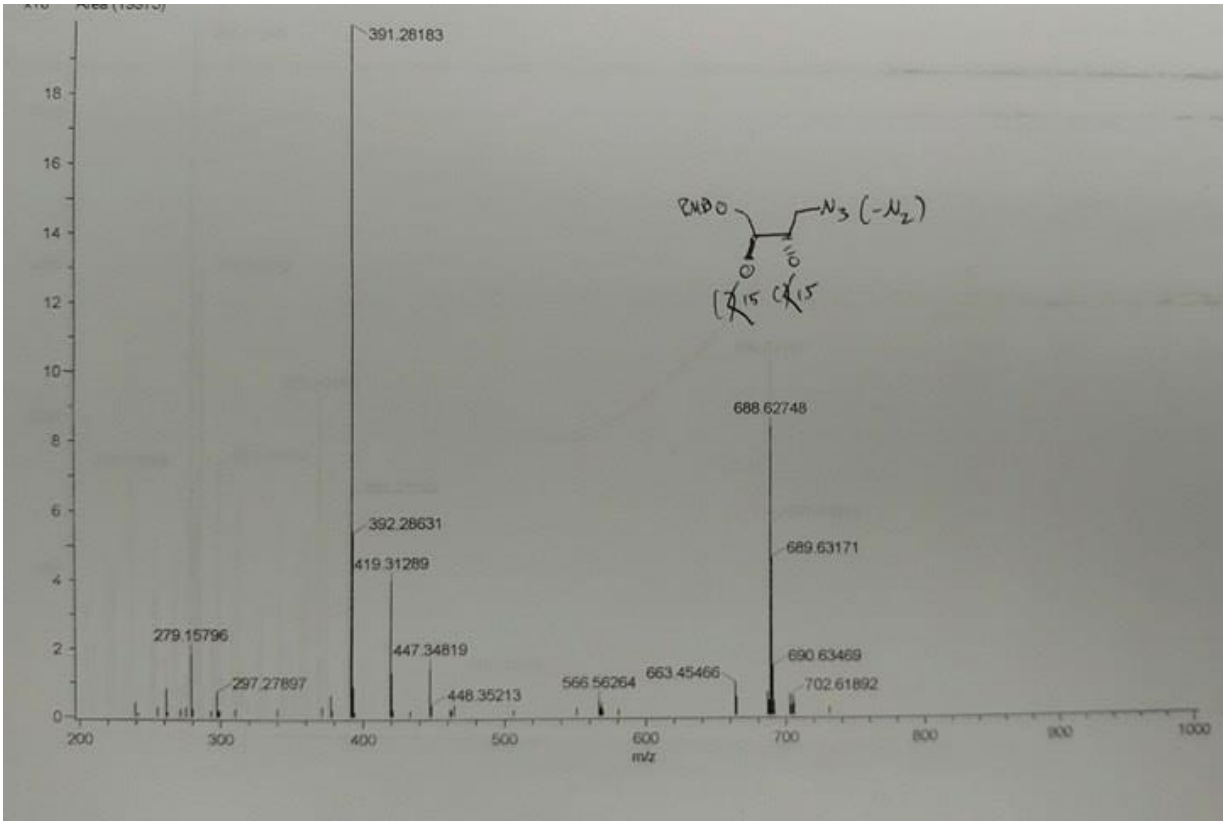

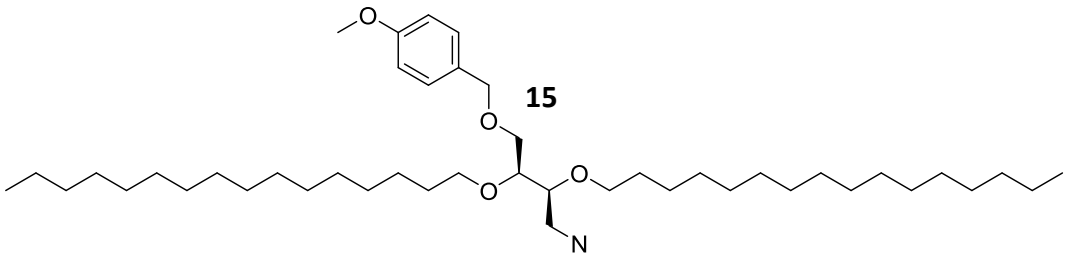

Exact Mass: 687.62

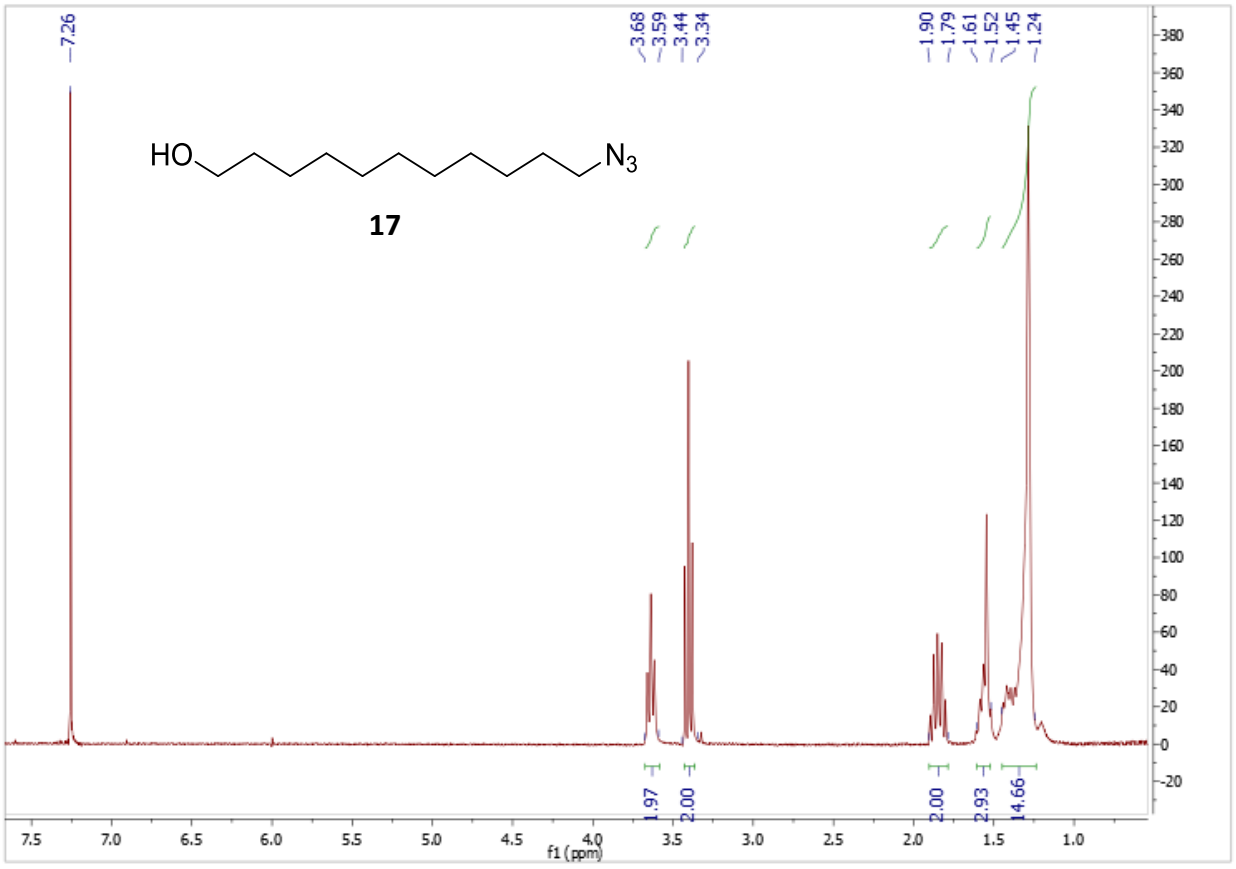
7.26
3.68
3.59
3.44
3.34
1.90
1.79
1.61
1.52
1.45
1.24
HO
N3
17
1.97
2.00
2.00
2.93
14.66
f1 (ppm)

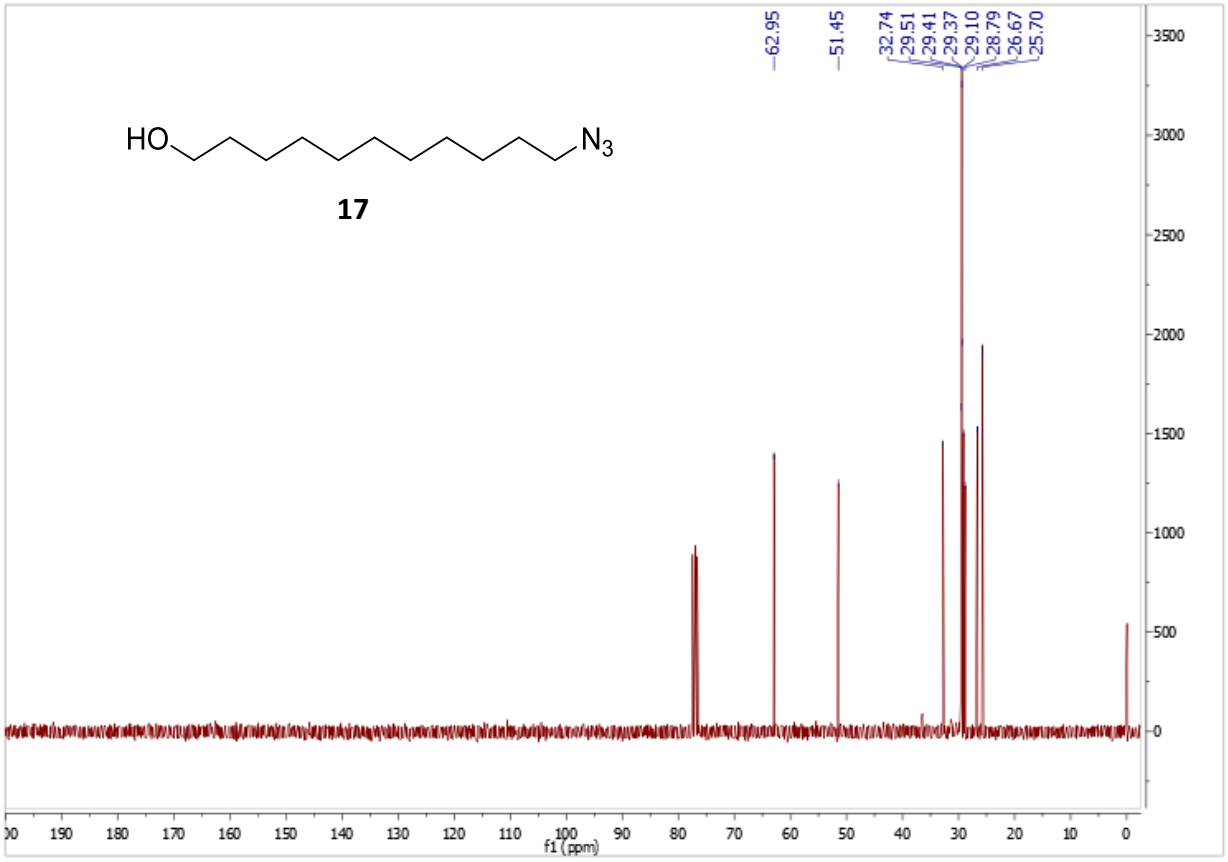
HO
N3
62.95
51.45
32.74
29.51
29.41
29.37
29.10
28.79
26.67
25.70
3500
3000
2500
2000
1500
1000
500
0
190
180
170
160
150
140
130
120
110
100
90
80
70
60
50
40
30
20
10
0
f1 (ppm)

17

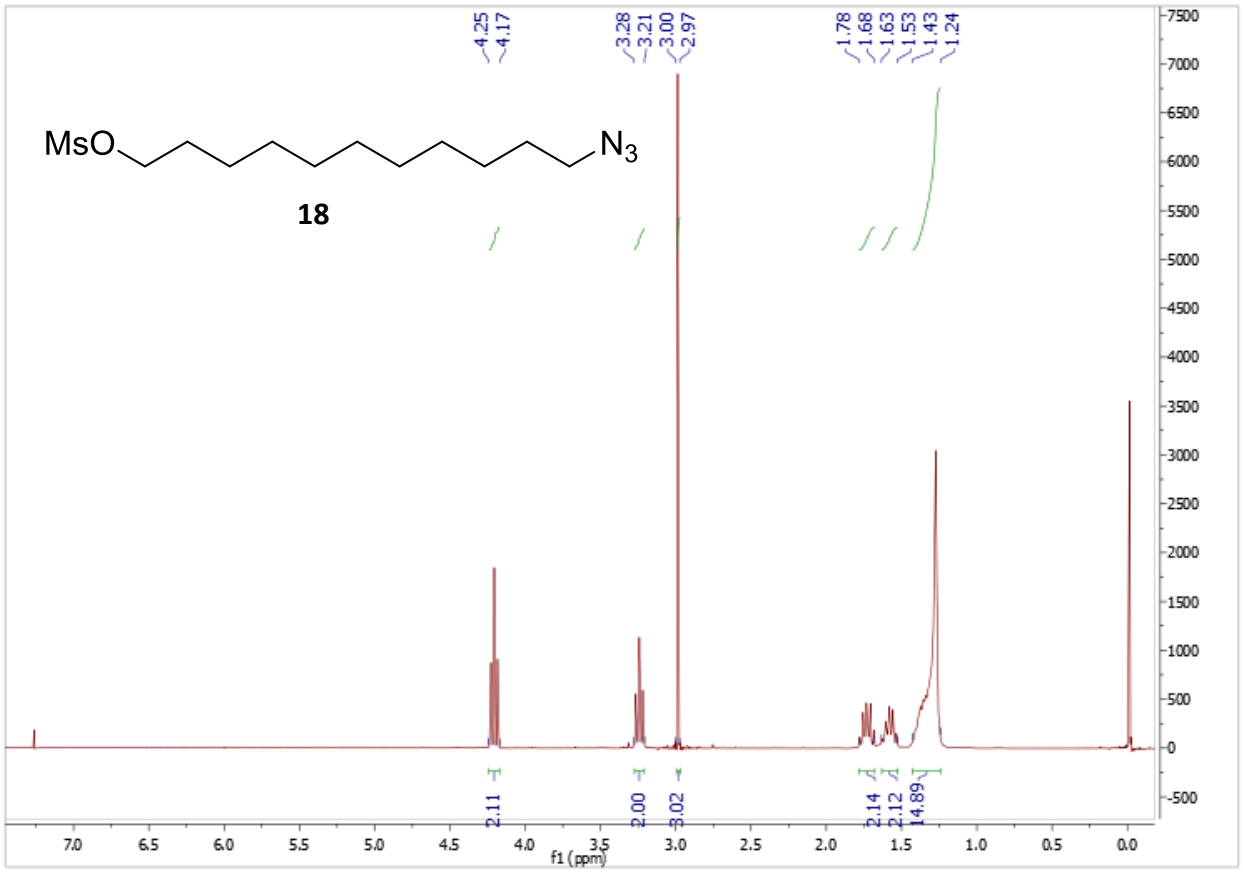
MsO
N3
18
4.25
4.17
3.28
3.21
3.00
2.97
1.78
1.68
1.63
1.53
1.43
1.24
2.11
2.00
3.02
2.14
2.12
14.89
f1 (ppm)

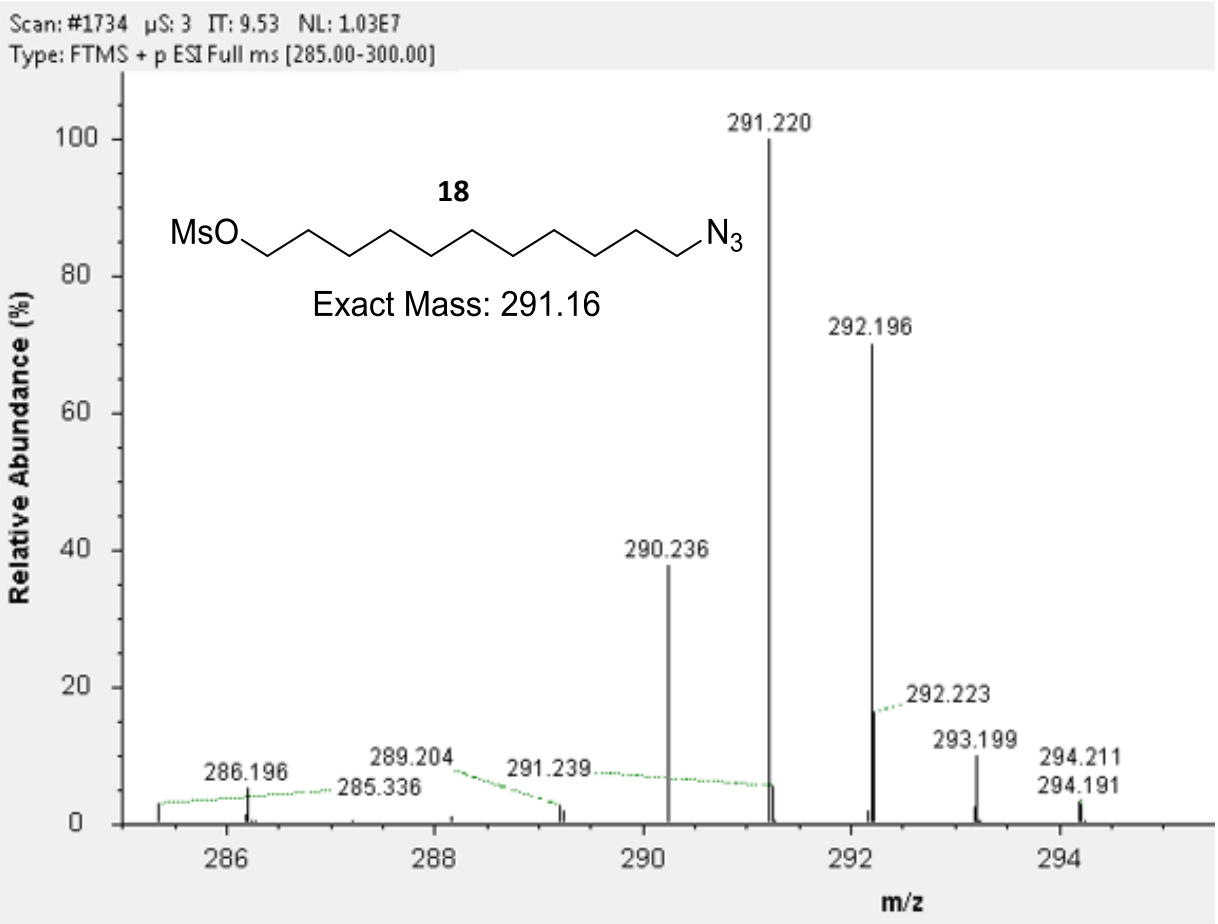
Scan: #1734 µS: 3 IT: 9.53 NL: 1.03E7
Type: FTMS + p ESI Full ms [285.00-300.00]
18
MsO
N3
Exact Mass: 291.16
Relative Abundance (%)
m/z
291.220
292.196
290.236
292.223
293.199
294.211
294.191
289.204
291.239
286.196
285.336

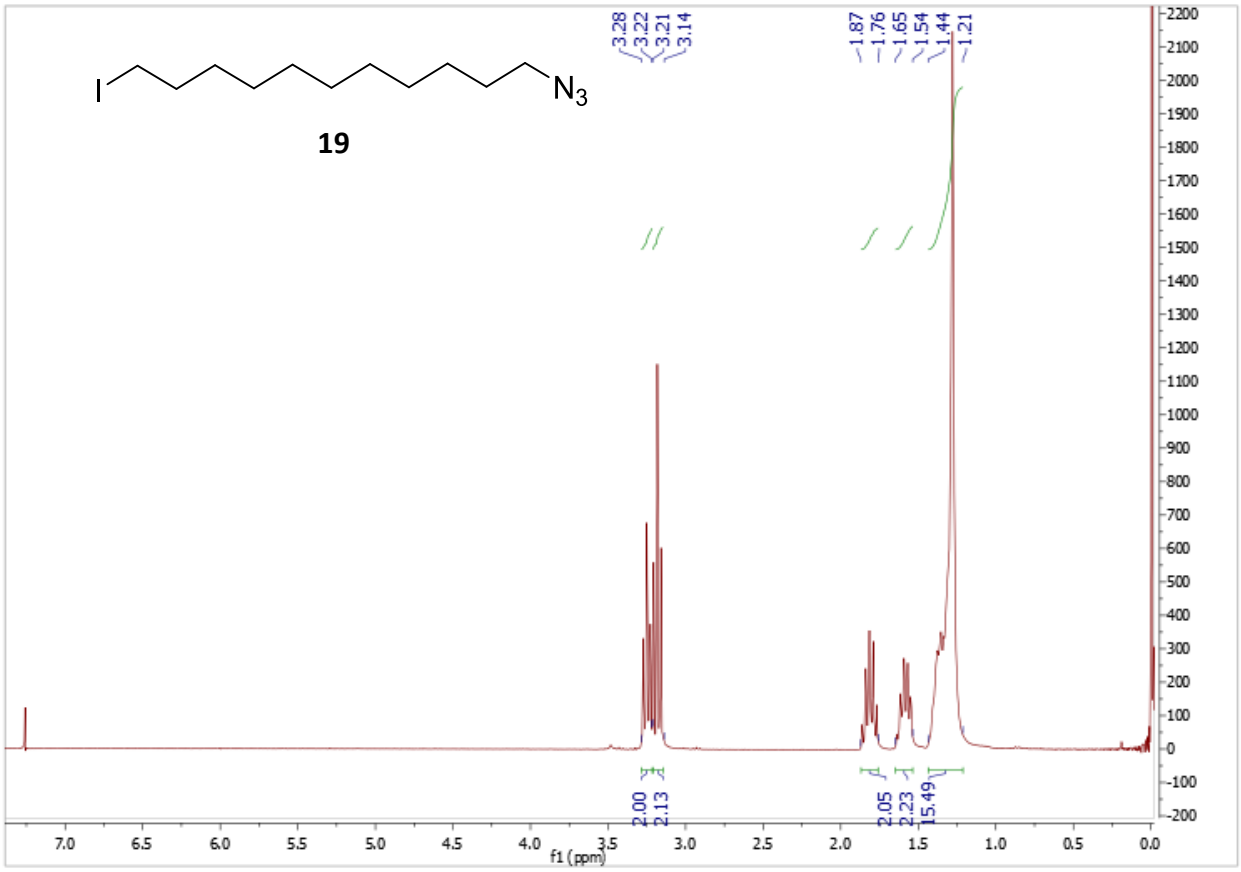
I
N3
19
3.28
3.22
3.21
3.14
1.87
1.76
1.65
1.54
1.44
1.21
2.00
2.13
2.05
2.23
15.49
f1 (ppm)

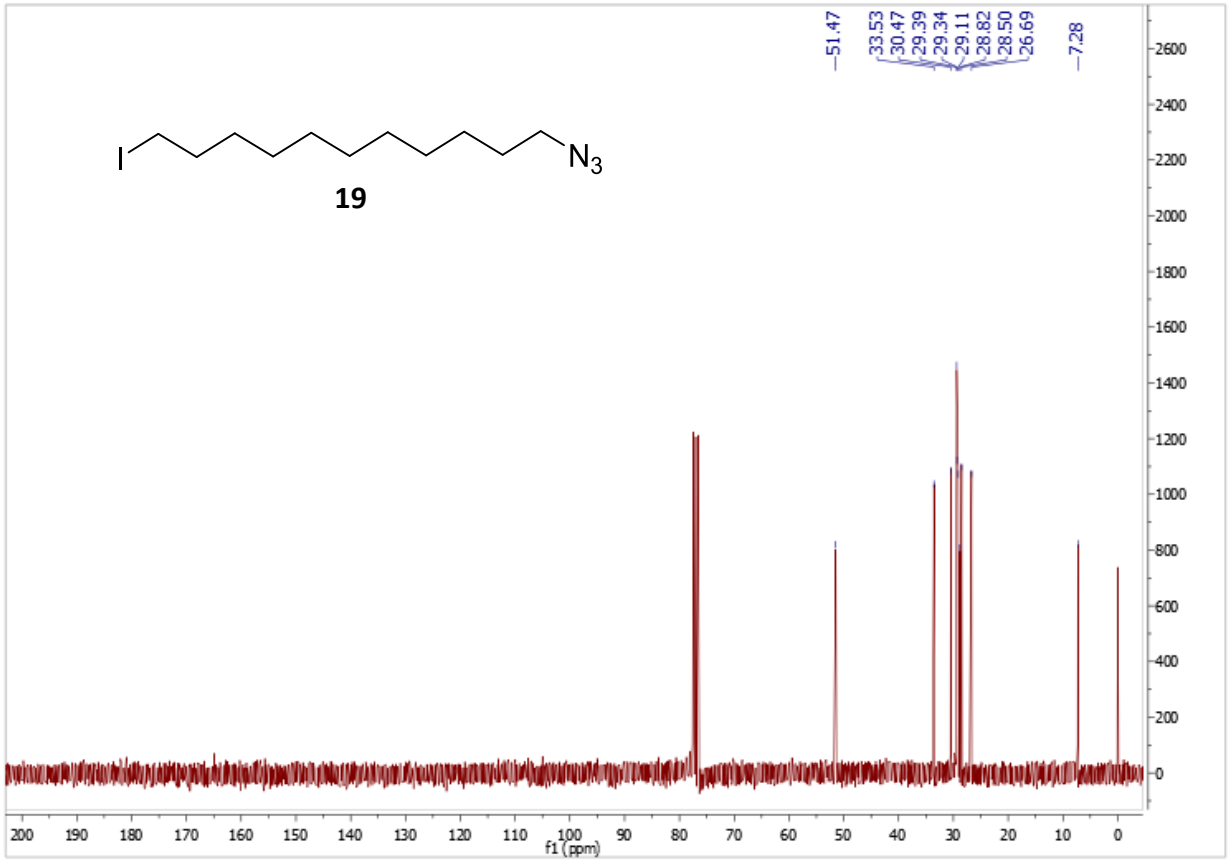
I
N3
19
51.47
33.53
30.47
29.39
29.34
29.11
28.82
28.50
26.69
7.28
f1 (ppm)

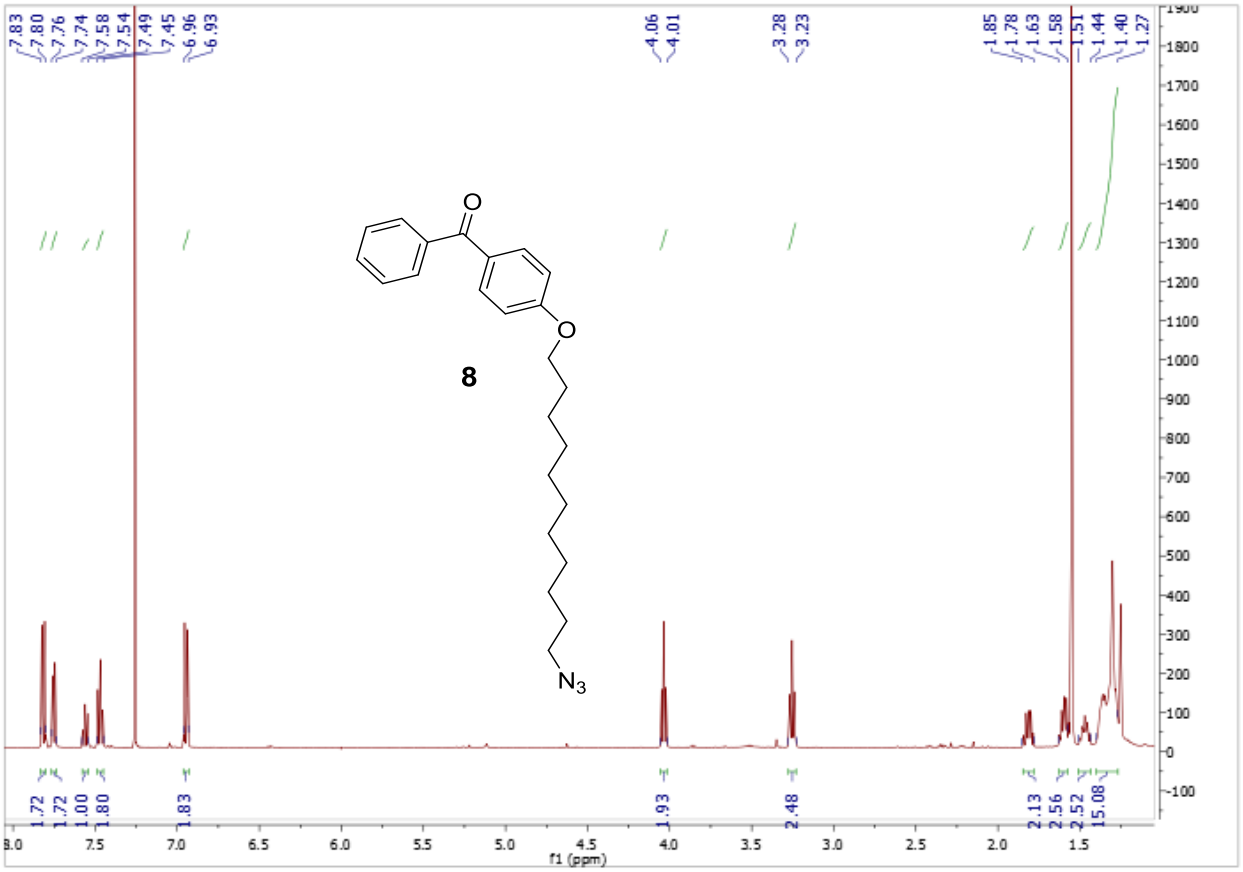
7.83
7.80
7.76
7.74
7.58
7.54
7.49
7.45
6.96
6.93
4.06
4.01
3.28
3.23
1.85
1.78
1.63
1.58
1.51
1.44
1.40
1.27
O
O
8
N3
1.72
1.72
1.00
1.80
1.83
1.93
2.48
2.13
2.56
2.52
15.08
f1 (ppm)

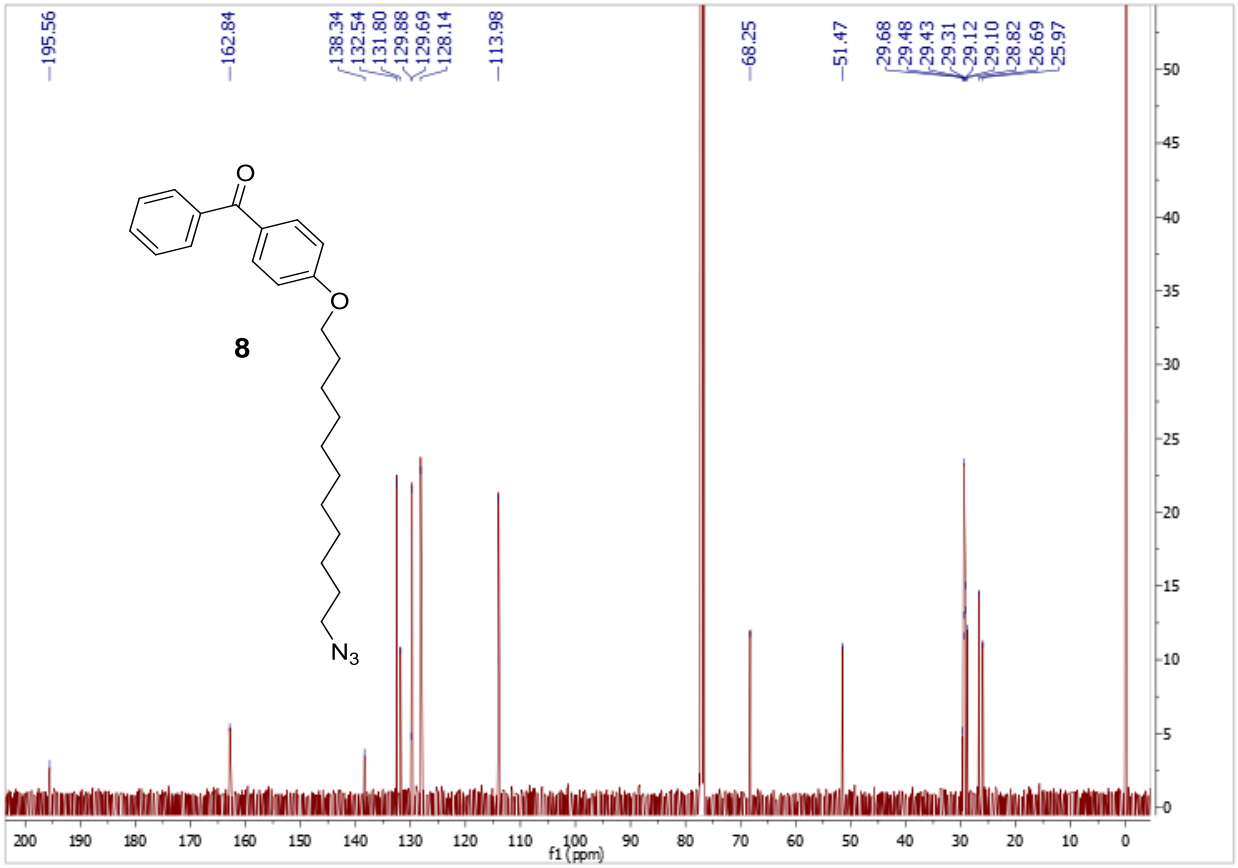
195.56
162.84
138.34
132.54
131.80
129.88
129.69
128.14
113.98
68.25
51.47
29.68
29.48
29.43
29.31
29.12
29.10
28.82
26.69
25.97
O
O
8
N3
f1 (ppm)

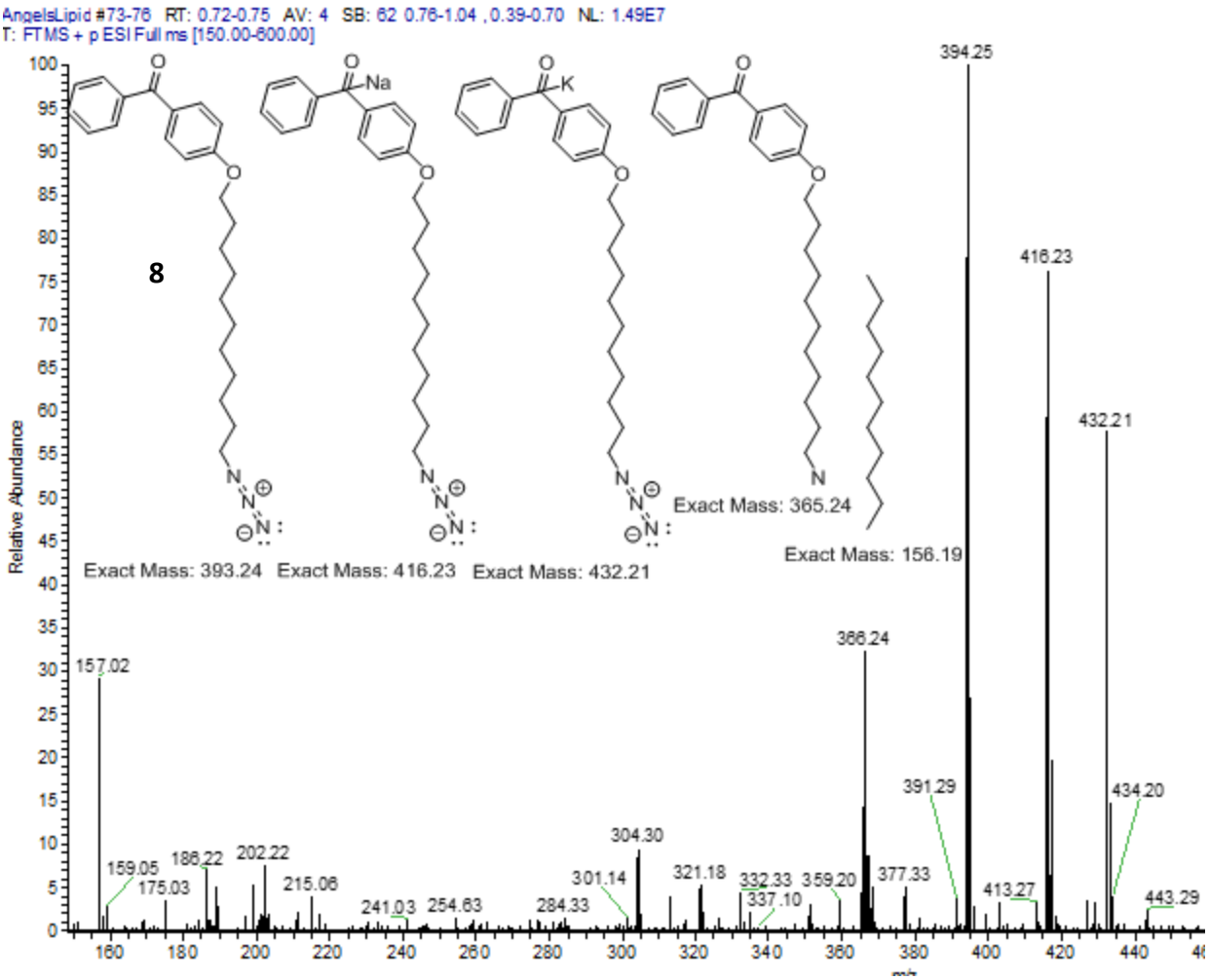
AngelsLipid #73-76 RT: 0.72-0.75 AV: 4 SB: 62 0.76-1.04 , 0.39-0.70 NL: 1.49E7
T: FTMS + p ESI Full ms [150.00-600.00]
8
Exact Mass: 393.24
Exact Mass: 416.23
Exact Mass: 432.21
Exact Mass: 365.24
Exact Mass: 156.19
Relative Abundance
394.25
416.23
432.21
366.24
157.02
391.29
434.20
304.30
159.05
186.22
202.22
175.03
215.06
301.14
321.18
332.33
359.20
377.33
337.10
413.27
443.29
241.03
254.63
284.33

VITA

Sam was raised with his sister, Adrienne, in Northwood, NH by his parents Grace Mattern and Eric Schain. Sam was creative and constructive from a young age. He worked as a carpenter for a master builder through high school and into his undergraduate years. Sam is an avid writer, he graduated *cum laude* from Clark University in Worcester, MA with a BA in English. After being certified as an English Foreign Language instructor in Costa Rica, Sam lived in Japan teaching English at several universities. He took his first Organic Chemistry class with Dr. Michael Best in 2011. In doing so, Sam found insight into the natural world that hooked him on chemical biology. He went on to work in Dr. Best's lab as a research assistant. Sam became fascinated by liposomes and how cellular pathologies may be exploited by nanotherapies. Sam trained many high school and undergraduate students working in Dr. Best's lab and he enjoys mentoring young scientists. Before graduate school, Sam lead a youth basketball team and taught soccer to kids. Of late, Sam has applied his passion for coaching to his work as a teaching assistant. He also enjoys clinical work; Sam served as a medical intern at the Pat Summit Alzheimer's Clinic during his graduate career. In his spare time, Sam can be found trail running with his dog.